AFRL-ML-TY-TR-2006-4545

ADVANCED FT-IR GAS ANALYSIS

James Markham; Patrick Bush; Peter Bonzani, Jr.; James Scire, Jr.

Advanced Fuel Research, Inc.
87 Church Street
East Hartford, CT 06108-3728

Final Report, December 2005

DISTRIBUTION STATEMENT A:

Approved for public release; distribution unlimited.

Air Force Research Laboratory
Materials and Manufacturing Directorate
Airbase Technologies Division
139 Barnes Drive, Suite 2
Tyndall AFB, FL 32403-5323

NOTICE

Using Government drawings, specifications, or other data included in this document for any purpose other than Government procurement does not in any way obligate the U.S. Government. The fact that the Government formulated or supplied the drawings, specifications, or other data does not license the holder or any other person or corporation; or convey any rights or permission to manufacture, use, or sell any patented invention that may relate to them.

This technical report was reviewed and cleared for public release by the Air Force Research Laboratory Tyndall Site (AFRL/MLQ) Public Affairs Office (PAO) and is releasable to the National Technical Information Service (NTIS). Reference PAO Case Number: AFRL/MLQ-06-051.

This report is releasable to the National Technical Information Service (NTIS) where it will be available to the general public, including foreign nationals.

5285 Port Royal Road
Springfield VA 22161
Telephone (703) 487-4650, (703) 487-4639 (TDD for the hearing impaired)
e-mail: orders@ntis.fedworld.gov
http://www.ntis.gov/index.html

This technical report is approved for publication.

//SIGNATURE//
HOWARD T. MAYFIELD
Work Unit Manager

//SIGNATURE//
SANDRA R. MEEKER
Chief, Airbase Sciences Branch

//SIGNATURE//
WENDELL D. BANKS
Chief, Airbase Technologies Division

This report is published in the interest of scientific and technical information exchange and its publication does not constitute the Government's approval or disapproval of its ideas or findings.

REPORT DOCUMENTATION PAGE

Form Approved
OMB No. 0704-0188

PLEASE DO NOT RETURN YOUR FORM TO THE ABOVE ADDRESS.

1. REPORT DATE *(DD-MM-YYYY)*	2. REPORT TYPE	3. DATES COVERED *(From - To)*
19-12-2005	Final Technical Report	16-10-2002 to 13-12-2005

4. TITLE AND SUBTITLE
Advanced FT-IR Gas Analysis (Phase III SBIR)

5a. CONTRACT NUMBER
F40600-02-C-0018

5b. GRANT NUMBER

5c. PROGRAM ELEMENT NUMBER
63716D

6. AUTHOR(S)
James Markham (PI)
Patrick Bush
Peter Bonzani, Jr.
James Scire, Jr.

5d. PROJECT NUMBER
OAFT

5e. TASK NUMBER
00

5f. WORK UNIT NUMBER
OAFT0161

7. PERFORMING ORGANIZATION NAME(S) AND ADDRESS(ES)
Advanced Fuel Research, Inc.
87 Church Street
East Hartford, CT 06108-3728

8. PERFORMING ORGANIZATION REPORT NUMBER
526056

9. SPONSORING/MONITORING AGENCY NAME(S) AND ADDRESS(ES)
Air Force Research Laboratory
Materials and Manufacturing Directorate
139 Barnes Drive, Suite 2
Tyndall AFB, FL 32403-5323

10. SPONSOR/MONITOR'S ACRONYM(S)
AFRL/MLQL

11. SPONSOR/MONITOR'S REPORT NUMBER(S)
AFRL-ML-TY-TR-2006-4545

12. DISTRIBUTION/AVAILABILITY STATEMENT
DISTRIBUTION STATEMENT A: Approved for public release; distribution unlimited.

13. SUPPLEMENTARY NOTES
AFRL/MLQ Public Affairs Case # 06-051. Document contains color images.

14. ABSTRACT
The Applied Technology Department at the Arnold Engineering Development Center (AEDC) of Arnold Air Force Base developed a "technology vision" for a rapid, continuous-sweep emissions measurement system that would provide cost-savings benefits and added-value benefits to large-nozzle military engines under development. The project described in this report resulted in a critical component of a system that was demonstrated to accomplish the multiple-species emissions survey of a full nozzle exit within the spatial resolution required by the regulatory agencies within a ten-minute time scale. At the pace emission measurement requirements were accomplished, there was no impact to other engine test objectives. The impact to this and future development engine test programs in terms of avoiding the cost of additional test time is significant. The critical component now available as a result of this project is an advanced prototype Fourier transform infrared (FT-IR) gas analyzer. Successful advanced development of the instrumentation hardware and software improved the measurement capabilities for advanced turbine engine programs, and for other applications in the Air Force and private sector. On-site demonstration trials are reported at the AEDC Aeropropulsion Systems Test Facility, at the AEDC Tunnel 9, and at facilities in the private sector.

15. SUBJECT TERMS
Infrared Spectroscopy, FT-IR, Gas Analysis, Turbine Engine, Emission

16. SECURITY CLASSIFICATION OF:			17. LIMITATION OF ABSTRACT	18. NUMBER OF PAGES	19a. NAME OF RESPONSIBLE PERSON
a. REPORT	b. ABSTRACT	c. THIS PAGE			Howard T. Mayfield
U	U	U	UU	236	19b. TELEPHONE NUMBER *(Include area code)*

Standard Form 298 (Rev. 8/98)
Prescribed by ANSI Std. Z39.18

Abstract

The Applied Technology Department at the Arnold Engineering Development Center (AEDC) of Arnold Air Force Base developed a "technology vision" for a rapid, continuous-sweep emissions measurement system that would provide cost-savings benefits and added-value benefits to large-nozzle military engines under development. The project described in this report resulted in a critical component of a system that was demonstrated to accomplish the multiple-species emissions survey of a full nozzle exit within the spatial resolution required by the regulatory agencies within a ten-minute time scale. At the pace emission measurement requirements were accomplished, there was no impact to other engine test objectives. The impact to this and future development engine test programs in terms of avoiding the cost of additional test time is significant. The critical component now available as a result of this project is an advanced prototype Fourier transform infrared (FT-IR) gas analyzer. Successful advanced development of the instrumentation hardware and software improved the measurement capabilities for advanced turbine engine programs, and for other applications in the Air Force and private sector. On-site demonstration trials are reported at the AEDC Aeropropulsion Systems Test Facility, at the AEDC Tunnel 9, and at facilities in the private sector.

Table of Contents

Note: The reader is strongly encouraged to view the referenced publications and appendices when prompted in the text of this report. Note the appendices may carry page numbers from the original document in the bottom center of the page, and in these cases, the page number for this table of contents is printed in the bottom right of the page.

List of Figures and Tables

List of Tables

Foreword

This report describes Phase III activities continuing developments from the Phase I and Phase II SBIR Projects, "Advanced FT-IR Gas Analysis Instrument for Improved Process Monitoring and On-Site Characterization," sponsored by the Air Force Research Laboratory, Airbase Technologies Division, Tyndall AFB, FL. The work was carried out by Advanced Fuel Research, Inc. acting in collaboration with Arnold Engineering Development Center, Aerospace Testing Alliance (AEDC/ATA), Arnold AFB, TN. These SBIR activities have developed an extractive FT-IR gas analysis instrument to produce near real-time quantitative analyses of environmentally significant species in gas streams, to include gas turbine engine exhaust gases. This instrument, termed a multigas analyzer, is now commercially available, after demonstration with civilian power generating gas turbine installations and with turbine engine test facilities at Arnold AFB, TN. Arrays of multigas analyzers have been used to provide rapid emission maps from turbine engines at Arnold AFB, TN and at a civilian academic research facility at Middle Tennessee State University.

Preface

The work reported herein was conducted by Advanced Fuel Research, Inc. (AFR), 87 Church Street, East Hartford, CT 06108 under U.S. Air Force Contract No. F40600-02-C-0018 for the Arnold Engineering Development Center (AEDC) with project monitoring by the Aerospace Testing Alliance (ATA), 690 Second Street, Arnold Air Force Base, Tennessee 37389. The AEDC/ATA Technical Points of Contact were Paul Jalbert, Vince Zaccardi, Denise Bryant and Don Gardner. Additional project support was provided by Tom Bentley (AEDC/ATA), Bill Phillips (AEDC/ATA), Ron Bishel (AEDC/DOT), and Howard Mayfield (AFRL/MLQL, Tyndall AFB).

This project demonstrated and provided both technology and cost saving benefits to the Air Force by improving gas analysis capabilities at Air Force facilities, with particular focus on emissions measurements from gas turbine engines undergoing developmental testing. The project consisted of the design, construction, testing, delivery, installation and operation of advanced prototype multiple-gas analyzers. The core technology of these analyzers originated at AFR and is currently manufactured by the MKS Instruments On-Line Products Group in Methuen, MA. Advancements were implemented to both hardware and software to provide added-value to the Air Force. Testing and demonstrations were performed: 1) in the AFR laboratory; 2) at an AEDC/ATA field demonstration site located at an airfield utilized by the Middle Tennessee State University (MTSU) in Murfreesboro, TN; 3) at Pratt & Whitney (P&W) in East Hartford, CT; 4) at Solar Turbines, Inc. in San Diego, CA; 5) at the University of California-Riverside (UCR) in Riverside, CA; 6) at AEDC, Arnold AFB, TN; 7) at AEDC Tunnel 9, White Oak, MD; and 8) at NASA Dryden Flight Research Center in Edwards, CA.

AFR expresses appreciation to the following individuals for important guidance and interactions during the project:

AEDC/DOT	**AEDC/ATA**	**MTSU**	**AFRL/MLQL**	**University of California (Riverside)**
Ron Bishel	Vince Zaccardi	Bill Allan	Howard Mayfield	Wayne Miller
	Paul Jalbert			Aniket Sawant
Pratt & Whitney	Don Gardner	**MKS/On-Line**	**Solar Turbines**	David Cocker
Chu Vu	Denise Bryant	Marty Spartz	John Lee	
Dick Strange	Bill Phillips	Dave Marran	Wasseem Nazir	**NASA GRC**
Bob Johnston	Tom Bentley	Bill Murphy	Andrew Russell	Changlie Wey
	Kent Wilcher	Nicole Bush	Nordine El Hafidoun	
UTRC			Bernie Blutinger	
Dave Liscinsky				

AFR also appreciates the many others at AEDC, MTSU, Pratt & Whitney, Solar Turbines, UCR, and NASA GRC who contributed time and effort to arranging and/or aiding the field demonstrations of this project; and to those who interacted with us at the NASA APEX test at

NASA Dryden Flight Research Center. AFR extends gratitude to independent consultants Jack Vaught and James Elwood for their efforts with AFR and ATA towards completion of the SAE Aerospace Information Report (AIR) 5917.

AFR was pleased and appreciative to be included as part of the ATA team to receive the First Quarter 2004 AEDC *Technical Achievement Excellence Award* from the AEDC Commander (Brigadier General David Stringer) for the outcome of this project. The Continuous Sweep Emissions Team members include: Mr. Ron Bishel, AEDC/DOT; Capt. Troy Christensen, AEDC/DOP; Dr. Charles Vining, AEDC/DOT; Dr. Howard Mayfield, AFRL/MLQL; Mr. Bill Allen, MTSU; Advanced Fuel Research Inc.'s Mr. Jim Markham, Mr. Peter Bonzani, and Mr. Patrick Bush; and ATA's Mr. Vince Zaccardi, Mr. Bob Hiers, Jr., Mr. Danny Catalano, Ms. Heather MacKinnon, Mr. Larry Wilhite, Mr. Jacob Cashion, Mr. Paul Jalbert, Dr. Brad Winkleman, Ms. Denise Bryant, Mr. Brad Besheres, Mr. Roy Carrol, Mr. John King, and Mr. Gary Storey.

Detailed Report

a. Introduction

Advanced Fuel Research, Inc. (AFR) of East Hartford, Connecticut, previously completed a Small Business Innovation Research (SBIR) Phase II project under Contract No. F41624-97-C-0003 awarded by the Air Force Research Laboratory, Tyndall AFB, Florida, entitled "Advanced FT-IR Gas Analysis Instrument for Improved Process Monitoring and On-Site Characterization." Phase II work in response to topic AF96-005e included key collaboration and technical support by Jacobs/Sverdrup, AEDC Group, the support contractor at the Arnold Engineering Development Center (AEDC) at Arnold AFB, Tennessee. The Instrumentation & Diagnostic Branch of Jacobs/Sverdrup, AEDC Group provided personnel and access to facilities during the Phase II project to demonstrate the new, advanced technology for gas phase emissions (pollution) monitoring from turbine engines. Phase II work was completed 10 March 2000, and included delivery of the Phase II prototype "MultiGas Analyzer" (MGA) to AEDC. The Jacobs/Sverdrup, AEDC Group continued with application of the Phase II deliverable in support of an improved extractive sampling and measurement methodology for turbine engine emission quantitative analysis. AFR successfully continued with efforts to bring the MGA to a production version: the product is now manufactured by MKS Instruments through its On-Line Products Group of Methuen, MA. Three published technical papers relevant to the success of the completed Phase II project are:

- Nelson, C.M., Marran, D.F., and Markham, J.R., **"Gas Turbine Testing,"** *Sensors*, vol. 16, no. 5, May 1999.

- Marran, D., Kenny, P., and Markham, J., (AFR), and Jalbert, P., Moyers, R., and Gardner, D., (Jacobs/Sverdrup AEDC Group), **"The Application of FT-IR Spectroscopy to Turbine Engine Exhaust Monitoring,"** invited paper presented at the 21st AIAA Ground Test Conference, Denver, CO (June 19-22, 2000). Paper AIAA 2000-2211.

- Jalbert, P.A. and Zaccardi, V.A. (Jacobs/Sverdrup, AEDC Group), **"Improved Methodology for Turbine Engine Emission Measurements,"** presentation/ publication at the 47th ASME International Gas Turbine & Aeroengine Technical Congress, Turbo Expo 2002, June 3-6, 2002, Amsterdam, The Netherlands. Paper GT-2002-30606.

The Air Force Impact Story pertaining to the completed Phase II project was previously available at www.afrl.af.mil/sbir/impact/af96-005e.pdf, and is presented in **Appendix A** to provide a project overview.

This Air Force Phase III contract no. F40600-02-C-0018 with AFR called for the delivery of additional units and advanced development. This effort was to provide both technology and cost saving benefits to the Air Force by improving gas analysis capabilities at Air Force facilities. Also, the effort would increase the commercial application of the Air Force supported research and development. This would be accomplished with multiple units of the now manufactured version of the SBIR Phase II prototype instrument. The units would be further advanced by AFR to meet specific measurement needs of the Air Force. The advanced R&D would increase measurement capability, and hence, increase value to the Air Force. The increased capability would also add value for commercial applications.

First installations with continued development of applications would occur at the Arnold Engineering Development Center (AEDC) at Arnold Air Force Base, the most advanced and largest complex of flight simulation test facilities in the world. Cost is increasingly important to future aircraft systems such as the Joint Strike Fighter (JSF). In response to this, DoD future technology development efforts are to aggressively pursue approaches to reduce development, production, and maintenance cost. The new technology offered here is such an approach.

The application and advanced development focused on military turbine engine exhaust monitoring for engine design testing, qualification and environmental control. Improved gas analysis capabilities at significantly lower costs than the current method would be proven and documented. A new aerospace recommended practice would result from this effort. Continued development of the instrumentation hardware and software would further improve the measurement capabilities for advanced turbine engine programs and other applications in the Air Force and private sector. Two long term demonstrations would be completed in the private sector.

Under the Phase III contract, six Advanced FT-IR Gas Analysis units were put into service (Figure 1). Four were utilized at AEDC to prove technology and cost saving benefits to the Air Force, and two were utilized at a major U.S. manufacturer of electric power generating gas turbine engines in the effort to increase commercial applications. Funding provided to this contract was effectively used for manufacture and delivery of the six Advanced FT-IR Gas Analysis units, to support the planned field demonstrations, and advanced development needs of the project.

Note that during the project, the support contractor at AEDC transitioned from the Jacobs/Sverdrup AEDC Group to the Aerospace Testing Alliance (ATA/AEDC).

MultiGas™ Analyzer

Figure 1. The FT-IR unit. 17.5" wide x 12.5" tall x 25.5" deep. 19" rack mount chassis.

The highlighted titles of the following published technical papers of the Phase III project serve to introduce the reader to the technology advancements and benefits provided to the Air Force. The papers are listed in chronological order with the most recent as the last entry.

- Gardner, D.G., Zaccardi, V.A., Jalbert, P.A., and Bryant, M.D. (AEDC), **"Reducing the Cost of Aircraft Engine Emission Measurements,"** ISA vol. 443, Proceedings of the 49th International Instrumentation Symposium, Orlando, FL (May 8, 2003).

- Markham, J.R., Bonzani, P.J., Bush, P.M., and Scire, J.J. (AFR), **"Integrated Gas Analyzer for Measuring Combustion Exhaust and Excess Oxygen,"** ISA vol. 443, Proceedings of the 49th International Instrumentation Symposium, Orlando, FL (May 8, 2003).

- Markham, J.R., Bush, P.M., Bonzani, P.J., and Scire, J.J. (AFR), and Zaccardi, V.A., Jalbert, P.A., Bryant, M.D., and Gardner, D.G. (AEDC), **"Integrated Gas Analyzer for Complete Monitoring of Turbine Engine Test Cells,"** Applied Spectroscopy, Volume 58, Number 1, January 2004.

- Jalbert, P.A., Zaccardi, V.A., Bryant, M.D., Winkleman, B.C., (AEDC), and Markham, J.R., Bush, P.M., Bonzani, P.J. (AFR), **"Rapid, Complete Nozzle Exhaust Gas Measurement Capability for Gas Turbine Engines,"** ISA vol. 451, Proceedings of the 50th International Instrumentation Symposium, San Antonio, TX (May 9-13, 2004).

- Jalbert, P.A. (AEDC) and Markham, J.R. (AFR), **"Fourier Transform Infrared for Turbine Engine Health Monitoring,"** Applied Spectroscopy, Volume 58, Number 12, December 2004.

The annual symposium in 2003 and 2004 used to present 3 of these papers provided a particularly good forum sponsored by the ISA Aerospace Industries Division, and the papers were presented during sessions held in conjunction with the spring 2003 and spring 2004 meetings of the Propulsion Instrumentation Working Group (PIWG). Applied Spectroscopy is the official publication of the Society for Applied Spectroscopy (3,000 members) and each of our articles benefited from two expert peer reviews as well as input from the journal editor.

Appendix B presents an article from the AEDC newspaper *High Mach* (vol. 51, no. 5, March 11, 2004) which provides an overview of the impact of this project on AEDC test customers. Also relevant to the accomplishments of the Phase III project, a provisional application entitled "Analyzer for Measuring Multiple Gases" was filed by AFR on 3 March 2003 at the United States Patent & Trademark Office (USPTO) and assigned provisional application no. 60/451,484. Its non-provisional counterpart was filed on 27 February 2004, and assigned non-provisional application 10/789,651. This patent pending was still in review at USPTO as of the submission of this report.

b. Significant Results

In the time period between the completion of the previous SBIR Phase II project and the start of this Phase III contract, AFR and the On-Line Products Group of MKS Instruments provided significant investment to advance the operational and analysis software of the instrument, and to establish a production line for the next generation MultiGas Analyzer, the model MGA 2030. In addition to the earlier Phase II prototype (MGA 2010) delivered under the Phase II contract to AEDC, one of the first MGA 2030's produced was purchased by AEDC. In support of AEDC's use of these instruments, a two-day advanced training session supplied by AFR and MKS to ten AEDC personnel for operation and maintenance of the MGA was completed 6-7 February, 2002 (about 7 months before the start of the Phase III project). The early stage of Phase III completed the manufacture and delivery of six production MGA 2030 systems. Four were delivered to AEDC, and two were delivered to Solar Turbines, Inc., San Diego, CA. Collaborative development and applications work has further proved and advanced the measurement capabilities for current and advanced turbine engine programs, other advanced aeropropulsion programs, and other applications in the Air Force and private sector. The effort has strived to advance the MGA platform towards a complete engine emissions measurement system.

Significant results of the project are now reviewed for each of the six Work Plan Tasks. During the reading of this section, the reader will often times be directed to the project's published articles and/or unpublished documents exhibited in the appendices of this report for important details and demonstration results. **The reader is strongly encouraged to view these referenced publications and appendices when prompted.**

Task 1 – Manufacture and Delivery of Six MGA Systems (AFR Responsibility)

Goals Targeted for this Task:

- Deliver MGA 2030 systems to AEDC, AFR, and Solar Turbines (2 each) for testing and applications of subsequent tasks.

Significant Results:

Six MGA 2030 systems were called for and purchased with project funds. Table 1 identifies these systems by serial number and main location during the project. The two systems provided to Solar Turbines during the project were purchased with a significant 54% cost-share discount

provided by MKS Instruments. **All six systems are Air Force property and would be delivered to AEDC by the end of the project.** Table 1 also identifies the earlier version Phase II MGA 2010 prototype and the post-Phase II/pre-Phase III MGA 2030 purchased by AEDC. Both of these earlier units were also advanced (hardware and software) as key refinements and improvements were completed and implemented for the six units in subsequent tasks of the project.

Table 1. MGA systems delivered

MGA Serial Number	Application Locations During Project
07-121 MGA 2030	AEDC
07-126 MGA 2030	AEDC
07-127 MGA 2030	AEDC
07-128 MGA 2030	AEDC
07-129 MGA 2030	Solar Turbines
07-131 MGA 2030	Solar Turbines
07-101 pre-phase III MGA 2030	AEDC
04-008 Phase II prototype MGA 2010	AEDC

The photograph in the preface section of this report presents five MGA 2030s in place for measurements at the AEDC engine test cell C-1.

Conclusion for this Task in Regard to Goal Targeted:

AFR achieved the goal of this task – MGA 2030 systems were delivered to AEDC and Solar Turbines (2 each) for testing and applications of subsequent tasks.

Task 2 – Development of the Gas Turbine Engine Application (AEDC & AFR Responsibility)

Goals Targeted for this Task:

- Demonstrate that the MGA 2030 is acceptable for emission measurements during engine development and certification testing to result in a new aerospace recommended practice (ARP).
- Identify 5 MGA 2030 turbine installation points within AEDC.
- Convince Solar Turbines of 24/7/365 performance.

Significant Results:

AEDC Gas Turbine Applications: Pertaining to technology benefits and cost savings benefits now available to the Air Force as a result of this task, **the reader is directed to view the project-generated publications [1- 5].**

A summary of the key points/results expressed in these publications is as follows:

- Success in combining the spectroscopic technique of FT-IR gas analysis with a solid-oxide (zirconia) sensor run in amperometric mode to result in a "single instrument"

approach for the simultaneous measurement of infrared-active combustion exhaust gases and infrared-inactive excess oxygen.

- Successful field-demonstrations at the AEDC/MTSU (low-cost) test location to validate the project approach to reducing both the time required to collect data and the associated cost of emissions measurements during tests of development aircraft turbine engines.
- Successful on-base demonstrations at the AEDC C-1 test cell that achieved the necessary exhaust emissions profile data at rake traverse rates as high as 27 in/min. At that rate a complete ten-probe engine survey can be completed in less than 5 minutes. A complete engine survey on this time scale is invisible to the customer and eliminates the typical 16-hour test period dedicated to emissions. Avoiding each currently performed test period dedicated to emissions testing results in significant cost-savings per test cycle in labor, altitude-test facilities usage, jet fuel and materials. **The magnitude of these savings are pointed out in the AEDC *High Mach* article that was presented in Appendix B.**
- Successful on-base demonstration at AEDC C-1 that also provided on-line data that proved to be particularly useful towards engine health monitoring. For the first time at AEDC, the measured value of the emission index for sulfur dioxide (SO_2) from a gas turbine engine was used effectively. The value measured by the MGA 2030 was used to unambiguously identify an oil leak within an engine and confirm repair.

A significant part of this effort was to perform development work and implement improvements to the operational and quantitative analysis software of the Multigas analyzer systems. To benefit AEDC users/operators, these improvements were documented in an addendum to the MGA 2030 user-manual. **Appendix C** displays this important addendum document.

One objective in the first part of this project was to compare the performance of four MultiGas Analyzers (MGA) when operating simultaneously. During MTSU Test #8 (11 June 2003), MGA performance was quantified in terms of MGA-to-MGA measurement agreement. Data Point #14 is of particular interest because extra effort was made to ensure that all four MGAs received the same JT-12 engine exhaust gas sample. A single sample line from the heated valve box routed the gas sample through two two-stage boost pumps to a manifold where the sample was distributed to the four MGAs. Note that the flow rate to the four MGAs was limited to 2.5 lpm in order to raise the sample pressure at the AEDC total hydrocarbon flame ionization detector (HFID) inlet to 2.5 psi.

The probe rake was positioned at 50.50 inches above the ground, just slightly below the engine centerline. Probes 2,3,4,5, and 6 were selected for sample. At the start of the engine power sweep, the engine had already been running for about 22 minutes so both the engine and gas sampling system had achieved thermal stability. The engine power sweep consisted of 5 percent power incremental changes in throttle setting from 45 percent power to 75 percent power and back to 45 percent power. The power sweep took about 40 minutes to complete. Good agreement was observed during the incremental power changes and also during two distinct continuous sweeps of the rake at a constant power setting. The measurement precision of the major species about the average of the four MGA readings is summarized below. In addition, the precision of the fuel / air ratio (FAR) was calculated for each MGA (based on MGA measurements of CO, CO_2, and NO_2 and HFID measurements of C_xH_y).

CO_2 = ± 0.03 percent
CO = ± 10 ppm
NO = ± .5 ppm
THC = ± 10 ppmC at power settings above 65 %, THC levels < 20 ppmC
H_2O = ± 0.05 percent
FAR = ± 0.0015

The conclusion from this analysis was: the measurement precision of four MGA's is as good as any single standard gas analyzer. Note: this analysis of data point #14, MTSU test #8 was provided by P. Jalbert of ATA/AEDC (reference document: email to J. Markham of AFR on July 1, 2003).

The acceptable performance of the multiple MGA 2030 systems used in this project provided data that supported the project-generated SAE Aerospace Information Report 5917, shown in **Appendix D**. The first draft of AIR 5917 was generated by AFR, then subsequent drafts 2-4 benefited from the cooperative efforts of AFR, ATA, and independent consultants Jack Vaught and James Elwood. ATA/AEDC representatives presented the AIR 5917 to the SAE Committee E-31 at the Committee's annual meeting held 8 June 2004. The AIR is to be placed on the Committee's ballot, and if accepted by member vote could then be developed into an Aerospace Recommended Practice (ARP).

The project's successful effort to identify 5 MGA 2030 turbine installation points within AEDC is summarized in Table 2.

Oxygen Sensor for Integration with the MGA 2030: Pertaining to the details of the oxygen sensor integration, the reader is directed to view **Appendix E** for:

1. Description of the sensing technology
2. Calibration
3. Construction and installation of sensors and modules
4. Electronic schematics and printed circuit board layout
5. Software schematics and screenshots
6. Notes on operation
7. Selection of vendor

Table 2. MGA Turbine Applications at AEDC*

Application	Location	Requirement	Task	Impact
1. Continuous Sweep Emissions	ASTF C-1	Reduce the cost, in terms of wear on the engine at high power, fuel usage, and test cell time, of an exhaust gas emissions survey.	Measure the gas species required for analysis of local F/A and combustion efficiency within 5 min.	A gas analysis system including five MGA's has been demonstrated to have sufficient time response to complete a nozzle exit survey in five minutes.
2. Combustor Exit Emissions	T-3	Reduce the cost of emission measurements during developmental combustor tests.	Provide on-line measurements of the gas species for analysis of F/A, combustion efficiency, and low NO_x.	A single MGA has been used to provide on-line measurements of the gas species in the exhaust of combustors being developed for low-NO_x stationary power gas turbines.
3. Ambient Air Quality	SL Test Cell Recirculation	Determine whether excessive gas turbine engine wear was caused by air-borne contaminants.	Measure the composition of the inlet air over a range of engine operating conditions.	Exhaust gas re-circulation and local air pollution was eliminated as a cause of the anomaly.
4. Engine Combustion Efficiency	T-11	Evaluate the performance of an expendable gas turbine engine.	Provide rapid, on-line measurements of the gas species during highly transient engine operation.	Fast response measurements of exhaust gas species were used to derive F/A and combustion efficiency during simulated missions profiles.
5. Afterburner Fuel/Air Ratio and Performance	FX621 and XTE67 ASTF C-1	Resolve deficiencies with military aircraft engine afterburner ignition and operation.	Provide rapid, on-line measurements of the gas species during highly transient engine operation.	Fast response measurements of exhaust gas species were used to define local A/B zone F/A.

* Credit is given to Paul Jalbert (ATA/AEDC) as the original author of the information in this table.

The MGA software has been updated regarding measurement from the integrated O_2 sensor. Data from the O_2 sensor manufacturer indicates that some gases present a small interference to the O_2 sensor's response. Equation 1 presents the correction for any gas "i" on the O_2 measurement:

$$O_2\%_{(real)} = O_2\% \text{ (measured)} - k_i \text{ (i\%)} \quad (1)$$

The value "k_i" is a constant specific to gas "i" and the manufacturer provided values for many combustion-relevant gases. During engine testing at MTSU, for example, typical concentrations of 17% O_2 and 2.3% CO_2 were measured. Using k_{CO_2} and eq. 1, the calculated deviation in $O_2\%_{(measured)}$ to $O_2\%_{(real)}$ would be -0.058%, which is -0.3% of the reading. While this level is below the sensor manufacturer's accuracy specification (±0.5% of reading) and also well within the typical accuracy of calibration certified standards (± 2%), the real time data availability from the MGA can be used to adjust the measured O_2 concentration. The MGA software was initially updated to perform this function for CO_2. Typical CO levels are less interfering than CO_2, and other combustion gases (NO_x, SO_x, etc) present negligible interference at the ppm levels typically encountered. The current version of the MGA software corrects the O_2 sensor response for CO_2 and CO measured in the sample flow. The software can easily be configured to correct for any interfering gas species.

All of the MGA systems of the project (Table 1) were retrofitted with an integrated oxygen sensor, with the exception of MGA 07-129. This unit was significantly damaged during a commercial field trial at Solar Turbines and not repaired due to a high cost estimate (discussed later in this report). Project publications presenting the successfully implemented sensor capability include **references 2-4**. An objective of the development of the integrated oxygen sensor was complete integration. Figure 2 indicates the system morphogenesis from the early version to the final completely integrated version. The first completely integrated oxygen sensor system was finalized in July, 2004. Solar Turbines requested the system to be installed in a new Multigas Analyzer model 2030 supplied by MKS, complete with the new electronics package. This new system allows for the direct importation of the oxygen data directly into the MGA hardware, eliminating the need for the additional serial port cable. All of the components of the oxygen sensor suite were placed within the MGA package. A single version of the now standard heating and current-to-voltage module was installed. A linear power supply was chosen to replace the earlier used switching supply, in order to reduce potential noise contributions from the system. The new data acquisition system used in the MGA to collect temperature and pressure measurements of the gas cell is identical to the one employed by the previous integrated oxygen sensors, the B+B 232SDA12. Using a modified circuit design, an additional channel was added to this module to import the oxygen data stream. Figures 3 and 4 show the placement of the components.

An integral lighted indicator switch was also incorporated into the design in order to provide a way of turning off power to the oxygen sensor when so desired. Figure 5 shows the location of the On/Off power switch.

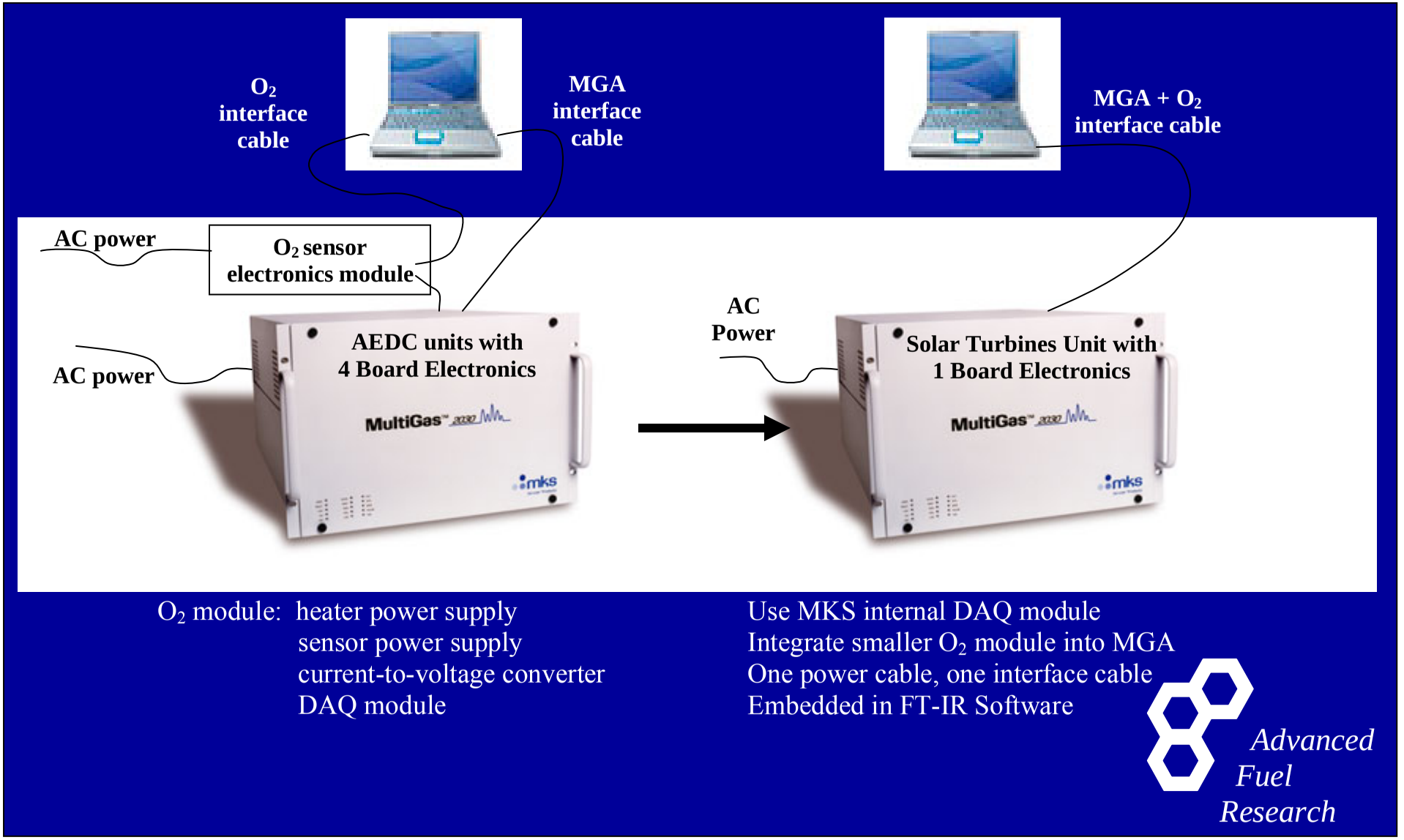

Figure 2. Integrated oxygen sensor morphogenesis from early version (left) to final version (right).

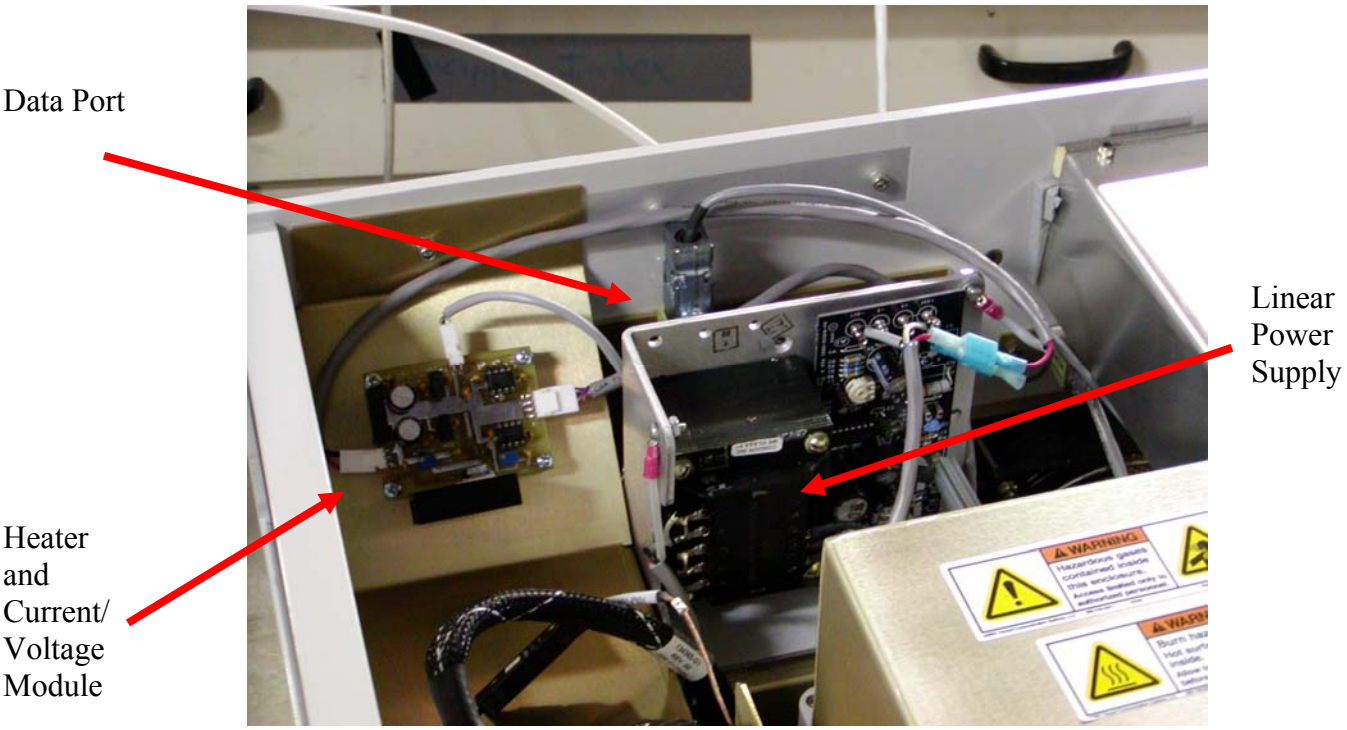

Figure 3: Location of internal components.

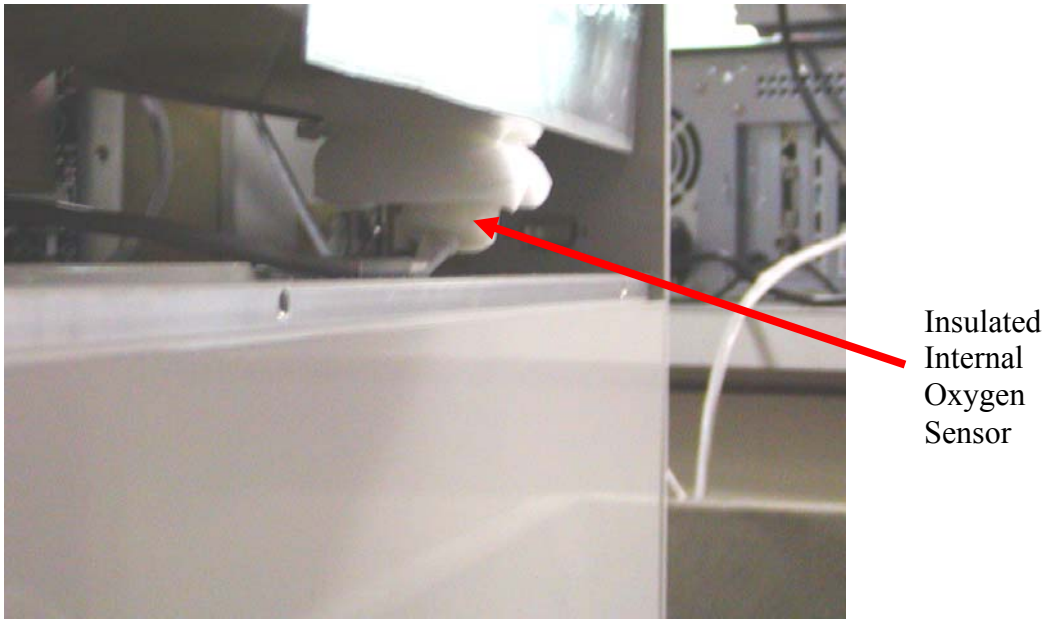

Figure 4: Oxygen sensor placement.

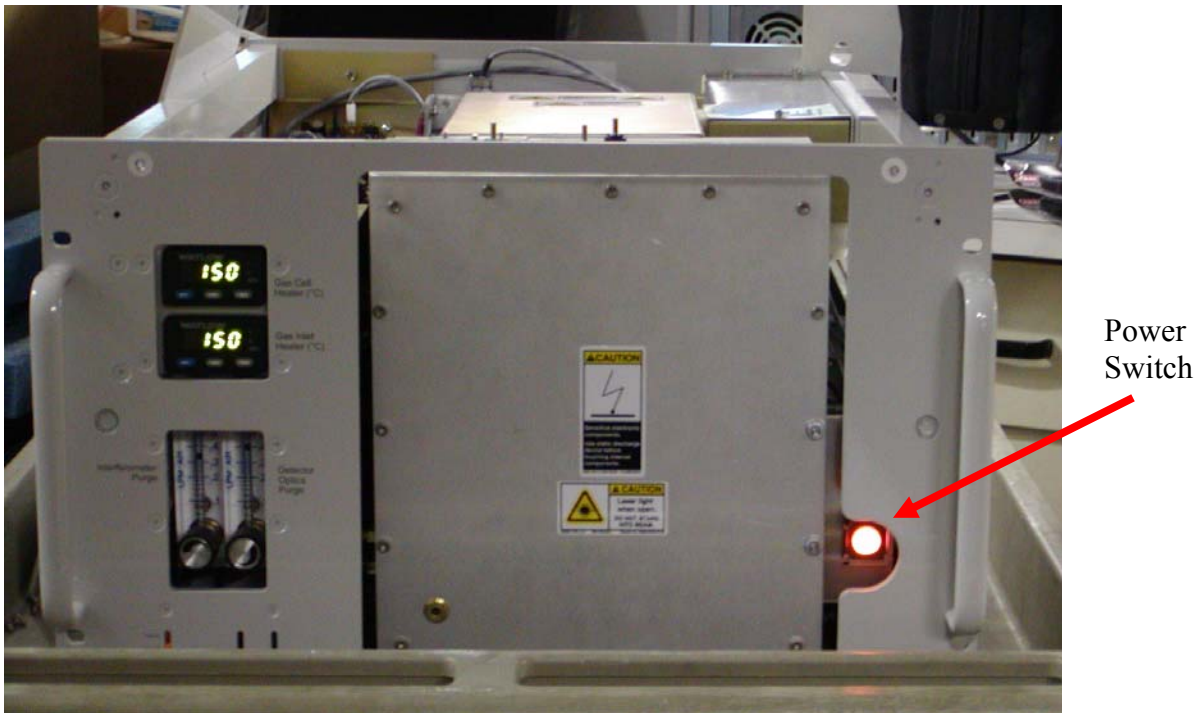

Figure 5: Location of power switch on front of instrument

Final improvements were then implemented in September 2004 on the MGA 2030 purchased by the University of Dayton Research Institute. Improvements to the O_2 installation occurred with the UDRI unit resulting in the O_2 sensor mounted directly (i.e., straight) into the gas flow path of the MGA (Figure 6). This new location results in a more compact installation of the O_2 sensor, which will reduce temperature instabilities for both the gas exhaust and the O_2 sensor. Another improvement to the installation was the power design of the O_2 sensor to run at both 120 and 240 VAC making the sensor more compatible with the universal use of the MGA. The O_2 sensor documentation indicated these new improvements and provides more detail to the installation of the O_2 sensor with the MGA.

In addition to successful internal integration and application of the oxygen sensor technology with the MGA, AFR also designed and constructed a prototype stand-alone oxygen sensor unit. The design incorporates the power supply, data acquisition (DAQ) module, and sensor unit in a temperature-controlled enclosure. The only electrical connections required are input 120 VAC and an output communications port. The unit is totally self-contained, heated and insulated. Detail is provided in **Appendix F**.

Investigation Pertaining to Hydrocarbon Speciation: Significant focus in this project has been to document the capability of the MGA 2030 for speciation of hydrocarbon gases in engine exhaust and other samples, and to improve the MGA capability towards closure of total hydrocarbons measured with the traditionally used flame ionization detector (FID). The next several pages of this report provide details of the progression of work during the project. If the reader desires to view the final results of this investigation, **Appendix G** presents our manuscript entitled

"Advances in Quantifying Total Hydrocarbons and Individual Species during the Rapid, Continuous-Sweep Method of Measuring Turbine Engine Exhaust."

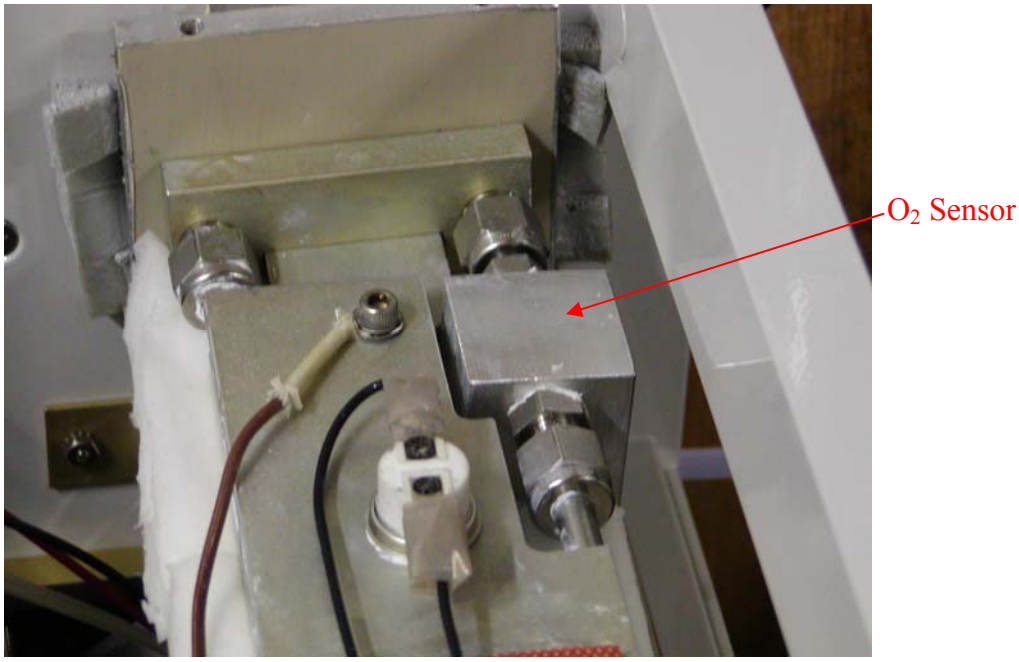

Figure 6: O_2 Sensor installed directly into the gas exhaust path of the MGA.

Work in this area performed measurements during JT-12 engine operation at MTSU that would provide comparative data between the MGA and FID instruments. As background, Figure 7 presents previous Phase II project data of hydrocarbon emissions measured from a natural gas fired combustor that was tested at AEDC. In this plot, total hydrocarbons are measured by AEDC using a flame ionization detector (FID), which is not capable of speciating hydrocarbons. The Multigas, on the other hand, does speciate hydrocarbons, and the total hydrocarbons are summed from the species indicated in Table 3. This table lists all the hydrocarbon compounds quantified in the turbine exhaust, and includes the approximate percent contribution to the total hydrocarbon concentration as reported by the FID. Since the FID results are normalized to C_1 (i.e., equivalent methane), the relative contribution for each compound in the table has also been normalized to C_1. As seen in Figure 7 the Multigas results are typically within about 2.5% of the FID results, which is well within the experimental uncertainty of the measurements.

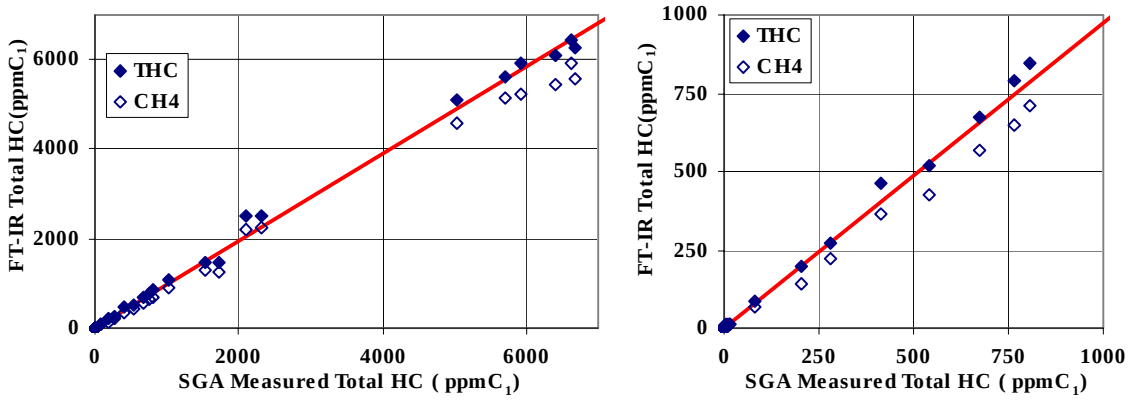

Figure 7. Correlation plot for Total Hydrocarbons. The graph on the left covers the entire dynamic range of the data, while the right expands the data from 0-1000 ppm. The total Hydrocarbons measured with the Multigas is calculated using the species listed in Table 3. The best linear fit shown has a slope of 0.975 and zero offset. Also plotted is the correlation between Multigas measured methane and the THC's. See text for details.

Table 3. Hydrocarbons detected in the turbine combustor exhaust, and the relative contribution of each. These contributions are normalized to the FID analyzer results, and have been corrected by the number of carbon atoms in each molecule.

Species	Fraction of total C_1(%)
Methane	80-90%
Formaldehyde	7-8%
Ethylene	8-9%
Methanol	<1%
Propylene	<1%
Formic acid	<1%

So when CH_4 was the primary hydrocarbon in the exhaust, good correlation in total HC was observed for the two measurement techniques. However, comparisons performed in this project when using diesel fuel were not close in agreement. Figure 8 presents overlaid MGA hydrocarbon concentration traces measured during the 21 March 2003 test (test #7). Concentration traces for the major non-methane organic compounds, ethylene (C_2H_4), propylene (C_3H_6), acetylene (C_2H_2), and formaldehyde, (H_2CO) are shown. Each gas shows the step-wise changes with power level and are reversible from start-to-finish of the sequence. Methane (not shown on the plot) was stable at about 4.5 ppm at 45% power and dropped to about 1.5 ppm at 75% power. With liquid fuel firing at 45% engine power, formaldehyde, ethylene, and acetylene exhibited higher concentrations than methane.

Figure 9 compares MGA vs. FID data for total hydrocarbon (ppm C) at 45% engine power, holding the engine power stable over 5 minutes. Wet and dry samples streams are compared. During wet exhaust sampling, the FID (~180 ppm C) exhibits about 4 times the total hydrocarbons as the MGA (~45 ppm C). During dry exhaust sampling, only about a factor of 2

difference is observed between FID (~90 ppm C) and MGA (~40 ppm C) since the dry FID exhibits a 50% reduction compared to wet FID. The MGA exhibits only about a 10% reduction comparing wet to dry. Note that the MGA total hydrocarbon values presented here are made up of only measured ethylene, methane, acetylene and propylene.

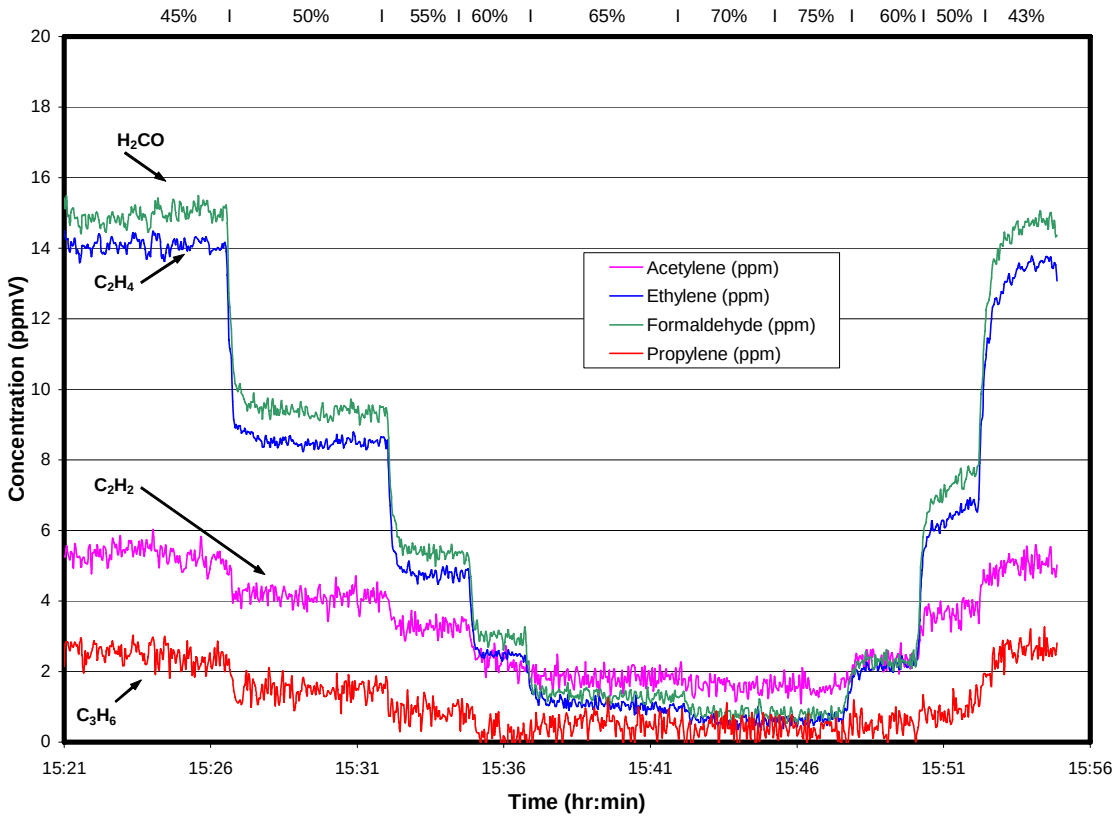

Figure 8. Non-methane hydrocarbons measured during JT-12 firing with diesel fuel, 21 March 2003 (test #7). Engine power is indicated at the top of the plot.

In an effort to explain the large drop in the FID data (wet vs. dry), and the lack of agreement of the MGA to the FIDs, the MGA spectral data is first considered. Figure 10 presents a hydrocarbon absorption region in the infrared spectrum (2800-3100 cm^{-1}), overlaying a spectrum collected for each the wet and dry JT-12 exhaust. Also overlaid is a measured spectrum of the vapor above a liquid Jet-A fuel sample (the liquid being at ambient temperature with its ambient temperature vapor phase being pulled into heat-trace tubing and measured at 150°C in the MGA). Although the figure is comparing Jet-A vapor components to diesel exhaust, the "three humps" present in the jet fuel vapor are evident in both the wet and dry exhaust. When comparing the two exhaust spectra, clearly evident when going from wet to dry are: 1) the loss of narrow moisture absorption bands; 2) the loss of formaldehyde; and 3) about a 50% intensity reduction of the "three humps" that line up with the jet fuel vapor. Figure 11 provides a comparison of the measured spectra to qualitative spectra (concentrations unknown) of several pure alkanes (C_4 - C_{16}) available on a NIST web site (http://webbook.nist.gov). The relative intensities of the "three humps" in the exhaust spectra are best visually matched to the C_6H_{14} features.

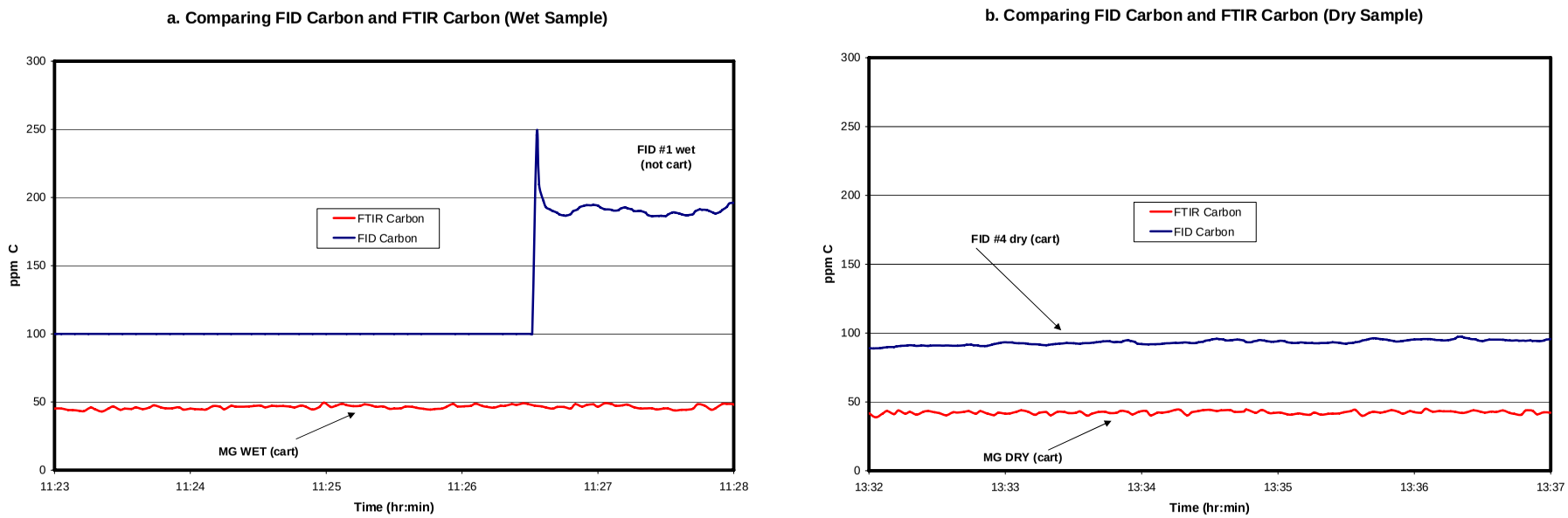

Figure 9: MGA versus FID measurements of total hydrocarbon concentration; JT-12 exhaust, 45% power, diesel fuel 21 March 2003 (MTSU test #7). a) wet gas sample over a 5 minute dwell time; b) dry gas sample over a 5 minute dwell time. Drying was accomplished with a PermaPure™ dryer. Formaldehyde is not included in all traces since 1) the FID documentation suggests that the instrument is not sensitive to aldehydes, and 2) since aldehydes are efficiently removed by the dryer. In plot a, the measurement range of the FID was appropriately set at the 11:26:30 mark. The same MGA is used, but two FID instruments were used for wet vs. dry samples.

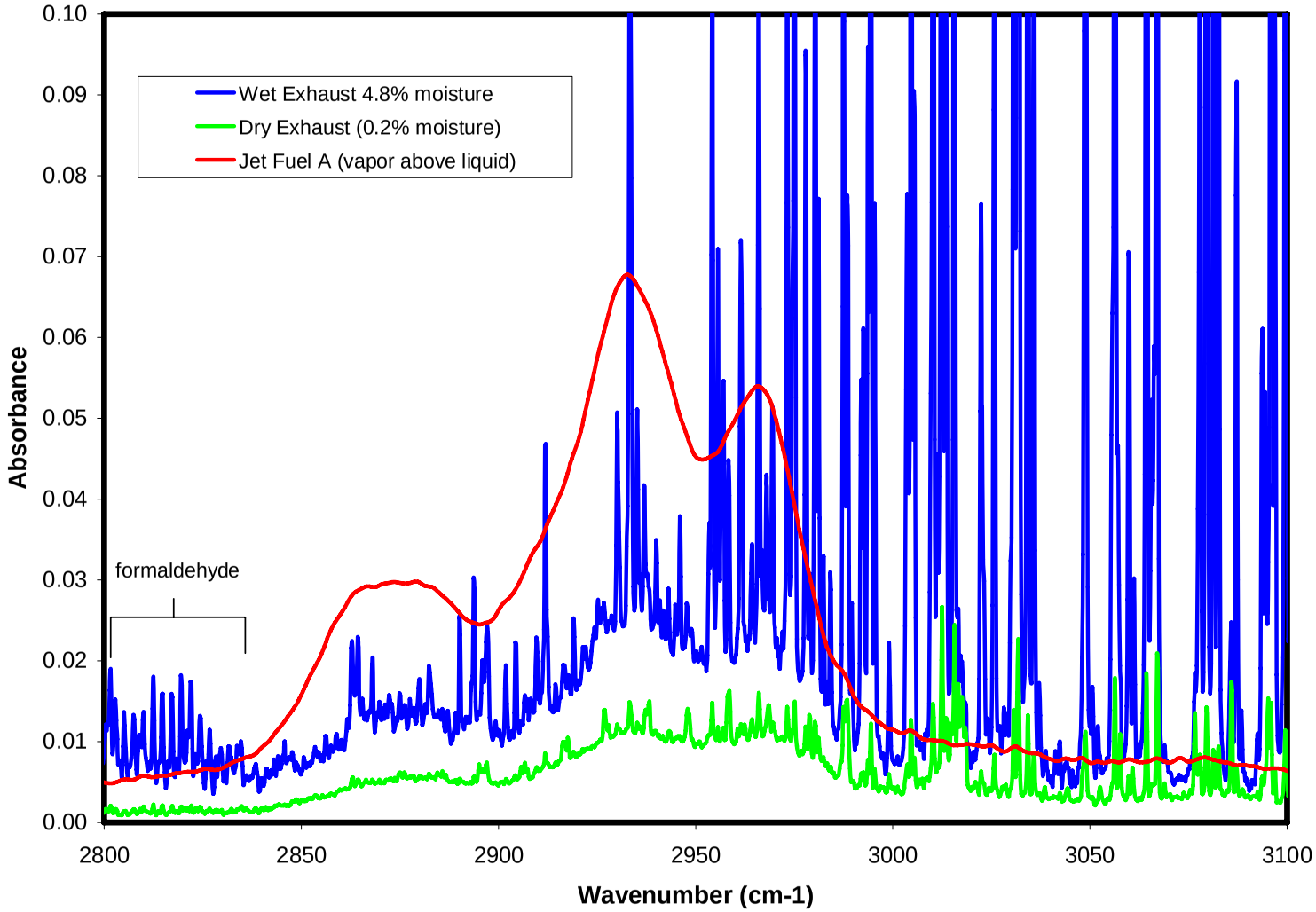

Figure 10: Hydrocarbon absorption region in infrared spectrum for wet and dry Jet-12 exhaust, 45% power, diesel fuel, 21 March 2003 (MTSU test #7). A spectrum of the vapor above a liquid Jet A fuel sample is overlaid.

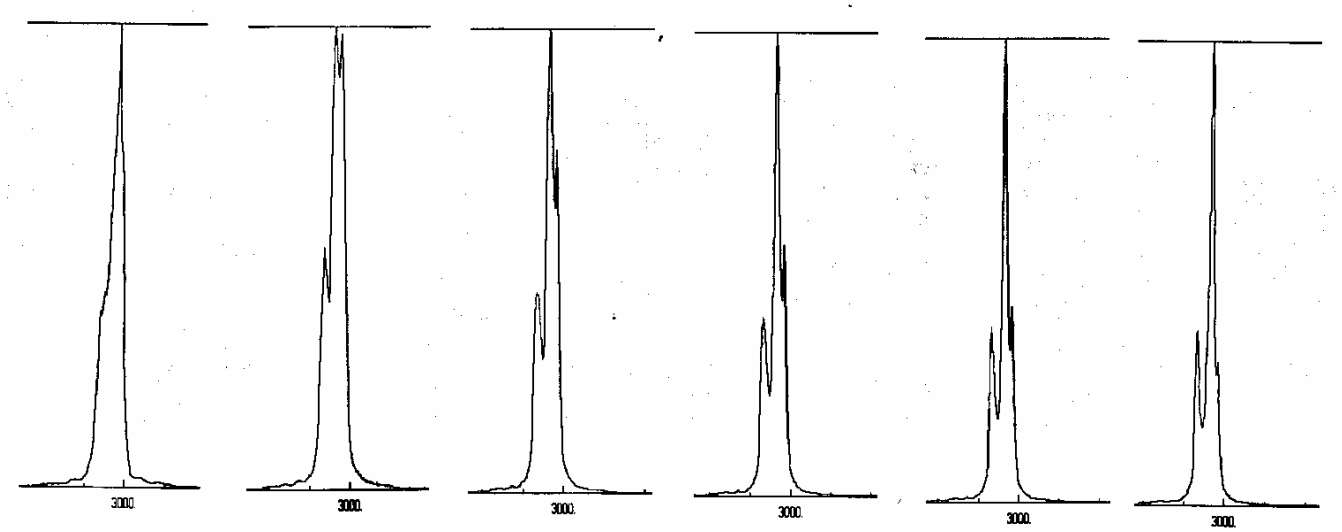

C_4H_{10} **C_6H_{14}** **C_8H_{18}** **$C_{10}H_{22}$** **$C_{12}H_{26}$** **$C_{16}H_{34}$**

Figure 11: Qualitative vapor phase infrared spectra of straight chain hydrocarbons from a NIST website (http://webbook.nist.gov).

Table 4 lists the boiling point temperatures for C_1 through C_{14} straight chain alkanes. Since the PermaPure dryer at the MTSU test did not have an external heat source, it is likely that a significant fraction of the higher boiling point compounds condensed in the dryer. This may account for the ~50% concentration loss in the FIDs (wet to dry) and the intensity reduction in the MGA spectra of Figure 5 (wet to dry).

Table 4. "Straight Chain" Alkanes

Name	**C_xH_y**	**M.p., °C**	**B.p.,°C**
Methane	C_1H_4	-183	-162
Ethane	C_2H_6	-172	-88.5
Propane	C_3H_8	-187	-42
n-Butane	C_4H_{10}	-138	0
n-Pentane	C_5H_{12}	-130	36
n-Hexane	C_6H_{14}	-95	69
n-Heptane	C_7H_{16}	-90.5	98
n-Octane	C_8H_{18}	-57	126
n-Nonane	C_9H_{20}	-54	151
n-Decane	$C_{10}H_{22}$	-30	174
n-Undecane	$C_{11}H_{24}$	-26	196
n-Dodecane	$C_{12}H_{26}$	-10	216
n-Tridecane	$C_{13}H_{28}$	-6	234
n-Tetradecane	$C_{14}H_{30}$	5.5	252

AFR had confidence in the MGA for quantification of key C_1 and C_2 hydrocarbons, but for larger hydrocarbons the reference library provided by MKS was either of high uncertainty or non-existent. Improved closure with FID data should be a result when the library is more

extensive and with lower measurement uncertainty. Work in this effort would expand the hydrocarbon reference library.

AEDC had available two compressed certified gas mixtures of hydrocarbon species, as shown in Table 5:

Table 5: Manufacturer gas species concentrations reported for hydrocarbons in the two calibration mixtures used to evaluate the MGA.

Mixture #1		Mixture #2	
Acetylene	97.6 ppm	Butane	102.0 ppm
Methane	100.0 ppm	Ethane	100.0 ppm
Ethylene	98.6 ppm	Hexane	102.0 ppm
Propane	100.0 ppm	Methane	100.0 ppm
Propylene	100.0 ppm	Pentane	100.0 ppm
Toluene	100.0 ppm	Propane	100.0 ppm
Total	**596.2 ppm**	**Total**	**604.0 ppm**

AFR used these mixtures as calibration checks to ensure that the instrument was working properly, as well as to observe the capability of the MGA to distinguish between several overlapping hydrocarbon species. Figures 12 and 13 show spectral data, between 2650 and 3490 cm^{-1}, which illustrates the overlap of each gas species found within these particular mixtures. Please note that the colored spectra represent the MGA calibration gases and only show the spectral regions that the MGA uses for quantifying those particular gases.

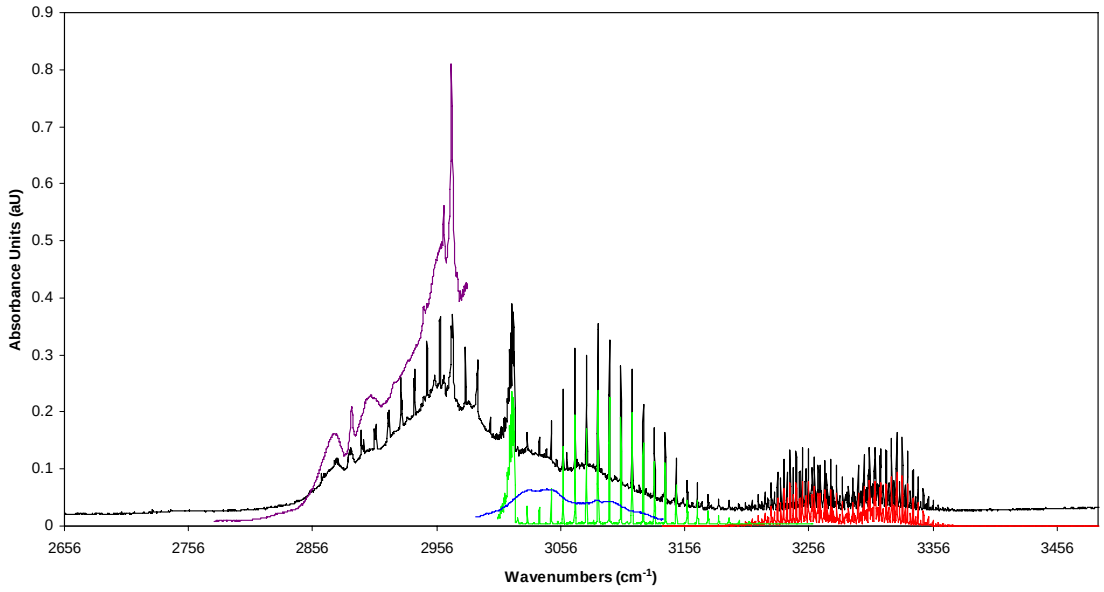

Figure 12: Absorbance spectrum for mixture 1 (black), indicating the quantifying regions for acetylene (red), methane (green), propane (purple), and toluene (blue). Ethylene and Propylene are not shown because these gases are quantified using absorbance bands located around 1100 cm^{-1}, but do absorb within the above region.

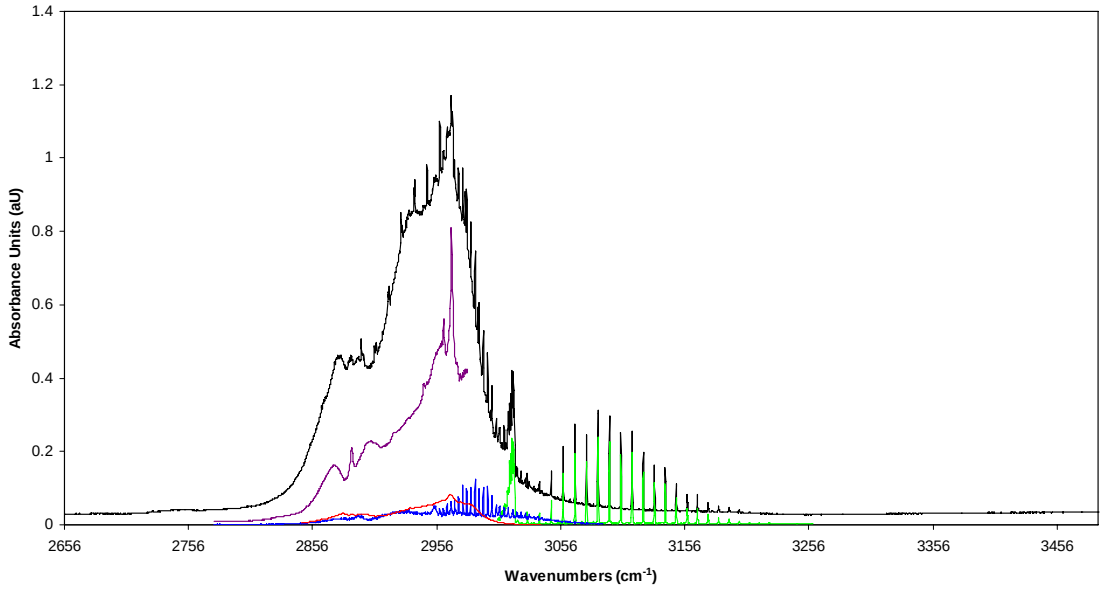

Figure 13: Absorbance spectrum for mixture 2 (black), indicating the quantifying regions for butane (red), ethane (blue), methane (green), and propane (purple). Hexane and Pentane are not shown because the MGA does not currently have a calibration routine for these gases, but do absorb within the above region.

Tables 6 and 7 show the average concentration for each mixture that was reported by the MGA. Since the MGA has a calibration routine for all of the species found in mixture 1, the MGA showed excellent results in distinguishing all of the species and calculating the concentration of each gas within 2% of the bottle. The total hydrocarbon concentration was determined to be 594.76 ppm, greater than 99% of the total concentration specified by the manufacturer in mixture 1. Because the MGA does not currently have calibration routines for hexane and pentane the accuracy of each gas found in mixture 2 is not relevant information from an accuracy point of view, but does show that the MGA is closing in on this mixture and the calibrations for hexane and pentane are needed. Since the MGA can not currently distinguish between these two species and the other species present, their spectral contributions affect the calculated concentration of butane (~230 ppm) and propane (~116 ppm). Yet the total hydrocarbon concentration was determined to be 548.15 ppm, approximately 91% of the total concentration specified in the bottle.

Table 6: Comparison of MGA reported concentration to Manufacturer bottle concentration for mixture #1.

Mixture #1			
	Bottle Concen.	**MGA Concen.**	**% Difference**
Acetylene	97.6 ppm	96.88 ppm	-0.74%
Methane	100.0 ppm	99.31 ppm	-0.69%
Ethylene	98.6 ppm	97.06 ppm	-1.56%
Propane	100.0 ppm	101.6 ppm	+1.60%
Propylene	100.0 ppm	100.3 ppm	+0.30%
Toluene	100.0 ppm	99.61 ppm	-0.39%
Total	**596.2 ppm**	**594.76 ppm**	**-0.24%**

Table 7: Comparison of MGA reported concentration to Manufacturer bottle concentration for mixture #2.

Mixture #2			
	Bottle Concen.	**MGA Concen.**	**% Difference**
Butane	102.0 ppm	233.1 ppm	+128.5%
Ethane	100.0 ppm	98.35 ppm	-1.65%
Hexane	102.0 ppm	N/A	N/A
Methane	100.0 ppm	100.1 ppm	+0.10%
Pentane	100.0 ppm	N/A	N/A
Propane	100.0	116.6 ppm	+16.60%
Total	**604.0 ppm**	**548.15 ppm**	**-9.25%**

The above data and subsequent analysis provided confidence that expansion of the MGA reference library with additional compounds as a function of concentration should improve the MGA-determined total hydrocarbon concentration for exhaust gas emissions from liquid fuel fired engines. Components were identified for purchase to proceed with construction of a pulse-free flow station for quantitative liquid hydrocarbon vaporization into the MGA. The station was assembled. Prior to the final installation of mass flow controllers into the calibration station, a calibration of kerosene was generated using manually controlled rotameters to dilute the kerosene vapor to concentrations of approximately 50, 66, and 79 ppm. (The distribution of hydrocarbons in kerosene based fuels nominally ranges from C5 to C20, with the highest percentages of hydrocarbons in the C11 to C13 range.) Also, several calibrations were generated for 1,3-butadiene, benzene, naphthalene, and acrolein by downloading the absorbance spectra for these species from the EPA Fourier Transform Infrared (FTIR) Reference Spectra website (http://www.epa.gov/ttn/emc/ftir/refsym.html) and converted into LabView spectra.

The kerosene calibration along with the other species were added to the standard calibration library and previously collected JT12 data was reprocessed for hydrocarbon speciation and comparison of the total hydrocarbon concentration (THC) between the MGA and FID. The data reprocessed was for data point #14 comparing the FID inline with MGA-1 (MG-07-126) on 11 June 03. Data point #14 incorporates data collected at several engine power settings ranging from 45% to 75%, which allows for THC comparison at the different power settings. Figure 14 compares the FID total hydrocarbon data to the original MGA total hydrocarbon data (which calculated ppmC using only acetylene, butane, ethylene, methane, and propylene), and the reprocessed MGA total hydrocarbon data (ppmC calculated using 1,3-butadiene, acetylene, butane, ethane, ethylene, kerosene, methane, and propylene). Note that kerosene is a blend of hydrocarbons chains ranging from C5 up to C20 with the highest percentage being C12. Therefore calculating the total hydrocarbon concentration the ppmC contribution of kerosene was determined by multiplying the MGA concentration by 12. A more accurate calculation could be obtained by doing an integration of the MGA concentration between C5 and C20.

Figure 14 shows the total hydrocarbon comparison between the FID (Blue), MGA original (yellow), and the MGA reprocessed (red). The initial analysis of the reprocessed data shows a 40% increase in the total hydrocarbon concentration compared to the FID at 45% engine power when adding in 1,3-butadiene, ethane and kerosene to the total hydrocarbon concentration that the MGA reports. At the high engine power settings the total hydrocarbon concentration

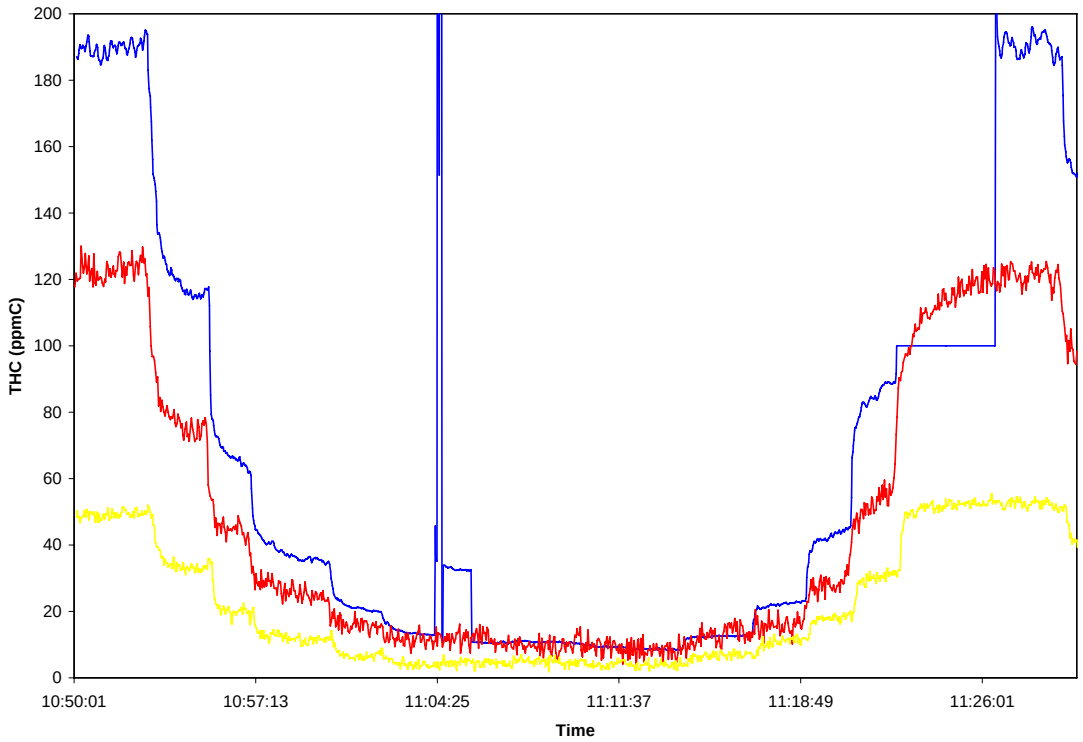

Figure 14: Total hydrocarbon comparison of the FID (blue), the original MGA (yellow) and the reprocessed MGA (red).

reported by the FID and the reprocessed MGA appear to agree relatively well. This makes sense in that at high power settings the hydrocarbons present tend to be the lower chain hydrocarbons (ethane, methane, ethylene, etc.) which the MGA can measure. Whereas, at the lower power settings the higher chain hydrocarbons are present but the MGA can not measure these species because of the lack of calibration files. Further analysis of this data and improved hydrocarbon calibration files will increase the ability of the MGA to report total hydrocarbon concentration comparable to what the FID reports.

Table 8 presents the concentrations measured for the speciated hydrocarbons at engine power settings of 45%, 65% and 75%. Note that formaldehyde, acetone, and the two alcohols (IPA and methanol) were not included in the MGA data for total hydrocarbons in Figure 14.

Table 8. Identifies the different C-H containing gas species determined by the MGA at three different power settings for the JT-12 engine located at MTSU (average concentration in ppm).

Gases (ppm)	45% Engine Power	65% Engine Power	75% Engine Power
1,3 Butadiene	0.904	0.322	0.164
Acetylene	3.11	0.863	0.218
Acetone	0.755	0.568	0.554
Butane	1.96	0.418	<0.100
Ethane	1.08	0.264	0.144

Ethylene	12.05	2.02	0.765
Formaldehyde	12.60	2.49	0.521
IPA	2.16	0.482	0.751
Kerosene (fuel)	5.76	0.718	0.523
Methane	4.44	2.10	1.55
Methanol	2.38	0.775	0.614
Propylene	3.55	0.223	0.130

Table 9 was generated as a guide to expanding the MG2030 reference library for the combustion exhaust application. Compounds in the two columns at the left were originally available in the

Table 9: Reference Species for MG2030 Library (may be expanded)

Currently Available and Validated	Currently Available†	New from AFR	Future Species
Acetaldehyde✓	Butane	1,3 butadiene††✓	1-butene
Acetone	Cyclohexane	Benzene††✓	1-butyne
Acetylene	Ethyl-benzene✓	Kerosene (K1 Clear) ††	1-heptene
Ammonia	n-butanol	m-xylene††✓	1-hexene
CH4 %	n-propanol	Naphthalene†✓†	1-octene
CH4 ppm	o-xylene✓	p-xylene††✓	1-pentene
CO %	Propane	Toluene††✓	1-pentyne
CO ppm	SO3	Ethylene Glycol††✓	2-hexene
CO2 %		Oxygen *	Acrolein✓
Ethane		Hydrogen **	Cumene✓
Ethylene			Decane
Formaldehyde✓			Diesel Blends
Formic Acid			Ethanol
H2O %			Gasoline Blends
H2SO4			Glyoxal
Isopropyl-alcohol			Heptane
Methanol✓			Hexane✓
N2O			Isopentane
NO			Isobutane
NO2			Isoprene
Ozone			Jet-A
Propylene			Jet-A1
SO2			Jet-B
			JP-4
			JP-5
			JP-8
			MTBE✓
			Nonane
			Octane
			Phenol✓
			Propyl-benzene
			Propyne
			Styrene✓

Notes:

† To be verified or updated for 150°C sample temperature

†† To be updated over a multi-point concentration range

* Non FT-IR

**Non FT-IR, Experimental

✓ Hazardous Air Pollutants (HAPs)

MKS reference library, but it is indicated that several need to be verified or updated for the 150°C sample temperature used during combustion exhaust gas measurements. The compounds in the column second from the right were added by AFR during this project, but would be updated once the project's calibration station is in service. The compounds in the far right column are also to be added. This table also indicates compounds that are on the Federal list of Hazardous Air Pollutants (HAPs).

Calibration measurements were initiated to increase the hydrocarbon species reference library. Calibrations for hydrocarbons between C4-C9 would be collected from a combination of gas calibration bottles and liquid samples. Listed below (Table 10) are the targeted C4-C9 hydrocarbons. Also, the MGA calibration library will be expanded for measuring unburned fuel concentration. The fuel concentration will be integrated over C10-C18 to determine a more accurate THC concentration of ppmC. Since hydrocarbon species are broad band absorbers over a certain number of carbons the MGA is limited in distinguishing between the extremely small concentrations of the individual species between C10-C18. Listed in Table 10 are the targeted fuel blends to be calibrated using the liquid calibration system.

Table 10: The targeted hydrocarbon species to generate MGA calibrations. Each species is identified as either a gas mixture calibration or a liquid calibration.

C4-C9 Hydrocarbon Species	Fuel Blends
Butane (gas) 1-Butene (gas) 1,3-Butadiene (gas) Ethane (gas) Propane (gas) Hexane (liquid) 1-Hexene (liquid) Heptane (liquid) Cumene (liquid) o-Xylene (liquid) p-Xylene (liquid) m-Xylene (liquid) Ethyl Benzene (liquid) Benzene (liquid) Toluene (liquid)	Kerosene (liquid) Jet-A (liquid) Jet-A1 (liquid) JP-4 (liquid) JP-5 (liquid) JP-8 (liquid) Diesel Blends (liquid) Gasoline Blends (liquid)

AFR received an FID sensor system from ATA, to set up and quantify the suspected partial response of the FID to aldehydes, ketones, and alcohols. This effort will benefit the closure of measurements between the MGA and FID.

The benzene derivatives were measured using the liquid injection pump and calibrations were generated for the following compounds: benzene, toluene, m-xylene, o-xylene, p-xylene, and cumene. The infrared signature of the benzene derivatives contains subtle differences, which

potentially makes distinguishing these species possible in combustion data. Yet, these derivatives are all broadband absorbers and therefore are sensitive to increases and decreases in the baseline noise, especially at very low concentrations. Figure 15 shows the corresponding calibration region for several of the benzene derivatives and kerosene. The sample spectrum (white) was generated by adding the individual species together along with water and CO_2 to illustrate the overlapping dependency the benzene derivatives have with each species.

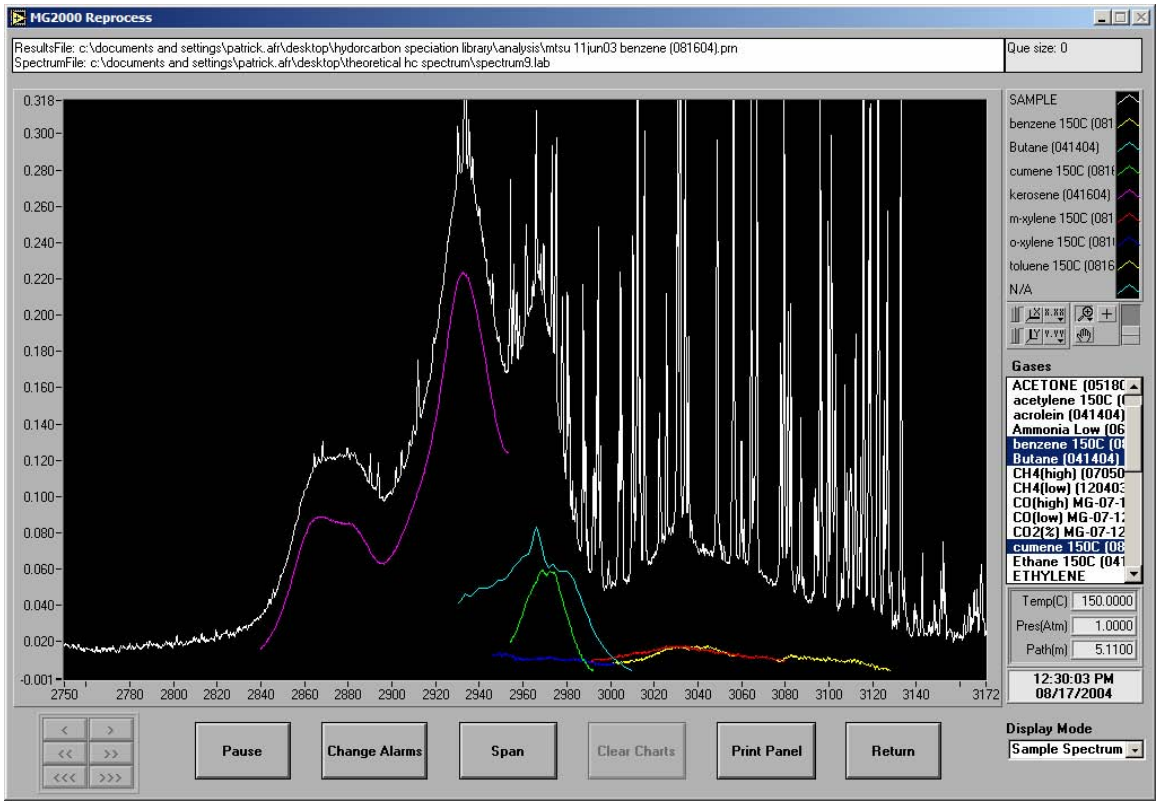

Figure 15: Sample spectrum (white) generated for the individual gas species: H_2O, CO_2, kerosene (purple), butane (light blue), cumene (green), o-xylene (dark blue), m-xylene (red), p-xylene (not shown), toluene (yellow), and benzene (yellow), which illustrates the overlapping dependency each benzene derivative has with the other gas species in this infrared region.

The final results of this investigation pertaining to hydrocarbon speciation are described in **Appendix G**, which presents our manuscript entitled "Advances in Quantifying Total Hydrocarbons and Individual Species during the Rapid, Continuous-Sweep Method of Measuring Turbine Engine Exhaust."

Commercial power generation gas turbine applications: Solar Turbines had interest towards integrating an emissions analyzer to their stationary turbine engines for monitoring and control of the combustion process, with an emphasis on being able to measure total NO_x under 1 ppm. Two MGA 2030s were purchased on the contract (with 54% cost-share provided by MKS Instruments) and lent out to Solar for a one year shake down demonstration. During the demonstration one MGA (unit 1) was installed at the University of California at San Diego for a long term durability test, while the other MGA (unit 2) was designed as a mobile unit for

laboratory and field testing (when needed). AFR has been analyzing data generated by the two MG 2030 systems that were installed at Solar Turbines. A portion of the data was provided to the MKS On-Line Products Group for inclusion to their most recent formal presentation at Solar Turbines in San Diego on 7 November 2003. The "conclusions" page from the MKS presentation is as follows:

- MKS supplied two MultiGas 2030 Systems that continuously operated in the field with no operational or calibration issues.
- Solar Turbines supplied MKS with a list of 13 items they wished for in an ideal analyzer
- MKS has demonstrated that it can meet or exceed the requirements and current CEM analyzers in all categories
- MKS 2030 analyzer
  - New electronics showed less than 1% standard deviations for NO_x
  - Old electronics showed less than 2% standard deviation for NO_x
  - Both systems had larger random error than CEMs
  - However mean concentrations were within specifications demonstrated by cal gas
- Standard NOx analyzers showed significantly higher systematic error
  - Both traditional systems compared to showed baseline drift
  - One traditional system may have showed loss of NO_x conversion

A document presenting AFR's analysis is attached in **Appendix H.**

As indicated above, one of the MGA units had undergone an upgrade to its data collection electronics. MKS had designed the new electronics and had tested preliminary versions in advance of this Air Force project. **Successful implementation of the final version is important with respect to improved performance of future MGA units that may be procured by the Air Force.** Since the installation of the upgraded instrument at Solar Turbines, the measurement stability of the instrument has been shown to be improved. Figure 16 compares the stability of the MGA before (red) and after (blue) MKS upgraded the instrument. The data was collected at 0.5 cm^{-1} resolution, and co-added over 128 scans (approximately 70 second time intervals) measuring a bottle concentration of 20.1 ppm ± 0.4 ppm of nitrogen oxide (NO). The stability after the instrument upgrade has improved by a factor of 3.5 times that of the stability before the instrument upgrade (the standard deviation for before and after the instrument upgrade has been calculated to be 0.329 and 0.094 σ, respectively). A reproducibility test was also conducted on the instrument after being upgraded to evaluate how long the instrument can measure accurately before a new background must be collected. Figure 17 shows several days where the instrument measured the 20.1 ppm bottle of NO without collecting a new background before each sample. Once the instrument stabilized, the reported concentration for each day averages to be 19.83 ppm (σ = 0.10), within the specification for the bottle concentration.

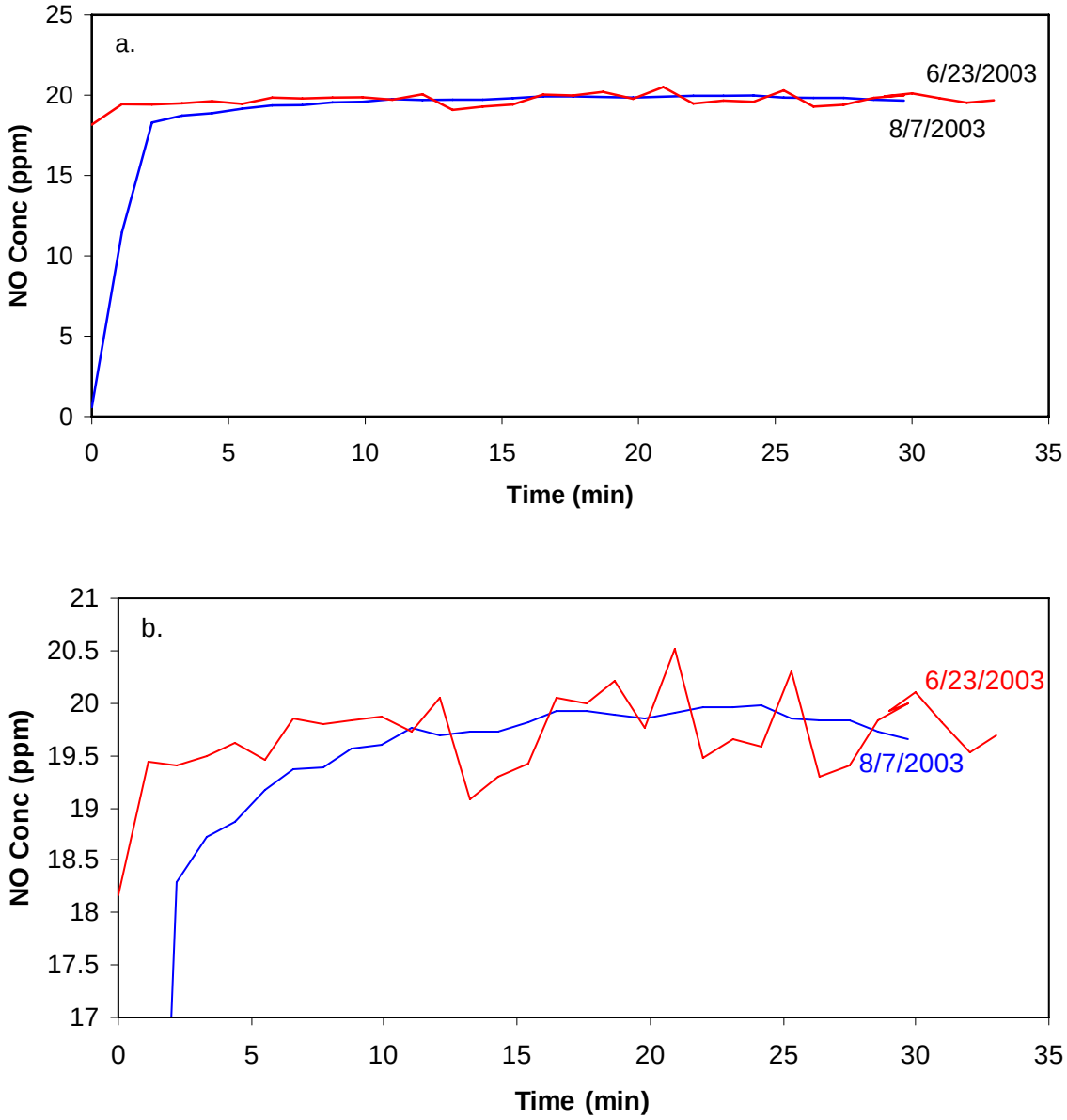

Figure 16: Comparison of total NO concentration before (red) and after (blue) instrument upgrade. The 17 to 21 ppm region of (a) is expanded in (b).

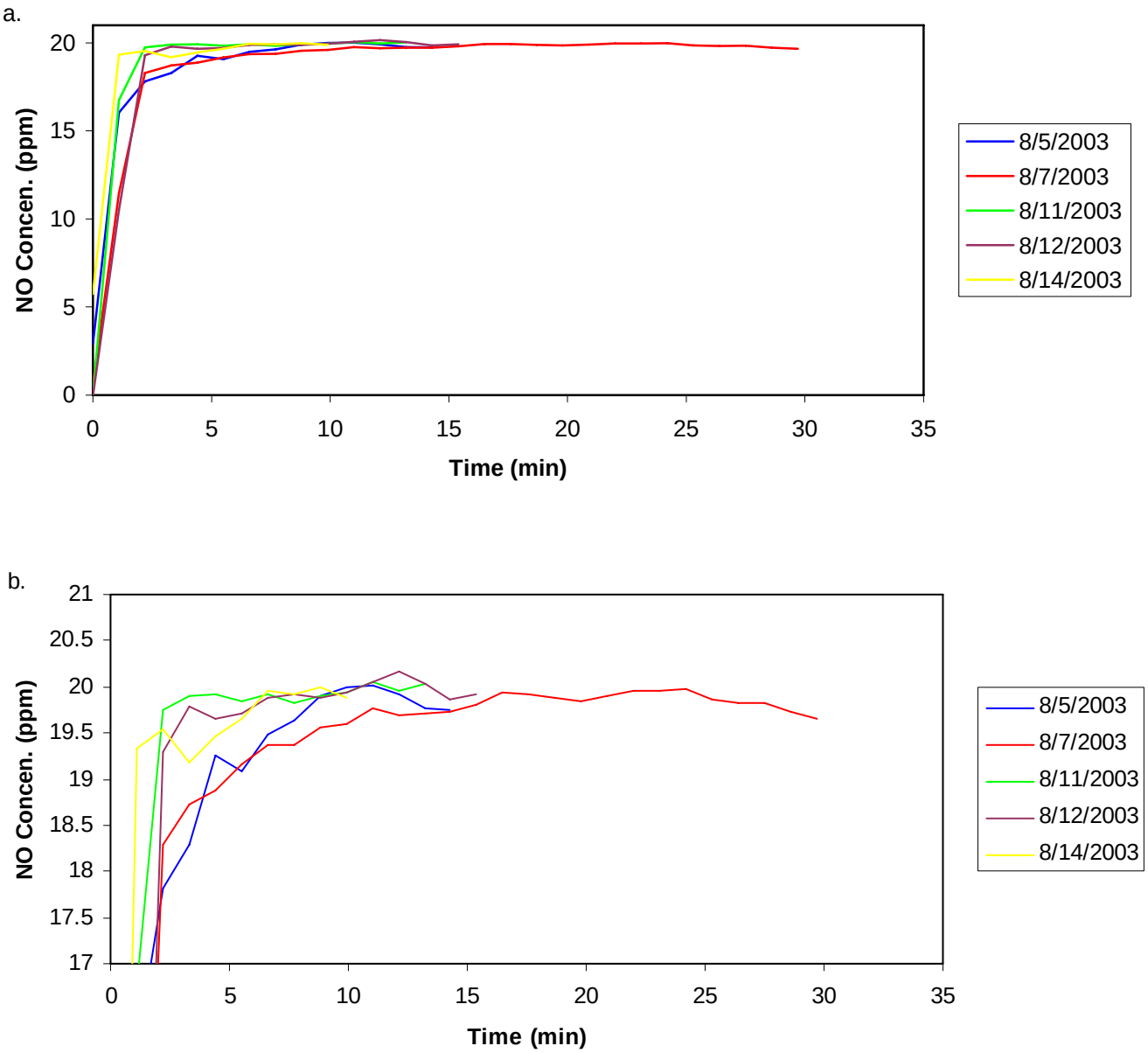

Figure 17: Comparison of NO concentration for several days after instrument upgrade without taking a new background. The 17 to 21 ppm region of (a) is expanded in (b).

As a result of the demonstration work of this project (see **Appendix H**), Solar Turbines ordered an MGA 2030 from MKS for their permanent use and continued evaluation. This project, therefore, did not convince Solar Turbines that the MGA 2030 could provide the 24/7/365 performance originally proposed/desired. Solar was impressed with the system performance once the new MKS electronics in place, but had reservations in reliability. As solar expressed to the PI, they were not expecting to be subjected to the "growing pains" of the new electronics. The unit was reworked by MKS several times (at Solar and at MKS). However, this project peaked Solar's interest enough to result in their direct-purchase of a new MGA 2030. Solar Turbines

also requested a cost-quotation from AFR for integration of the solid oxide sensor into their new MGA, which they accepted. AFR completed the oxygen sensor installation and shipped the completed system to Solar before the end of June. An MKS representative was on-site at Solar on 29-30 July 2004 to provide installation and training. Solar then shipped to AFR the mobile unit on loan to them from this project, which was received by AFR on 8 September 2004. On 13 September, AFR was informed by Solar that their direct-purchased MGA 2030 was shipped back to MKS for repair due to another problem with its electronics. Solar has been pleased with the oxygen sensor performance.

Solar Turbines had previously shipped back to AFR the MGA that was installed at the UCSD power generating station. Significant damage to the MGA has occurred. It appears that, for a long time period, combustion exhaust gas was flowed through the MGA with the sample lines and sample cell at ambient temperature instead of the required 150 °C. Water condensation occurred to the extent that the sample cell filled with liquid water to the level of the infrared transparent salt-windows (KBr), which then dissolved to result in the corrosive brine spilling into the adjacent chamber holding the detector, detector electronics, and optical components (first-surface mirrors, adjusters, and supports). Based on AFR photographs of the damage and description, MKS estimated a repair cost of $26,600 in replacement parts plus $6,000 in labor for a total of $32,600. This is 54.3% of the retail price for a new unit. It is noted that this unit was purchased new under the contract for about $30,000 since MKS provided significant cost-share to this part of the program.

AFR held off on implementing repair as alternatives were considered. Alternatives included: 1) only buying the replacement parts from MKS and having AFR investigators perform the installation, performance testing, and re-calibrations of the unit; 2) postpone the repair until if and when FY05 funding to the project is available, at which time the system electronics would also be upgraded; or 3) do not repair the unit. AFR does not feel that Solar Turbines should be held responsible for repairs since it was an evaluation system supplied to them for which they contributed much in-kind labor and hardware support. The unit has to-date been treated as a consumable of the project.

Conclusion for this Task in Regard to Goals Targeted:

AFR achieved two out of the three goals of this task:

- The MG 2030 was demonstrated as acceptable emission measurements during engine development and certification testing. This allowed the generation of the SAE Aerospace Information Report (AIR) 5917 that was submitted by ATA/AEDC to the SAE Committee E-31 at the Committee's annual meeting held 8 June 2004. The AIR is to be placed on the Committee's ballot, and if accepted by member vote could then be developed into an Aerospace Recommended Practice (ARP).

- Five MG 2030 turbine installation points were identified within AEDC (see Table 2 for summary).

- Solar Turbines Inc. was not convinced that the MG 2030 was ready for continuous 24/7/365 monitoring and control of stationary power generating turbine engines, but

significant impression resulted in Solar purchasing an MG 2030 directly from MKS for continued evaluation (see Task 5). Solar Turbines also purchased (from AFR) an integrated solid oxide oxygen sensor for their new MG 2030.

Task 3 – Development of Related Aeropropulsion Applications (AFR Responsibility)

Goals Targeted for this Task:

- Demonstrate other applications at AEDC, such as ambient air monitoring, cabin air monitoring, other propulsion systems
- Establish list of target HAPs at AEDC
- Improve HAP speciation and detection limits

Significant Results: On-site measurements were performed for two related aeropropulsion applications: 1) test cell air monitoring during engine icing tests at AEDC; and 2) test cell gas exchange monitoring in AEDC Tunnel 9 at White Oak, Maryland. Both applications and measurement results were included in the January 2004 article published in Applied Spectroscopy **[3]**, but the discussion and data presentation as originally submitted were significantly shortened on the advice of the peer reviewers and editor, in order to shorten the overall length of the article. Key data from both applications are presented below.

In addition Table 11 presents a brief descriptive listing of several applications identified and performed at AEDC facilities by AEDC personnel.

Test cell air monitoring during engine icing tests: Under existing Federal Aviation Administration (FAA) and Joint Aviation Authority (JAA) certification regulations, an airplane must demonstrate the ability to operate safely in a wide range of icing conditions. The icing system at AEDC was designed to provide the complete range of atmospheric icing conditions occurring in nature, with the system capable of providing simulated-altitude icing testing of large turbine engines, inlets, windshields, wings and other test articles. Airflows to 1,600 lbm/sec and higher can be obtained for icing testing in test cells depending on temperature and pressure.

However, ice inhibitors such as ethylene glycol (1,2 – ethanediol) are used upstream of the engine in the test cell in heat-exchange systems and to de-ice surfaces such as air louvers. Carryover in the air stream originating from upstream leaks or surface residue will have a negative impact on the desired ice accretion on aircraft and engine surfaces. The FT-IR unit was used for its ability to monitor trace quantities of ethylene glycol vapor in the air flow that may be originating from upstream sources. The FT-IR unit was set to collect data at 0.5 cm^{-1} spectral resolution (2 scans per second) and report signal-averaged data for every 30 seconds. From the concentration reference data generated prior to these tests, a low detection limit of about 1 ppm was determined for this number of signal-averaged scans. Only data from the second of two icing test monitored during the project indicated a positive identification of glycol in the air stream. Figure 18 shows a sample absorbance spectrum overlapped with the ethylene glycol spectrum indicating a positive identification of ethylene glycol being present within the sample stream. During particular test runs the ethylene glycol concentration cycled between 0-25 ppm along

Table 11. MGA Applications at AEDC*

Application	Location	Requirement	Task	Impact
Landfill Gas Monitoring	AEDC	Monitoring for hazardous substances.	Determine the composition of gases escaping from the AEDC landfill.	AEDC was able to confirm compliance with State and Local landfill management regulations.
Test Area CO Contamination	G Range Gun Room	Monitoring for hazardous substances.	Locate the source of high CO levels in G Range following a light gas gun shot.	The source of the high CO levels was found to be a leaking gun seal which was repaired.
Test Area HCN Contamination	Tunnel 9 White Oak, MD	Monitoring for hazardous substances.	Determine whether any HCN is produced during blow down of Tunnel 9.	No HCN or other harmful compounds were detected.
Work Area Contamination	AEDC Clean Shop	Monitoring for hazardous substances.	Determine whether the processes in the AEDC Clean Shop produce locally high levels of HAP's.	No harmful compounds were detected.
Evaluate/Confirm Operation of other Analyzers	AEDC Mobile Emissions Lab	Serve as a transfer standard during check-out of other instrumentation.	Confirm that the alarm limits on hand-held CO / LEL meters are correct.	The alarms on hand-held CO /LEL meters is routinely confirmed within the Emissions Lab avoiding the need for costly outside calibrations.
Evaluate/Confirm Operation of Other Analyzers	AEDC Mobile Emissions Lab	Serve as a transfer standard during check-out of other instrumentation	Determine the performance characteristics of new NO_X MEMS chemical gas sensors.	A MEMS chemical gas sensor test bench has been assembled for characterization of various new MEMS gas sensing configurations.
Air Contamination Monitor	APTU VAH Stilling Chamber	Ramjet / scramjet test facility inlet air contamination	Measure the unburned hydrocarbons, CO and NO in the stilling chamber before expansion in the supersonic nozzle.	Contamination of the inlet air from the VAH in APTU was measured to be less than 70 BTU/lbm or less than 0.4% for a JP-10 fueled engine.
Clean Air Quality	F119 in ASTF C-1	Reduce the cost of performing a cabin air quality certification test.	Provide measurements of the major species and some trace air contamination species per ARP 4418.	A single MGA has been used to provide rapid on-line measurements of the gas species and avoided hours of simulated altitude test time.
Fuel and Additive Evaluation	MTSU (JT-12)	Evaluate the effectiveness of fuel additives in reducing emissions.	Provide rapid, on-line measurements of the gas species for analysis of CO, HC, and NO_x emission indices.	The CO, NO, and speciated hydrocarbon measurement resolution of the MGA provided conclusive results concerning the effectiveness of the fuel additives.

Application	Location	Requirement	Task	Impact
I/C Aircraft Engine Emissions	MTSU Continental 0470 fired with 100 octane low lead AVGAS	Determine the environmental impact internal combustion aircraft engine operation.	Provide rapid, on-line measurements of the gas species for analysis of percent – level CO, HC, and NO_x emission indices.	The impact of providing this measurement is unknown at this time.

* Credit is given to Paul Jalbert (ATA/AEDC) as the original author of the information in this table.

with the presence of water vapor. Figure 19 shows this cycling phenomenon of water and ethylene glycol throughout this particular test run. This pattern and relationship between these two gas species were seen throughout the entire test. Also, trichloroethylene (TCE) was monitored during these test runs; the MGA indicated no presence of TCE within the sample stream. A TCE lower detection limit of 0.232 ppm was estimated.

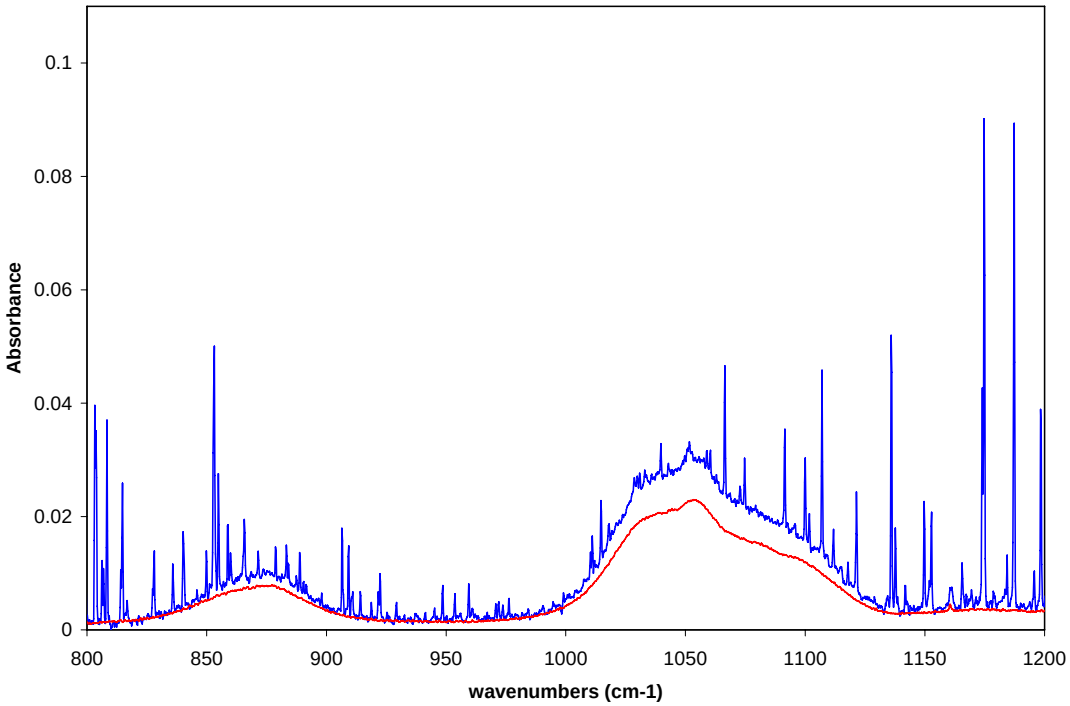

Figure 18: Sample absorbance spectrum (blue) compared to ethylene glycol (red) positively identifying the presence of ethylene glycol within the sample stream.

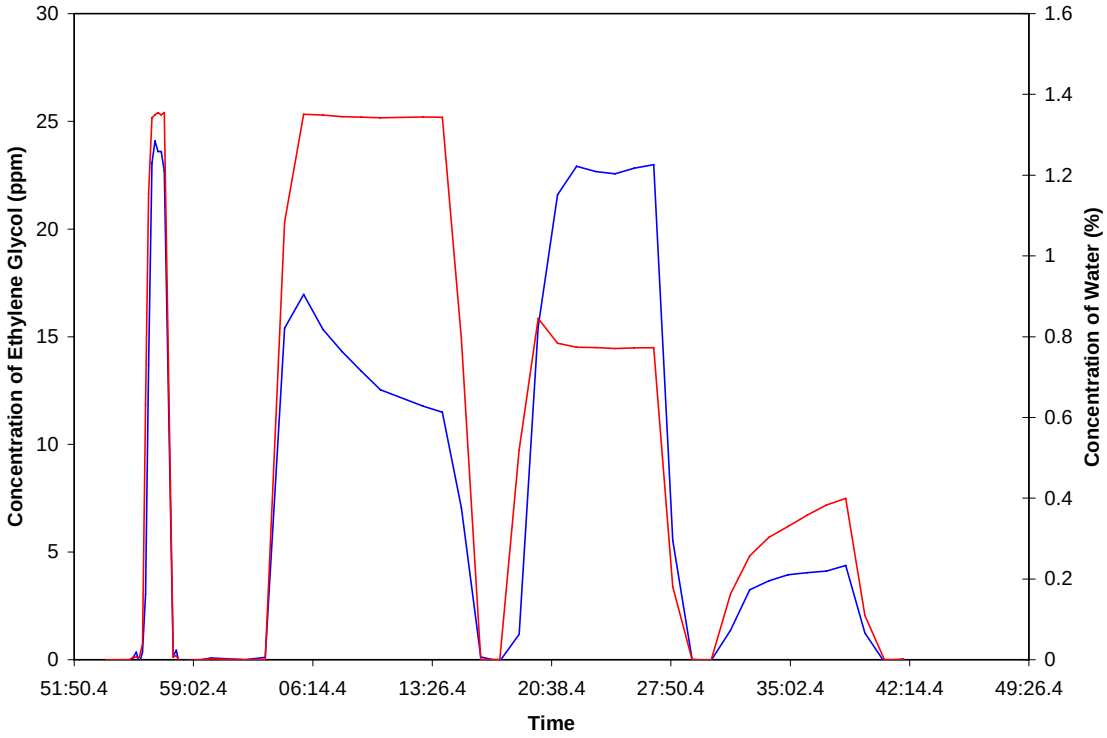

Figure 19: Plot indicating the cycling of ethylene glycol (blue) and water (red) with respect to time.

Test cell gas impurities and exchange monitoring: Hypervelocity wind tunnels are high-Mach-number, high-Reynolds-number facilities which provide aerodynamic simulation in critical altitude regimes for reentry and hypersonic vehicles technologies. The AEDC Tunnel 9 facility is a blow down type with an operational envelope of Mach 7 and above. This facility provides nitrogen gas supply pressures up to 1430 atmospheres and temperatures up to 3460 degrees Rankine (1922 degrees Kelvin) and sustains long-duration, constant-condition runs. Crew safety is a primary concern, and the FT-IR sensor has been used as a survey tool for hydrogen cyanide (HCN), formaldehyde (H_2CO) and other harmful gases. The concern was that toxics could be present in the test cell and vacuum sphere from outgassing of liners, other components in the heating system, from test articles, or from surface reactions with the high temperature nitrogen gas.

HCN, with absorption bands in the spectral regions of 712 cm^{-1} and 3310 cm^{-1}, was not detected. At the signal averaging time used of 5 seconds, a low detection limit of 0.21 ppm was estimated in the fairly dry test cell gas with the 5.11 meter effective-path length cell. Formaldehyde, as shown in Figure 20, was detected with concentrations as high as 3.75 ppm. This is almost twice the fifteen minute Short Term Exposure Limit (STEL) set by the U.S. Occupational Safety & Health Administration. A low detection limit of 0.20 ppm was estimated. Of interest is that on-site measurements at Tunnel 9 that were performed a few months earlier and a few months after the measurements presented here indicated formaldehyde at about 20 ppm and 1 ppm, respectively. The source of the formaldehyde vapor in Tunnel 9 appears to be depleting over time and/or test cell use. In addition, the MGA spectral data showed evidence of longer-chain

hydrocarbons present in the tunnel gas, possibly oil vapor from some source. Figure 21 plots the relative intensity of the longer-chain hydrocarbons measure by setting the highest signal measured to 1. The highest concentration of the hydrocarbons is measured soon after the cell is fired and slowly decreases as the gaseous nitrogen (GN2) purge process forces all of the gases through the test cell and towards the collection sphere. Tunnel 9 operators have expressed interest in continued measurements and monitoring. The work performed to improve the hydrocarbon speciation capability of the MGA (discussed previously) would certainly benefit this Tunnel 9 effort.

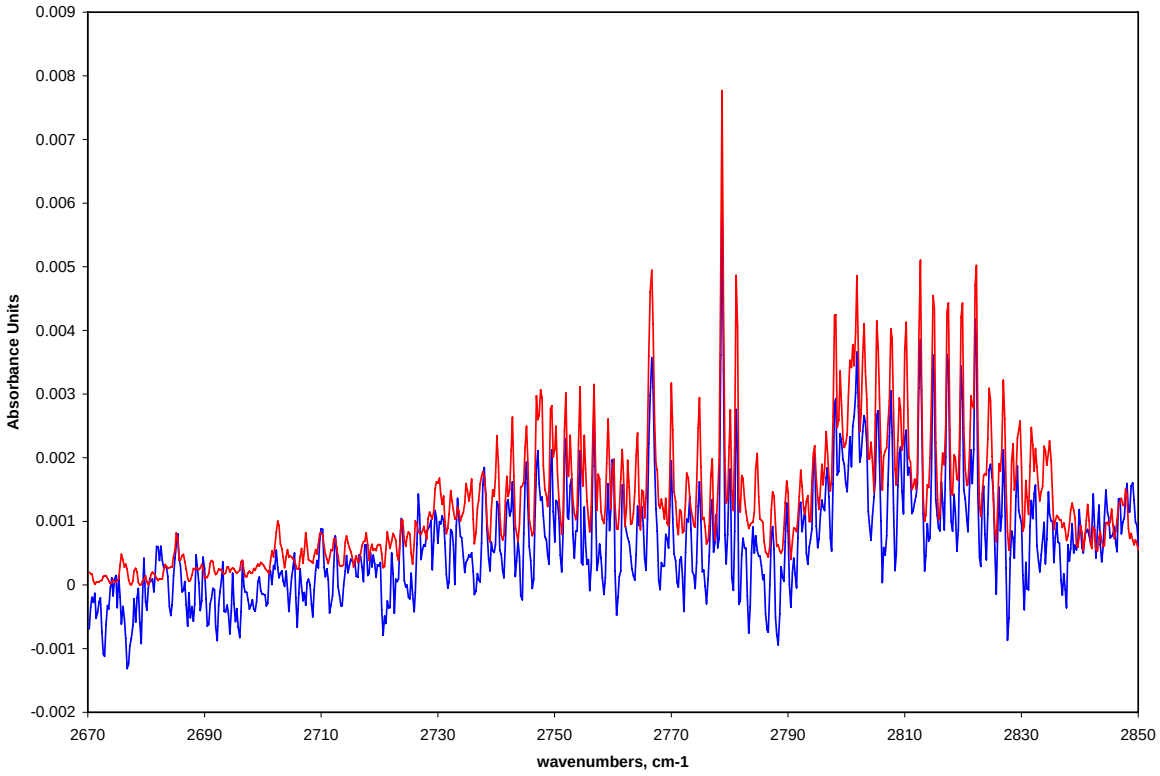

Figure 20: Spectrum of test cell gas (blue) overlaid with a reference spectrum (red) of formaldehyde. The reference spectrum (top, 20 ppm) is scaled down in absorption intensity for convenient overlay with the sample spectrum (bottom, 3.75 ppm).

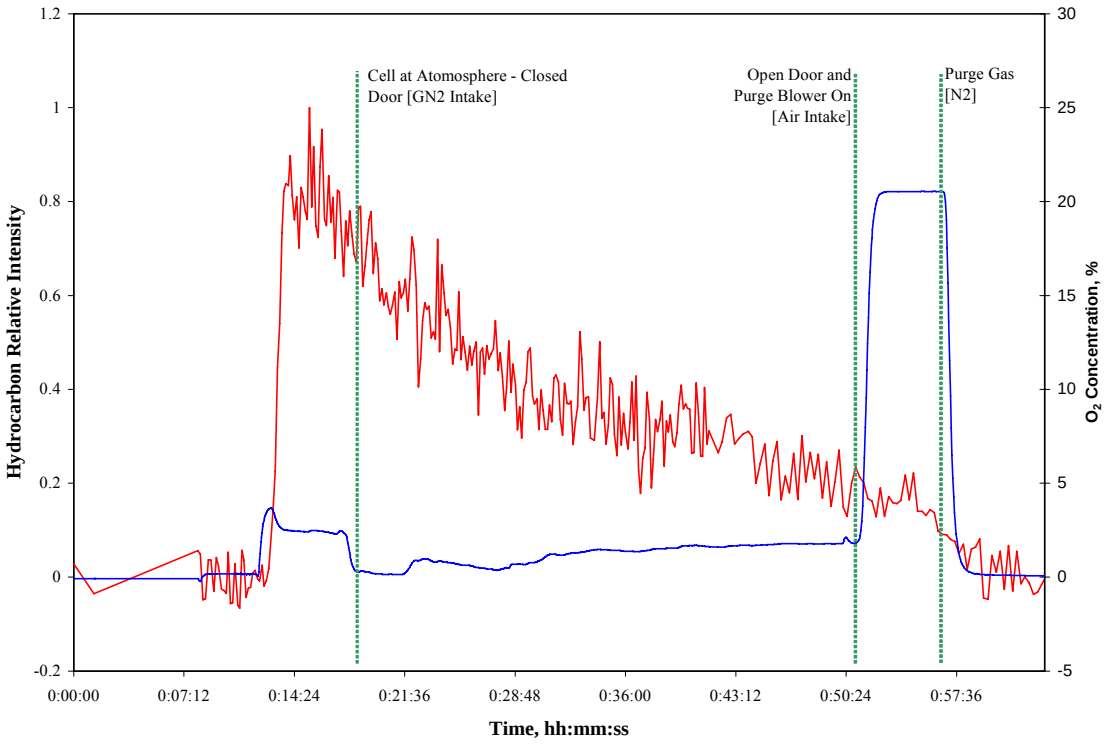

Figure 21: Longer-chain hydrocarbons relative intensity (red) and O_2 concentration (blue) measured in the hypervelocity wind tunnel (21Jul03).

The integrated O_2 sensor proved to be an additional convenience for monitoring the wind tunnel for conditions for safe entry of personnel. Symptoms of oxygen deficiency in humans are well documented to begin at an atmospheric concentration of approximately 16%. The effects become progressively more severe with further reduction in oxygen content. Figure 22 plots O_2 concentration measured over a 1 hour 15 minute time period. Through about the first 55 minutes, the O_2 concentration level is very low during the gaseous nitrogen (GN2) purge process through the cell. When the GN2 purge process is completed, a ventilation door into the cell is opened, and the O_2 level rises to about 15% in the local area of the gas extraction probe in the cell. At this time a purge blower is turned on to force air through the cell. The O_2 level drops back down to about 2% as the plug of GN2 is forced past the extraction probe. The GN2 is then displaced by air as the O_2 level recovers to the ambient air level of 20.9%.

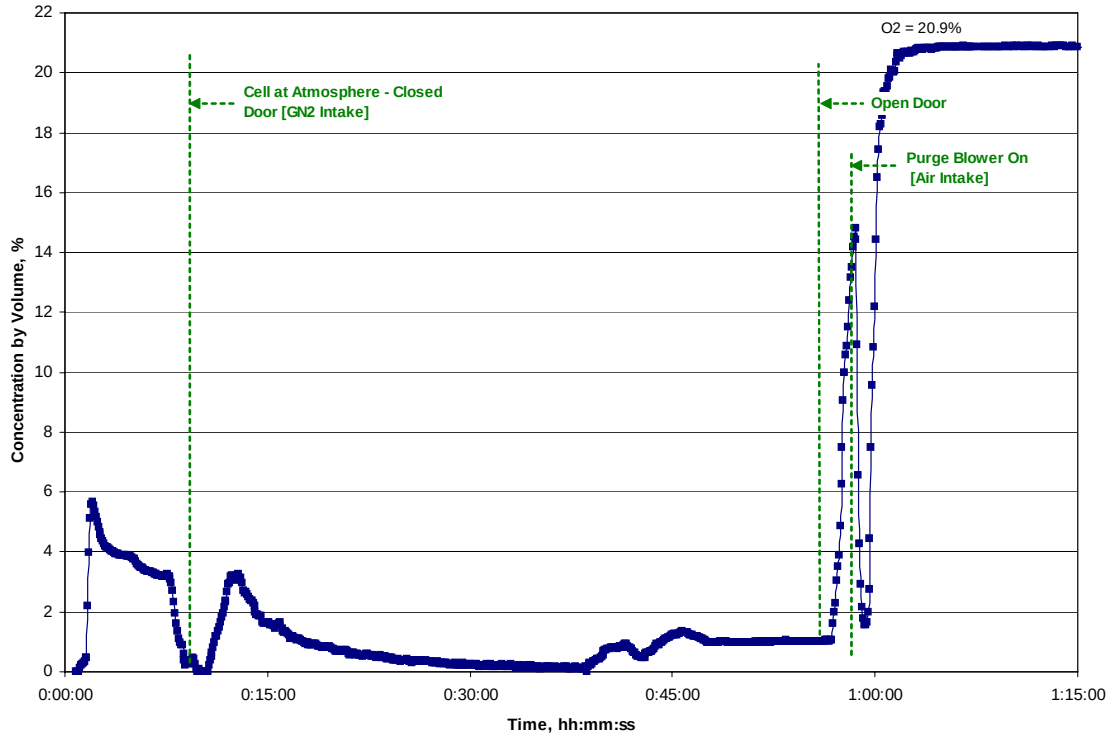

Figure 22: Oxygen concentration measured in the hypervelocity wind tunnel. Note that time 0:00 indicates time of test cell firing.

HAPs at AEDC: As indicated on the AEDC Environmental Compliance web site http://www.arnold.af.mil/aedc/compliance.htm (indicated as last updated 11 June 2003): "AEDC is committed to protecting and improving air quality by insuring all of its operations comply with existing and future state and federal air regulations. All of the research and development operations conducted at AEDC are critical to the nation's defense. AEDC presently has 33 air quality operating permits. These permits allow AEDC to operate research heaters, engine test facilities, steam plants, fuel storage tanks, etc. Because AEDC is a major industrial source, it has applied for a Title V Operating Permit according to the Clean Air Act of 1990. Because most of the research involves engine (rocket and turbine) testing, some of the criteria air pollutants such as nitrogen oxides, sulfur dioxide, carbon monoxide, particulate matter, and ozone are released. AEDC uses engineering control methods to reduce these emissions to the lowest levels possible and well below allowable levels specified by the State of Tennessee and US EPA."

As indicated on the EPA Air Toxics Website Pollutants & Sources http://www.epa.gov/ttn/atw/pollsour.html : "Hazardous air pollutants (HAPs), also known as toxic air pollutants or air toxics, are those pollutants that cause or may cause cancer or other serious health effects, such as reproductive effects or birth defects, or adverse environmental and ecological effects. EPA is required to control 188 hazardous air pollutants."

ATA/AEDC provided AFR with a "report on engine emissions analysis," prepared by Dr. Ngee-Sing Chong from MTSU. Dr. Chong's exhaust sample collections during engine testing at MTSU and subsequent GC-MS analysis provide guidance on larger molecular weight hydrocarbon species to search and analyze for in the MGA infrared spectral data. Dr. Chong's

report to ATA/AEDC is shown in **Appendix I**, and tentatively identifies 17 compounds in the engine exhaust (Jet A and diesel fired). The list is reproduced below in Table 12, and by matching these compounds to the EPA list of 188, HAPs are indicated.

It is emphasized that: 1) Dr. Chong tentatively identifies these compounds; and 2) the measurements were performed from an old, out of production JT-12 engines at the MTSU airfield (approximately 40 miles from AEDC). As discussed above in this task, the HAP formaldehyde was positively identified by MGA analysis at MTSU and at the AEDC Tunnel 9 facility in White Oak, MD. The HAP ethylene glycol was positively identified by MGA analysis during an engine icing test at AEDC.

The above compounds provide an initial set of target HAPs to focus upon with the MGA technology. In addition, publications of other investigators **[6- 9]** provide additional potential compounds from turbine engine exhaust. As the capability to detect and speciate hydrocarbons is improved by: 1) expanding the hydrocarbon reference library (see Task 2); and 2) utilizing the procedural improvements implemented in this project (**Appendix C**) for calibration and reduction of cross-talk for quantitative analysis, the opportunity to identify additional species including HAPs in enhanced.

Table 12: GC-MS Identified Compounds (Tentative) from Engine Exhaust at MTSU (See **Appendix L** for Full Report).

Compound	HAP
1,3-Butadiene	√
Ethanol	
Acetone	
Methylene chloride	√
1-Propanol	
Acetic acid	
Hexane	√
Ethanol, 2-methoxy	
Benzene	√
Toluene	√
Naphthalene	√
1,5-Dimethylnaphthalene	√
Acenaphthylene	√
Fluoren-9-one	
Anthracene	√
Phenanthrene	√
Pyrene	√

Conclusion for this Task in Regard to Goals Targeted:

AFR achieved the three goals of this task:

- AFR demonstrated other applications of the MGA at AEDC including test cell air monitoring during icing tests (see text and Appendix C) , and test cell gas impurities and exchange monitoring (see text and Appendix C). In addition, see Table 10 for a brief descriptive listing of ten other applications identified and performed at AEDC facilities by AEDC personnel.
- This task combined with the effort of Task 2 established a list of target HAPs at AEDC see (Table 8 and 11).
- This task combined with the effort of Task 2 improved the speciation for several HAPs. Detection limits are shown in **Appendix G**.

Task 4 – Advanced Development for Vaate Application (AFR Responsibility)

Goals Targeted for this Task:

- Identify VAATE requirements
- Reduce detection limits with shorter sampling time
- Improve speciation of hydrocarbons and HAPs

Significant Results: AFR and AEDC/ATA representatives have discussed the status of AFRL VAATE requirements several times during this project. Discussion at the 5th quarterly meeting held at Tyndall AFB (25 November 2003) maintained agreement that VAATE requirements have not yet been established by the Air Force. The PI then attended the spring 2004 Propulsion Instrumentation Working Group (PIWG) meeting (13-14 May 2004), at which a session for "VAATE Instrumentation Sensor Needs & Roadmap," was presented by Brian Beachkofski of AFRL. The PI was hopeful that discussion pertaining to VAATE emissions would be included. However, the presentation was focused on future instrumentation needs for engine health management (damage detection) and self-diagnostics (TBC health). Exhaust emissions requirements were not addressed in this presentation.

This task was then discussed at the 7th quarterly meeting held at AEDC. Still the consensus was that emissions requirements for VAATE are not available at current time. The effort of Task 2 is working to reduce instrument detection limits and improve speciation of hydrocarbons and HAPs. Results of Task 2 should provide benefit to future VAATE measurements. It was agreed that the advanced development would be approached again in FY05 funded work, if continued funding is provided in the FY05 DOD appropriations bill.

The effort in this task did achieve improvement to the MG quantitative analysis routine, which benefits this task as well as above tasks with reduction of measurement uncertainty and detection limits. Analysis of the gas species concentrations is performed by the MG 2030 using a classical least squares (CLS) routine that compares the spectra recorded from the exhaust to a standard library of calibrated reference spectra. References are recorded at multiple concentrations in order to account for any non-linearity of the absorbance with concentration. This non-linearity is most pronounced for small molecules with narrow rotational lineshapes, such as CO, and is caused by the 0.5 cm^{-1} resolution of the spectrometer not fully resolving the true lineshape (~0.1 cm^{-1} at 1 atmosphere). These non-linearities, as well as species crosstalk, are minimized by using

analysis software that is designed to automatically select the reference spectrum that is closest to the concentration found in the sample being analyzed.

To further minimize crosstalk, work performed here has modified the MG 2030 software with optimum definition of spectral analysis region for each species to be measured. Described as the "picket fence" component of the analysis, select spectral regions have been carefully chosen that maximize the species signature component in the spectrum while minimizing overlap by other species. Table 13 compares the measurement uncertainty obtained when both CLS and picket fence are combined. A significant improvement is obtained. **Appendix C** provides additional detail on the function and use of the picket fence component with the CLS analysis. As indicated previously, to benefit AEDC users/operators the appendix provides the information in user-manual form.

Table 13: Lower Measurement Uncertainty with Improved Quantitative Analysis Routine. Data for 64 scans at 0.5 cm^{-1} resolution (32 seconds), liquid nitrogen cooled detector.

	Standard Deviation			
Gas Species	**No Least Squares No Picket Fence**	**Least Squares No Picket Fence**	**No Least Squares Picket Fence**	**Least Squares and Picket Fence**
Carbon Monoxide (0-50ppm)	+/- 2.5 - 3.0 ppm	+/- 0.7 - 1.2 ppm	+/- 0.4 - 0.44 ppm	+/- 0.05 - 0.1 ppm
Carbon Dioxide (3.5%)	+/- 4.5%	+/- 0.1-0.2%	+/- 0.2 - 0.22%	+/- 0.02 - 0.03 %
Water (6-10%)	+/- 0.25 - 0.5%	+/- 0.1 - 0.25%	+/- 0.05 - 0.1%	+/- 0.05 - 0.06 %
Nitrogen Monoxide (0-10ppm)	N/A	+/- 5.0 - 6.1ppm	+/- 2.4 - 3.0 ppm	+/- 0.1 - 0.2 ppm
Nitrogen Dioxide (0-10ppm)	N/A	+/- 0.5 - 1.0 ppm	+/- 2.4 - 3.0 ppm	+/- 0.05 - 0.1 ppm
	worst ←			→ best

Conclusion for this Task In Regard to Goals Targeted:

AFR achieved two of the three goals of this task:

- VAATE requirements could not be identified. Discussions with the TPOCs of the project came to the agreement that VAATE requirements for emissions had not been established by the Air Force. The PI also established that the spring 2004 AFRL presentation on VAATE Instrumentation Sensor Needs & Roadmap did not address exhaust emissions sensor or measurement requirements.
- The work performed in this task to improve the quantitative analysis routine resulted in a significant decrease in measurement uncertainty for most species, generally a factor of ten or more for species such as CO, NO and NO_2. Previously in Task 2, the new MKS electronics when retrofitted into one of the project's MGA units was shown to also

decrease the measurement uncertainty, by a factor of 3.5. These improvements result in reduced detection limits and allow for shorter sampling times.

- The improved quantitative analysis routine resultant from this task combined with the effort of Task 2 improved the speciation of hydrocarbons and HAPs, and also improved the capability of the FT-IR method to quantify total hydrocarbons. Detection limits are shown in **Appendix G**, Table 2.

Task 5 – Advanced Development for Performance, Health and Condition Monitoring of Aeropropulsion Systems (AFR Responsibility)

Goals Targeted for this Task:

- Development of performance, health and condition analysis system

Significant Results: This task has investigated the development of an engine health monitoring system. AFR's experience in FT-IR instrumentation and FT-IR gas phase spectral measurements, analysis, and interpretation developed with previous SBIR funding has resulted in a related FT measurement methodology that is currently in the SBIR Phase II research and development stage (AEDC Contract F40600-01-C-0014). If successful, detection of incipient combustion instability may be afforded by non-intrusive measurements in exhaust flows of afterburners, ramjets, scramjets, and advanced turbines engines. Combustion instability can have negative consequences on exhaust emissions and also result in combustor/engine damage. Advanced gas analysis for the emissions profile would benefit by advanced gas analysis for condition of the combustion system (i.e., confirming stability or indicating incipient instability).

The above mentioned contract is limited to the augmentor application, but the collaborative work with Solar Turbines under Task 2 of this project resulted in an opportunity to develop the measurement technique for non-augmented turbine engines and increase the commercial applications of the technology. Solar Turbines expressed significant interest in the project's sensor technology under development and offered to provide private sector support to our technology development and demonstration (i.e., private sector cost-share via test engine operation and labor) at their San Diego engine manufacturing/testing facility. Specifically, Solar Turbines would provide the project with an operating test turbine engine in one of their test cells that includes traditional pressure sensors for combustion-oscillation detection. A test with traditional pressure sensors in place has yet to be available at AEDC, increasing the value of the test offer by Solar Turbines. Also, the test engine that Solar offered to the project can be operated to induce combustion instability at both low and moderately high frequencies. Figure 23 is a digital picture of the test engine facility showing the exhaust exit duct that would be modified for optical access.

Two field tests at Solar Turbines were accomplished, over 26-27 February 2004 and 17-21 May 2004. Optical heads were built following the stand-off design of the Phase II augmentor project, but modified to allow direct mounting to the Solar engine exhaust duct. Pictures are shown in Figure 24.

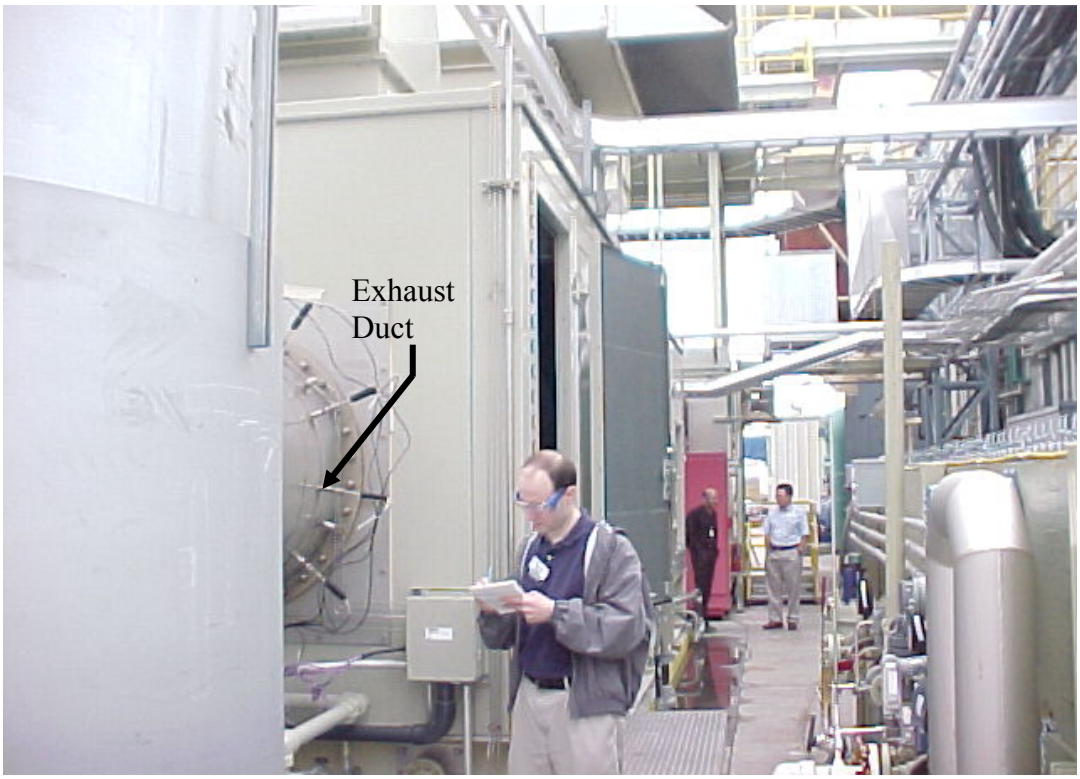

Figure 23: Test engine facility with exhaust duct for optical access labeled.

The tests at Solar provided valuable data in terms of showing the capabilities of the senor method. AFR has demonstrated that the optical method described above could be applied to turbine engines without afterburners, to sense combustor instabilities when measuring at the engine exhaust exit plane, downstream of the turbine. The innovative concept is elegant in that the optical sensor measures the exhaust flow at the exit of the engine and does not require undesired penetrations into the high-temperature, high-pressure combustor in front of the turbine. The innovative concept works by optically monitoring fluctuations or oscillations in the concentration and temperature of hot exhaust gas species. **This is possible because the operation of the sensor is not hindered by the presence of the turbine in the engine gas path.** With small passages, high-speed flows, fast-moving parts, and significant inertia, the turbine is expected to distort or destroy the passing pressure waves that on-engine pressure transducers monitor through penetrations upstream of the turbine. **However, axial variations in species concentration and temperature are maintained as gas flows through the turbine.** In addition, the high-speed flows and small passages also help to maintain variations that are present along the entrance plane of the turbine.

Figure 25 compares measurements from a single AFR SBIR Optical Sensor (exhaust-duct-mounted lens/fiber optic pair with remote detector, viewing a narrow line-of-sight across the exhaust diameter) to a traditional dynamic pressure sensor (combustor mounted on a stand-off tube) from a diesel-fuel-fired ground electric-power turbine engine that has been forced into oscillation. Both sensors readily exhibit the 460-Hz oscillation, demonstrating that the exhaust-mounted optical sensor is indeed sensitive to the oscillation that originated in the combustor. The optical sensor data presented here was acquired at an 8-kHz sampling rate over a one-second

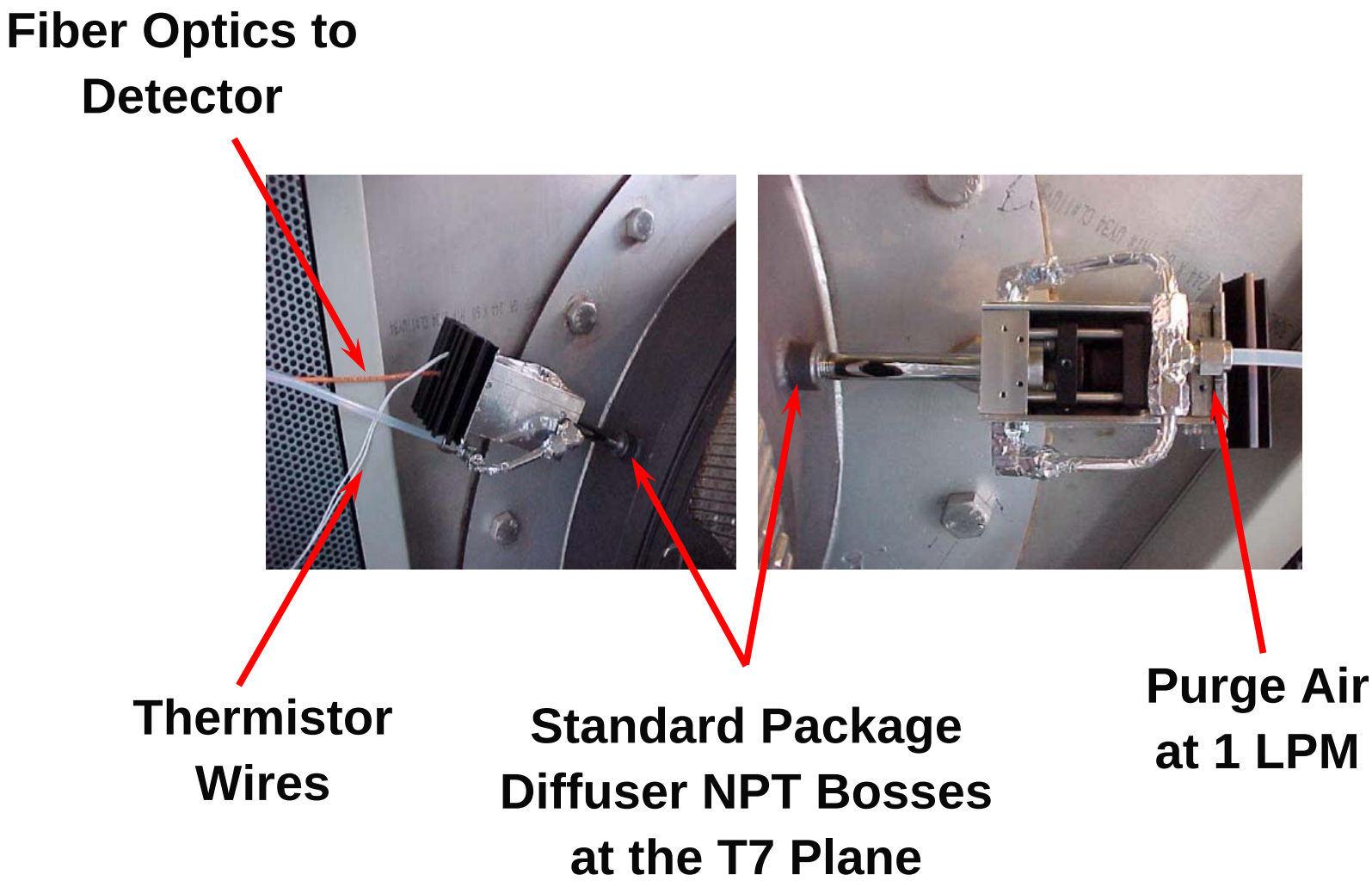

Figure 24: AFR SBIR Optical Sensor Mounted on Exhaust Plane of a 6,000 Hp Turbine Engine.

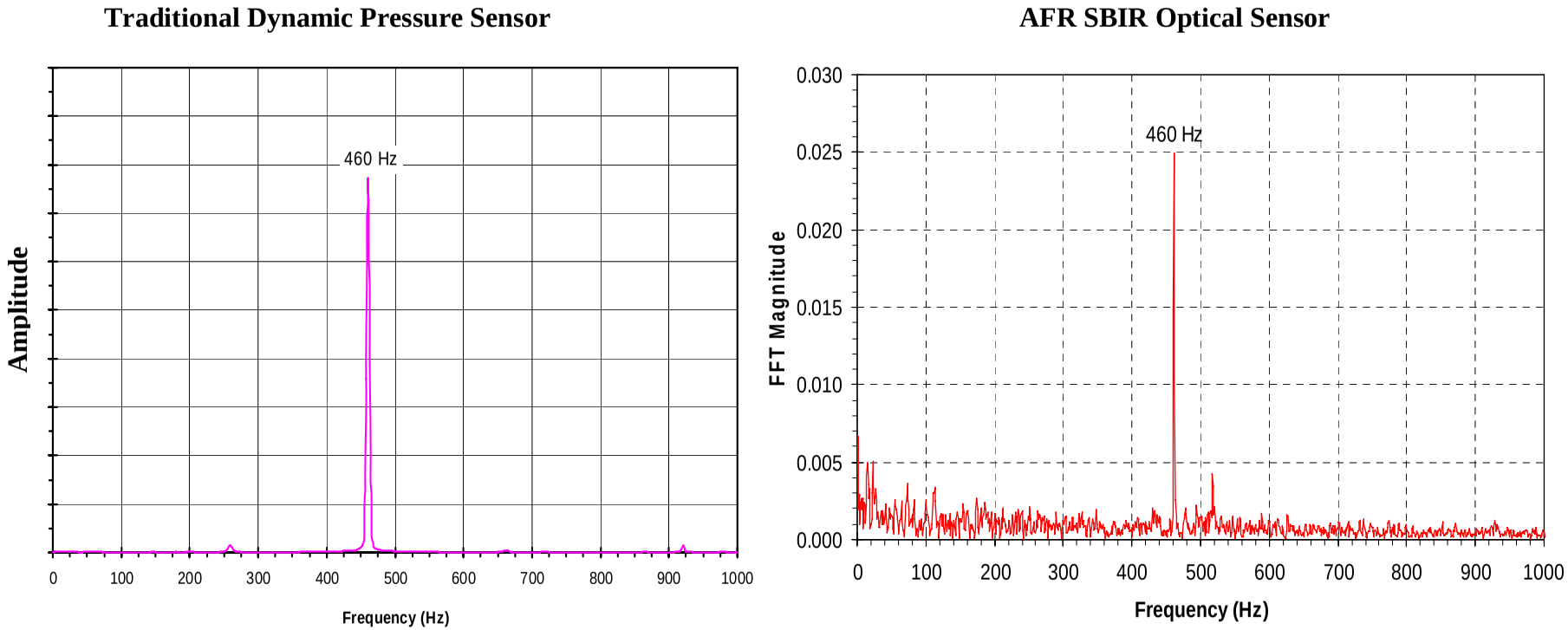

Figure 25: Data demonstrating that a passive optical-based sensor (right) mounted on the exhaust duct of a ground-power turbine engine observes the same frequency oscillation as a traditional combustor-mounted dynamic pressure sensor (left). The engine was fired with diesel fuel, 27 February 2004.

scan time. We note here that the traditional combustor-mounted pressure sensor was blown off the engine at one point during the field test.

Figure 26 (with a much expanded y-axis compared to Figure 25) presents time-averaged data from the exhaust-mounted optical sensor for the ground power engine when fired with natural gas at normal operating conditions.

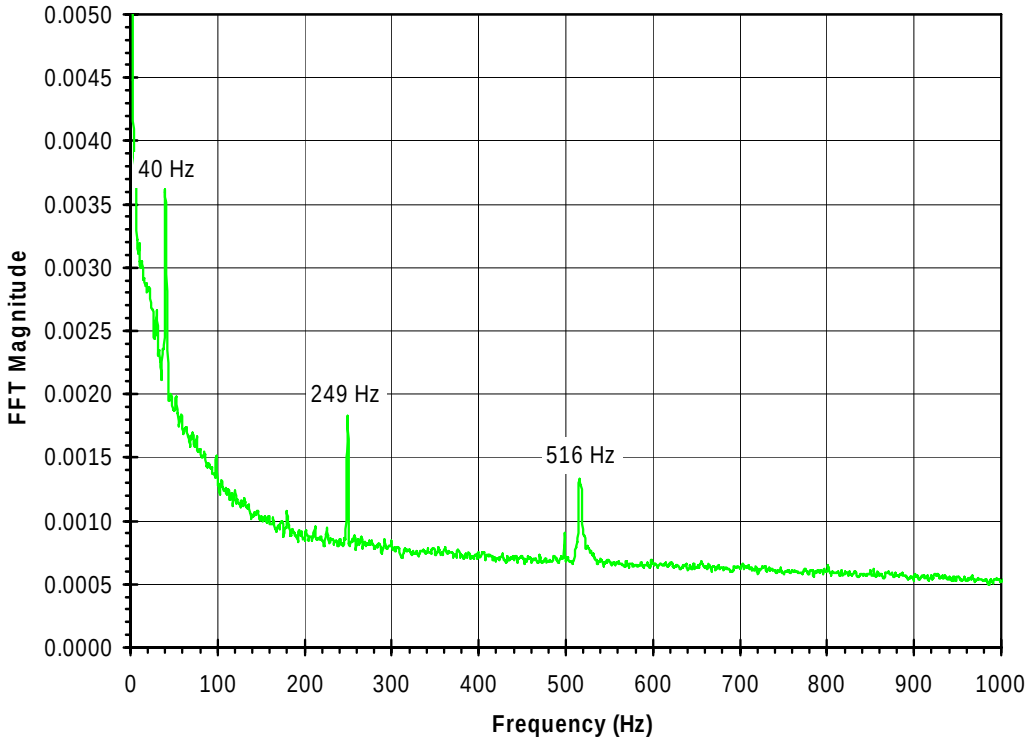

Figure 26: Time-averaged data from the passive optical-based sensor mounted on the exhaust duct of a ground-power turbine engine fired with natural gas (normal operating condition). The sensor records the set turbine rotational speed of 249 Hz and also both low and high frequency signatures of the engine. 26 February 2004.

The engine is on-load (producing electricity for the grid) and the turbine rotational speed is set at 249 Hz. The passive optical data from the exhaust shown in Figure 26 exhibits the turbine rotational speed, as well as a harmonic of less intensity (not labeled) at 498 Hz. But the data also presents evidence of both low frequency (40 Hz) and high frequency (516 Hz) oscillations in this engine that we were told was being operated at normal condition. Of interest is that the 516 Hz frequency also presented itself in the optical exhaust data in Figure 25 during diesel firing with induced oscillation, whereas the traditional combustor-mounted pressure sensor was not sensitive to this frequency. The exhaust sensor is providing additional engine health information that is not observed with the traditional sensor.

The two field tests at Solar Turbines confirmed that the sensing method could detect high frequency oscillations (screech) and low frequency oscillations (rumble), and also provide signals of flame-on and flame-off for the engine.

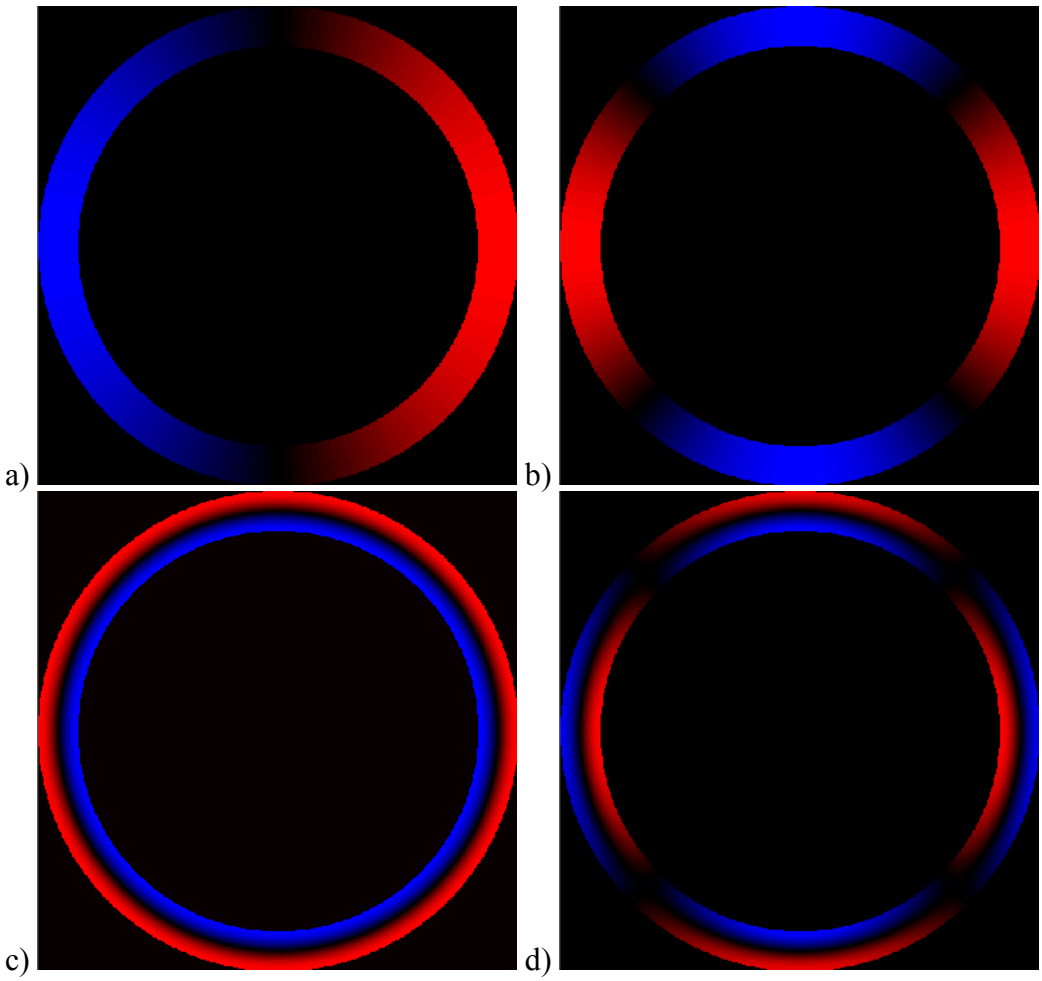

Figure 27: Acoustic mode shapes for an annular region with hard boundaries (zero normal velocity at all boundaries): a) first circumferential mode, b) second circumferential mode, c) first radial mode, d) combined 2 and 3.

However, a complication needs to be addressed in association with the mode shape of the higher frequency oscillations (circumferential modes). Our optical heads used to-date measure oscillations integrated across their line of sight. Figure 27 shows four acoustic mode shapes for a cylinder with an annular cross section and rigid walls. Positive and negative pressure fluctuations are shown as red and blue. Black corresponds to zero. If the pressure fluctuations in the combustor induce changes in the extent of reaction, the gas entering the turbine is expected to have temperature and concentration profiles that are qualitatively similar to the mode shapes shown in the figure. As the gas passes through the turbine, the radial profile is altered and the gas expands toward the engine axis. The circumferential profile is rotated through the turbine but the turbine blades help to maintain the variations from blade passage to blade passage. Therefore, as a first approximation, different sensor responses can be obtained by reference to the circumferential variation in the Figure 27 results.

We have demonstrated this with two optical heads that both viewed the entire diameter of the exhaust stream (looking through the engine centerline), but with the heads mounted 120° apart.

For the mode shown in part (a), both heads would be integrating over positive and negative portions of the wave, leading to cancellation of the fluctuations in the perfectly linear (optically thin) case. For the mode shown in part (b), both heads would be integrating over either positive or negative portions of the wave, so the diametrical line of sight is ideal for detecting this mode. However, the mode shapes shown in the figure may be oriented at any angle as standing waves (the nodes maintain their angular position with time) or may also exist as spinning waves (the nodes rotate around while the peak fluctuation in space remains constant), or combinations of the two. For standing waves oriented as in part (b), the horizontal line of sight has the greatest sensitivity, while a line of sight at 45° from the vertical passes through both nodes and therefore shows the least sensitivity.

During the on-engine measurements associated with Figure 25, oscillations were observed at frequencies from 450-470 Hz. Data from the two optical heads indicate that this corresponds to a mode with a circumferential component. Figure 28 shows a plot of the signal from one head vs. the signal from the other at the peak frequency. Very little correlation is seen between the two signals. This is dramatically different for rumble (longitudinal modes), where the oscillation is expected to result from bulk mode interactions and therefore exhibits only axial variations. Figure 29 shows a plot of the rumble magnitude for the two optical heads. There is a good correlation between these two signals, indicating very little in-plane variation in the lower frequency rumble oscillations.

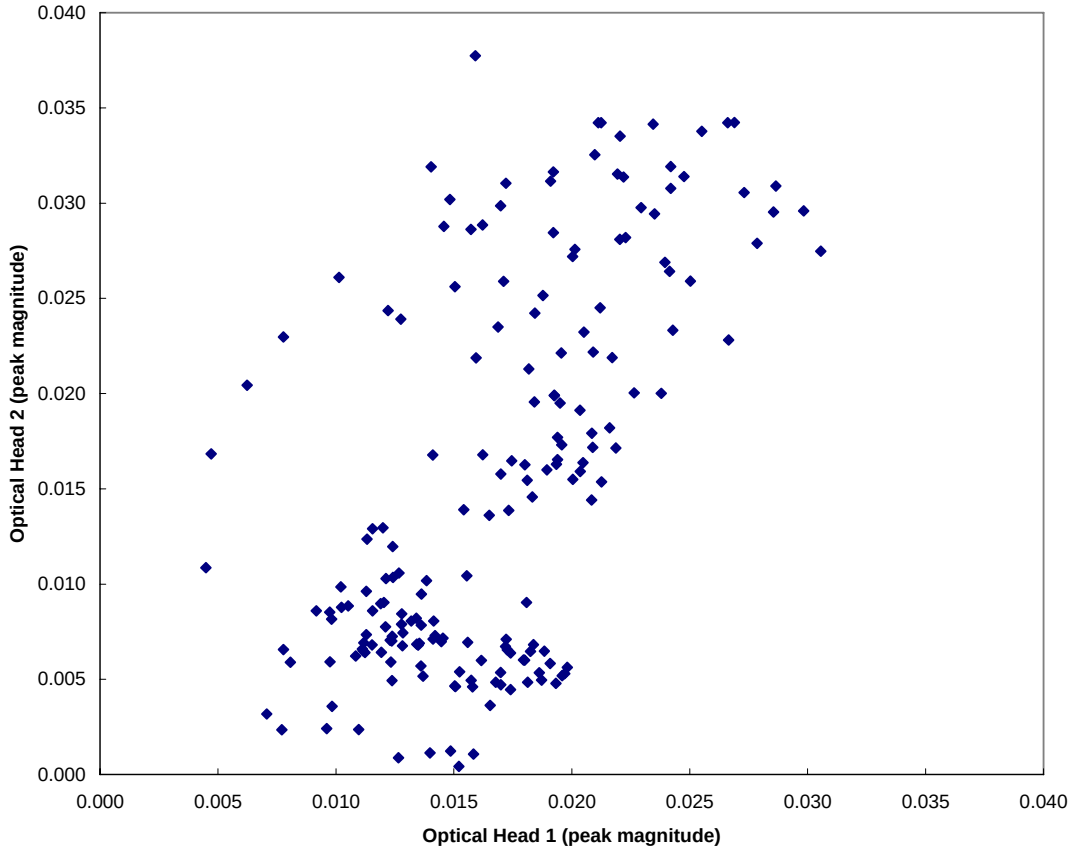

Figure 28: Comparison of magnitude for frequency peak during 450-470 Hz oscillations between the two optical heads.

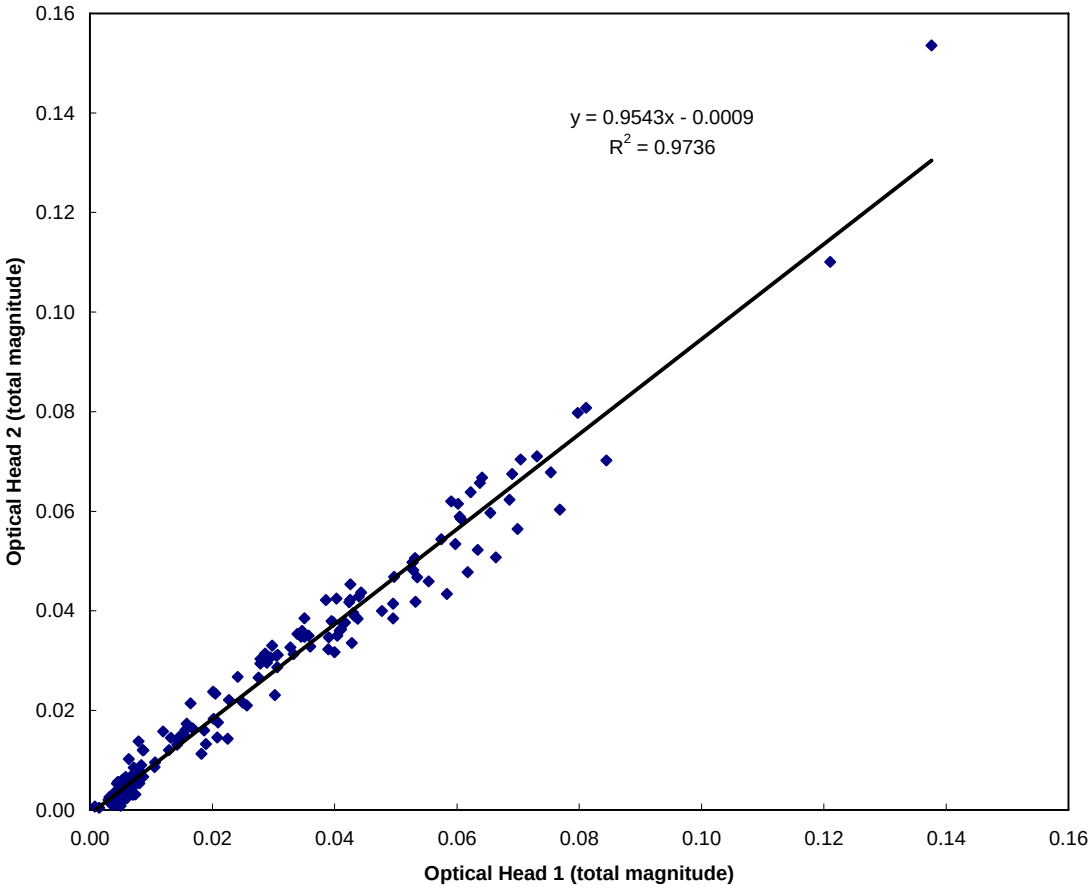

Figure 29: Comparison of total magnitude of the rumble signal between the two optical heads. The fundamental and first two overtones are used in the calculation.

For the higher frequency oscillations, the data from the two optical heads can be used to reconstruct the radiance fluctuations if a wavenumber for the mode is assumed (e.g., the mode is assumed to be the first circumferential mode). This can be used to illustrate if a standing wave, spinning wave, or some combination is present. These data can also be used to determine the orientation of the fluctuation at the position of the optical heads (note that the gases rotate about the engine axis as they pass through the turbine).

It is clear from the discussion above that multiple optical heads can be used to examine the spatial variations seen during oscillatory combustion. The discussion of Figure 27 illustrates that a system employing multiple heads would provide a more reliable indication of instabilities than a single head system, which could fail to indicate certain modes, depending on their in-plane shapes. **In fact, a system that can effectively characterize the in-plane mode shape can potentially detect oscillatory conditions in a much shorter time than a system employing a single point measurement.** For the single point measurement, the frequency resolution is determined by the length of the Fourier transform window (ignoring apodization issues). For 1-Hz frequency resolution, we need a 1-second window length. We can decrease the system response time only in so far as we can tolerate decreased frequency resolution (a 0.5-second window only gives 2-Hz frequency resolution). However, acoustic modes correspond to discrete

frequencies in time and discrete wavenumbers in space. By performing a spatial Fourier transform of the time Fourier spectra (from the different detectors), we can further reduce the signal-to-noise ratio and therefore tolerate reduced frequency resolution. **For spatially and temporally white noise, increasing the number of spatial points by a factor of two allows the response time to be halved while maintaining the same signal-to-noise ratio.** For these reasons, we propose to develop a system that employs an array of sensors to give both spatial and temporal radiance information.

We have provided Solar with a drawing of the modified exhaust duct, adding 6 pipe bosses, for future testing at Solar. Four of the bosses look across chords that do not pass through the duct axis. These should yield a higher sensitivity to oscillations than the existing ports. The other two ports will allow one optical head to view a cold blackbody backstop on the end of an extension tube, for flame-out, light-off, rumble, and oscillation detection.

Solar reviewed our drawing and agreed to modify and prepare the exhaust duct for the future test, scheduled for April 2005. Solar's goal is to demonstrate the following at this trial:

- Closed loop emissions control with MGA and AFR instability probe
- Flame on/off detection with AFR instability probe

Due to the ending of this Phase III project, this next test will be accomplished as part of the SBIR Phase II project identified at the beginning of this task. Note that a portion of the above analysis work was accomplished as part of the SBIR Phase II project.

Conclusion for this Task in Regard to Goals Targeted:

- AFR has made significant progress towards development of the engine performance, health and condition analysis system under this task. The collaboration established with Solar Turbines, Inc. has provided a key test-bed to the effort. Solar's private sector cost share of providing the turbine engine test-bed, providing engine operating costs including labor, and implementing modifications to the exhaust duct have to-date been unquantified but are recognized as significant.

<u>Task 6 – Meetings and Reporting Requirements (AFR & AEDC Responsibility)</u>

Goals Targeted for this Task:

- Monthly progress reports, 50% demonstration report, 85% demonstration report, and final report.

Conclusion for this Task in Regard to Goals Targeted:

Reporting was performed on schedule and satisfied the requirements of this task. Quarterly meetings were held generally on schedule, rotating meeting locations between AFR (East Hartford, CT), AEDC (Arnold AFB, TN) and AFRL (Tyndal AFB, FL).

Pertaining to the continued uses and future applications of the FT-IR MultiGas at AEDC and other Air Force facilities, contractor-developed costing data was delivered to allow a post-development technical support system to be developed that will allow support for an indefinite duration. This document was also a contract deliverable. (Please see **Appendix J** of this final report for the complete listing and status of contract deliverables.)

Conclusions

The project scope was to provide both technology and cost saving benefits to the Air Force by improving gas analysis capabilities at Air Force facilities. Also, the effort would increase the commercial application of the Air Force supported research and development. The application and development work was particularly focused on military turbine engine exhaust monitoring for engine design testing, qualification, and environmental control. Work of the project established that improved gas analysis capabilities at a significantly lower cost than the current method is now available. Successful advanced development of the instrumentation hardware and software improved the measurement capabilities for advanced turbine engine programs, and for other applications in the Air Force and private sector. Project accomplishments and highlights include the following:

- Delivery of six advanced prototype FT-IR multiple-gas analyzer systems.
  - Improved calibration algorithms and procedures
  - Improved quantitative analysis in multi-component samples
  - Integrated oxygen sensor (hardware and software)
  - Expanded reference library for organic vapors
  - Optimized for AEDC TECHMAT engine testing
    - Continuous sweep sampling
    - Move and dwell sampling

- Successful field trials at the Middle Tennessee State University (MTSU) airfield.
  - P & W JT-12 turbine engine
  - GE J-85 turbine engine
  - Continental 0470 6-cylinder engine

- Successful field trials with turbine engine manufacturers.
  - Solar Turbines, Inc.
  - Pratt & Whitney

- Successful field trials at AEDC facilities.
  - Emissions monitoring and engine performance monitoring during TECHMAT engine testing at AEDC's ASTF (Aeropropulsion Systems Test Facilities)
  - Glycol monitoring during icing testing at AEDC's ASTF
  - Toxic gas monitoring and oxygen monitoring at AEDC's Tunnel 9

- Generation of the draft Aerospace Information Report (AIR) 5917 for review by the SAE E-31 Committee and consideration as a new Aerospace Recommended Practice (ARP).

- Successful integration of five advanced prototype FT-IR multiple gas analysis systems with the AEDC Applied Technology Department's high temperature probe rake system, rapid gas transport system and pitot pressure measurement system.

- Success in delivering critical components that would help the AEDC Applied Technology Department meet its goal of moving forward with the new capability for multiple-species surveys of a full nozzle exit within the spatial resolution required by the regulatory agencies on a five-minute time scale (avoiding the previously typical 16-hour dedicated air-on period for emissions).

- Identification of more than a dozen measurement applications at AEDC.

- The first three commercial instrument sales as a result of the project have taken place. Solar Turbines, Inc. (San Diego, CA) purchased one, and the University of Dayton Research Institute (WPAFB, Ohio) purchased two advanced multiple-gas analyzer system (advanced FT-IR system with integrated oxygen sensor). The three deliveries were completed.

- A project-related commercial sale was made to the NASA Glenn Research Center. NASA Glenn submitted a purchase order to AFR for FT-IR technical support consisting of telephone/email technical support including data analysis support for data transmitted to AFR.

- Success in making progress towards development of an engine performance, health and condition analysis system.

- AFR and ATA/AEDC published five peer-reviewed technical articles pertaining to results and accomplishments of the Phase III project. These articles were in addition to the two articles published in Phase II and the one article published in the transition period between Phases II and III.

- The ATA team including AFR received the AEDC First Quarter 2004 *Technical Achievement Excellence Award*.

References

1 Gardner, D.G., Zaccardi, V.A., Jalbert, P.A., and Bryant, M.D. (AEDC), **"Reducing the Cost of Aircraft Engine Emission Measurements,"** ISA vol. 443, Proceedings of the 49th International Instrumentation Symposium, Orlando, FL (May 8, 2003).

2 Markham, J.R., Bonzani, P.J., Bush, P.M., and Scire, J.J. (AFR), **"Integrated Gas Analyzer for Measuring Combustion Exhaust and Excess Oxygen,"** ISA vol. 443, Proceedings of the 49th International Instrumentation Symposium, Orlando, FL (May 8, 2003).

3 Markham, J.R., Bush, P.M., Bonzani, P.J., and Scire, J.J. (AFR), and Zaccardi, V.A., Jalbert, P.A., Bryant, M.D., and Gardner, D.G. (AEDC), **"Integrated Gas Analyzer for Complete**

Monitoring of Turbine Engine Test Cells," Applied Spectroscopy, Volume 58, Number 1, January 2004.

4 Jalbert, P.A., Zaccardi, V.A., Bryant, M.D., Winkleman, B.C., (AEDC), and Markham, J.R., Bush, P.M., Bonzani, P.J. (AFR), **"Rapid, Complete Nozzle Exhaust Gas Measurement Capability for Gas Turbine Engines,"** ISA vol. 451, Proceedings of the 50th International Instrumentation Symposium, San Antonio, TX (May 9-13, 2004).

5 Jalbert, P.A. (AEDC) and Markham, J.R. (AFR), **"Fourier Transform Infrared for Turbine Engine Health Monitoring,"** Applied Spectroscopy, Volume 58, Number 12, December 2004.

6 Groth, R.H. and Robertson, D.J. **"Reactive and Nonreactive Hydrocarbon Emissions from Gas Turbine Engines,"** Air & Waste Manag. Assoc., Pittsburgh, PA (1974).

7 Moses, C.A. and Stavinoha., L.L., "Gas Chromatographic Analysis of Exhaust Hydrocarbons from a Gas turbine Combustor," Western States Section/The Combustion Institute, Paper 75-17, Stanford Research Institute (1975).

8 Spicer, C.W., Holdren, M.W., Smith, D.L., Hughes, D.P. and Smith, M.D., Trans. ASME/J. Eng. Gas Turbines Power, 114, 111 (1992).

9 Spicer, C.W., Holdren, M.W., Riggins, R.M., and Lyon, T.F., Ann. Geophysicae, 12, 944 (1994).

Appendix A

Air Force SBIR Impact Story: **"Portable Multi-Gas Analyzer"**

Air Force SBIR Impact

Portable MultiGas Analyzer

Company:
Advanced Fuel Research, Inc.

Location:
East Hartford, CT

Employees:
14

CEO:
James R. Markham

Project Officers:
Captain Gina Graziano and Bruce J. Nielsen AFRL Air Expeditionary Forces Technologies Division, Tyndall AFB, FL

Key Collaborators:
Paul Jalbert, Vincent Zaccardi and Donald Gardner, Jacobs/Sverdrup, Arnold Engineering Development Center Group, Arnold AFB, TN

The new MultiGas Analyzer (MGA), in a convenient shipping case, next to a traditional gas analysis system. The MGA measures more gases for a fraction of the traditional capital and maintenance costs.

Air Force Requirements:

Many Air Force programs require measurements of gas compositions and gas specie concentrations. However, to satisfy characterization and monitoring needs for hazardous and toxic chemicals, the majority of these programs would benefit from an advancement in measurement technology. Other branches of the DoD, and NASA, DoE and a large portion of commercial industry have similar characterization and monitoring needs, and all are calling for technology breakthroughs that result in "better, faster, and cost effective" products to fill these needs. Typically, what is called for is a rugged, reliable, on-location multi-component gas analyzing instrument that exhibits a fast response combined with the sensitivity to detect down to trace concentrations of the compound(s) of interest.

SBIR Technology:

The Air Force Small Business Innovation Research (SBIR) opportunity provided to Advanced Fuel Research, Inc. (AFR) stimulated technological innovation. Research and development on innovative optical designs, hardware designs, and software designs resulted in a package of new technology that was demonstrated to provide

For more information on this story, contact Air Force TechConnect at 1-800-203-6451 or at www.afrl.af.mil/techconn/index.htm

benefits to the Air Force. By way of field demonstrations, the innovations were proven. The Air Force accepted delivery of new technology at the conclusion of Phase II, put it into immediate service, and continues to reap the benefits of the new capabilities provided by this SBIR project.

A particular focus of this effort became to improve exhaust gas characterization and monitoring capabilities during Air Force development and testing of gas turbine (jet) engines. Significant SBIR collaboration took place between AFR and the Arnold Engineering Development Center (AEDC) at Arnold Air Force Base, TN, the Air Force's premier flight simulation test facility. AEDC's engine test facilities are used routinely for testing combustor and full propulsion systems including turbojet, turbofan, and ramjet air breathing engines. Gas phase emissions testing before flight is a key responsibility of AEDC. AFR advanced the AEDC/Air Force measurement capabilities, and the new technology is being pursued to become a new aerospace recommended practice to government and industry for the analysis and evaluation of gaseous emissions from aircraft engines. In support of this, the DoD appropriations bill for FY2002 included a Phase III earmark for the delivery of additional multigas anlayzers to the Air Force.

Company Impact:

AFR sold the new technology to On-Line Technologies, Inc. (an SBIR generated product manufacturing/ sales spin-off of AFR). On-Line Technologies incorporated the new technology into a key product line. The successful sales growth was a factor when the spin-off company was purchased by the large company MKS Instruments. The On-Line Products Group of MKS now benefits from a worldwide sales, service and distribution force. For exemplary achievement in commercializing technology developed in the SBIR program, AFR received the U.S. Small Business Administration's prestigious Tibbetts Award in year 2000.

Company Quotes:

"This project was a pleasure for AFR, not only for the successes in technology advancements and commercialization, but also for the opportunity to meet and work with Air Force experts at Tyndall Air Force Base and Arnold Air Force Base. The Air Force SBIR program has strengthened AFR's business."

James R. Markham
CEO
Advanced Fuel Research, Inc.

"It is exciting to work with small businesses that think outside-the-box, without the constraints that may plague big companies. These companies often deliver technical innovation that improves a process and reduces cost for an Air Force customer much faster than technology development through other RD&A programs."

Bruce Nielsen
AFRL Air Expeditionary Forces Technologies Division
SBIR Project Officer

AF SBIR Program Manager
AFRL/XPTT
1864 4th Street, Room 1, Building 15
Wright-Patterson AFB, OH 45433

AF SBIR Program Manager: Steve Guilfoos
e-mail: stephen.guilfoos@wpafb.af.mil

Website: www.afrl.af.mil/sbir

DSN Fax: 785-2329
T: (800) 222-0336
F: (937) 255-2329

Appendix B

AEDC Newspaper Article: **"New Technology Adds Benefits, Saves Money for AEDC Test Customers."**

HIGH MACH

A publication for and about
Arnold Engineering Development Center

Vol. 51, No. 5 | Arnold AFB, Tenn. | March 11, 2004

New technology adds benefits, saves money for AEDC test customers

By Tina R. Barton
AEDC Public Affairs

A unique AEDC-developed gas sampling system is saving turbine engine test customers time and money and helping keep the skies environmentally friendly.

The Continuous-Sweep Gas Analysis System provides simultaneous sampling and analysis of more than a dozen gaseous species present in the exhaust of turbine engines.

AEDC's Paul Jalbert, Denise Bryant and Vince Zaccardi designed the system, and Brad Besheres, Roy Carroll and Gary Story assembled the equipment. According to Mr. Jalbert, no other test facilities in the nation can provide this multi-gas sampling.

The data helps military engine manufacturers ensure they comply with environmental regulations for emission control, as well as helping them understand engine fuel consumption.

"The basing of military aircraft is dependent on the exhaust gas emission levels the aircraft contribute to the local environment," Mr. Zaccardi said. "Before entering service, an engine design must be certified by the regulatory agencies to ensure it does not produce more than the allowable level of emissions during landing and takeoff."

Mr. Jalbert compared the sampling to that of NASCAR pit crews who insert a probe into the tailpipe of the racecar and collect samples of the gases in the exhaust stream. By analyzing the samples for the presence of carbon monoxide, carbon dioxide and oxygen in the exhaust, the manufacturer can determine how the engine burns fuel.

The same concept is behind the continuous-sweep system for turbine engine testing. However, the AEDC system can analyze more than a dozen different elements simultaneously instead of one at a time using separate instruments.

According to Mr. Zaccardi, gas sampling previously required many hours of steady-state engine exhaust-gas sampling and was expensive due to the added engine run time, test cell and personnel time and materials consumed during the test. Additionally, older gas sampling systems required large trailers located inside the test areas to house the computer analysis systems.

The new system consists of small orange-crate-size, multi-gas analyzers mounted on a cart that can be rolled into a test cell next to the engine. Each analyzer is connected by a heated gas sample tube to a rake containing 16 probes designed to withstand exhaust temperatures up to 4,000 degrees Fahrenheit. The gas sampling rake is then mounted on a sliding mechanism placed at the exit of an engine's exhaust nozzle.

During engine operations, the test conductor controls the rake as

See Gas Sampling, Pg. 3

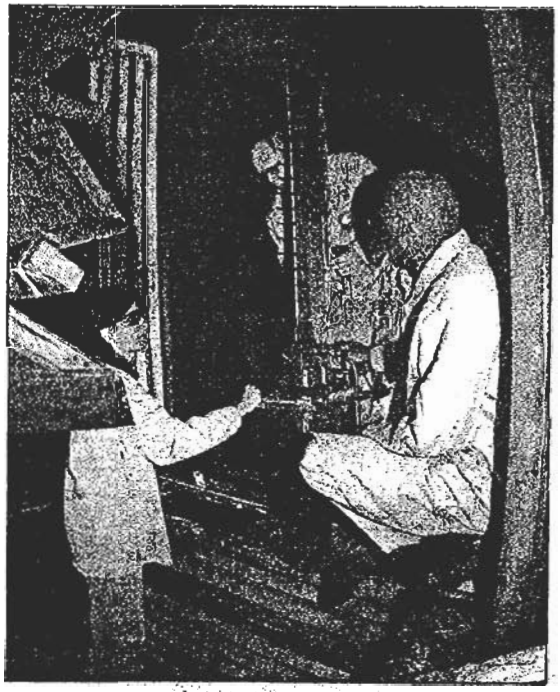

AEDC engineer, Denise Bryant, left, and outside machinists, Steve Lepley, center, and Elvy Davis, position the continuous-sweep gas analysis probe in the exhaust path of the Pratt & Whitney XTE67/SE1 experimental test-bed engine in C-1. (Photo by Gary Barton)

Gas sampling

(From Page 1)

it continuously sweeps through the exhaust at a controlled rate from two inches per second to two inches per minute. At this time, the probes gather samples of the gases in the exhaust stream. The samples travel through a special heated line to the gas analyzers, which immediately provide data on exhaust composition. The test conductor transmits the resulting processed data file to a computer in the test control room allowing the customer to view the results within five minutes of the sampling.

The system began development in 2001 under the Small Business Innovative Research (SBIR) program. Since there were no engines available at AEDC to validate the system, Bryant, Jalbert and Zaccardi teamed with Bill Allen, associate professor of Middle Tennessee State University's (MTSU) Aerospace Department to develop and test the system program while providing aerospace students an opportunity to learn more about turbine engine instrumentation. Mr. Allen operated a JT12 gas turbine engine, a 3,000-pound thrust class engine with a 13.5-inch nozzle exit diameter, to validate the system.

"Advanced Fuel Research, a Small Business Innovative Research company, teamed well with AEDC in providing new gas sampling technology to AEDC's turbine engine customers," said Ron Bishel, SBIR program manager. "The SBIR Phase III technology saved one customer over $350K in engine testing cost and provided excellent gas sampling data."

Since March 2001, the AEDC crew has conducted 13 validation test periods using the MTSU facility at the Smyrna airport. In 2002, the system provided exhaust gas analysis of the Tactical Tomahawk engine in Propulsion Development Test Cell T-11 and various combustor rigs in Propulsion Development Test Cell T-3. AEDC crews also used it for facility safety checkouts in Range G and Research Test Cell R1D. The latest use provided combustion analysis for the Dual Combustion Ramjet test in the center's Aerodynamic Propulsion Test Unit.

"The payoff for aeropropulsion testing will allow the customer to reduce the number of required test periods by being able to perform all exhaust analysis simultaneously while achieving other propulsion test objectives," Mr. Jalbert said.

Appendix C

Final Report Document: **Improvements Implemented to the Operational and Quantitative Analysis Software of the FT-IR MultiGas Analyzer System**

Improvements Implemented to the Operational and Quantitative Analysis Software of the FT-IR MultiGas Analyzer System

Patrick M. Bush

Advanced Fuel Research, Inc.
87 Church Street
East Hartford, CT 06108-3728

Table of Contents

Abstract

Improvements to the MGA software have been concentrated on upgrading the communications between the MGA host software and peripheral devices, improving the calibration files used for quantifying gas species, and increasing the MGA standard library. Using the peripheral hardware communication package, AFR has been able to incorporate an integrated oxygen sensor into the MGA data reporting stream. The addition of the integrated oxygen sensor to the MGA increases the ability of the system to monitor combustion applications for non-infrared active gas species. Other improvements have come in advancements to the calibration files by using classical least squares routine and a process known as "Picket Fence" Enhancement. The CLS routine and "picket fence" enhancement defines the quant region in greater detail by selecting the actual absorption bands to quantify over, as well as, to decrease the overlapping "cross talk" interferences from other gas species. Finally increasing the MGA reference library potentially improves the capability of the MGA for monitoring the combustion process by identifying and quantifying all gas species present.

I. Peripheral Hardware (Device) Communication

The MGA software has been designed to give the user an option of connecting peripheral hardware to the system and reporting the results in the gas concentration data stream. The user is still limited to informing MKS/AFR about the hardware to ensure the software and communication port are configure correctly before each new peripheral hardware is installed in the system.

The following peripheral hardware and software improvements are described in this section:

- Integrated Oxygen Sensor (B&B RS232DA communication package)
- Calibrate Oxygen Sensor Software

Integrated Oxygen Sensor (B&B RS232DA communication package)

AFR has designed an integrated oxygen sensor that communicates with the MGA as a peripheral device using the B&B RS232DA option from the MG2000 software (Refer to the integrated oxygen sensor manual for information on the actual sensor and design). The B&B RS232DA is one of several preset peripheral hardware communication options that the user can select, which uses a data acquisition card purchased from B&B Electronics and communicates with the host computer through a RS232 cable. The use of the B&B RS232DA communication option for the integrated oxygen sensor is described below. The other preset peripheral hardware communication options were designed for other MKS customers and are not discussed in this manual. The user should call MKS Inst. for further information of these options if needed.

Selecting Setup from the Multigas Main tab opens the MG2000 Setup Utility screen where the user can add the integrated oxygen sensor to the reporting stream. Clicking Add under External Device displays the External Device Selection menu. Highlight the B&B RS232DA option and click continue; this opens the B&B RS232DA Configuration Menu. If the B&B RS232DA Configuration Menu is **not** configured for the integrated oxygen sensor the menu should appear as shown in Figure 1. Make sure all the digital channels are disabled and channel 0 or 1 of the analog channels is enabled. The check-mark next to the channel name indicates if the channel is enabled and the user can switch between them by double clicking on the desired channel.

To configure the B&B RS232DA perform the following steps:

1. Select either Internal O_2 or External O_2 from Analog Ch. Config: Type pull down menu. (Make sure CH0 or CH1 is highlighted and enabled in the Analog Ch. List box.)

2. Set the Analog Ch. Config: Input mode to 0-5V. All other Analog Ch. Config parameters can be ignored.
3. The O_2 Sensor Config. section becomes enabled and the user can then load a calibration file, save a new calibration file, or calibrate the current oxygen sensor.
   -Load Calibration File:
   a. Click the Load Cal. Button and follow the computer prompts to load the desired calibration file.
   b. Once loaded the polynomial constants appear under the corresponding Quad, Linear, and Offset parameters.
   c. The user can manually change these parameters if needed.
   -Save Calibration File:
   a. If the polynomial constants have been changed or the oxygen sensor has been re-calibrated the new calibration curve can be saved by clicking the Save Cal. Button.
   b. Follow the prompts to select the directory and save the new calibration file.
   -Calibrate Oxygen Sensor:
   a. Refer to "Calibrate Oxygen Sensor" in this manual for a detail procedure.
   b. Once calibrated the new polynomial constants appear under the corresponding Quad, Linear, and Offset parameters.

Note  To calibrate the integrated oxygen sensor the user must have available several known concentrations of oxygen.

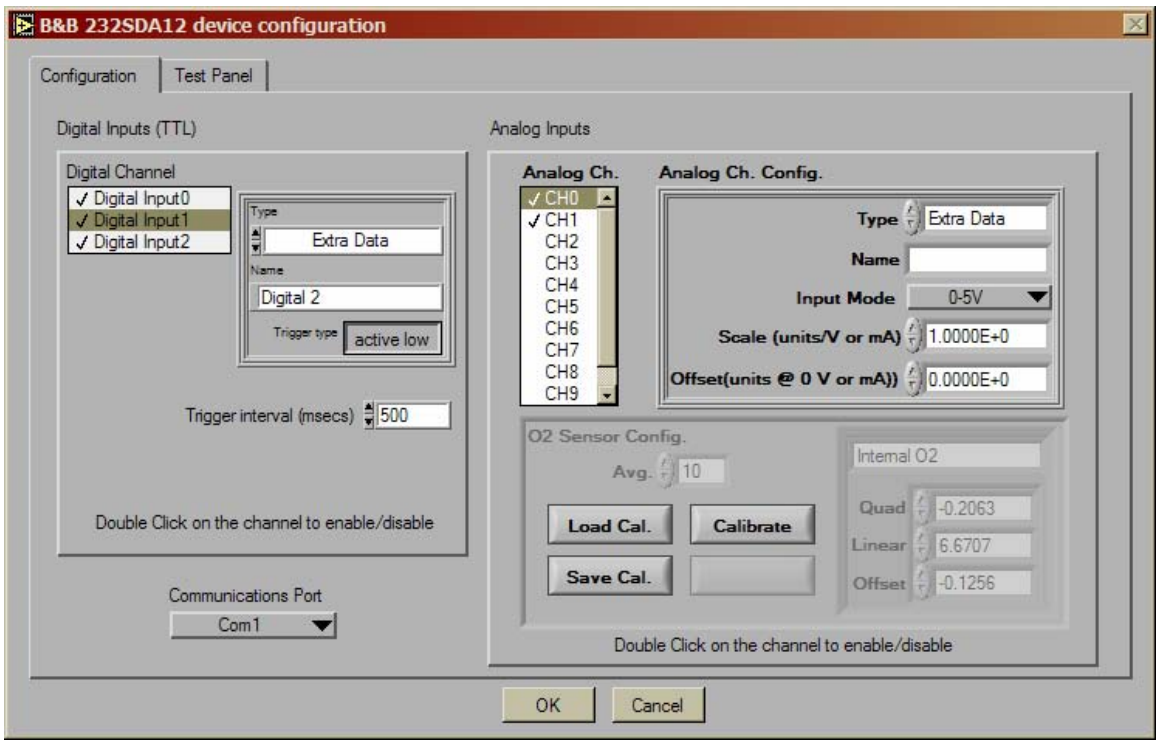

Figure 1: B&B RS232DA Configuration Menu

The following table describes the functions of the B&B RS232DA Configuration Menu:

Function	Description
Configuration *(tab)*	Displays all the channel parameters for both the digital and analog channel for the B&B data acquisition card.
Digital Inputs *(TTL) (control cluster)*	Configures the digital input channels for the B&B data acquisition card. The digital channels are not used for the integrated oxygen sensor and should be disabled by double clicking on each digital channel. (To change the status of each channel, highlight and double click on the desired channel. The check mark indicates that the channel is enabled.) All other digital parameter can be ignored.

Analog Ch. *(list box)*	Displays all of the active analog channels (check mark). For the integrated oxygen sensor make sure that only CH0 and CH1 are enabled and all other channels are disabled. (To change the status of each channel, highlight and double click on the desired channel. The check mark indicates that the channel is enabled.)
Analog Ch. Config: Type *(pull down menu)*	Assigns one of the preset functions to the analog channel that is highlighted (i.e. pressure, temperature, internal O2, external O2, or extra data). If the user is using the DAQ communication device to measure something other than one of the preset values, select extra data for channel type and identify the function under Analog Ch. Config: Name.
Analog Ch. Config: Name *(control string)*	Allows the user to identify the function for the highlighted channel if one of the preset channel types do not apply. Make sure that the channel type is configured to extra data before identifying the function.
Analog Ch. Config: Input Mode *(pull down menu)*	Assigns the channel input range for the selected channel. The integrated Oxygen sensor uses input mode of 0-5V.
Analog Ch. Config: Scale and Offset *(entered values)*	Allows the user to generate a generic linear regression to the input mode. (i.e. degrees Celsius vs. voltage). These parameters can be used only if the measured value follows a linear regression. The integrated O2 sensor does not use these parameters.
O_2 Sensor Config: Avg *(entered value)*	Allows the user to adjust how many points the O2 sensor co-adds. The signal-to-noise ratio increases as the number of scans to co-add increases.
O_2 Sensor Config: Load *(button)*	Allows the user to load a saved calibration file.
O_2 Sensor Config: Save *(button)*	Allows the user to save the current calibration curve parameters. The parameters are display as Quad, Linear, and Offset.
O_2 Sensor Config: Calibrate *(button)*	Allows the user to calibrate the integrated Oxygen sensor.
O_2 Sensor Config: Calibration Constants – *Quad, Linear, Offset*	Displays the current polynomial constants used for the calibration curve.

Once all of the channels are configured, the user can test all active channels by selecting the Test Panel tab (Figure 2). The test panel shows the channel name and the raw signal

data for each channel. The user can determine if the peripheral device is responding and working correctly from the data reported on this panel.

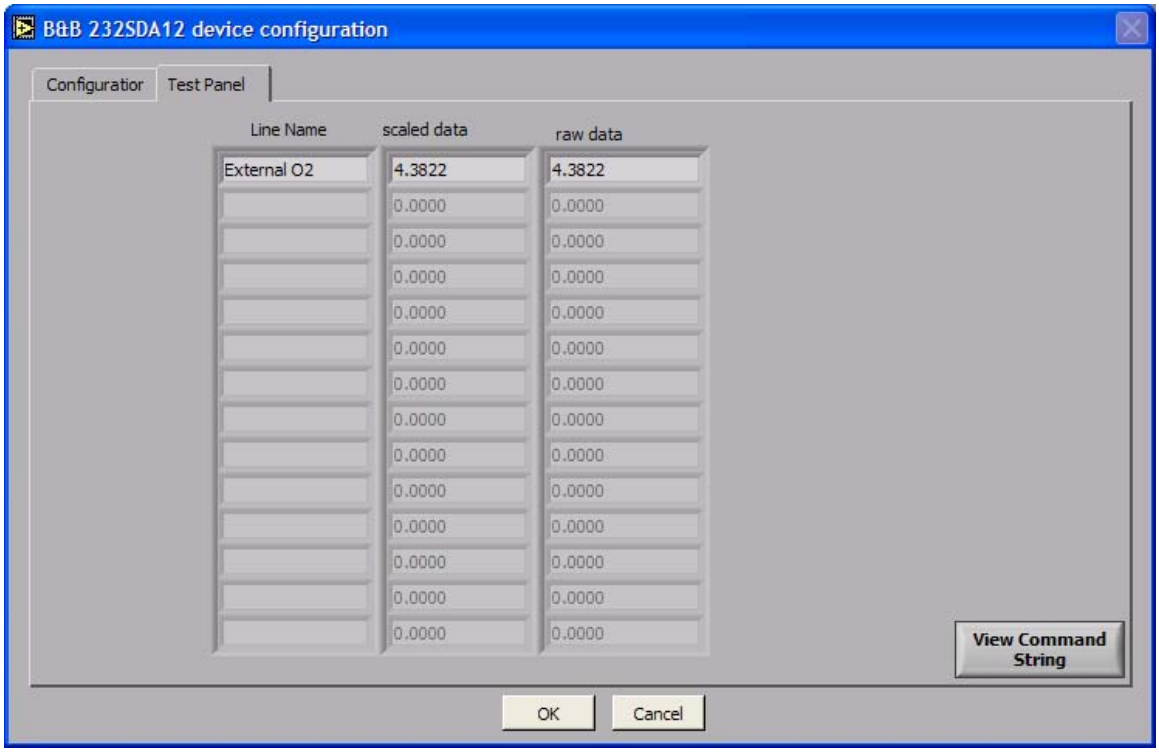

Figure 2: Peripheral Device Test Panel

Finally clicking on Ok exits back out to the MG2000 Setup Utility menu and the B&B RS232DA will show up in the main indicator box under External Devices and the active channels will appear in the lower indicator box (Figure 3).

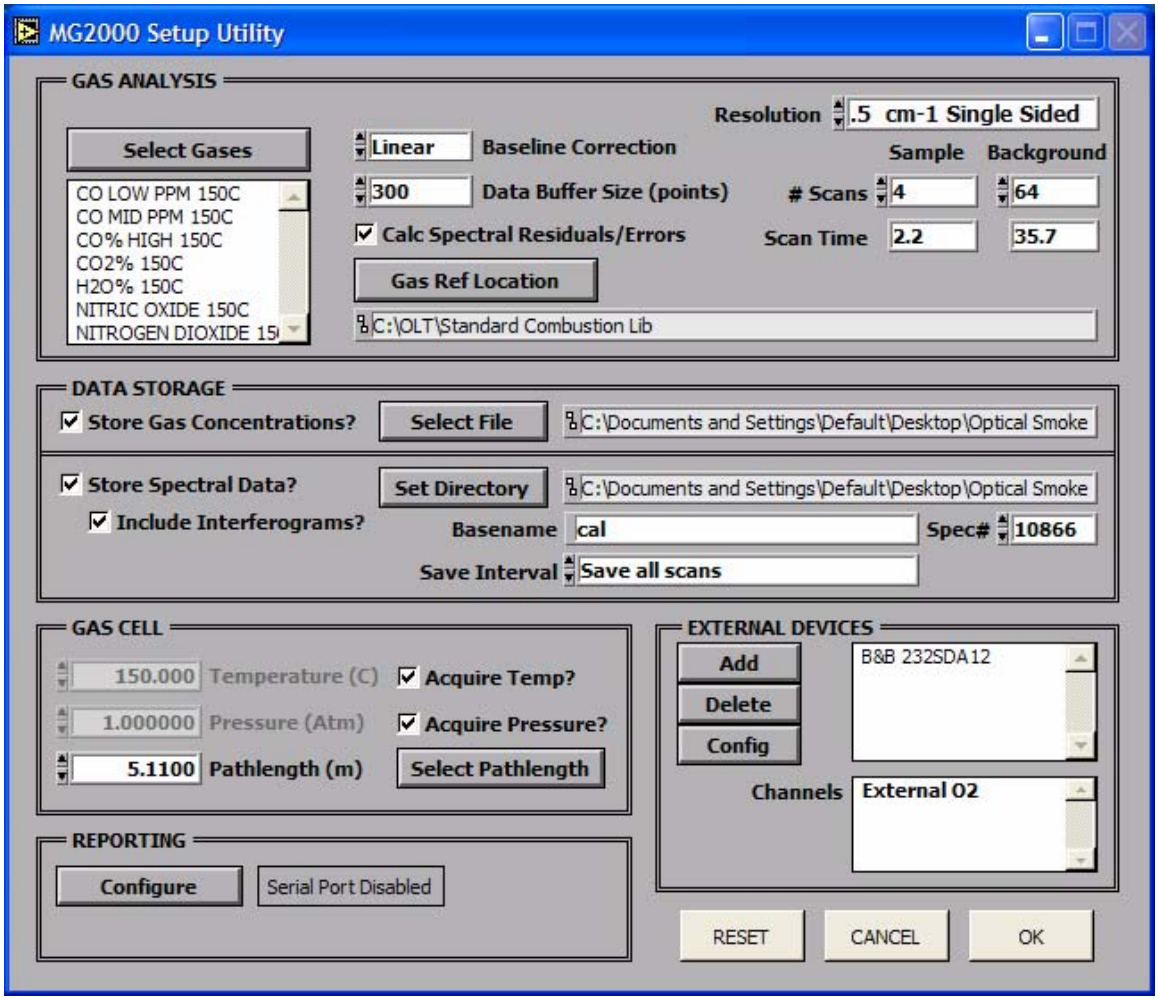

Figure 3: MG2000 Setup Utility

These indicator boxes tell the user if any peripheral devices are installed into the MGA reporting stream without going through the entire process each time the software is opened up on the computer. During data collection the user can view the integrated oxygen data by selecting either the timeline or data table display (Figure 4 and 5 respectively).

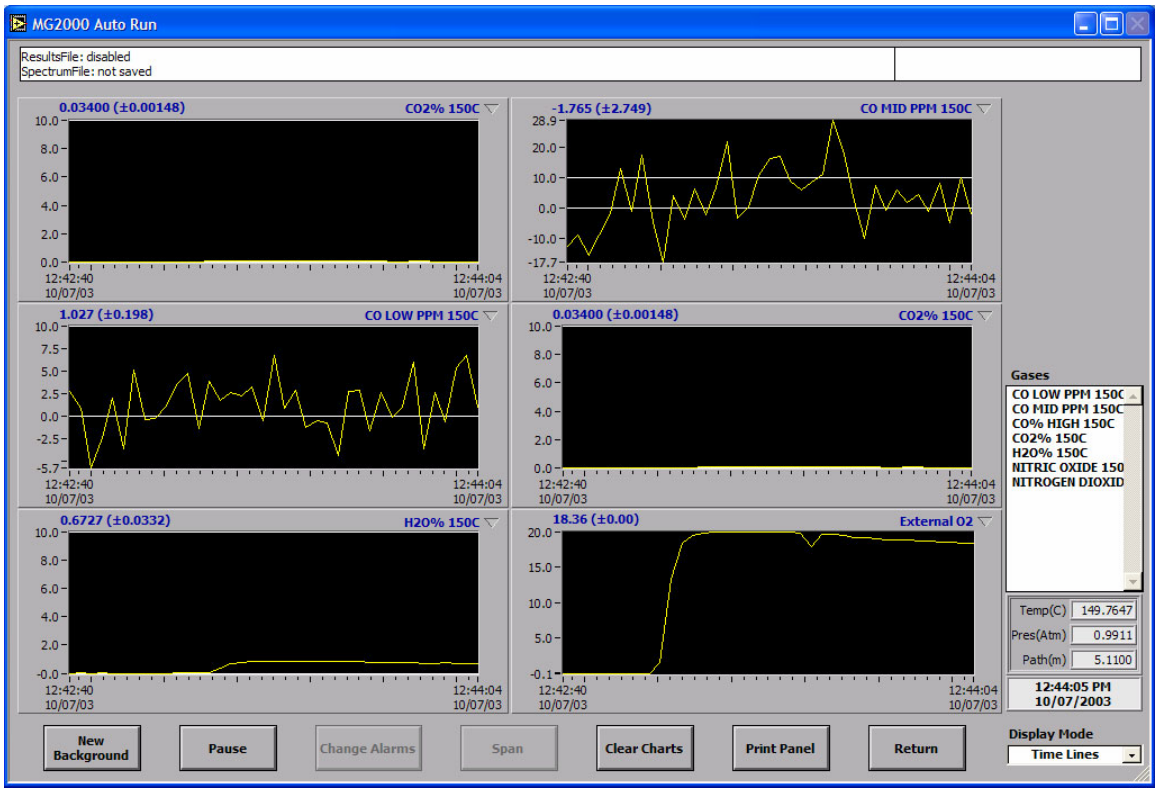

Figure 4: MG2000 Auto Run Time-line Screen

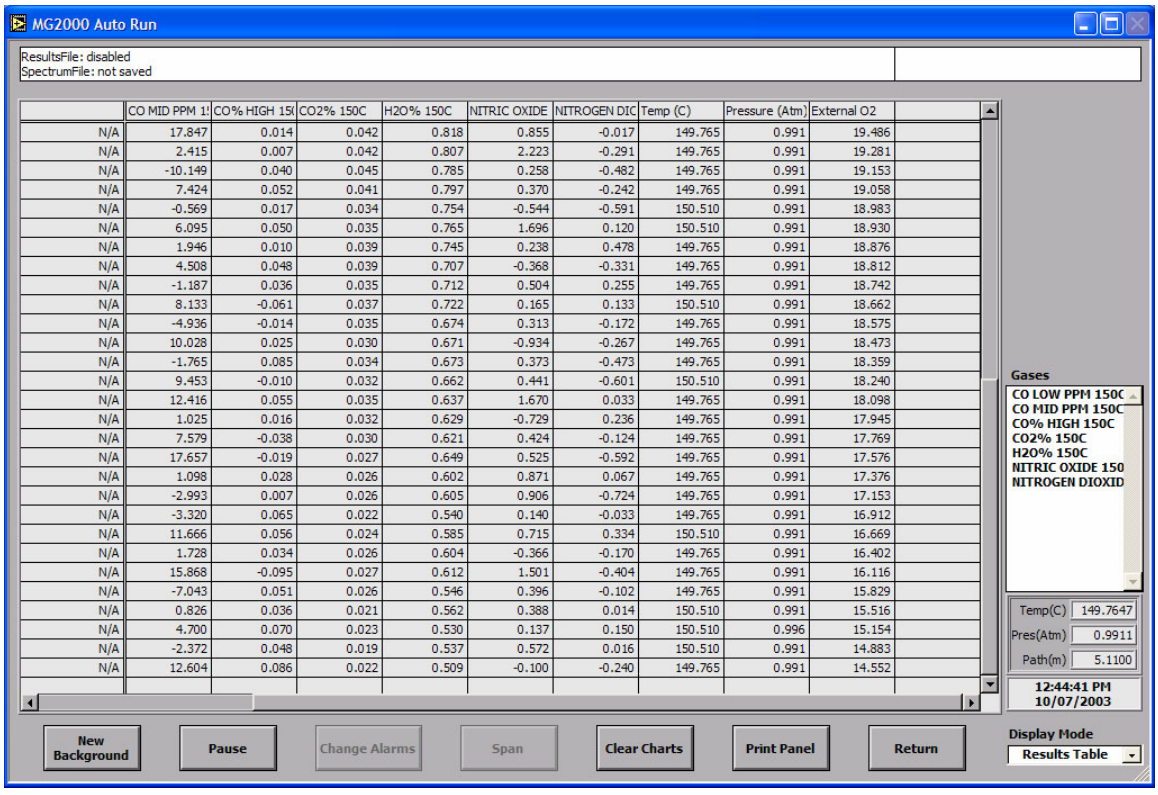

Figure 5: MG2000 Auto Run Data Table Screen

Calibrate Oxygen Sensor Software

The user has the ability to calibrate the oxygen sensor using the MG2000 software. By clicking on the Calibrate button, from the B&B RS232DA Configure Menu, the Oxygen Calibration display appears (Figure 6).

The O_2 Calibration screen shows both the sensor response (above plot) and the current calibration curve (lower plot). The sensor is calibrated by sending several known oxygen concentrations through the MGA and watching for the sensor response to stabilize. For each oxygen concentration an average response is computed and the concentration versus the average response is plotted. Once several points have been collected a polynomial regression can be fitted to the data points to generate a calibration curve. The O_2 Calibration screen can calibrate two oxygen sensors simultaneously if both sensors (internal and external) are connected to the MGA.

To calibrate the integrated oxygen sensor perform the following steps:

1. Click on the calibrate button from the B&B RS232DA Configuration Menu to display the O_2 Calibration screen. The sensor response will begin plotting automatically.
2. Send the first known oxygen concentration through the MGA and watch for the sensor response to stabilize.
3. Once the signal appears stable, click on collect to begin data collection. A green cursor appears on the above plot to indicate the time data collection began. Allow the instrument to collect data for a set time period.
4. Click the collect button again to stop data collection. A red cursor appears on the above plot to indicate the time data collection was stopped.
5. Enter the known oxygen concentration under the Calibration Plot parameters.
6. Click on the Plot Av. button to average the response data between the two colored cursors. The point will displayed in the lower plot.
7. Repeat step 2 through 6 for each known oxygen concentration.
8. Once each point is plotted in the lower plot, click Cal. Poly to compute the best polynomial regression for the current data points. The regression plot will appear in the lower plot overlaying the data points. The Quad, Linear, and Offset parameters are display in the bottom right corner of the screen (Calibration).
9. If satisfied, click done. This exits out of the Calibration screen and displays the calibration parameter in the B&B RS232DA Configuration Menu.

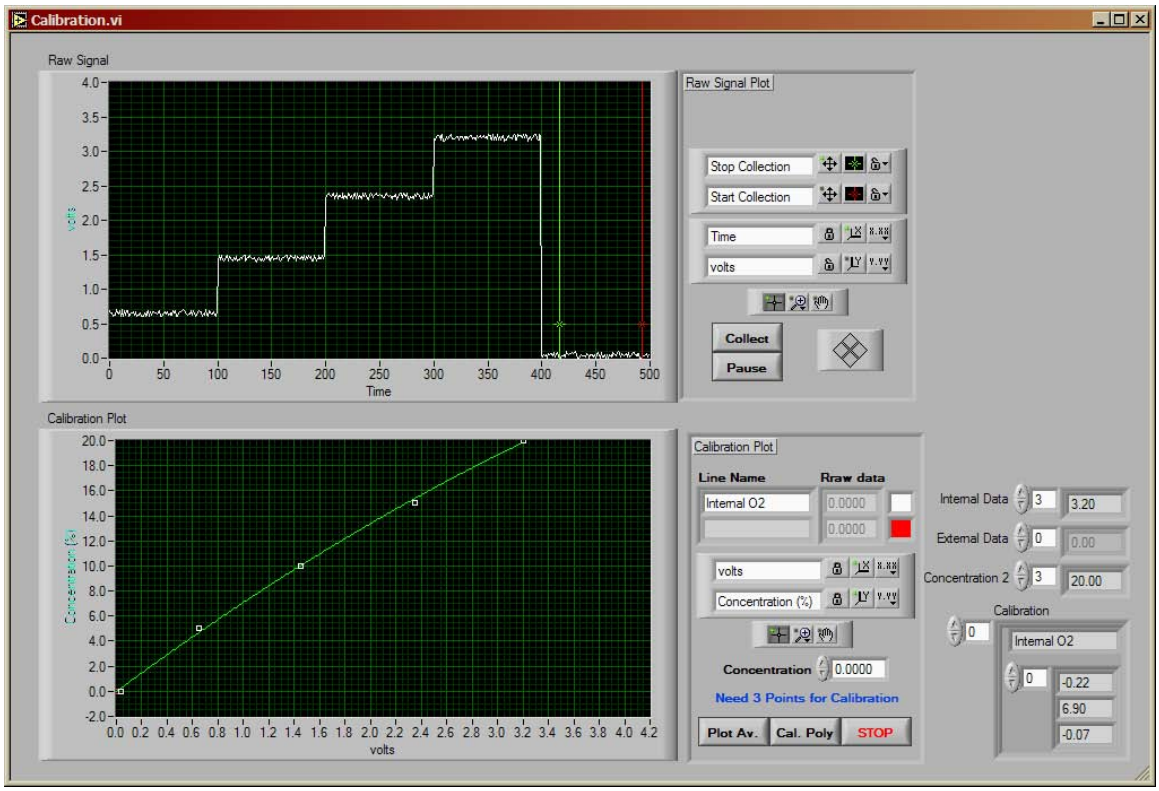

Figure 6: Oxygen Calibration Display

The following table describes the functions of the O_2 Calibration screen:

Function	Description
Signal Response *(plot)*	Plots the signal response for the integrated oxygen sensor. The signal automatically begins plotting when the Calibration screen is loaded.
Signal Plot Parameters *(control cluster)*	Allows the user to adjust the plot parameters (i.e. time scale, response scale, zoom in, zoom out, cursor position, etc). The cluster also identifies the two cursors, the x-axis, the y-axis, and contains the collect and pause buttons. The user can manually adjust the two cursors on the Signal Response Plot to obtain the optimal stable region.

Collect *(button)*	Starts and Stops the data collection for each data point. When the button is click for the first time the green cursor will appear on the Signal Response Plot to indicate the time at which data collection began. The second time the button is clicked data collection stops, indicated by the red cursor.
Pause *(button)*	Stops the signal response from updating.
Calibration Curve *(plot)*	Displays the data points for the integrated oxygen sensor as well as the polynomial regression if computed.
Calibration Curve Parameters *(control cluster)*	Allows the user to adjust the plot parameters (i.e. response scale, concentration scale, zoom in, zoom out, etc.). The cluster identifies the data points and regression curve by color if two sensors are being calibrated. Allows the user to enter the corresponding oxygen concentration, calculate the average signal response, compute the polynomial regression, and exits the Calibration screen.
Concentration *(entered value)*	The software assigns the entered value with the newly average signal responses and plots the data point on the calibration curve. The user needs to manually adjust this value with each known oxygen concentration.
Plot Av. *(button)*	Calculates the average signal response between the two colored cursors and plots the entered concentration vs. the average response for the new data point.
Cal. Poly *(button)*	Calculates the optimal polynomial regression for the current data points.
Calibration *(calibration cluster)*	Displays the calibration parameters for the polynomial regression.

II. MG2000 Gas Calibration Improvements

Advances to the MG2000 software since the MGA has been in existence have come in improvements to the gas calibration files. Improvements to the gas calibration curves have proven to decrease interferences within the quant region caused by other gases, as well as, increase the detection capability (i.e. decrease detection limits) for some particular combustion gases. The following improvements to the gas calibration routine are described in this section:

- Classical Least Squares Routine
- "Picket Fence" Enhancement of the Quant Region
- Determining if CLS and "Picket Fence" are Working Correctly
- Computing Regression Curves to the Calibration Points
- New Gas Calibration Species

Classical Least Squares Routine

In general, any FTIR based instrument measuring complex mixtures such as combustion gases uses a form of classical least squares to reduce the "cross-talk" of interfering gases. This process is nothing new, but gives an initial starting point of where the MGA software was and where it is today in reducing the interfering "cross-talk" within the quant region.

Note  Nitrogen monoxide will be used for all examples since water bands interfere in the preset quant region of NO.

Each gas calibration, found within the MGA library, is divided into several selected regions. Each selected region is a different part of the absorbance spectrum for that particular gas species. One of the selected regions is assigned as the primary region, which the software uses as the quant region to determine the concentration of that particular gas. The primary region is usually determined by selecting a portion of the gas absorbance spectrum where there is little or no interfering gases overlapping in that particular region, while ensuring that the desired gas specie has strong absorption bands within the region. All other preset regions are used for determining their interferences on other gas species. Figure 7 shows the primary quant region for NO (highlighted in blue) along with a water spectrum (red) to illustrate the interference water has within this region. The concentration of the water in figure 7 is approximately 10%, which can be a typical concentration seen within a combustion process.

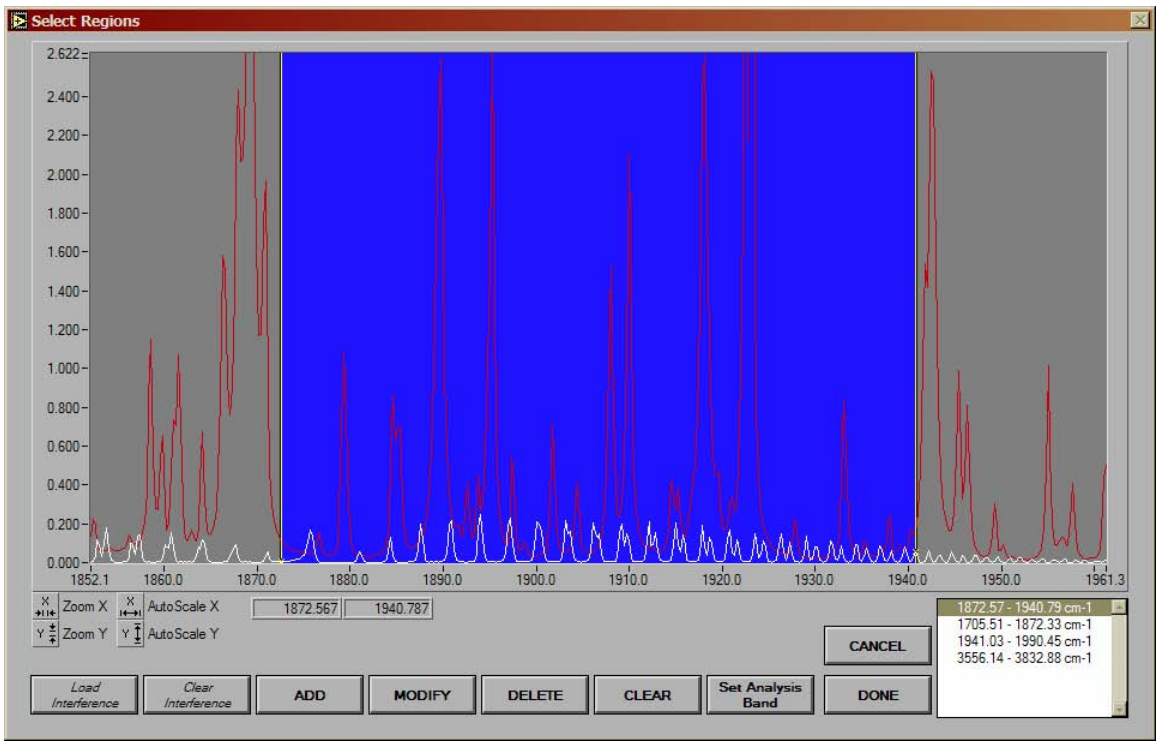

Figure 7: MG2000 Select Quant Region Screen

When the MGA collects data, the resulting absorbance spectrum (which is the sum of all the individual gas absorbance spectra) runs through a classical least squares routine for each reference gas (selected at instrument setup) to reduce the "cross-talk" between interfering gases and the quantifying gas. The CLS routine works by basically determining the absorbance contribution of each interfering gas species within the quant region and subtracts those contributions from the sample spectrum, before determining the concentration for that particular gas.

Since the CLS routine takes into account the entire quant region, the CLS reduces "cross-talk" interferences for all gas species but particularly broad-band absorbing gas species (i.e. NO_2, N_2O, aromatic hydrocarbons, etc.). The limitations to using CLS for reducing "cross-talk" interferences are the following:

1. The CLS routine only reduces the "cross-talk" of interfering gases if the user selects those interfering gases during instrument setup for quantification. For example, the CLS routine will only be able to distinguish between the interfering water bands from the NO absorbance bands within the primary quant region if water is one of the other gases selected for quantification. Therefore, depending upon the application, the user is required to select all probable gas species for quantification to ensure the CLS routine works properly and reduces the "cross-talk" from all interfering gases.
2. Since the user has to select all probable gas species for quantification, the user is limited to the current MGA library. If an interfering gas is not in the

current MGA library, the CLS routine will **not** be able to distinguish between that unknown interfering gas and the desire gas specie, resulting in an error in the calculated concentration.

3. For each gas found in the current MGA library, all of the absorption bands for that particular gas specie must be grouped into one of the several selected regions described above. The CLS routine uses all the selected regions for a particular gas to determine the interferences these regions have all other gases the MGA is measuring. If some absorbance bands are not within a selected region, the CLS routine can not distinguish between these interfering absorbance bands, and a gas that has a primary quant region that overlaps with that region. Figure 8 shows the standard water calibration file found within the current MGA reference library.

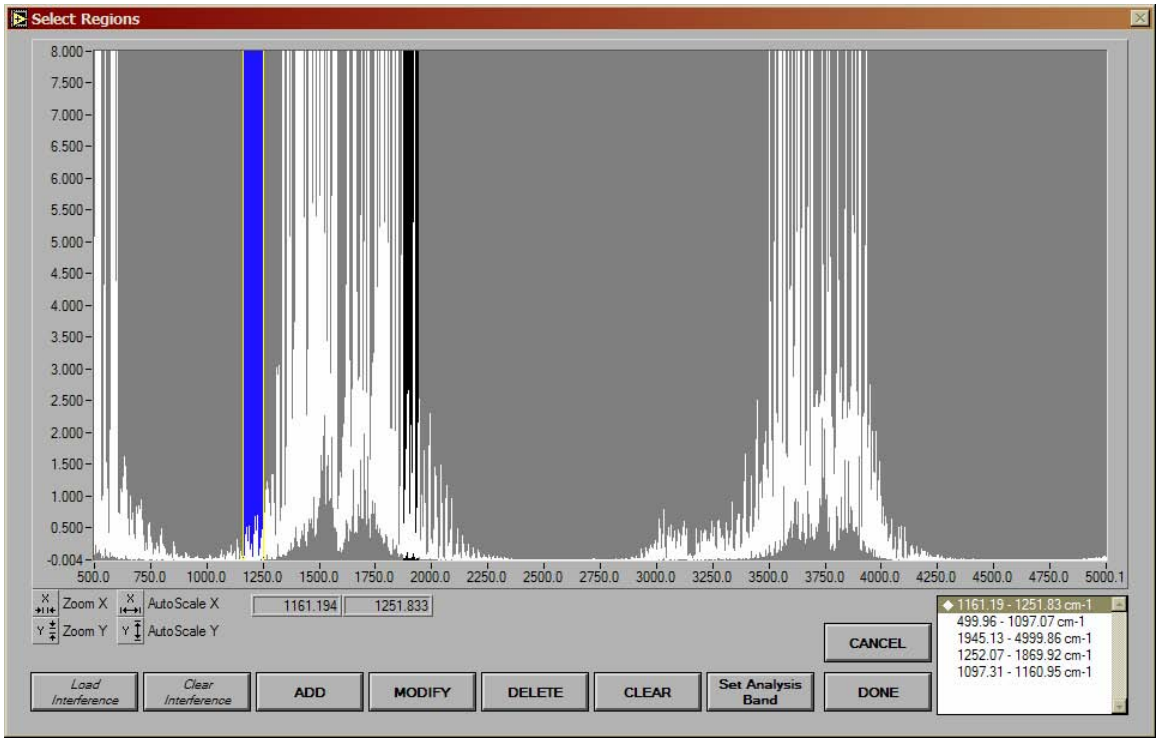

Figure 8: The current water calibration found in the current MGA reference library with the region between 1870 - 1940 cm^{-1} unselected (highlighted with black background).

The blue highlighted region indicates the primary quant region for water and the gray areas indicate all the other selected regions. Note that the black highlighted region between 1870 – 1940 cm^{-1} (the primary quant region for NO) is not selected as a region that water absorbs within for demonstration purposes only. If the MGA software uses figure 8 as the water calibration, the CLS routine will not distinguish the interfering water bands within this region (since it is not a selected region for water) when determining the concentration of NO. For the CLS routine to be able to distinguish the water interference

from NO absorbance bands, the water calibration file must indicate that water absorbs within that region (figure 9).

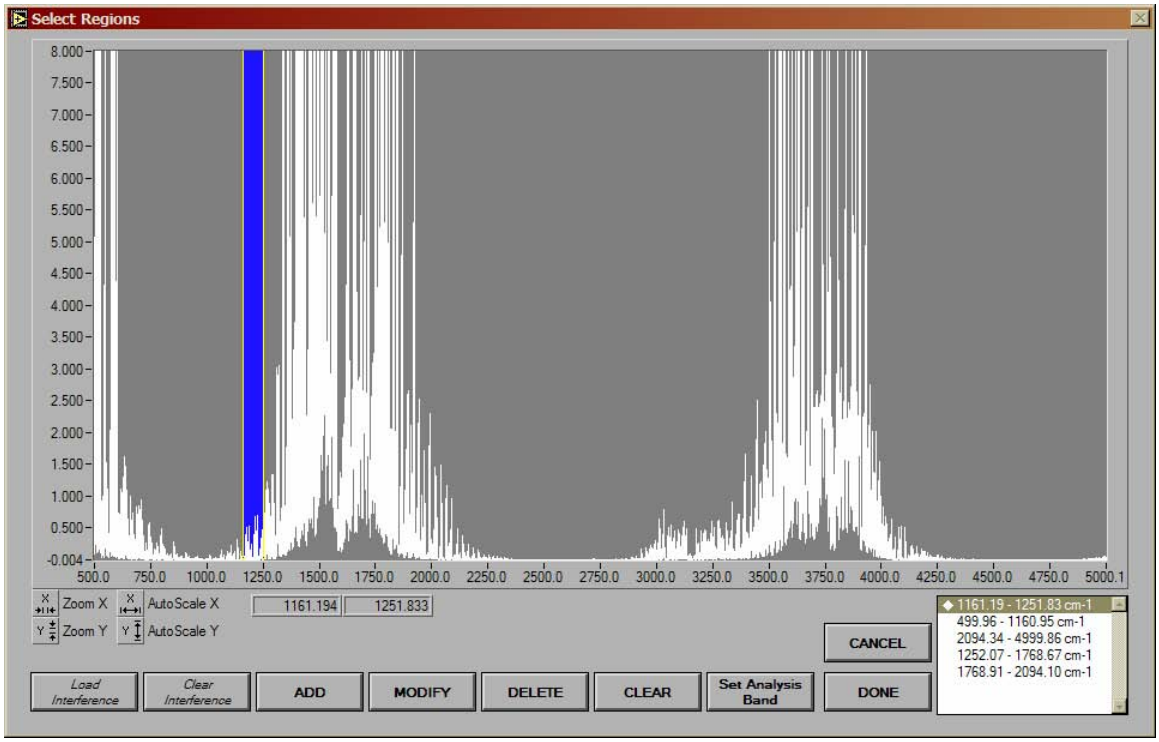

Figure 9: Water calibration spectrum found in the current MGA reference library indicating all selected regions.

"Picket Fence" Enhancement of the Quant Region

An improvement to the CLS routine for reducing "cross-talk" interferences is the addition of the "picket fence" enhancement to the primary quant region. With the "picket fence" enhancement, the MGA software no longer determines gas concentrations using the entire primary quant region, but uses specifically selected absorbance bands within the primary region to calculate concentration. Isolating the gas absorbance bands within the primary region dramatically reduces the possibility of overlapping interference bands, resulting in less "cross-talk" interferences. Therefore the need to rely completely on the CLS routine to eliminate "cross-talk" interferences is reduced. The limitation of using the "picket fence" enhancement option requires the data be collected at a high resolution setting (0.5cm^{-1} resolution), so the software can distinguish between actual absorption bands and interfering bands.

Figure 10 shows the primary quant region for NO with the "picket fence" enhancement. The gray-shaded regions where the interfering water bands appear are regions that the software no longer uses for calculating the concentration. Only the regions highlighted in back are used Comparing Figures 7 and 10 illustrates the dramatic reduction in the water

contribution that the CLS has to distinguish within the primary quant region. In Figure 7 the CLS routine is applied to the entire quant region (shaded in blue) and must distinguish between strong water absorbance bands (red) from weaker NO absorbance bands (white). Figure 10, the CLS routine is applied only to the small regions highlighted in black, where NO absorption bands exhibit good intensity and the small "cross-talk" interferences are only tail-offs of the water bands.

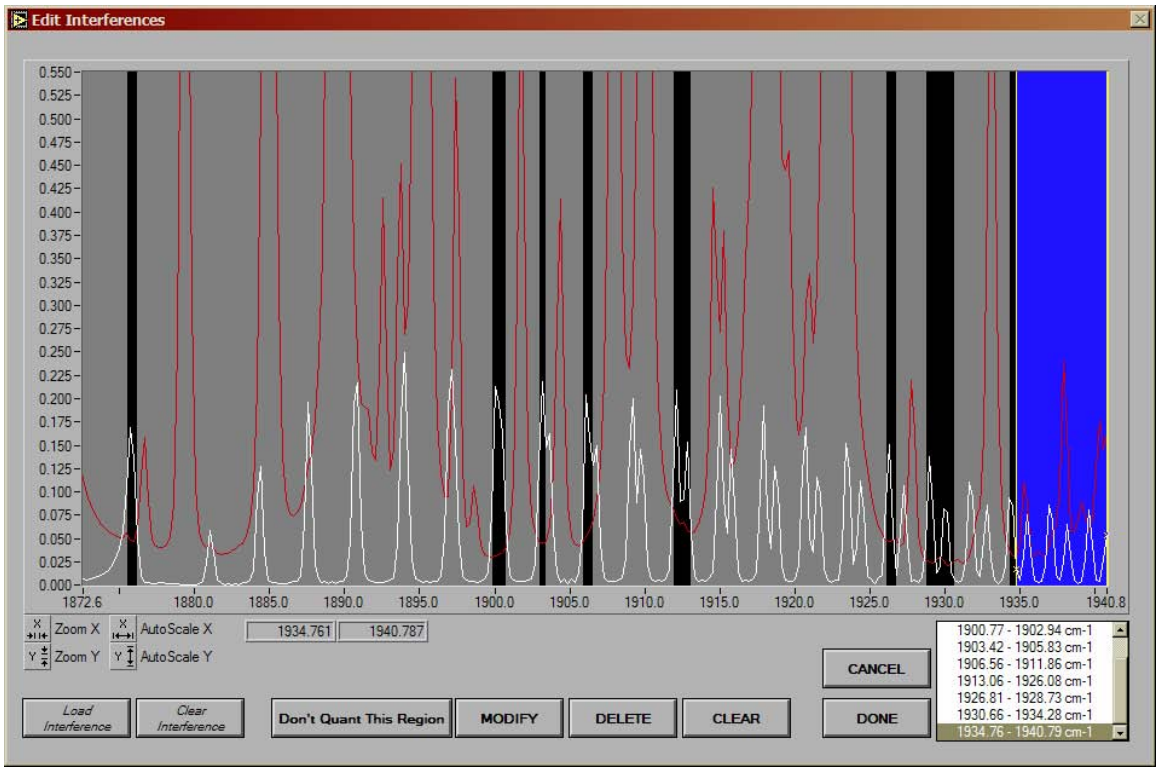

Figure 10: NO primary quant region with the "picket fence" enhancement.

The "picket fence" enhancement has been incorporated into the MG2000 software for the current library of combustion gases. Operators with suitable training can modify the current settings or add settings for new gas species.

Determining if CLS and "Picket Fence" are Working Correctly

The MG2000 software is equipped with a residual check during data collection to determine if the CLS routine and the "picket fence" enhancement are working correctly in reducing "cross-talk" interferences. The "Spectral Resids" screen which can be displayed during data collection or post-test provides an indication of magnitude for interference to each gas selected for quantification. The spectrum display shows all the primary quant regions in different colors to correspond to each gas species. The indication that the CLS routine and "picket fence" enhancement are working correctly is

when the spectral residuals contain minimal absorption bands. Figure 11 shows the high spectral residuals or interferences within the NO primary quant region when the MGA is only measuring for NO (no other gases are selected for quantification) and the calibration file being used by the software does not contain the "picket fence" enhancement. Since there are no other gases selected for quantification and the calibration file does not contain the "picket fence" enhancement, the software **cannot** distinguish between the water bands and actual NO absorption bands. Therefore the water interference bands show up in the spectral residuals within the NO primary quant region.

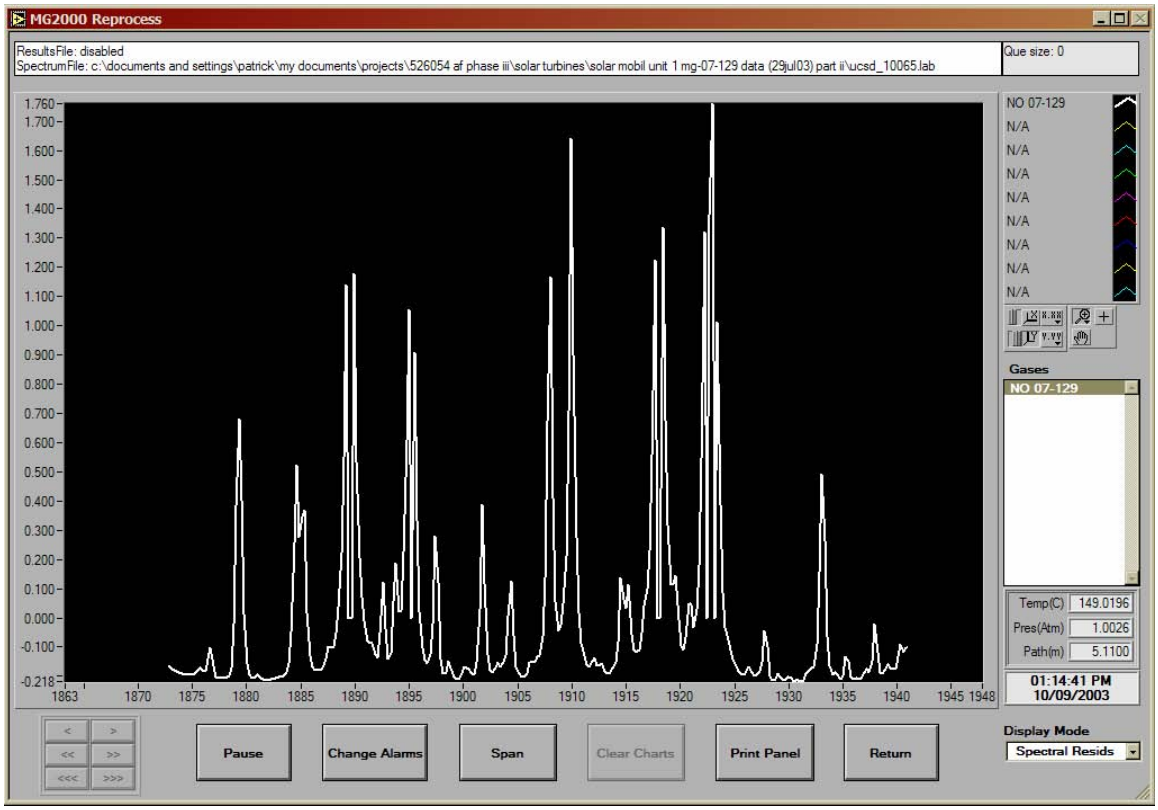

Figure 11: The spectral residuals within the NO primary quant region when the MGA is only measuring for NO (no other gases selected for quantification).

Once the MGA is setup to quantify multiple gas species including NO, the "cross-talk" interferences seen in the spectral residuals for NO (figure 12) are eliminated and the major interference becomes baseline noise. Figure 12 shows the spectral residual display when the MGA is measuring for multiple gas species and using calibration files that contain the "picket fence" enhancement. Comparing figure 12 to 11, the y-axis is identical in both figures to illustrate the absence of the interfering water bands from the spectral residuals for NO (white). The red, blue, green, and yellow regions correspond to NO_2, CO_2, H_2O, and CO, respectively. Figure 12 is a good indication that the CLS routine and the "picket fence" enhancement are working properly to reduce the "cross-talk" interferences when measuring each gas species.

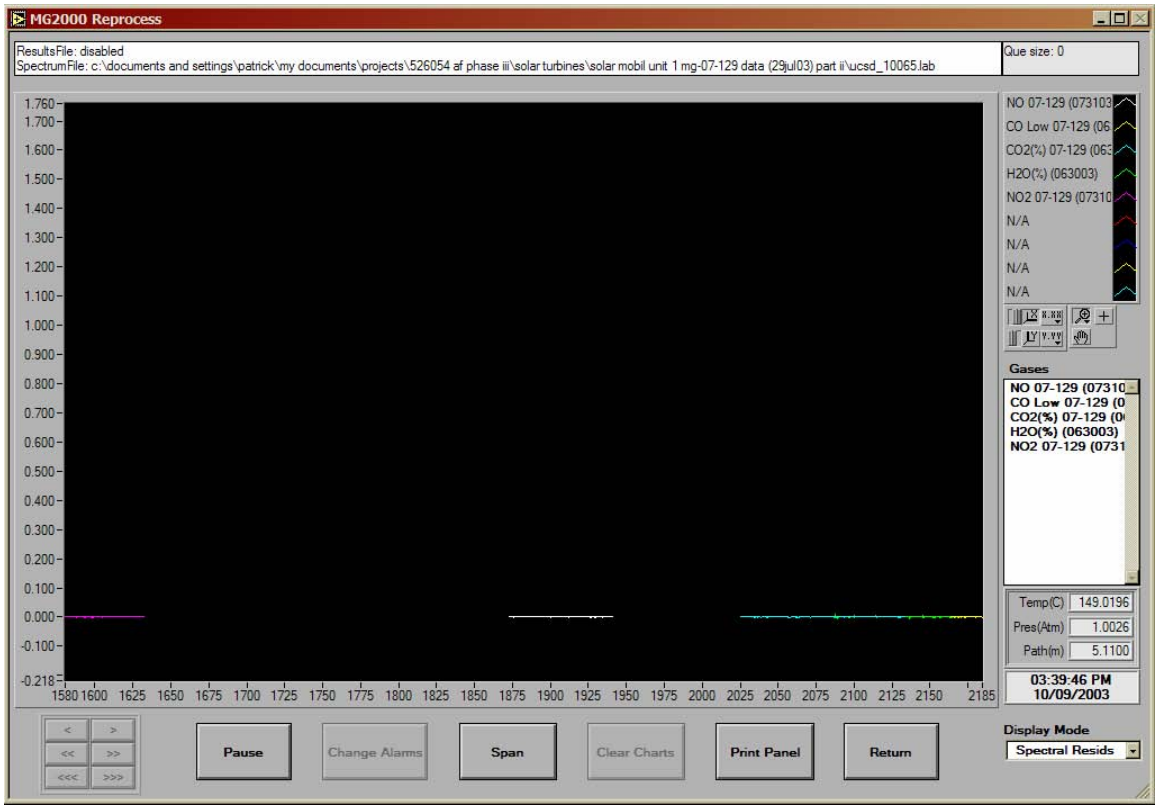

Figure 12: Spectral residuals for multiple gas species that the MGA is setup to measure, including NO (white).

Computing Regression Curves to the Calibration Points

Traditionally, the MGA was only able to compute a cubic spline regression to fit the data points for a particular gas species. Since a cubic spline regression forces the calibration curve to go through each data point, there are some limitations. One, the data points have to follow a smooth curve to ensure the regression curve is smooth, and two, if the data points are too close together the resulting cubic spline regression could contain local random areas of the curve. Figure 13 and 14 are of the same calibration data, but in figure 14 one data point has been altered to induce the random errors that are possible when using a cubic spline fitting.

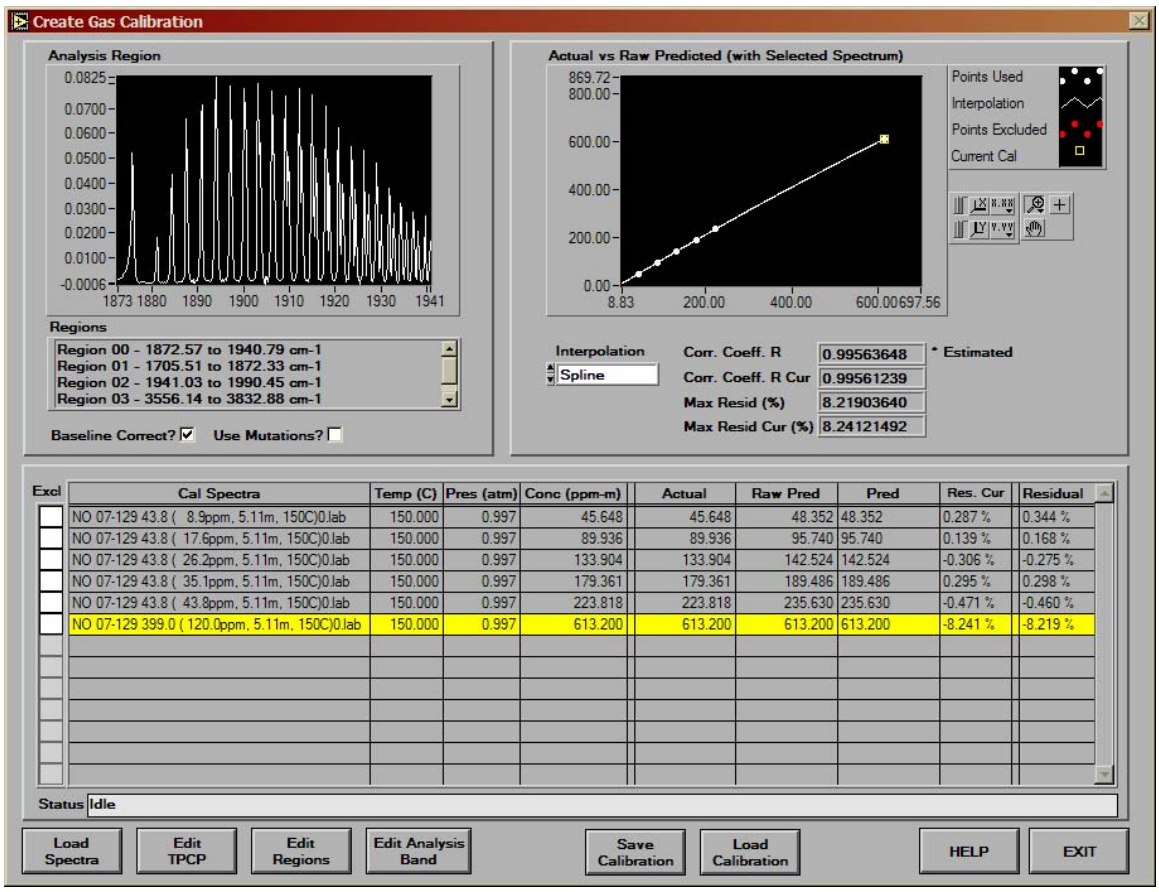

Figure 13: Nitrogen monoxide calibration curve using a cubic spline regression fitting.

The new calibration software also computes the residual error (given in percentage, far right column in figure) for each data point, as well as, the residual curve error (given in percentage, second column from right in figure). The maximum residual error and residual curve error are displayed below the second data plot (Actual vs. Raw Predicted). The maximum values give an indication of how well the regression curve fits the data points. In figure 13, both max. error values are approximately 8.2% indicating that the regression curve fits the data points relatively well. Anything below 10% is considered a decent relationship between the data points and regression curve. Yet, when one point no longer fits a smooth curve, figure 14, the maximum error values are now approximately 413%, well above the accepted error percentage. If the altered data point is de-selected, meaning the software no longer uses this point in fitting a regression curve, the error values drop back into the accepted region (approximately 7%). Figure 15 shows the new calibration curve with the de-selected data point, which is indicated by an "X" in the data table (far left column).

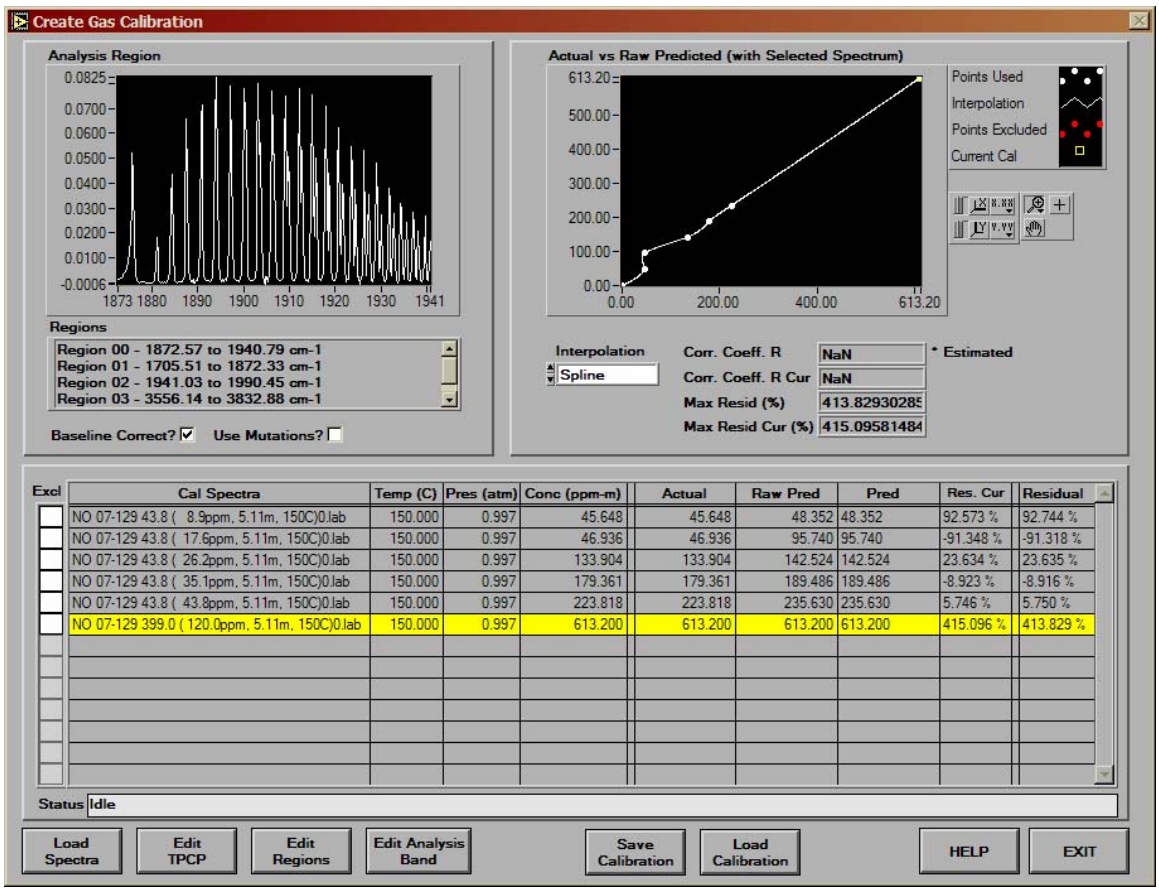

Figure 14: Nitrogen monoxide calibration curve using a cubic spline regression fitting. One of the data points has been adjusted.

Another option the user has available is to use a different regression fitting other than the cubic spline. The new software allows the user to analyze a linear regression curve, as well as, polynomial regressions (up to the 4^{th} degree). These new regression fittings and by de-selecting data points allow the user to generate the best calibration curves for each gas species. For example, taking the calibration curve shown in figure 15 and changing from a cubic spline regression to a quadratic the error values now drop to approximately 1.75%.

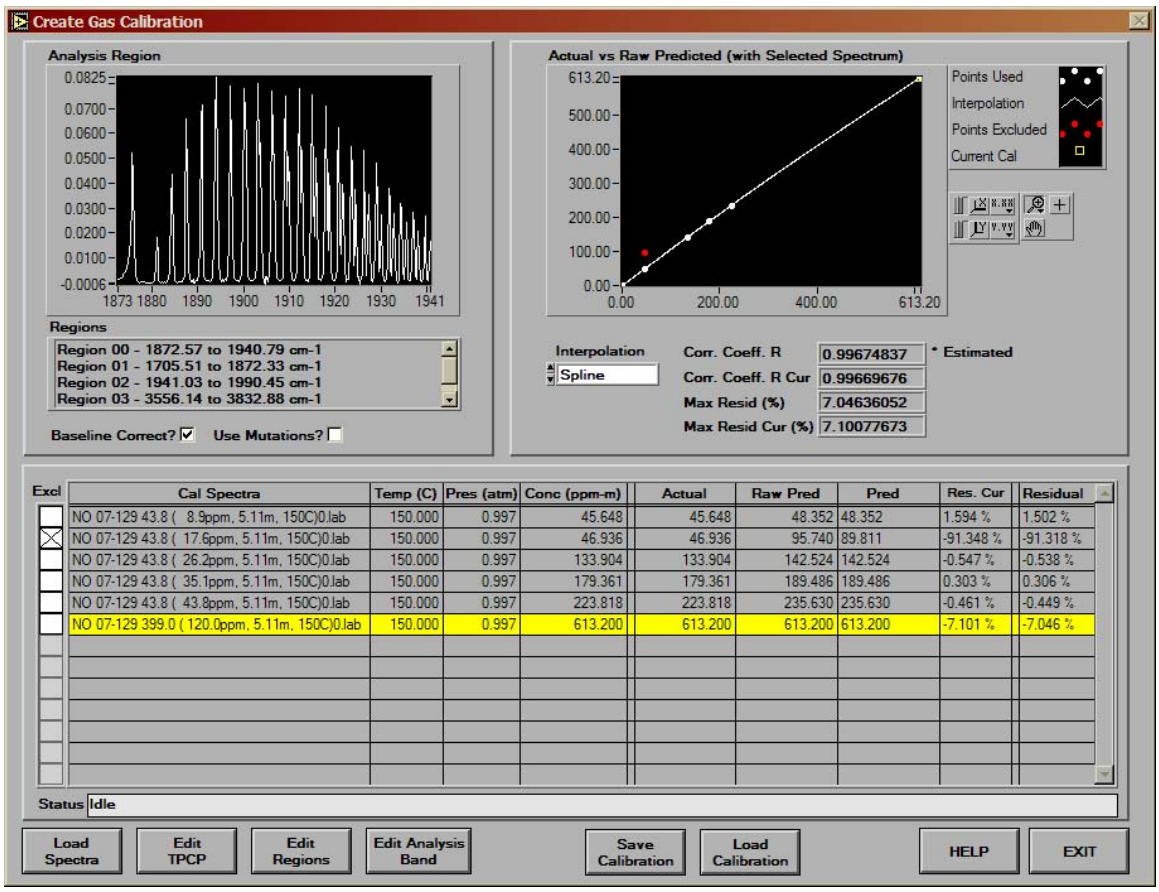

Figure 15: Nitrogen monoxide calibration point using a cubic spline regression fitting. The second data point has been de-selected.

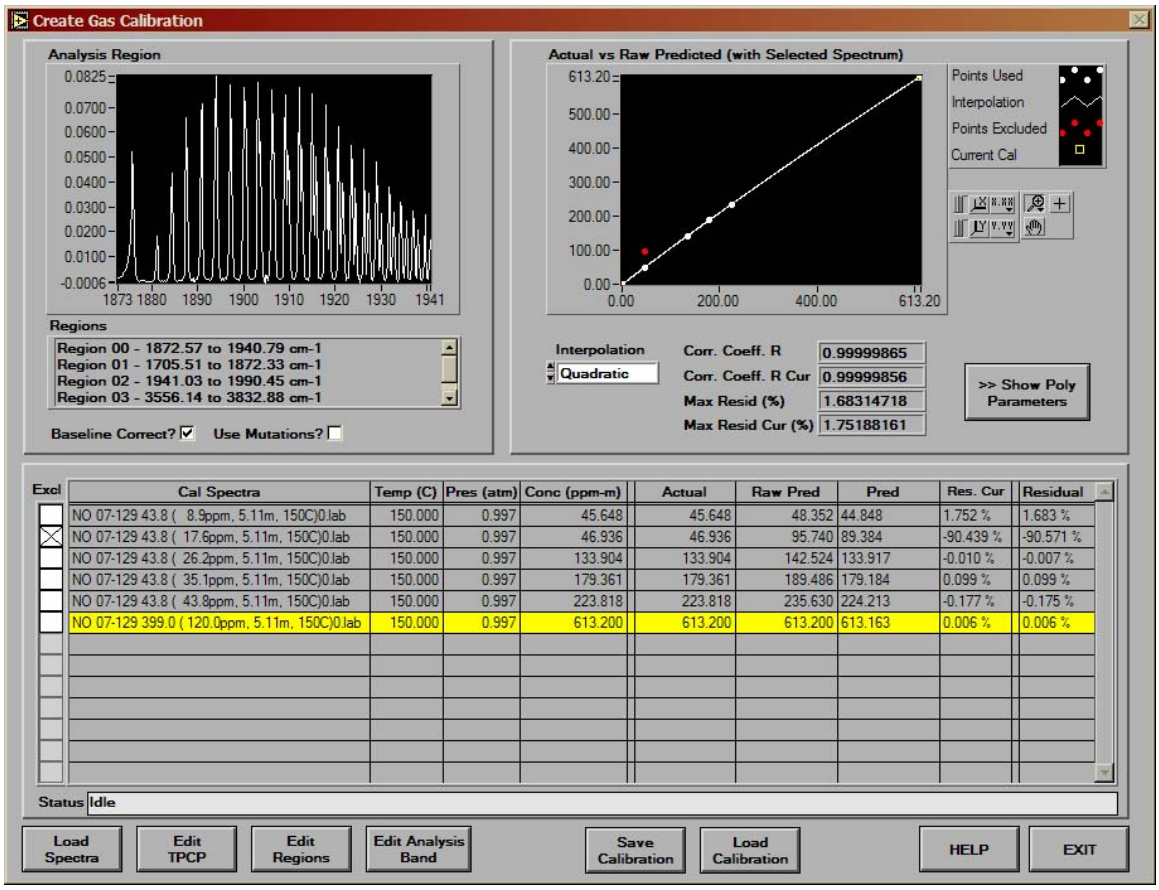

Figure 16: Nitrogen monoxide calibration curve using a quadratic regression fitting. The second data point has been de-selected.

New Gas Calibration Species

New gas calibration species recently introduced into the MGA library by MKS has been mainly limited to gas species typically needed for measurement applications in the semiconductor industry. For combustion applications the highest necessity from AFR's standpoint is on hydrocarbon speciation. Unfortunately, the majority of hydrocarbons seen in liquid fuel combustion applications are hydrocarbons that fall within the C_6 and higher families. Therefore, obtaining accurate gas calibration files for these species has been slow since they are predominantly liquids at room temperature.

AFR has recently evaluated a pulse free syringe pump that was tested using ethylene glycol for generating a calibration curve. The ethylene glycol was injected into a 150°C N_2 gas stream at different flow rates (ranging from µL to mL) to obtain several data points of varying concentrations of ethylene glycol. Figure 17 shows the calibration curve that was generated using these data points, which contains a relatively small residual error. This new calibration curve has been added to the MGA library. The syringe pump has since been ordered along with other components to build a flow

injection system to further add to the MGA library and potentially improve the capability for speciation of hydrocarbons.

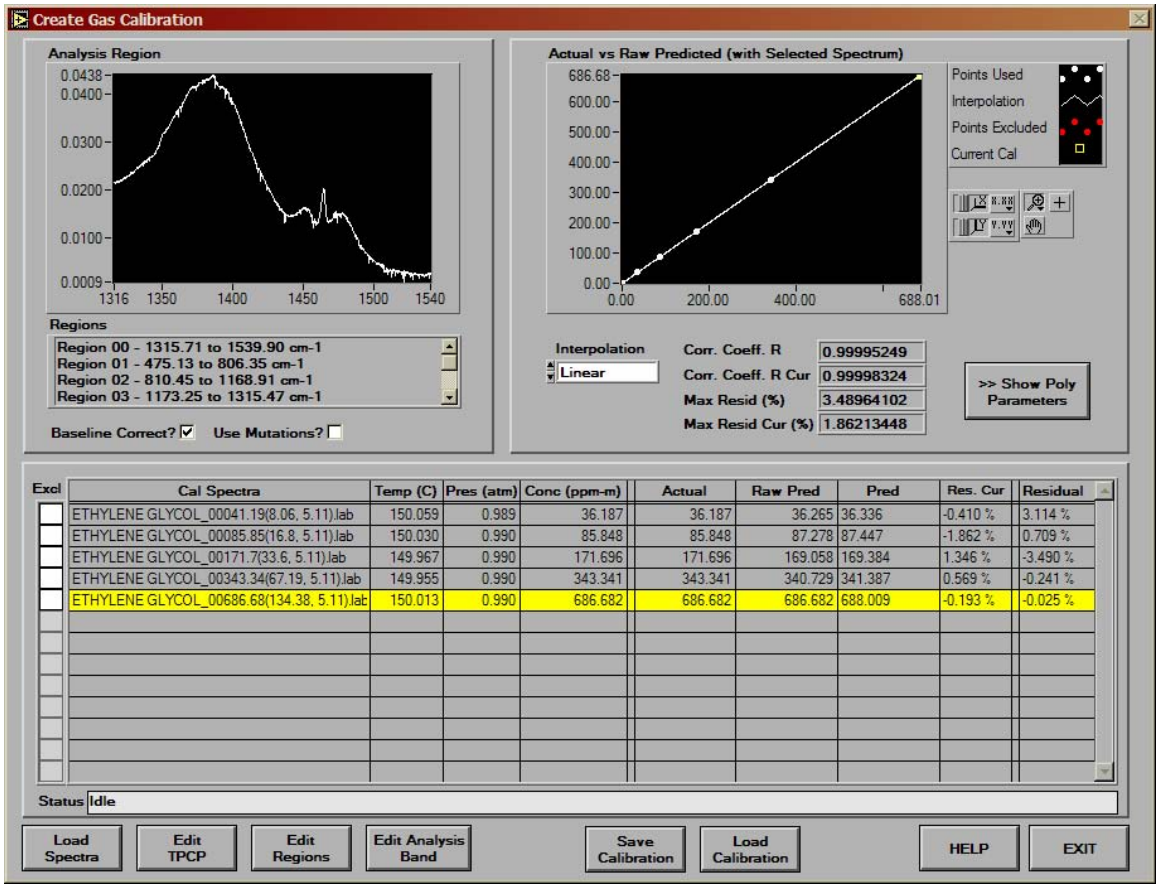

Figure 17: Ethylene glycol calibration curve using a cubic spline regression fitting.

Appendix D

Aerospace Information Report (AIR) 5917 Submitted by ATA/AEDC to the SAE Committee E-31 on 8 June 2004

SAE Aerospace
An SAE International Group

AEROSPACE INFORMATION REPORT

SAE AIR5917draft4

REV. X

Issue date
5-27-04
Proposed draft no.4

MEASUREMENT OF GASEOUS EMISSIONS FROM AIRCRAFT TURBINE ENGINES USING EXTRACTIVE FTIR GAS ANALYSIS

E31 Committee working draft-----do not cite or quote

FOREWORD

Fourier transform infrared (FTIR) analyzers measure gaseous emissions from combustion sources with significant improvement in precision. This results in improved overall accuracy over the present non-dispersive infrared (NDIR) and chemiluminescent type analyzers required by regulatory agencies. Equally important, FTIR analyzers provide almost real time data which results in substantial savings in testing costs.

This Aerospace Information Report (AIR) summarizes experience in the use of FTIR instruments in measuring turbine engine and combustion rig exhaust effluents using a protocol similar to the one meeting the measurement requirements of aviation governing bodies (FAA, ICAO, USAF, USN). This report is intended to provide a basis for the generation of an Aerospace Recommended Practice describing the use of the FTIR analyzer system to measure exhaust emissions from aircraft turbine engines.

TABLE OF CONTENTS

1. SCOPE

This Aerospace Information Report describes the continuous sampling and analysis of gaseous emissions from aircraft gas turbine engines and combustion rigs using gas analyzer systems that contain one or more Fourier transform infrared (FTIR) instruments. The use of FTIR analyzers is shown to be a suitable and cost effective equivalent to NDIR and chemiluminescent analyzers as defined in SAE ARP 1256B for the measurement of CO, CO_2, NO, and NO_2. These FTIR analyzers would also be suitable for use in emission testing to meet the U.S. EPA standards as defined in 40 CFR 87 through ICAO Annex 16 Vol. II.

2. REFERENCES, DEFINITIONS, TERMINOLOGY

2.1 SAE Publications. Available from SAE, 400 Commonwealth Drive, Warrendale, PA 15096-0001

2.1.1 ARP1256B Procedure for the Continuous Sampling and Measurement of Gaseous Emissions from Aircraft Turbine Engines

2.1.2 ARP1533A Procedure for the Calculation of Gaseous Emissions from Gas Turbine Engines

2.2 Other Applicable References:

2.2.1 General References. The following general references are provided for information purposes only and are not a required part of this SAE Aerospace Information Report.

ICAO Annex 16, Vol. 11, “Aircraft Engine Emission,” 2nd Ed. (July 1993).

Griffiths, P.R. and deHaseth, J.J., “Fourier Transform Infrared Spectrometry,” Wiley Interscience, New York.

Spellicy, R.L., "Challenges to CLS Analysis in the Real World," presented at the National Air & Waste Management Association (AWMA) conference, Salt Lake City, Utah (June 18-22, 2000).

14 CFR Part 34, Fuel Venting and Exhaust Emissions Requirements for Turbine Engine Powered Airplanes, Federal Register Vol. 64, Number 22, 1999.

40 CFR, Part 87 (1997). Control of Air Pollution from Aircraft and Aircraft Engines; Emission Standards and Test Procedures, Federal Register, Vol. 62, Number 89, p. 25355-25367, May 8, 1997.

2.2.2 Literature cited. The following literature is called out in this report.

1. ASTM Standard D 6348 – Revision #1: Standard Test Method for Determination of Gaseous Compounds by Extractive Direct Interface Fourier Transform Infrared (FTIR) Spectroscopy (March 2000).

2. "Energy Conserving Tool for Combustion Dependent Industries," Final Technical report for U.S. Department of Energy, Grant No. DE-FG41-R110915, October 2002.

3. "EPA Protocol for the Use of Extractive Fourier Transform Infrared (FTIR) Spectrometry in the Analysis of Gas from Stationary Industrial Sources," EPA document, Emission Measurement Technical Information Center Bulletin Board, 1995.

4. Gardner, D.G., Zaccardi, V.A., Jalbert, P.A., and Bryant, M.D., "Reducing the Cost of Aircraft Engine Emission Measurements," ISA Vol. 443, Paper 2302/IIS03-P081 (2003).

5. Jalbert, P. and Zaccardi, V., "Improved Methodology for Turbine Engine Emissions Measurement," IGTI Paper No. GT-2002-30306 (2002).

6. Jalbert, P.A., Zaccardi, V.A., Bryant, M.D., Winkleman, B.C., Markham, J.R., Bush, P.M., and Bonzani, P.J., "Rapid, Complete Nozzle Exhaust Gas Measurement Capability for Gas Turbine Engines," submitted for presentation and publication at the 50th International Instrumentation Symposium of ISA, San Antonio, TX (May 9-13, 2004).

7. Markham, J.R., Bush, P.M., Bonzani, P.J., Scire, J.J., Zaccardi, V.A., Jalbert, P.A., Bryant, M.D., and Gardner, D.G., "Integrated Gas Analyzer for Complete Monitoring of Turbine Engine Test Cells," Applied Spectroscopy, Volume 58, Number 1, 2004.

8. Marran, D., Kenny, P., Markham, J., Jalbert, P., Moyers, R. and Gardner, D., "The Application of FTIR Spectroscopy to Turbine Engine Exhaust Monitoring," AIAA Paper 2000-2211 (2000).

9. McIntosh, B.C. "Fourier Transform Infrared (FTIR) Analyzers," Chapter 29, Analytical Instrumentation, Instrument Society of America, 1996.

10. Oliver, W., Marran, D.F., Spartz, M.L., Lee, J.C.Y. , and Nazeer, W., "Evaluation of the MKS On-Line FTIR MultiGas Analyzer for Gas Turbine Applications," ASME/IGTI Paper GT-2003-38656 (2003).

11. "Procedure for the Continuous Sampling and Measurement of Gaseous Emissions from Aircraft Turbine Engines," Aerospace Recommended Practice ARP1256, Rev. B, Society of Automotive Engineers, Warrendale, PA, August 1990.

12. Unpublished results of U.S. Air Force Contract # C-F40600-02-C-0018.

2.3 Definitions and Terminology

2.3.1 Definitions and terminology specified in ARP1256B are applicable in this AIR.

2.3.2 Other definitions and terminology.

ABSORBANCE SPECTRUM: The resultant spectrum calculated from the negative logarithm of the quotient resulting from dividing the sample spectrum by the background spectrum.

BACKGROUND SPECTRUM: The spectrum taken in the absence of absorbing species or sample gas, typically conducted using dry nitrogen or zero air in the gas sampling cell.

ELECTROMAGNETIC SPECTRUM: The total set of all possible frequencies of electromagnetic radiation.

EXTRACTIVE FTIR: A means of employing FTIR to quantify concentrations of gaseous emissions. It consists of extracting an exhaust gas sample from the combustion exhaust stream and directing this sample to an FTIR gas-sampling cell without collection on sample media.

FTIR An abbreviation for Fourier transform infrared. Typically used as the short form of FTIR spectrometer: a spectroscopic instrument using the infrared portion of the electromagnetic spectrum. Also used as the short form of the method, FTIR spectrometry. For an in-depth description of FTIR, see Griffith and deHaseth, Section 2.2.1.

FTIR GAS SAMPLING CELL: The chamber of an FTIR where the gas sample is passed through and exposed to the infrared portion of the electromagnetic spectrum for measurement.

INFRARED PORTION OF THE ELECTROMAGNETIC SPECTRUM: The portion of the electromagnetic spectrum from about 20 cm-1 (500 microns) to about 12,500 cm-1 (0.8 microns).

SAMPLE SPECTRUM: The spectrum taken with the presence of absorbing species or sample gas in the gas-sampling cell.

SINGLE GAS ANALYZERS: Generalized description of the separate analytical instruments described in ARP1256B for measuring gaseous emissions from aircraft turbine engines.

SPECTRAL RESOLUTION: The minimum separation that two spectral features can have and still, in some manner, be distinguished from one another. The quality of the spectrum – the amount of spectral detail – increases as the number of resolution elements becomes larger or the frequency intervals between measurements become smaller.

WAVE NUMBER: The number of electromagnetic waves per centimeter. This term has units of reciprocal centimeters (cm-1) and is proportional to frequency.

3. INTRODUCTION

3.1 Background

ICAO gaseous emission measurement requirements for aircraft gas turbines are derived from SAE Aerospace Recommended Practice 1256B (Ref 11) and must be followed during emission certification testing. Cost analysis has shown that making these measurements is expensive in equipment, and in installation, test cell operation, and test analysis time. Marran et al (Ref 8) describes how turbine engine exhaust, using the methods called out in ARP1256B, is typically measured using an array of single gas analyzers. In the same test series, an FTIR gas analyzer was demonstrated to measure simultaneously the required concentrations of H_2O, CO_2, CO, NO, and NO_2. Methane, formaldehyde, ethylene, propylene, methanol, sulfur dioxide, formic acid, and nitrous acid were also measured by the FTIR analyzer. These tests showed how FTIR spectroscopy was demonstrated to have lower detection limits and provide the quantification of more compounds while offering a space saving and lower cost alternative to using an array of single gas analyzers. (Ref 4,7,10)

3.2 FTIR Analyzers

FTIR instruments have been used for over 40 years in research and industry to measure and control the concentration of specific gaseous compounds including the exhaust gases from stationary combustion sources (Ref 9). These instruments are well developed and commercially available. They operate on the principle that most molecules in gas phase show unique gas absorption spectra to mid-range infrared light. This IR absorption is related to concentration and is measured and recorded for multiple compounds simultaneously.

An FTIR can replace the suite of nondispersive infrared (NDIR) and chemiluminescent instruments required for most current exhaust emission measurement by ARP1256B (Ref 11).

An FTIR analyzer offers the capability to:

1. simultaneously measure CO, CO_2, NO, and NO_2 in a single instrument

2. measure other infrared-active gases if required

3. distinguish and quantify individual hydrocarbon species that are a subset of the total hydrocarbons (see below)

4. provide near real-time measurement and evaluation of exhaust constituents

5. measure wet exhaust gas

6. measure at concentrations far below that of the NDIR instruments currently used

3.3 Measurement of Total Hydrocarbons

The measurement of total hydrocarbons from aircraft gas turbine exhaust using an FTIR analyzer is under development. Results to date show considerable promise. A large number of the species present in exhaust have been identified and more are being determined as work progresses. The concentration of each of these species can be measured precisely with an FTIR analyzer providing the spectral data for each specie has been entered into the analyzer library. Total hydrocarbons as measured by FTIR would consist of the sum of all the species that were detected.

The measurement of total hydrocarbons as required by ARP1256B uses a flame ionization detector (FID). This instrument measures the sum of hydrocarbon ions present in the exhaust sample but under-measures some species, particularly halogenated and oxygenated hydrocarbons. Total hydrocarbons measured by FID is the sum of all the species detected but is reduced by the instrument's failure to measure oxygenates (aldehydes for example) accurately.

Work to obtain a useful correlation between the two measurement methods is proceeding with results expected in about one year.

3.4 Intent of this AIR

The intent of this AIR is to document the use of FTIR gas analyzer instrumentation so that the FTIR method may be included in an Aerospace Recommended Practice. Adoption of FTIR instruments in a measurement practice will reduce the number of analyzers needed, provide the capability to measure more gas species than present instrumentation, and allow a major reduction in test and analysis time.

4. MEASUREMENT METHOD

4.1 Background

FTIR analyzers measure the chemical composition of solids, liquids, and gases throughout industry. These analyzers have been used in laboratories since the 1960s, in process industries since the mid 1980s and to measure compounds in the effluent of stationary

combustion sources for the last 10 years. Their application range is extremely broad and extends from analyzing toxic gases in air in parts per billion to determining percentages of components in solids. (Ref 9)

FTIR instruments provide the fundamental and unique response to infrared radiation of each compound simultaneously. Because of the FTIR analyzer's rapid response, emission tests can be run during performance and other routine engine testing. FTIR measurement speed depends on instrument type along with spectral resolution and signal averaging settings. Depending on the instrument, the speed of measurement can vary from one measurement per fraction of a second to one every several minutes. Speed of measurement is a major advantage and allows FTIR analyzers to be used for process control. The ability to measure many compounds simultaneously is another advantage that allows one instrument to be used in place of many.

4.2 Principle of Measurement

FTIR gas analysis is a full spectroscopic technique that makes it possible to monitor many species simultaneously in a single instrument. Every molecule except homonuclear diatomic molecules (oxygen for example) has a unique set of rotational and vibrational frequencies that absorb and emit infrared energy in a characteristic manner. In general, it is possible to identify and quantify gases based on the location and magnitude of molecular absorptions. Since an FTIR spectrometer is capable of detecting the absorption of infrared wavelengths from approximately 500 to 7700 wave numbers (20 to 1.3 micrometers), it is capable of identifying an almost unlimited variety of compounds. (Ref 8) Figure 1 shows a composite infrared spectrum of many of the compounds detected in a gas turbine exhaust using an FTIR analyzer.

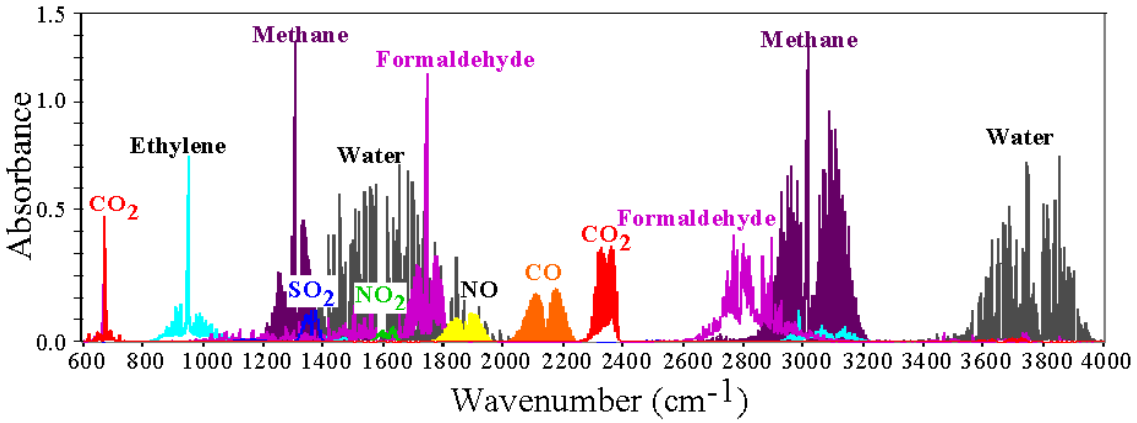

Figure 1. Composite infrared spectrum indicating many of the compounds in gas turbine exhaust detected by FTIR spectroscopy.

For FTIR analyzers used in measuring gas turbine exhaust components, the gas is extracted and brought to a specifically designed sample cell. A mid-range infrared beam is directed through the exhaust, producing the spectral pattern related to the concentration of each component of the exhaust. Such analyzers consist of:

- a source of mid-infrared radiation
- an interferometer
- an enclosed sample cell of known absorption path-length, temperature, and pressure
- an infrared detector
- optical elements for the transfer of infrared radiation between components
- gas flow control and measurement components
- a computer

Adjunct and integral computer systems are used for controlling the instrument, processing the signal, and performing Fourier transforms and quantitative analyses of the spectral data.

The absorption of pure gases and of mixtures of gases are described by Beer's Law. Using this law, modern FTIR systems use computerized analytical programs to quantify compounds by comparing the absorption spectra of known (reference) gas samples to the absorption spectrum of the sample gas. Some standard mathematical techniques used for comparisons are classical least squares, inverse least squares, cross-correlation, factor analysis, and partial least squares. Additional details describing the operating principles of FTIR analyzers are give in the EPA Protocols (Ref 3), the ISA text Analytical Instrumentation (Ref 9) and in the ASTM Standard Test Method D6348 (Ref 1).

4.3 Precision

ARP1256B defines precision as "The closeness with which a measurement upon a given, invariant sample can be reproduced in short-term repetitions of the measurement with no intervening analyzer adjustment." FTIR analyzers when properly handled and used exhibit high precision (Ref 12).

Figure 2 shows data measured right after installation of an FTIR analyzer over a period of 10 minutes at 40-second intervals. A background spectrum was taken before the first data point and used for all data points taken over the 10 minutes. The measured sample was a certified calibration gas mixture of 20.1 ppm ± 2% NO in dry nitrogen. The horizontal lines in the plot indicate the certified ± 2% concentration range for NO in the gas mixture. Two observations can be made of these data: (1)The independently calibrated FTIR analyzer falls comfortably within the ± 2% range of the certified calibration gas, and (2) the precision of the measurement is very close with very little variation (standard deviation of 0.04 ppm.)

Also plotted in the figure are data points for the measured summary concentration of NO and NO_2. The FTIR analyzer consistently detected trace amounts of NO_2 (<0.1 ppm) even though NO_2 was not specified by the manufacturer of the gas mixture. The trace amount of NO_2 detected was confirmed to be present by visual examination of the measured absorbence spectra.

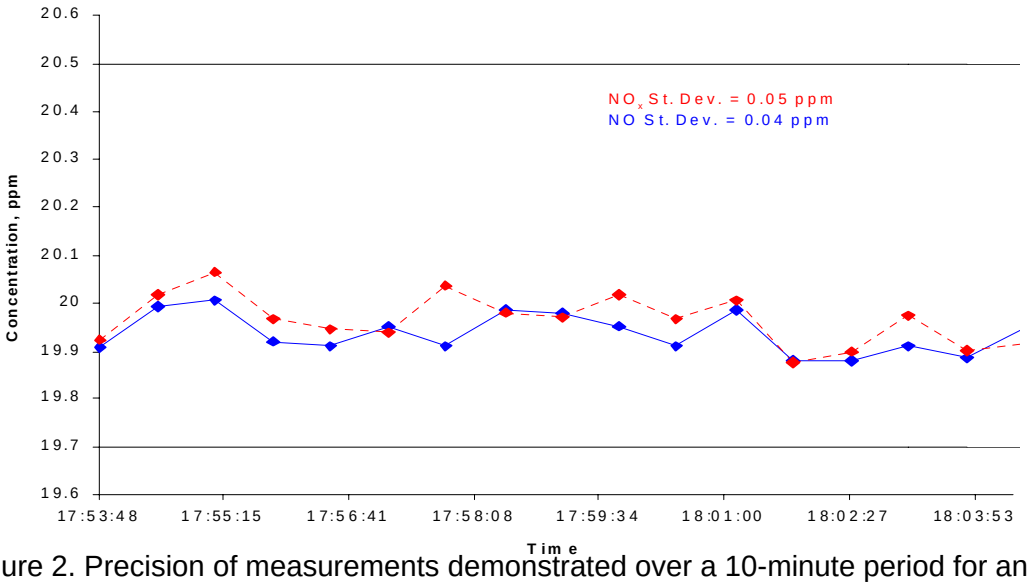

Figure 2. Precision of measurements demonstrated over a 10-minute period for an FTIR analyzer measuring a certified gas mixture containing 20.1 ppm ± 2% of NO.

Figure 3 shows data measured with the same FTIR analyzer and the same certified gas mixture over a period of 9 days. A background spectrum was taken before the first data point and used for all data points taken. Averaging these five NO data points (solid trace) results in a deviation of 0.05 ppm. Also plotted in the figure are data points for the measured summary concentration of NO and NO_2 = NO_x (dotted trace). The measured NO_2 is greater than that shown in Figure 2 for the same bottle of gas. The 9-day test used a longer gas transport line made of Teflon® than the earlier 10-minute test. It was assumed that the ambient water vapor diffusion through the Teflon® resulted in a conversion reaction of NO to NO_2. In Figures 2 and 3, the NO concentrations reported are within the ± 2% limits for the certified mixture. The total NO_x concentrations reported by the FTIR analyzer show a close correspondence to the 20.1-ppm label on the bottle.

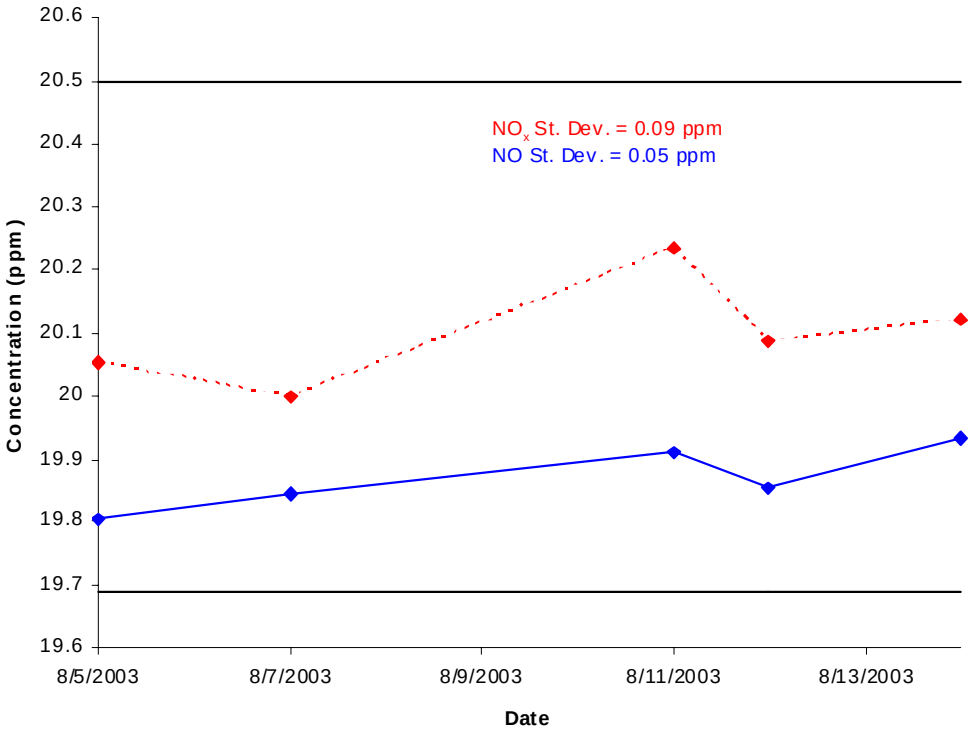

Figure 3. Precision of measurements demonstrated over a 9-day period for an FTIR gas analyzer measuring a certified gas mixture containing 20.1 ppm ± 2% of NO. NO (solid trace) and total NO_x (dotted trace) measurements are shown.

4.4 Detection Limits

Table 1 exhibits detection limits for an FTIR analyzer for a 0.5 cm-1 resolution that results in a 2-second measurement time. (Ref 10) These values are at or below the current detection limits for NDIR and chemiluminescent instruments used in ARP1256B.

Table 1. Detection limits for the species measured by an FTIR analyzer for a 2-second measurement time (0.5 cm^{-1} resolution).

Species	Detection Limits
NO	0.41 ppmv
NO_2	0.19 ppmv
CO	0.10 ppmv
CO_2	0.003%
H_2O	0.018%
CH_4	0.14 ppmv
H_2CO	0.29 ppmv
N_2O	0.12 ppmv
SO_2	0.30 ppmv
NH_3	0.070 ppmv

Increasing the measurement time will reduce the detection limits. Detection limits for other scan times can be estimated using the following equation:

$$DL(T) \approx DL(2)\sqrt{\frac{2}{T}}$$

Where DL (T) is the detection limit for a T second scan time and DL (2) is the detection limit reported in Table 1 for a 2-second scan time.

The detection limits posted in Table 1 are applicable to a dry sample stream but will be very similar in a sample stream of high water vapor content because of the analysis algorithms used. FTIR analyzers are well suited to monitor many species simultaneously over a very wide concentration range, from parts per billion to percent, even in sample streams with up to 30% water.

4.5 Application to Gas Turbine Engine Emission Measurements

For the measurement of gas turbine exhaust constituents, one or more extractive FTIR analyzers are integrated into a measurement system consisting of a sampling probe, sample transport line, flow controller, and a data recording and analysis computer. The samples are analyzed wet. The concentration values for NO, NO_2, CO, CO_2, SO_2, H_2O, and major hydrocarbon species can be read directly from the screen within a few seconds of sampling. An entire traverse based on ARP1256B point-to-point spacing can be run in five minutes or less. Emission measurement parameters can be calculated and presented simultaneously. Experience with engine and combustion rig measurement is given in Section 5.

4.6 Comparison with Present Measurement Method

4.6.1 Size

A comparison of the size of the FTIR and SGA analyzers used in ARP1256B is shown in Figure 4. ARP1256B defines the present measurement method. In it, gaseous emissions are defined as "gases emitted downstream of the combustion chamber and limited to carbon monoxide, carbon dioxide, nitric oxide, nitrogen dioxide, and hydrocarbons." The ARP specifies measuring these gases using nondispersive infrared (NDIR) analyzers for CO and CO_2, a chemiluminescence analyzer with a nitrogen dioxide converter for NO_x, and a flame ionization detector (FID) for total hydrocarbons.

Figure 4. An FTIR analyzer, in shipping case, next to a traditional gas analysis system. Photograph courtesy of Aerospace Testing Alliance.

4.6.2 System Layout

Figure 5, taken from ARP1256B, shows the system layout currently accepted for the continuous sampling and measurement of gaseous emissions from aircraft turbine engines. Figure 6 shows a modified system layout incorporating an FTIR analyzer that replaced the CO, CO_2, and NO_x analysis instruments.

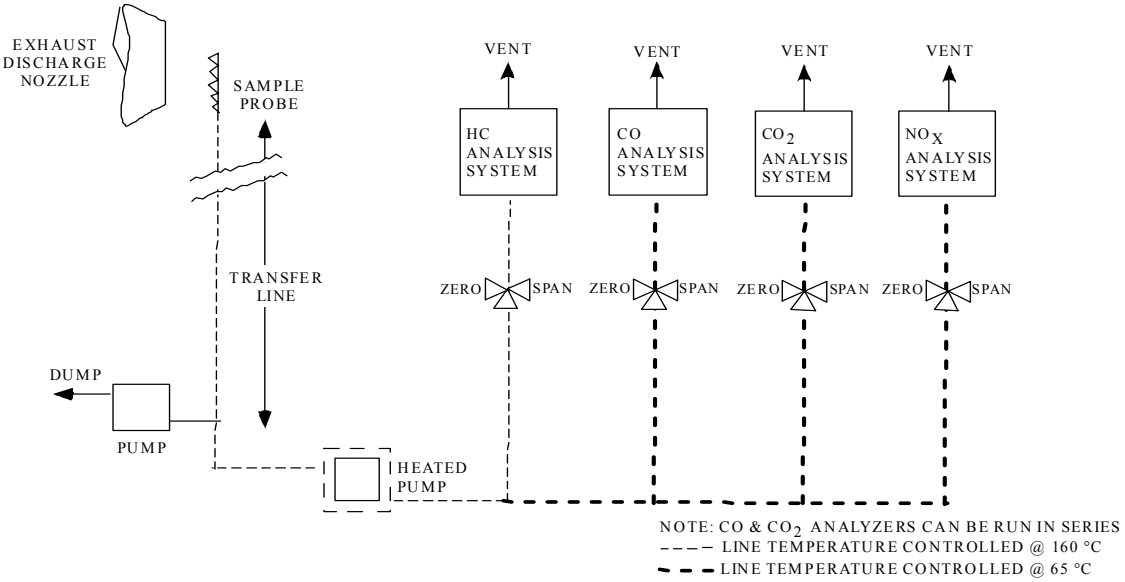

Figure 5. Current sampling system and analyzer specified in ARP 1256B.

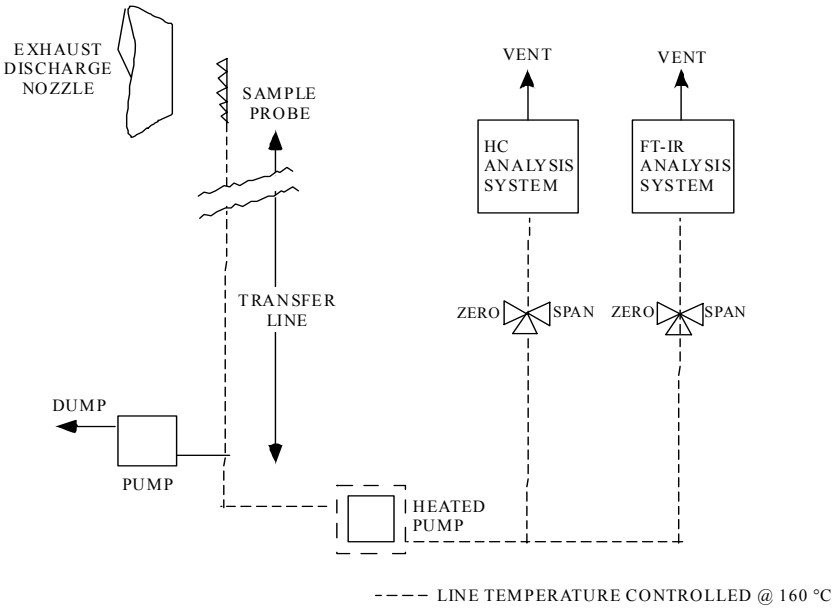

Figure 6. Sampling system and analyzer arrangement used for FTIR analyzer.

4.6.3 Comparison of Precision

The precision of measurement of an FTIR analyzer was compared experimentaly with that of an NDIR CO single gas analyzer. ARP1256B lists the specifications shown below for the precision of NDIR CO and CO_2 analyzers and for chemiluminescence NO/NO_x analyzers. Full scale refers to the analyzer range selected.

CO: Better than ± 1% of full scale for ranges above 100 ppm full scale

Better than ± 2% of full scale for ranges below 100 ppm full scale

CO_2: Better than ± 1% of full scale for all ranges

NO/NO_x: Better than ± 1% of full scale

FTIR analyzers are capable of measuring at ± 1% of any scale selected. For example, one instrument manufacturer states that this accuracy is provided for the above listed gases based on 1% NIST traceable standards.

Table 2 compares a typical NDIR CO analyzer with an FTIR analyzer and shows how each satisfied the ARP1256B precision requirement when measuring certified gas mixtures. (Ref 2) CO gas mixture concentrations from 62.70 ppm to 1,790 ppm were measured as shown in Column 1. The NDIR analyzer measurement ranges used were 0-200 ppm, 0-500 ppm, and 0-2000 ppm. One percent of these scale values, the precision requirement of ARP1256B, is shown in Column 2. Column 3 shows the concentration values for which the NDIR analyzer satisfied the ARP precision specification. For the highest CO concentration, the NDIR analyzer was unsatisfactory. FTIR measurements were made simultaneously using the same ± 1% of full-scale criteria. As shown in Column 4, the FTIR was satisfactory at all concentrations.

Table 2. Comparison of Precision Measuring Certified Gas Mixtures of CO.

CO Cal Gas Concentration Named by Manufacturer	± 1% of NDIR ranges Full Scale	NDIR compliance ± 1% of Full Scale Precision	FTIR compliance ± 1% of Full Scale Precision
62.70 ppm	± 2 ppm	Yes	Yes
120.00 ppm	± 2 ppm	Yes	Yes
180.00 ppm	± 5 ppm	Yes	Yes
298.0 ppm	± 5 ppm	Yes	Yes
448.8 ppm	± 20 ppm	Yes	Yes
1,202 ppm	± 20 ppm	Yes	Yes
1,790 ppm	± 20 ppm	No	Yes

Comparison of simultaneous FTIR analyzer measurements with typical single gas analyzer measurements for CO_2, NO, and NO_x shows that an FTIR analyzer could

perform as well as single gas analyzers in complying with the current ARP-defined precision requirements (Ref 2).

5. ENGINE AND COMBUSTION RIG EXPERIENCE

FTIR measurement of exhaust constituents from engine and rig tests is summarized below. These measurements show that extractive FTIR instruments produce rapid, valid values applicable to combustion research, engine development, and compliance testing. The evaluation of FTIR analyzers used to measure aircraft engine exhaust emissions was started modestly by measuring the effluent from combustion test rigs. These measurements made with FTIR instruments were found to compare favorably with those made using the NDIR instruments specified in ARP1256B and were expanded to include engine emissions testing. The following tests are summarized in this report and more detailed test results can be found in literature in the public domain:

- JT12 turbojet engine
- Military turbofan engine
- CFM56-2 turbofan engine (APEX Tests)
- Combustion rig tests at AEDC

5.1 JT12 Turbojet Engine

5.1.1 Test Setup

Emission measurements were made of the exhaust of a JT12 turbojet engine operated by the Aerospace Department at the Middle Tennessee State University (Ref 7). The JT12, a 3000 lb. thrust class engine, was fired with diesel fuel and ran with a 13.5 inch diameter exhaust extension duct.

Exhaust samples were collected using a rake-type probe. The probe tips of the rake were located 3.8 inches from the exit plane of the nozzle extension (Ref 5). Exhaust temperature at the rake location varied from approximately 300 °C at 45% to approximtely 400 °C at 75% of full power. Measurements were taken with the probe rake held at the nozzle centerline during acceleration/deceleration of the engine and during a continuous sweep of the probe rake across the nozzle exit at constant engine power.

Emissions were measured with a multiple gas analyzer that contained an FTIR analyzer and integrated oxygen sensor. The FTIR analyzer collected data at 0.5 wavenumber spectral resolution (2 scans per second) and reported signal-averaged data every 2 seconds. The O_2 sensor collected data at 50 Hz and also reported signal-averaged data every 2 seconds.

5.1.2 Engine Acceleration Tests

The plots on Figures 7 and 8 illustrate how precisely and accurately the FTIR measurement system tracked engine events as they were reflected in the concentration values of exhaust gas components.

Upper Figure 7 gives overlays of the measured concentrations of O_2, H_2O, and CO_2 as functions of time during acceleration and deceleration of the engine. Oxygen concentration is shown on the right side and percent engine power is shown at the top of the plot. As engine power was increased to 70%, the excess O_2 concentration in the exhaust rose from 17.4% to 17.8%. The compressor air bleed started to close at 70% to 75% power. Acceleration to 75% power resulted in a drop in the excess O_2 concentration and corresponding increases in H_2O and CO_2 concentrations. These trends were reversed for all three gases during deceleration.

The O_2 concentration trace correlates inversely with the fine features of the H_2O and CO_2 concentration traces. Fine features at the engine power transition points are exhibited for each gas. Fine features are characteristic of FTIR measurements and are actual indications of concentrations and not simply “sensor overshoots” during rapid transitions. All three concentration traces also demonstrate reversibility from start to finish of the time (i.e., power) sequence.

Lower Figure 7 shows FTIR measured concentration traces for CH_4, NO, NO_2, SO_2, and CO. Note that the CO concentration is scaled down by a factor of 100. Concentration traces for the major non-methane organic compounds: ethylene (C_2H_4), propylene (C_3H_6), acetylene (C_2H_2), and formaldehyde (H_2CO), are also shown in Figure 8. Each gas trace clearly displays the step changes with power level and tracks exhaust concentrations through out the test sequence.

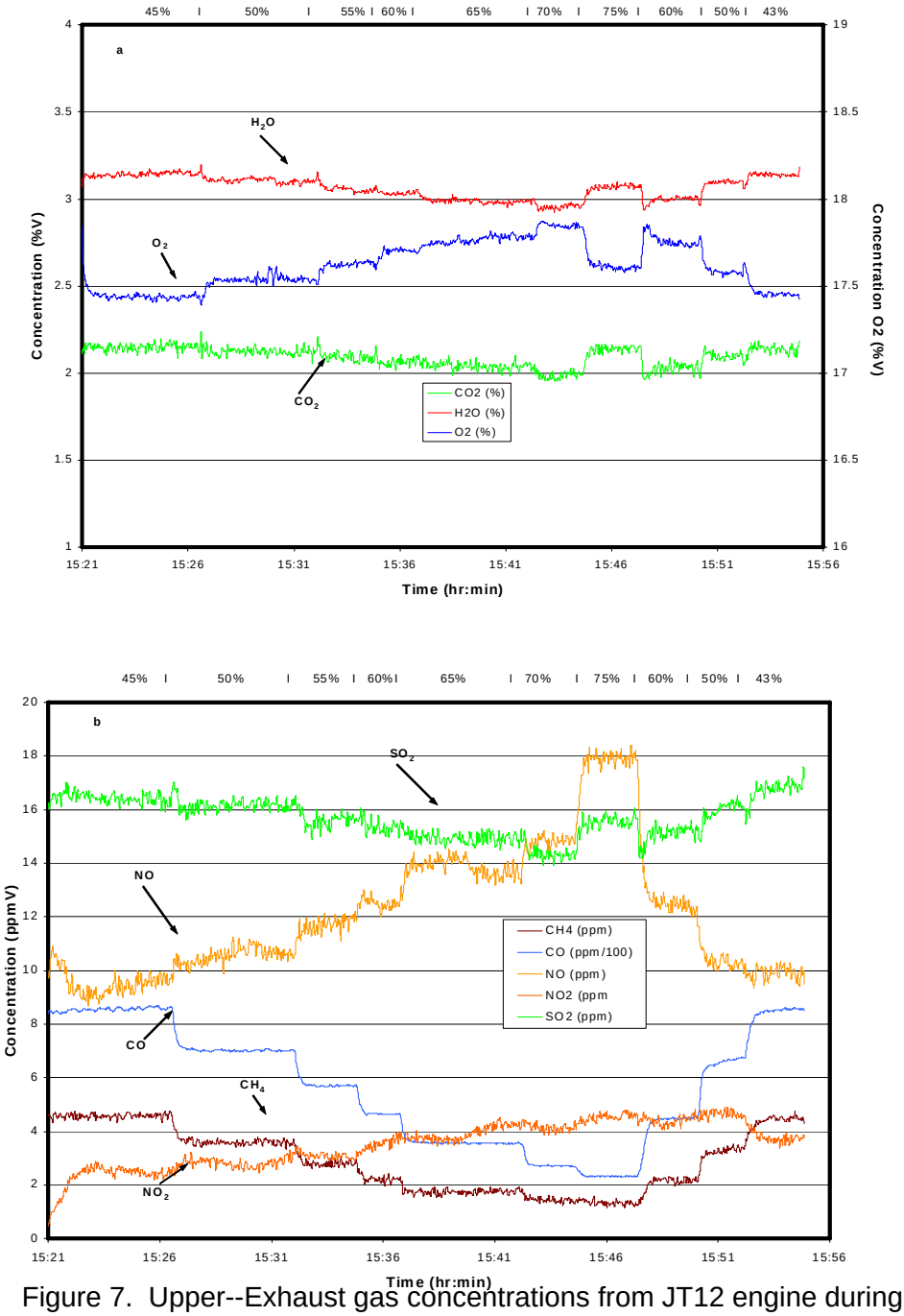

Figure 7. Upper--Exhaust gas concentrations from JT12 engine during acceleration/deceleration test measured with FTIR and integrated O_2 instruments. Lower--Exhaust emissions concentration from JT12 engine during the same test.

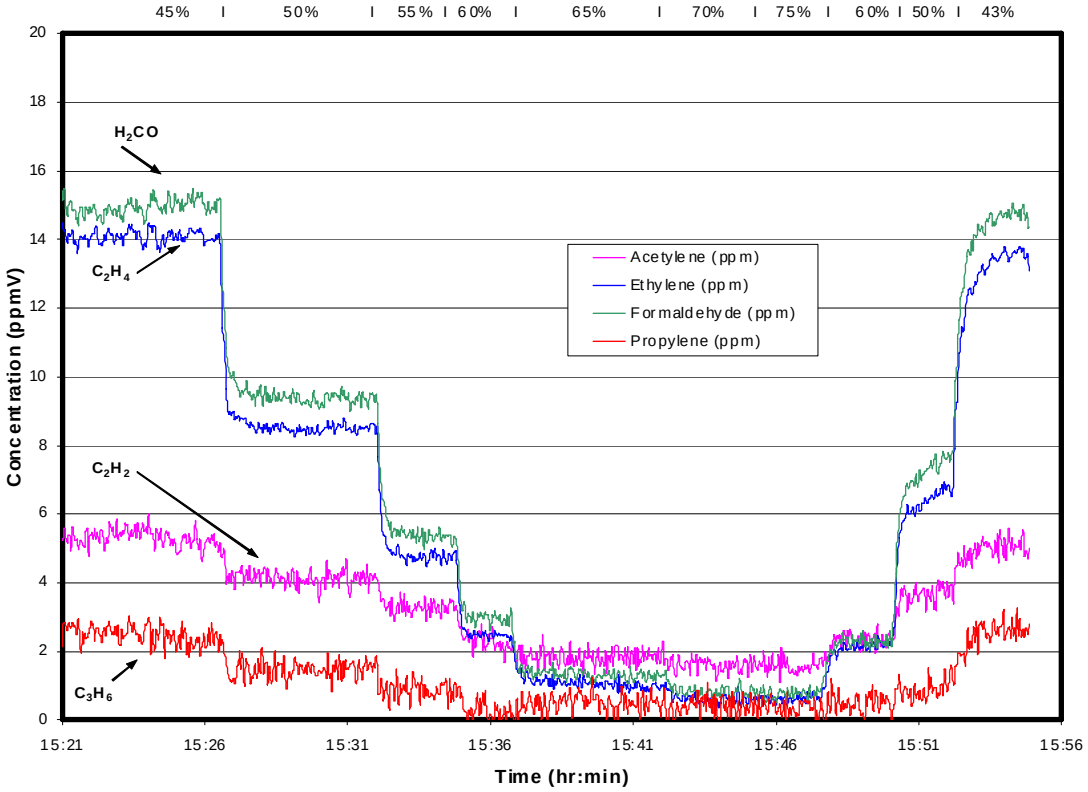

Figure 8. Nonmethane hydrocarbons obtained from acceleration/deceleration test of JT12 engine measured with FTIR analyzer.

5.1.3 Exhaust Nozzle Traverse

The ability of FTIR instruments to respond rapidly to changes in concentration was demonstrated when the exhaust nozzle was rapidly traversed with the sampling probe. Continuous sweep of the probe rake across the nozzle exit with FTIR measurements was found to be a useful and valid approach for rapid emission surveys of engines (Ref 4). Figure 9 shows the concentrations measured for CO and O_2 at rates of 1, 4, 5.5, and 6.2 inches per minute as the rake was traversed downward through the exhaust stream of the JT12 engine. As the rake moved outside the nozzle exit flow, the CO concentration dropped toward zero, and the O_2 concentration rose rapidly to ambient air level (20.9%). A narrow concentration "spike" for each gas occurred when the rake was quickly raised through the exhaust in preparation for the next downward traverse. The important feature to note from the downward sweep measurements is that both sensors maintained the concentration features through the exhaust plume at all sweep rates. Spatial resolution was not lost with the sampling rates used.

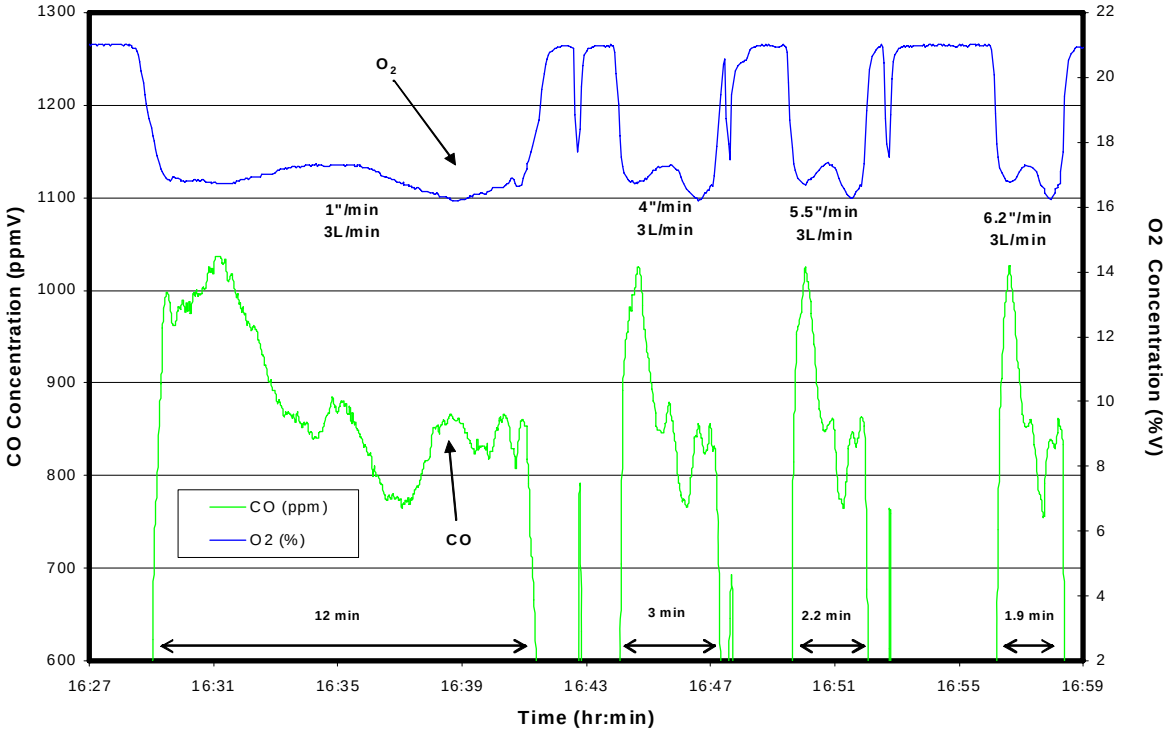

Figure 9. CO and O_2 concentrations from continuous sweep of JT12 exhaust nozzle.

5.1.4 Summary

The use of FTIR analyzers to reduce the time required to collect data and the associated cost of emission measurements during the development testing of aircraft turbine engines was validated. A five-minute survey of the nozzle exit, which yields profiles of the major products of combustion, is feasible. A steady-state, 44-point emission survey was completed in 45 minutes, and a continuous-sweep profile containing hundreds of data points was completed in five minutes. Agreement between the steady state and continuous-sweep emission measurements for the centerline probe averaged ± 0.1 percent CO_2, ± 10 ppm CO, ± 1 ppm NO, and ± 1 smoke numbers.

5.2 Large Engine Test

Jalbert et al (Ref 6) reported the first demonstration of a rapid, continuous-sweep emission measurement system on a large engine. The goal of demonstrating the multiple-species emissions survey of a full nozzle exit within a five-minute time scale was met. The goal also required that the survey meet the minimum spatial resolution specified by the regulatory agencies. The continuous sweep emission profiles that were generated were assessed to be more representative of the actual exhaust gas profile and were a great improvement over previous methods. The emission measurement requirements were accomplished with no impact on other test objectives. Reducing the cost of of engine

development testing by reducing current emission test time is a significant contribution to present and future programs.

5.2.1 Background

A major factor in determining where military and civilian aircraft are based depends on the exhaust gas emission levels that these aircraft contribute to the local environment. The emission indexes (mass of CO, NO, NO_x, SO_2, and HC produced per 1000 mass units of fuel consumed) for existing aircraft are measured during engine certification tests. The test procedures are used are equivalent to or better than those defined in ARP1256B and prescribe many hours of point-by-point sampling of the engine exhaust plume. The current process is expensive due to the amount of added engine run time and the associated test costs. The impetus for a new measurement system design was three-fold:

1. The protocol required in ARP1256B prescribes point-by-point sampling, which has become expensive due to the hours added to engine run time, test cell time, personnel time, and materials consumed.

2. New, high performance turbofans with large exhaust nozzles, run time constraints at high power conditions that are not compatible with the time required for typical exhaust gas sampling, and analysis using present protocols.

3. The value in obtaining a routine exhaust gas analysis to verify engine performance during engine development testing. Emission values for CO, CO_2, NO, NO_2, and hydrocarbons are powerful diagnostic tools if they are available while the engine is being tested.

5.2.2 Test set up

The FTIR tests were conducted during engine performance testing at the USAF, Arnold Engineering Development Center in the engine high altitude facility.

The measuring system used for these tests included a high temperature capable probe rake system, a rapid gas transport system, a pitot pressure measurement system, and five separate gas analysis systems centered around advanced FTIR gas analyzers with integrated oxygen sensors, and four HFID total hydrocarbon analyzers.

The time response of the gas sampling and analysis system was measured during pretest checkout. An ambient temperature calibration gas containing 900-ppm propane balanced by dry air was diluted by nitrogen through a gas divider to rapidly change the gas composition measurable by the FTIR, HFID and oxygen sensors. Each of the three measurement devices in the five gas-sampling systems transported and measured step increments in the propane and oxygen concentration at greater than 90 percent in 17 seconds (Fig. 10).

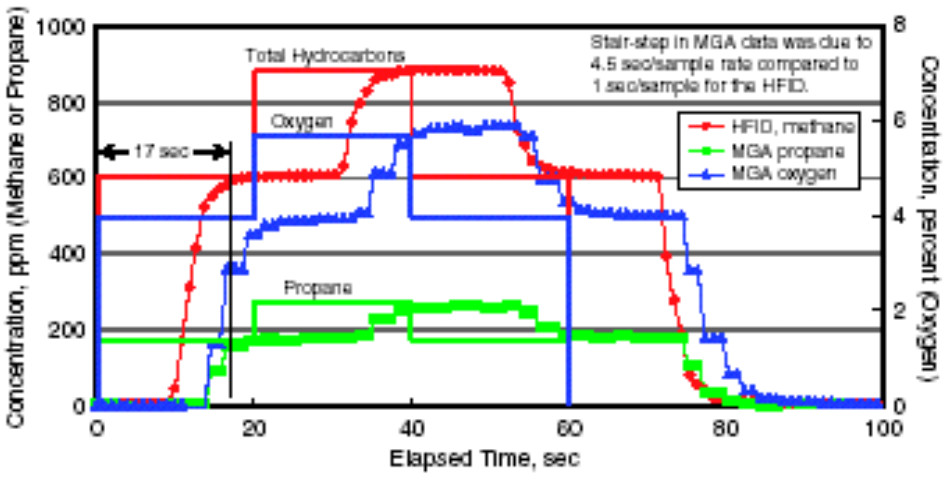

Figure 10. Typical gas-sampling and analysis system response to step changes in calibration gas composition.

5.2.3 Test Results

All emission measurements collected during these tests were obtained on a noninterference basis with other engine test objectives.

Five gas analysis systems were capable of measuring CO, CO_2, O_2, NO, NO_2, H_2O, and SO_2, plus 18 trace species and 4 systems total hydrocarbons. The measurable trace species for the JP-8+100 fuel used with the nominal formula $C_{7.19}H_{13.60}O_0N_0S_{0.0019}$ included acetaldehyde, formaldehyde, acetylene, isopropanol, methane, propane, butane, and toluene.

Pretest system development tests at Middle Tennessee State University did not duplicate the altitude test cell environment. Therefore, the amount of exhaust gas recirculation into the test cell was not anticipated. Outside the plume, the CO levels failed to drop below 200 ppm and water vapor exceeded 10% at some periods during testing. Since gas composition was not a reliable indicator of the plume boundary, a pitot pressure survey, shown on Figure 11, was used to define the plume boundary.

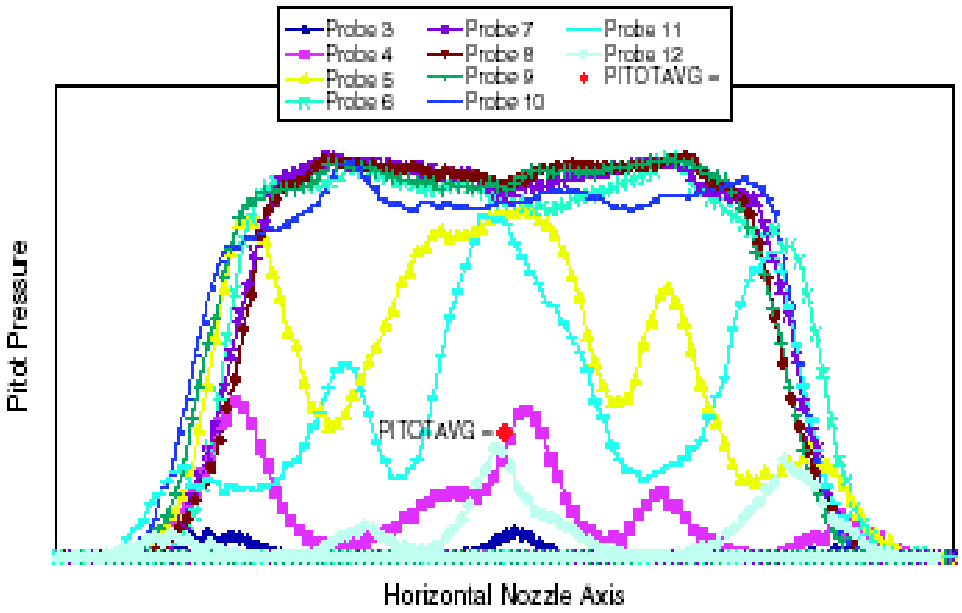

Figure 11. Pitot pressure profile of the exhaust gas plume collected during the continuous-sweep emission measurement survey.

5.2.4 Continuous Sweep Tests

The continuous-sweep method produced an emission profile representative of the entire plume by spanning the nozzle side-to-side and top-to-bottom. In contrast to previous emission surveys of this type of engine (core only), a full plume survey includes an annulus of low F/A flow about the core. The same emission survey at 100% engine power was analyzed to determine the impact of plume boundary assignment on the plume-averaged parameters such as emission index, fuel/air ratio, and combustion efficiency. Emission indices except total hydrocarbons were lower when calculated over the entire plume.

A major issue considered during the development of the continuous-sweep measurement methodology was how to correct for the system time delay. With an FTIR analyzer, a rigorous approach using measured gas transport velocities and instrument time response was found unnecessary. Figure 12 illustrates the fidelity of the time-delay correction as the steep gradients for the entire sweeps overlay on the steady-state data set.

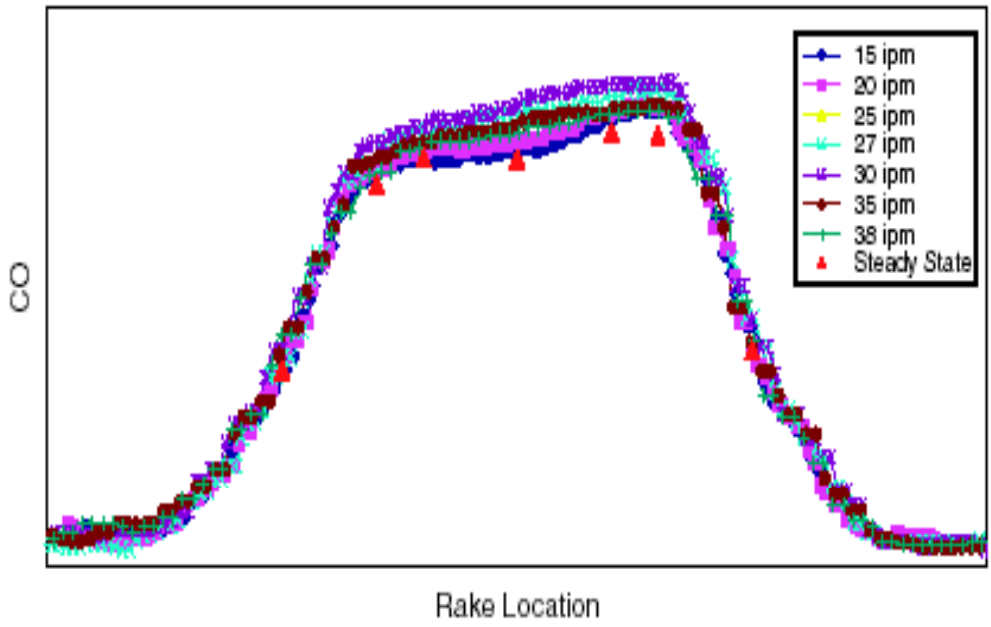

Figure 12. Tests to determine the maximum probe rake traverse velocity illustrate the fidelity of the time-delay correction methodology.

The maximum rake traverse velocity was defined empirically during several sweeps with various rake traverse velocities at similar engine and test cell conditions. Even at rake traverse velocities of 38 in./min there was no difference in the plume-averaged parameters and no loss of detail in the plume structure. Differences in CO levels were attributed to slight variations in engine or test cell operation. A maximum sweep rate of 27 in./min was specified because, at that rate, a complete extend-and-retract emissions survey could be completed within the five-minute target.

5.2.5 Power Transients

The test matrix included many slow throttle transients programmed from idle to intermediate power and back to idle at each altitude/Mach number condition. During these transients, the probe rake was parked at fixed locations in the plume to determine whether the emissions system could follow the changing engine operating conditions. Figure 13 shows the results of these surveys. Profiles for CO, HC, and CO_2 stabilized at intermediate power. The O_2 profile stabilized a few seconds later. When using this methodology, an emissions profile at every altitude/Mach number condition can be pieced together with five points from each different rake location collected during several throttle transients. Even though they are lacking the resolution of the continuous-sweep profiles, these data provide anchor points from which to extrapolate high-resolution profiles for other test conditions. These extrapolated profiles, while not acceptable to regulatory agencies, serve to screen altitude/Mach number conditions where emission variations are not significant.

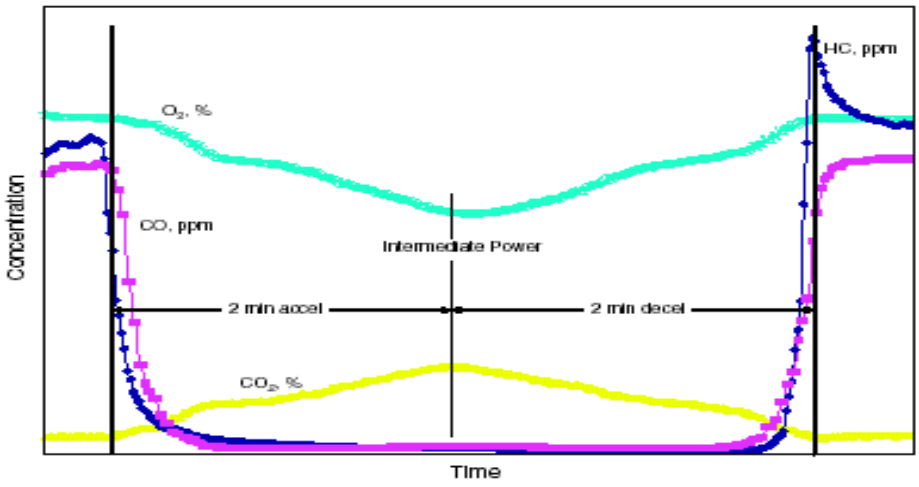

Figure 13. Response of the gas-sampling and analysis system to a slow engine transient from idle to intermediate power shows that stable data was achieved at intermediate power.

5.2.6 Engine Health Monitoring

The capability of the FTIR to measure many species economically during engine test periods enables the gas analysis system to serve as an engine health monitor. For example, the emission index of sulfur dioxide may be calculated from the FTIR measured SO_2 concentration instead of using the percent of sulfur by weight in the fuel as an estimate. Figure 14 shows clear evidence of an oil leak into the gas path of a gas turbine engine as the measured emission index of SO_2 ($EISO_2$) diverged from the estimated $EISO_2$. Lubricating oil was the only other source of sulfur in the exhaust gas, and once the leak was repaired, the measured $EISO_2$ returned to the expected level.

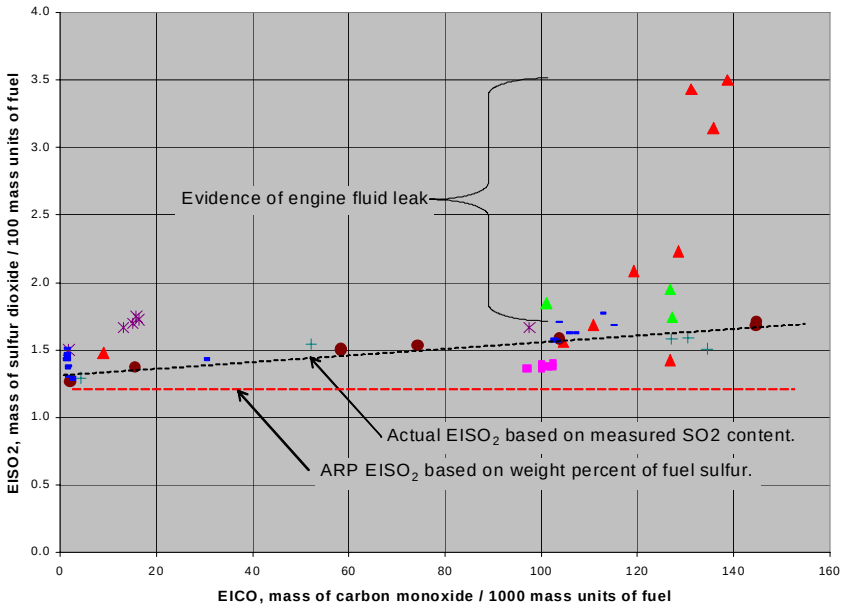

Figure 14. A plot of EISO2 vs. EICO illustrates the value of the FTIR gas analyzer as an engine health monitor. An engine oil leak was detected and the repair was confirmed.

5.2.7 Summary

The purpose of the emission tests was to prove the design goal of the measurement system. For this proof, the measurement system was required to demonstrate a multiple-species emissions survey of a full nozzle exit within a five-minute time period. The minimum spatial resolution required by the test protocol used by regulatory agencies (ARP1256B) also was required. This goal was met.

Three emission data acquisition methods were demonstrated during the first implementation of the system. The continuous-sweep method was the most productive approach and required the least amount of engine run time. The steady-state “traverse and dwell” method provided the lowest measurement uncertainty but required almost 15 min. per survey. Finally, data were also collected during slow engine throttle transients, which yielded a single, vertical profile.

Following each survey, regardless of the method of emission data acquisition used (profiles of fuel/air ratio or of combustion efficiency), the emission indexes were calculated as well as several data quality-check parameters that immediately indicated the health of the gas-sampling system. Within five minutes, the processed data file was sent on the emission network to the control room allowing an evaluation of engine performance before changing run conditions.

Application of the continuous-sweep emission measurements made feasible by FTIR instruments had a major positive impact on the scope, schedule, and cost of the emission data collection of a major engine test program. Because emission surveys

were collected at every altitude/Mach number condition tested, the volume of useful emission data was much greater than would have been obtained at the minimum emission test conditions. The required emission surveys were obtained simultaneously with other test objectives eliminating from the test program 12 to 18 hours of previously dedicated emission testing. The total cost of measuring emissions was reduced to less than the cost of one hour of test stand operation.

5.3 DC8 Tie-down Tests (APEX)

Exhaust emission tests were made on a NASA DC8 aircraft in April. A number of runs were made measuring the exhaust from the CFM56-2 engines using both ARP1256B single gas and FTIR analyzers. Results are to be summarized and included in this report as soon as they become available.

5.4 AEDC Combustion Rig

As a part of their program to improve the emission measurement methods used to evaluate USAF engines at Arnold Engineering Development Center, a combustion rig operating on natural gas fuel was used as a source of engine exhaust. In the testing described by Marran et al, (Ref 8) side-by-side measurements were made using a single gas analyzer instrument system designed to meet ARP1256B (SGA) and an FTIR system. Both systems sampled the same filtered exhaust gas except the analyzers used for the SGA required water removal from the analyte.

One hundred twenty-three test points were run in conjunction with rig tests that mapped out the combustor operational limits. Many of these test points were not normal operating conditions. Correlation plots were generated for CO_2, CO, NO, NO_x, and total hydrocarbons (Figures 15-19). These plots showed that good linear relationships between the measurement methods existed for all data.

FTIR spectral references that perform the same function as calibration data can be transferred between identically manufactured instruments. The spectral references used to quantify the above species were acquired on a different FTIR analyzer using a 5.11 meter low volume (200 cc) cell. A 5.6 meter (1,600 cc) cell was used to obtain the test data.

5.4.1 CO_2 Comparison

Early in the program, CO_2 was analyzed using a band centered on 1000 cm^{-1}. This band originated from a vibrationally excited state, so it was extremely temperature dependent, i.e. about 5% error in the analysis corresponded to a 5°C change in temperature. The analysis was moved to the 2200 cm^{-1} region that originated from a ground state vibration level. This change resulted in improved agreement between the SGA and the FTIR systems which read about 1% high (Figure 15).

5.4.2 CO Comparison

Figure 16 plots the correlation for CO. The single gas analyzer was limited to concentrations below 1000 ppm, but about 15% of the test points had levels above this value. The FTIR analyzer was calibrated to operate from sub-ppm up to 20% CO and was able to provide quantitative results well above the SGA cutoff. Eighty-four % of the data were below 150 ppm, where the FTIR data were consistently 1% higher than the SGA results. There were three data points between 150 ppm and 1000 ppm and these analyzed about 3% high. The CO concentration values from the FTIR analyzer appear to have a 1.3 ppm offset when compared to those from the CO analyzer. This offset highlights the advantage of FTIR post-test validation, not available to single gas analyzer systems. On re-examination of the FTIR spectral data for the test points reported to have near zero concentration by the SGA, the CO by FTIR analysis was verified. The discrepancy was thought to be due to SGA zero drift or incomplete FTIR gas cell volume exchange.

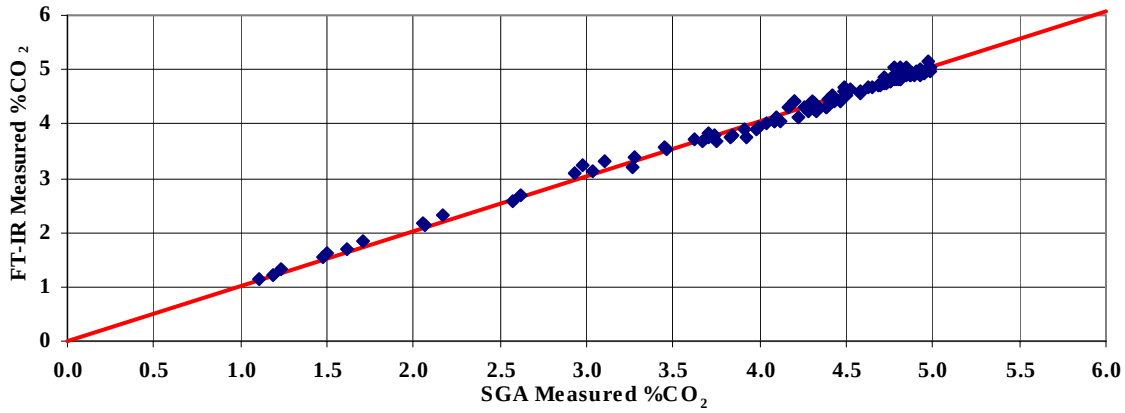

Figure 15. Correlation plot for CO_2. The best linear fit shown has a slope of 1.01 and zero offsets.

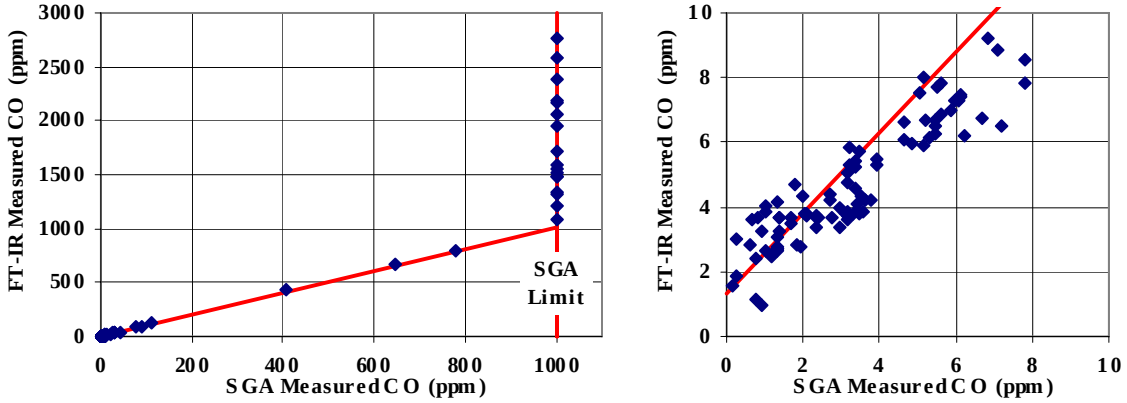

Figure 16. Correlation plot for CO. The graph on the left covers the entire dynamic range of the data, while the right expands the data from 0-10 ppm. The best linear fit shown has a slope of 1.01 and a +1.3 ppm offset.

5.4.3 NO and NO_2 Comparison

Figures 17 and 18 plot the correlation between the analyzers for NO and NO_x. In Figure 17, the FTIR NO data is consistently 4% higher when compared to the SGA results. Although this result is well within the combined uncertainties of the two measurement techniques (approximately 6.7%), experience has shown that sample drying systems have a tendency to shift NO_2 to NO. This shift was seen in the present data as well. The total NO_x appears to be largely conserved and is usually the best way to compare the FTIR performance for NO_x. In Figure 18, the total NO_x measured with the FTIR (NO + NO_2) reads approximately 2% higher when compared to the SGA results and is still well within the uncertainty of the two measurements. A third nitrogen-containing compound, nitrous acid (HNO_2), was detected in the exhaust stream:. This compound correlated best with NO_2 and ranged from 0.03 to 1.3-ppm concentration.

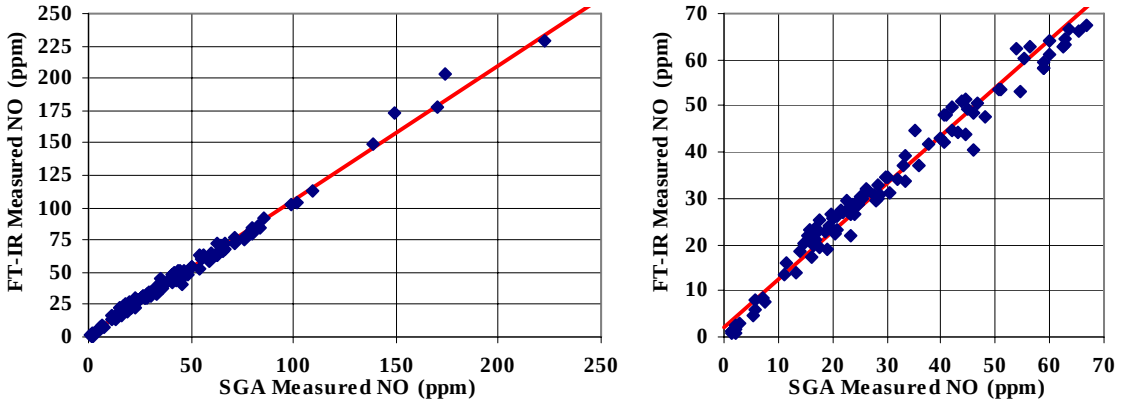

Figure 17. Correlation plot for NO. The graph on the left covers the entire dynamic range of the data, while the right expands the data from 0-70 ppm. The best linear fit shown has a slope of 1.04 and a +2 ppm offset.

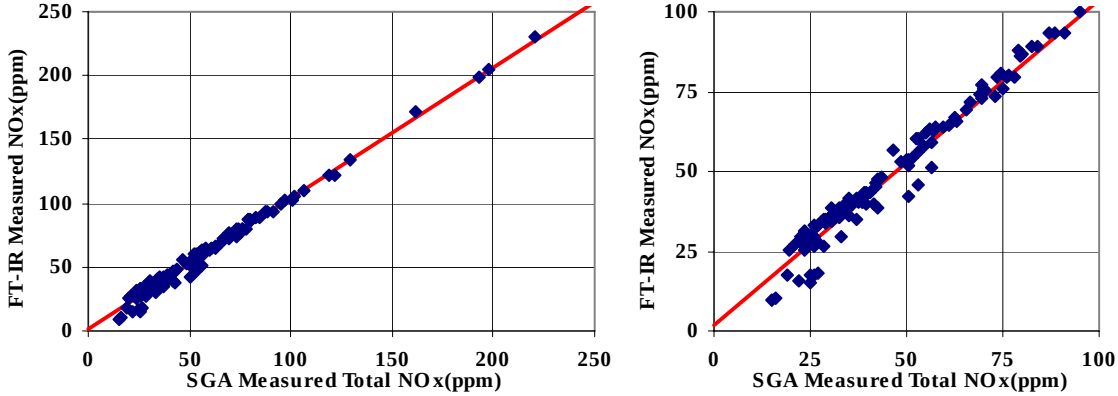

Figure 18. Correlation plot for NO_x. The graph on the left covers the entire dynamic range of the data, while the right expands the data from 0-100 ppm. The best linear fit shown has a slope of 1.02 and a +2 ppm offset.

5.4.4 Total Hydrocarbon Comparison

The correlation between the FTIR analyzer and total hydrocarbons measured using a flame ionization detector (FID) is shown in Figure 19. The FID is not capable of speciating hydrocarbons, while the FTIR measures each species for which spectral data are entered into the analyzer. The total hydrocarbons from the combustion of natural gas were summed from the species given in Table 3. This table lists the concentration of each of these compounds detected in the turbine exhaust and the approximate percent contribution to the total hydrocarbon concentration as measured with the FID. The data in Table 3 were normalized to C1 (i.e. equivalent methane) to be compatible with the FID results. Table 3 and Figure 19 show that the FTIR analyzer results are within approximately 2.5% of the FID results, which is well within the experimental uncertainty of the measurements.

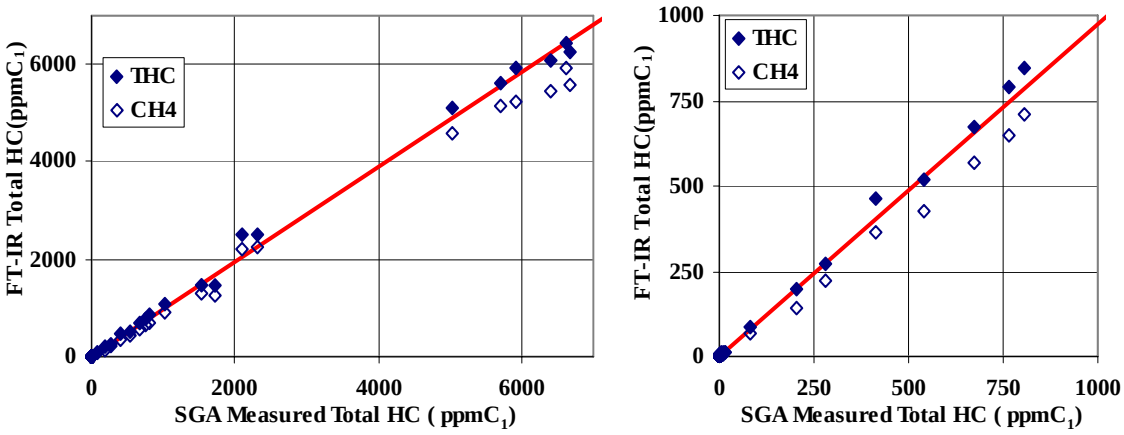

Figure 19**.** Correlation plot for total hydrocarbons. The graph on the left covers the entire dynamic range of the data, while that on the right expands the data from 0-1000 ppm. The best linear fit shown has a slope of 0.975 and zero offset. Also plotted is the correlation between FTIR measured methane and the THC's.

Table 3. Hydrocarbons detected in the turbine combustor exhaust, and the relative contribution of each.

Species	Fraction of total C_1(%)
Methane	80-90%
Formaldehyde	7-8%
Ethylene	8-9%
Methanol	<1%
Propylene	<1%
Formic acid	<1%

5.4.5 Measured and Calculated Water Comparison

The water concentration in the exhaust was calculated based on the test rig stoichiometry, inlet humidity, and known fuel C-H ratio and measured directly with an FTIR analyzer. The measured concentration values had excellent linear correlation with the calculated water concentration but were systematically low by 5%. Because of the inherent errors in the precision with which water concentration can be calculated, the water reference concentrations were re-scaled by a constant factor of 1.05 to agree with the measured values of the FTIR analyzer.

5.4.6 Summary

The FTIR analyzer successfully monitored the exhaust composition from a gas turbine combustion rig over a wide range of emission values. The instrument not only measured the species traditionally measured at the facility (CO_2, CO, NO, NO_x, and total hydrocarbons) but also detected and measured many other species, including water, formaldehyde, ethylene, propylene, methanol, formic acid, and nitrous acid.

The side-by-side comparison of the single gas analyzers currently employed and the FTIR analyzer showed excellent agreement. The FTIR analyzer's relatively small footprint, ease of use, minimal daily calibration, and low maintenance were found to make it an ideal instrument for both laboratory and field measurements of turbine engine exhaust composition.

6. SUMMARY AND RECOMMENDATION

Fourier transform infrared (FTIR) analyzers provide many advantages in measurement capability and cost reduction. SAE E31 Committee recommends that an Aeronautical Recommended Practice be implemented at this time that specifies the use of FTIR analyzers to measure CO, CO_2, and NO_x from aircraft gas turbines, or alternately, that ARP1256B be amended to include the use of FTIR analyzers as an option to the present (single gas) instruments for the measurement of CO, CO_2, and NO_x.

ACKNOWLEDGEMENT

PREPARED WITH SUPPORT FROM ARNOLD AIR FORCE BASE.
AIR FORCE SBIR PHASE III, CONTRACT NO. C-F40600-02-C-0018 OF

Appendix E

Final Report Document: **A System to Permit the Quantitative Measurement of Oxygen Simultaneously with the FT-IR MultiGas Analyzer System**

A System to Permit the Quantitative Measurement of Oxygen Simultaneously with the FT-IR MultiGas Analyzer System

Peter J. Bonzani, Jr., Patrick M. Bush, James R. Markham
and James J. Scire, Jr.

Advanced Fuel Research, Inc.
87 Church Street
East Hartford, CT 06108-3728

Table of Contents

Abstract

In emissions related testing, FT-IR has proven to be a reliable and accurate technique to be used in analysis. One limitation of this method is the inability to measure infrared inactive species. The quantity of excess oxygen in particular is important to combustion applications to provide insight into how well an engine is performing. An integrated single-instrument system was developed and tested. A solid oxide zirconia current-limiting sensor was integrated into the existing MKS MultiGas Analyzer. It was determined that the sensor be located in the exit gas stream of the instrument. Hardware to install the sensor, measure and report the concentrations and related software was developed. Multiple field trials were performed to evaluate the sensor's performance. Multiple measurements were completed on two Pratt and Whitney engines: an FT-8 power generation stationary gas turbine and an aviation JT-12 engine. Oxygen balances and reversibility were seen and maintained with these lean-burning engine applications. Calibrations and stability were performed on two vendors, NTK of Japan and Electrovac of Austria. It was determined that the Electrovac sensor had some distinct advantages over the NTK version. This integrated "single instrument" approach proved successful and its results verified against existing standards and equipment.

The Problem

Recent articles have demonstrated the advantages and benefits of Fourier transform infrared (FT-IR) spectroscopy toward improving the methodology for the reliable quantification of gas composition in gas turbine engine exhaust [1-3]. FT-IR gas analysis is a full spectroscopic technique that makes it possible to monitor many species simultaneously in a single instrument. It is based on the fact that every molecule, except homonuclear diatomics, has a unique set of rotational and vibrational frequencies that absorb and emit infrared energy in a characteristic manner. In general, it is possible to identify and quantify gases based on the location and magnitude of these absorptions, which occur throughout much of the infrared region of the electromagnetic spectrum. Since an FT-IR spectrometer is capable of recording infrared absorptions through the wide wavelength range from about 50 to 1 microns, or as wavenumbers, 200 to 10,000 cm^{-1}, it can be used to identify and quantify an almost unlimited variety of compounds [4].

FT-IR has been shown to provide lower detection limits and quantification of more compounds while offering a space saving and lower cost alternative to using an array of single gas analyzers [1-3]. Figure 1 presents a photograph comparing the physical size of an FT-IR gas analyzer product to a rack of single gas analyzers for measuring combustion exhaust gases. Turbine engine exhaust is typically analyzed for species such as oxides of carbon (CO_2, CO), oxides of nitrogen (NO, NO_x), total hydrocarbons, water (H_2O), and excess oxygen (O_2) using an array of single gas analyzers. An FT-IR gas analyzer was then demonstrated to simultaneously measure H_2O, CO_2, CO, NO, NO_2 and methane (CH_4), plus formaldehyde, ethylene, propylene, methanol, sulfur dioxide, formic acid, and nitrous acid. However, it is well known that FT-IR is deficient in that it cannot measure O_2 (i.e., O_2 is an infrared-inactive homonuclear diatomic gas).

Figure 1: An FT-IR MultiGas Analyzer (MGA), in a convenient shipping case, next to a traditional gas analysis system. The much smaller MGA measures more gases for a fraction of the traditional capital and maintenance costs [1-3] Photograph courtesy of Vince Zaccardi, Jacobs-Sverdrup/AEDC Group.

In theory, for any combustion system, there is a specific amount of oxygen that will completely burn a specific amount of fuel. In practice, burning conditions (e.g., mixing of fuel and oxygen) are never ideal, so excess air (roughly 20.9% oxygen, 79.1% nitrogen and minor components by volume) must be supplied to drive the burning conditions closer to ideal. For most combustion devices (engines, boilers, incinerators, etc.), an insufficient amount of air leads to unburned hydrocarbons (including unburned fuel), carbon monoxide, and soot, fume, and smoke in the exhaust [5-6]. This can result in the fouling of heat transfer surfaces, lower energy efficiency, pollution, and flame instability. However, excess air can lead to higher levels of thermally generated NO_x produced in the flame region while also decreasing device efficiency through exhaust gas cooling. It is generally beneficial to quantitatively measure the oxygen concentration in exhaust gas simultaneously with the combustion-generated emissions for process understanding, optimization, and control.

Opportunity for Solution

An obvious solution to the O_2 measurement deficiency of FT-IR gas analysis products is to pair them off with typical single-gas analyzers for O_2. Two individual instruments instead of six or more single-gas analyzers can be considered attractive, but traditional O_2 analyzers (i.e., paramagnetic, chemical cells, laser/optical cells) require the added complexity of moisture removal from the sample gas stream [1-2]. Physical size, sampling complexity and cost are all significantly increased by the pairing in comparison with a stand-alone FT-IR.

A better solution to the deficiency of FT-IR gas analysis products is to integrate the capability to measure O_2 in a manner that does not increase the overall packaged product dimensions and that does not require moisture removal from the sample gas stream. Close-coupling of an O_2 measurement device with the optical sampling cell of an FT-IR gas analyzer ensures that the measurements for the infrared-active molecules and infrared-inactive O_2 are from the same gas sample.

Technology Description

Due to the above mentioned problems with traditional O_2 analyzers, a solid oxide type sensor was chosen for integration. Solid oxide sensors have the advantage that they can function in very high humidity conditions, are proven rugged and reliable and are much smaller in overall dimensions than the other types.

One obvious choice was to explore the possibility of using an automotive type zirconia sensor, shown in Figure 2.

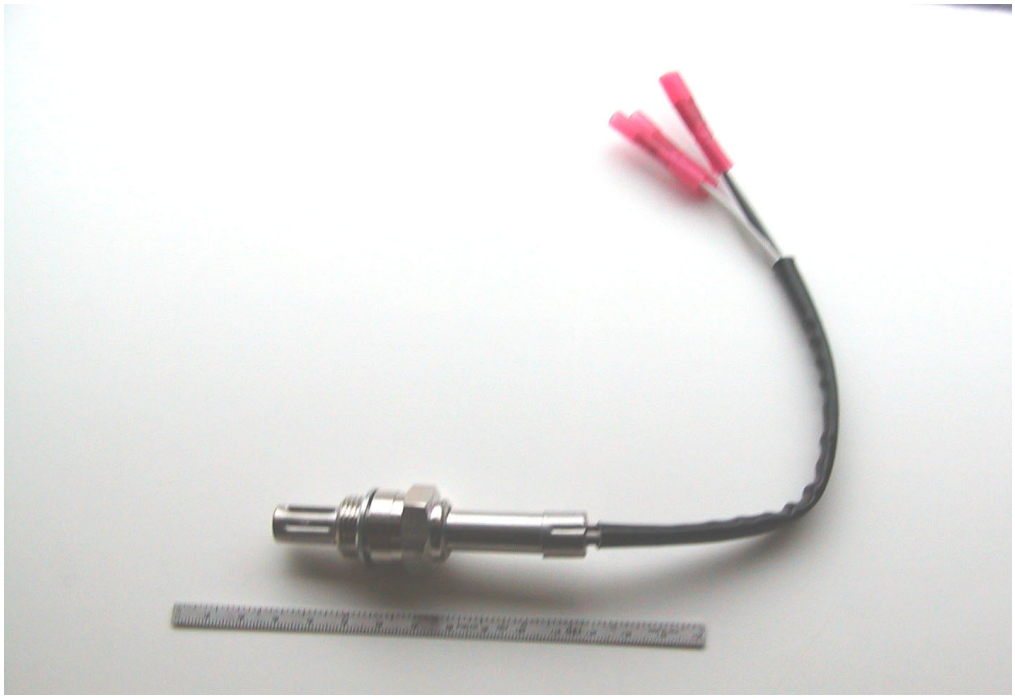

Figure 2: A typical heated zirconia automotive application oxygen sensor (Robert Bosch)

Automotive type sensors for the most part rely on making a comparison between two distinct gasses, the sample and a reference. In the automotive application, outside air is used as a reference gas, while the exhaust output gas of the internal combustion engine is the sample. When applied in this mode of operation, a voltage potential is developed between the two gases in the zirconia electrolyte. This is why the sensor is called a "potentiometric" sensor. The response is proportional to the deficiency of oxygen in

comparison to outside air. Two major drawbacks to this sensor are that a reference gas is always required and must remain constant concentration in order to give viable results and the sensor response is asymptotic, making accurate calibrations difficult, as show in Figure 3.

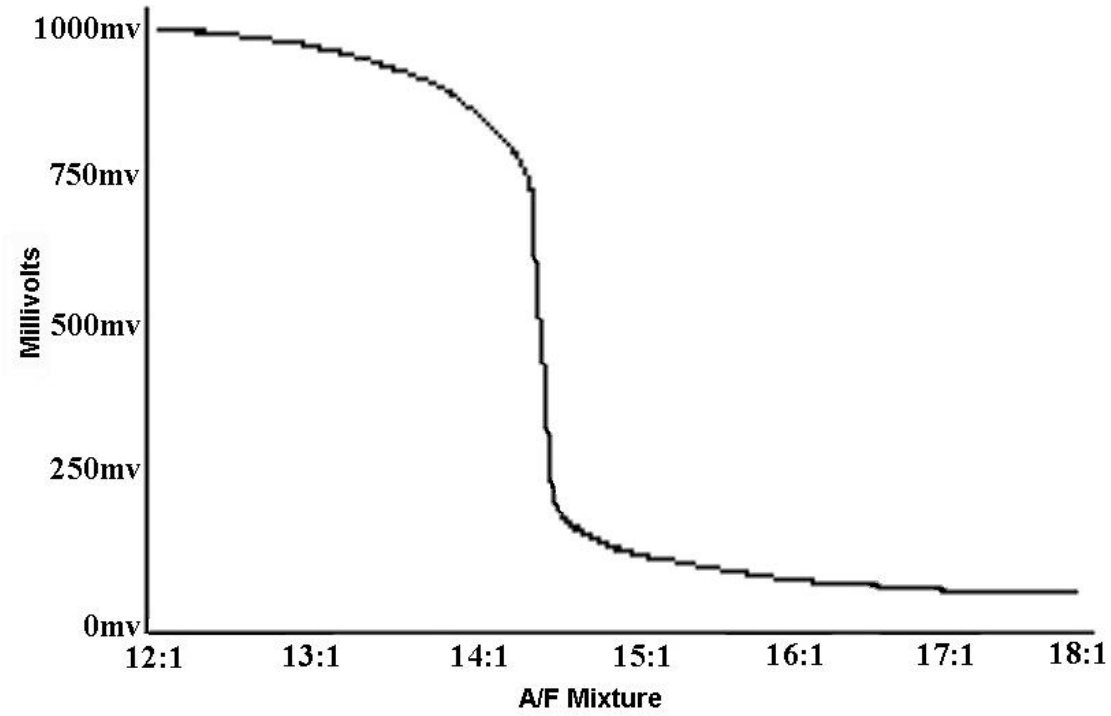

Figure 3: Typical potentiometric zirconia sensor response

Another drawback to this type is they are usually unheated or only heater assisted. This means that some or all of the heat energy is supplied by the exhaust stream, which is not problematic when mounted in the exhaust flow close to the engine in an automobile. In the needed application, an additional heater would be needed to bring the sensor element to the required ~650 ºC for operation, because the gas sample temperature flowing through the optical cell of the FT-IR system is too low at a temperature range from ambient to 150 ºC.

A more simple and reliable method for measuring oxygen had to be found. It is prior knowledge that the oxygen concentration of a gas can be determined by the limiting

current of an electrochemical pumping cell when coupled to either a normal-type or Knudsen-type diffusion barrier [7-9]. The amount of current flowing through the electrolyte is limited by the concentration or partial pressure of oxygen present in the sample. This method of operation is called "amperometric mode". These types of amperometric sensors are typically called limited current-type oxygen sensors. The response, unlike in potentiometric mode, is roughly linear at low concentrations (below 25% Volume) as shown in Figure 4, avoiding the asymptotic behavior. The added advantage is that in this mode of operation, the sensors do not require a reference gas.

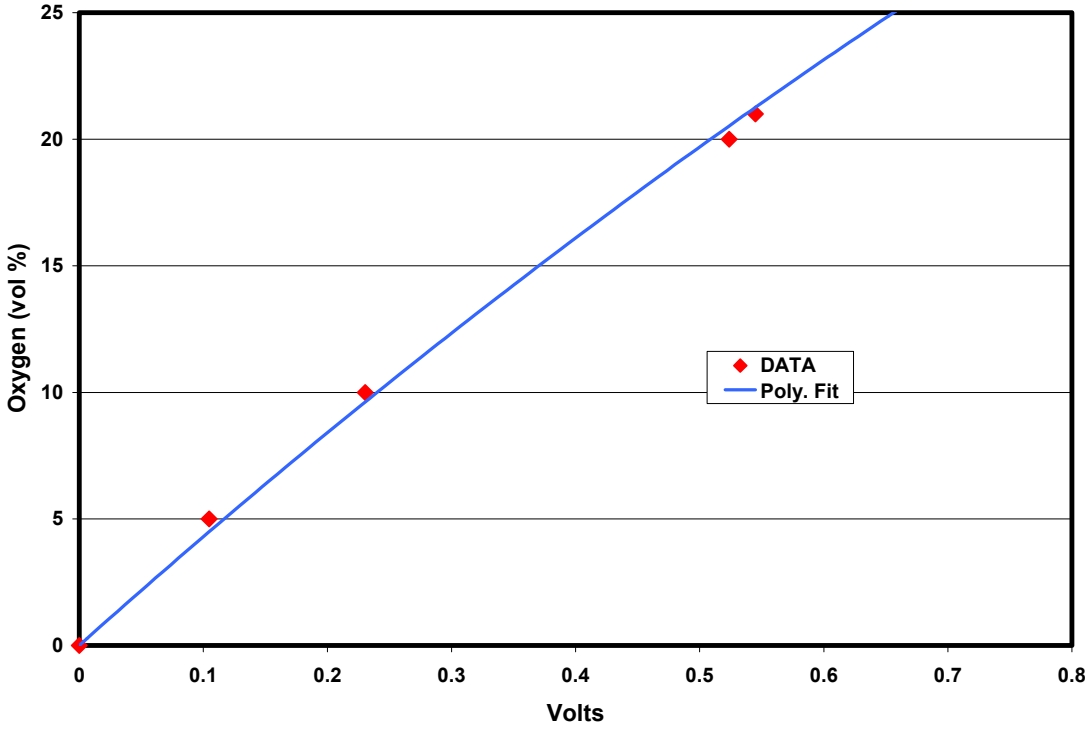

Figure 4: Near-linear response of a limited current-type solid oxide sensor.

Taking into account these distinct advantages, self-heating solid oxide (zirconia) sensors run in amperometric mode were chosen for integration and testing with an FT-IR gas analyzer. Figures 5 a. and b. present pictures of the commercially available oxygen sensors chosen for this study, operating at an element temperature of ~650 °C.

After determining the type of sensor needed, two vendors were identified. NTK, a division of the Japan-based NGK Spark Plug Company and Electrovac, an Austrian based company specializing in zirconia sensors and related products.

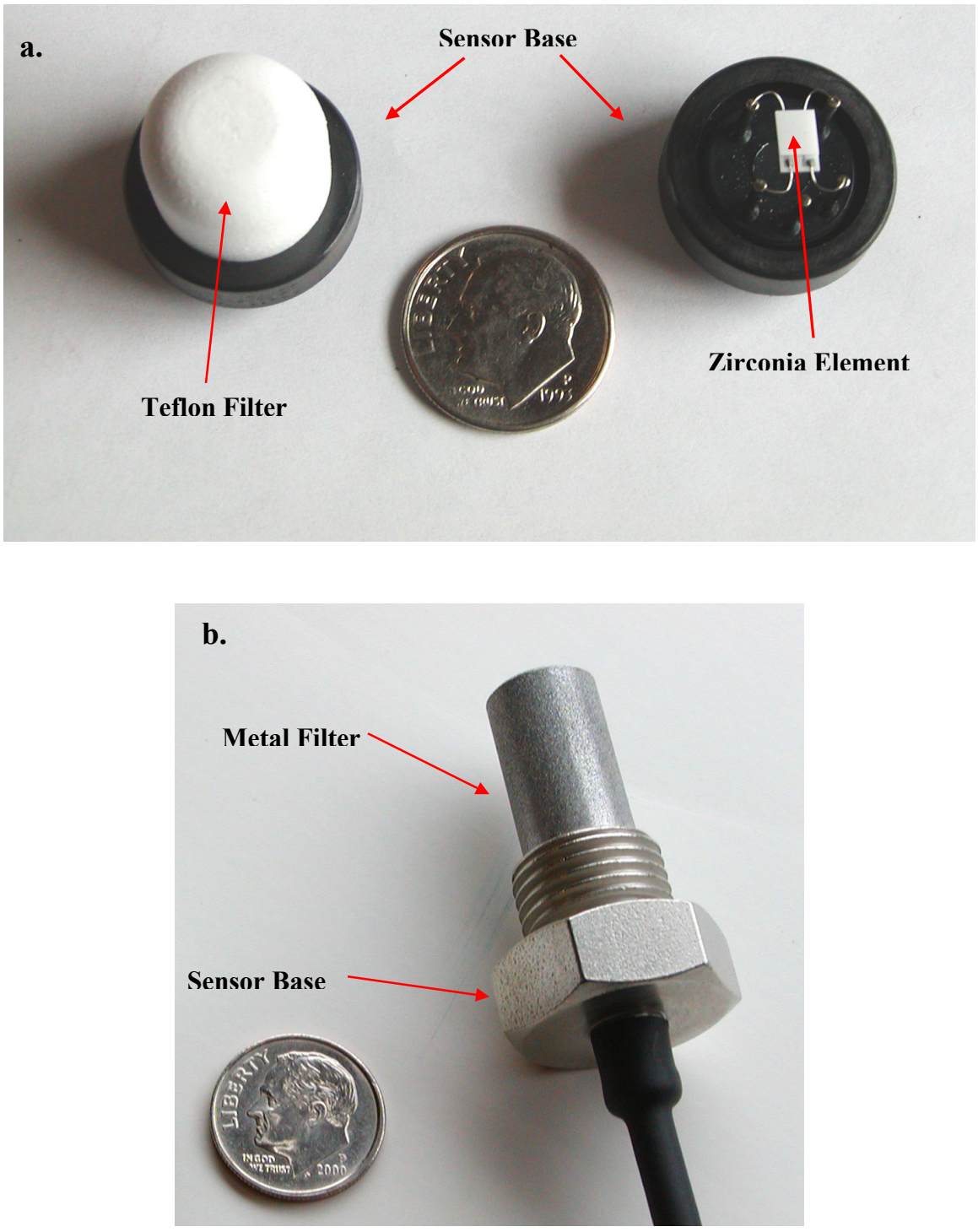

Figure 5: The a. NTK amperometric oxygen sensor package with and without protective Teflon particle Filter and b. Electrovac equivalent with metal filter.

In order to integrate the sensor into an FT-IR gas analyzer, some design issues has to be considered. The porous barrier of the oxygen sensor is required to be in contact with the gas sample being measured by the instrument. This can be accomplished in any one of five locations described here and shown in Figure 6: #1) in the sample transfer tube prior to the sample gas entering the instrument; #2) in the sample transfer tube within the instrument prior to the sample gas entering the gas sampling cell containing the infrared light beam; #3) in the gas sampling cell containing the infrared light beam; #4) in the sample transfer tube within the instrument that receives the sample gas as it exits the gas sampling cell; and #5) in the sample transfer tube after the sample gas exits the instrument.

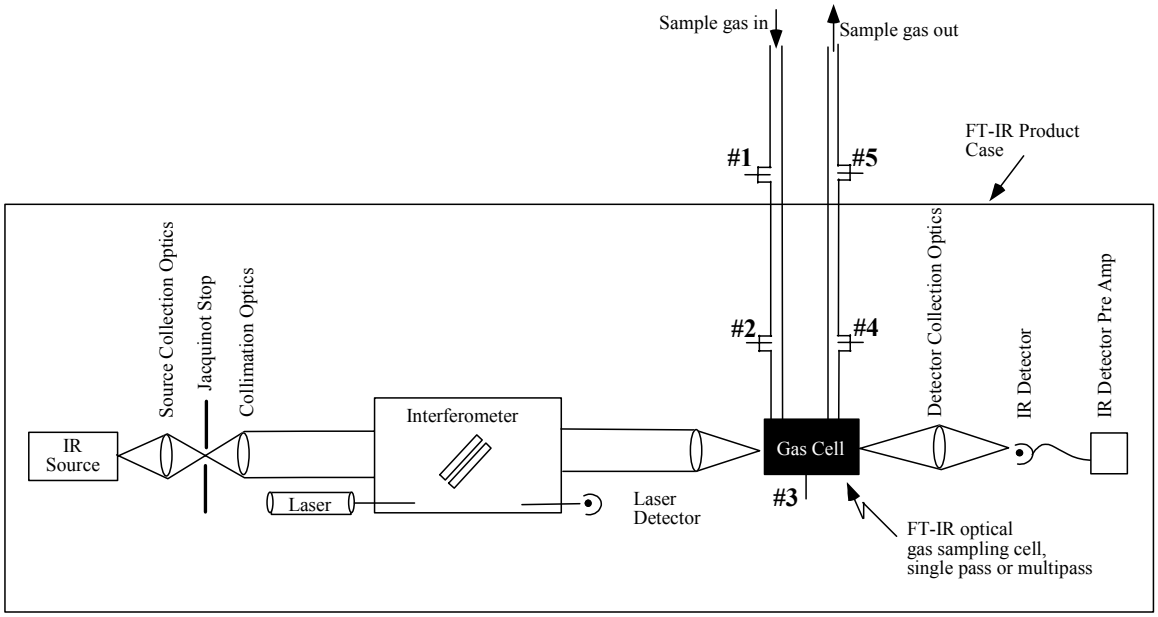

Figure 6: Generic schematic of an FT-IR gas analyzer product showing five locations (#1-#5) in the sample gas path where the oxygen sensor can be integrated.

The small size of the O_2 sensors presented in Figure 5 allows installation at location #3 (in the gas sampling cell with the infrared light beam) by means of a small access hole and gas tight seal, positioned to not interfere with the infrared light beam.

The small size also makes it suitable for installation at locations #1, #2, #4 or #5 in the gas transfer tubes, where a small assembly such as that shown in Figure 7 can be incorporated for sensor contact with the flowing gas sample. Figure 8 illustrates both the NTK and Electrovac sensors mounted in such an assembly.

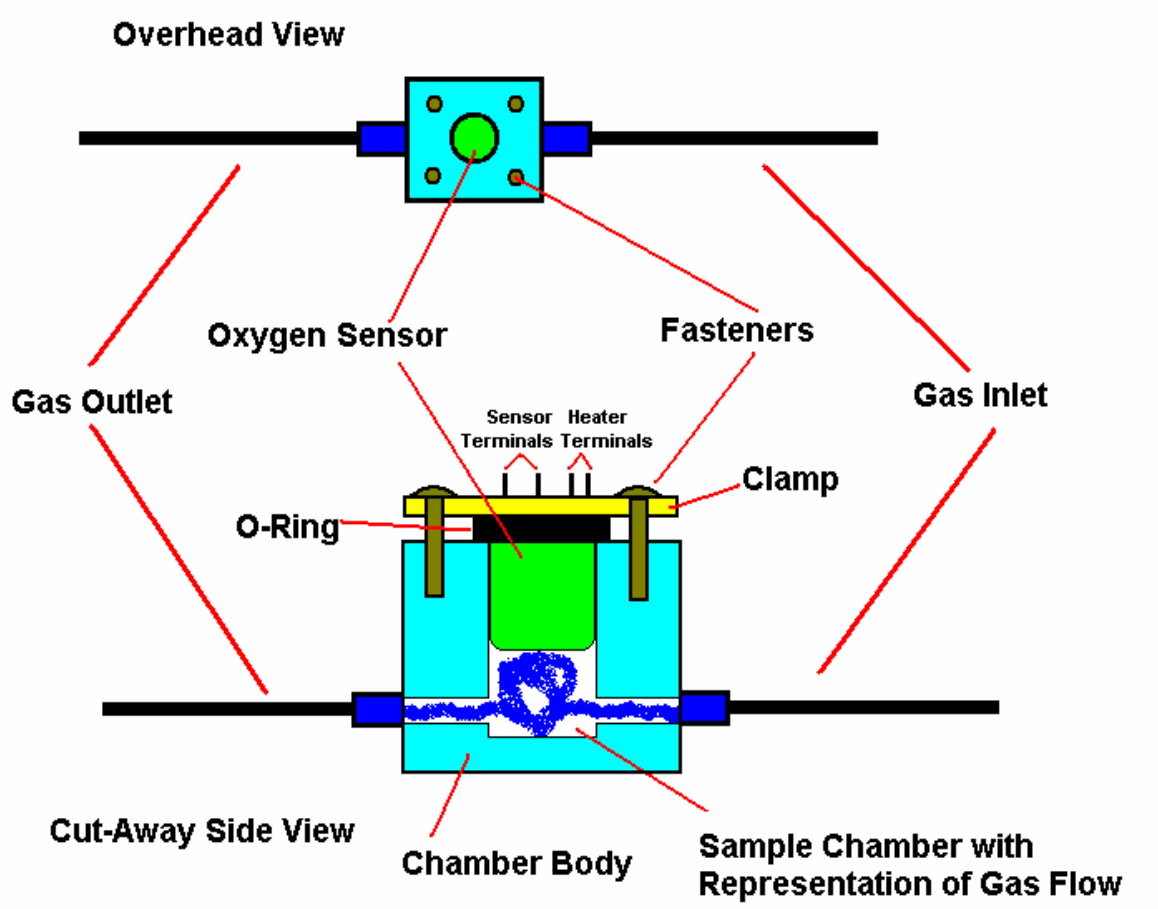

Figure 7: Schematic of a representative flow-through assembly showing the oxygen sensor and sample gas flow.

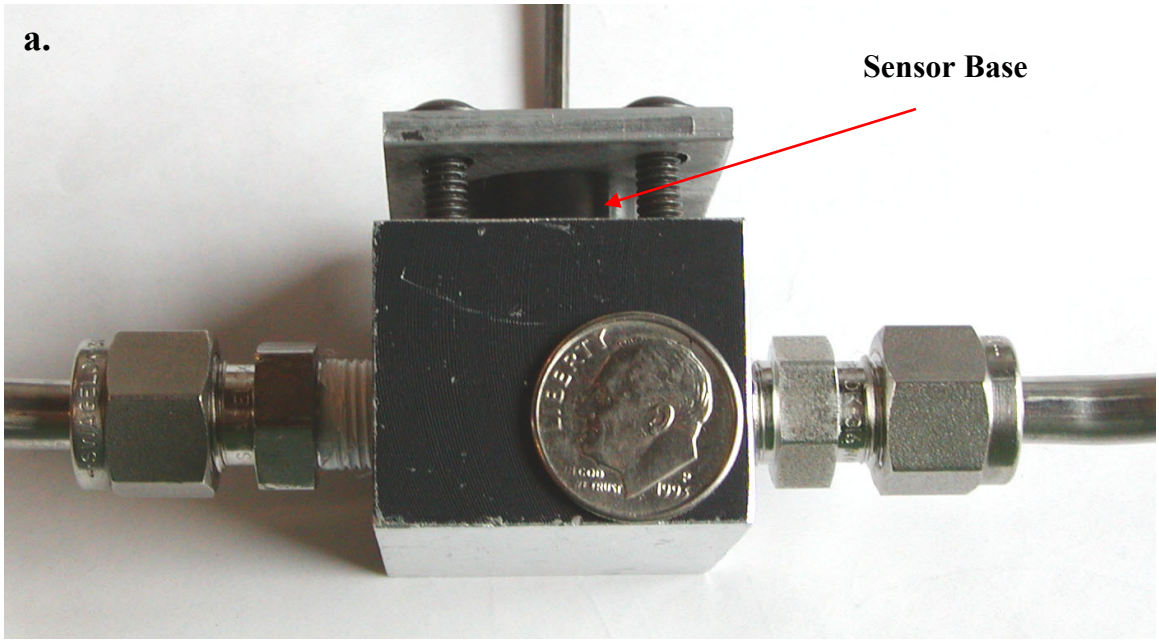

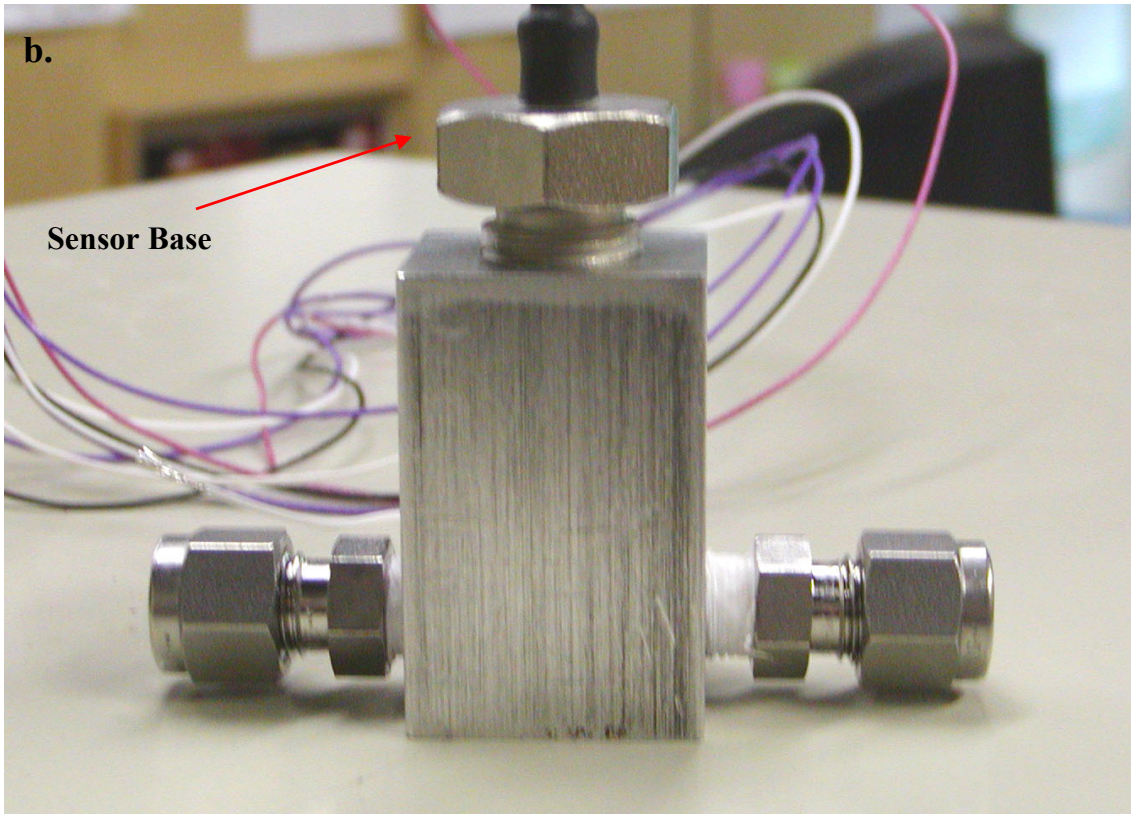

Figure 8: Photographs of both the a. NTK and b. Electrovac sampling cells

Figure 9 presents a photograph of one of the FT-IR units used in the measurements presented in this study. The MultiGas™ 2030 is available from MKS Instruments. Figures 10 a. & b. show the placement of oxygen sensors relative to the gas sampling optical cell within the MultiGas 2030 and its predecessor model 2010. The gas cell with folded optical path provides a 5.11 meter effective measurement path length within a 200 cm^3 sample volume. At 10 SLPM sample flow, gas exchange in the cell takes 4 seconds. The oxygen sensor is integrated into the ¼ inch tubing just downstream of the gas sample exit from the cell. The assembly of optical cell and oxygen sensor are encased in an insulated box in the FT-IR unit and maintained at 150 °C to avoid gas condensation for most applications. This is of course important for the turbine engine exhaust application and other exhaust applications since combustion-generated moisture is included in the sample stream for both FT-IR and O_2 sensor measurements.

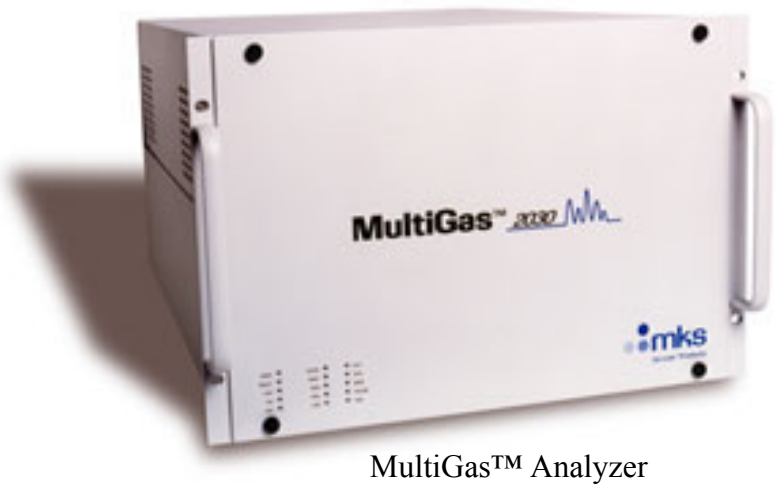

MultiGas™ Analyzer

Figure 9: The FT-IR unit. 17.5” wide x 12.5” tall x 25.5” deep. 19” rack mount chassis.

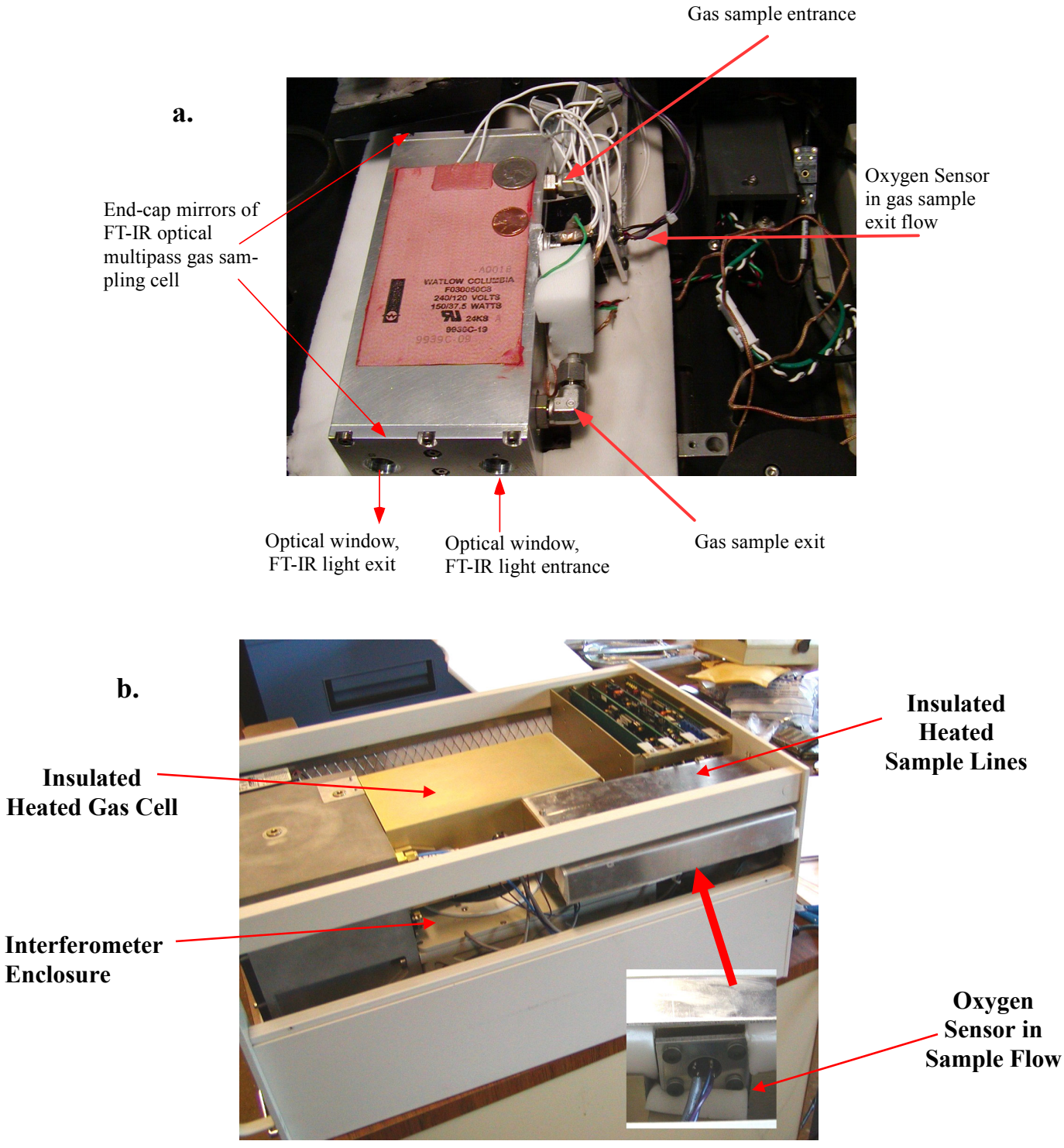

Figure 10: Close-coupled oxygen sensor and FT-IR gas sampling cell. A penny and a quarter are in the top photograph to indicate size of components. a. MultiGas model 2010 and b. model 2030.

In order to acquire the data from the oxygen sensor package and supply necessary heating, an electronics module was fabricated. The module consists of five distinct parts: heater supply, sensor supply, current to voltage converter, data acquisition module (DAQ) and optional ranging. The sensor being of the limiting current type shows a quantifiable change in current with oxygen concentration. This current is converted to a 0 to 5V DC signal that is then digitized and sent to the serial port of the computer using a commercially available DAQ module. The heater circuit provides the recommended operating voltage to the platinum thick-film heater. The optional ranging is a simple gain modification made to the current converting circuit using the same commercially available DAQ module to signal the change. This is for applications that might require higher than atmospheric oxygen conditions.

Three different circuits were designed, fabricated and tested during the development and application of the integrated sensor. The first system used during the February 2003 measurements on exhaust from a Pratt and Whitney FT-8 engine employed the use of four power sources. Only one prototype of this version was produced. The second system used at a March 2003 AEDC/MTSU test of a Pratt and Whitney JT-12 engine eliminated the need for the using a multiple-source power supply, of which two were built. Figure 11 shows all three of the modules used in testing. The third and final version differed from the previous two in that it was designed to run two oxygen sensors simultaneously. This would allow for a direct real-time comparison of both sensors (NTK and Electrovac) during testing. Appendix A describes in more detail the progression of power supplies for the modules. Due to the fact that six of the final version were needed for the project's test plan, a PC board service was employed. This allowed for faster assembly and troubleshooting of problems. A complete single-circuit and PC board layouts are available for review in Appendix B. Also included within the final package is the DAQ module, monitor light, the capability to run two sensors simultaneously and a cooling fan.

Figure 11: All three modules used in testing, advancing in design from left to right.

Throughout construction of the various modules, noise level in the response signal was considered. When placed inside of the MKS FT-IR units, the sensors were found to be fairly noisy in response. In order to reduce the EMF noise picked up by the electronics, the sensor wires were fed through shielded twisted pair and the sheath was grounded to the case. This greatly increased the signal-to-noise ratio. In the final module design, the PC board and circuit both incorporated methods to reduce noise such as power supply and signal filters as well as large centrally located grounds. Figure 12 shows these details.

Additional information, notes and Figures on the fabrication of the sensors, housings and modules is available for review in Appendix A.

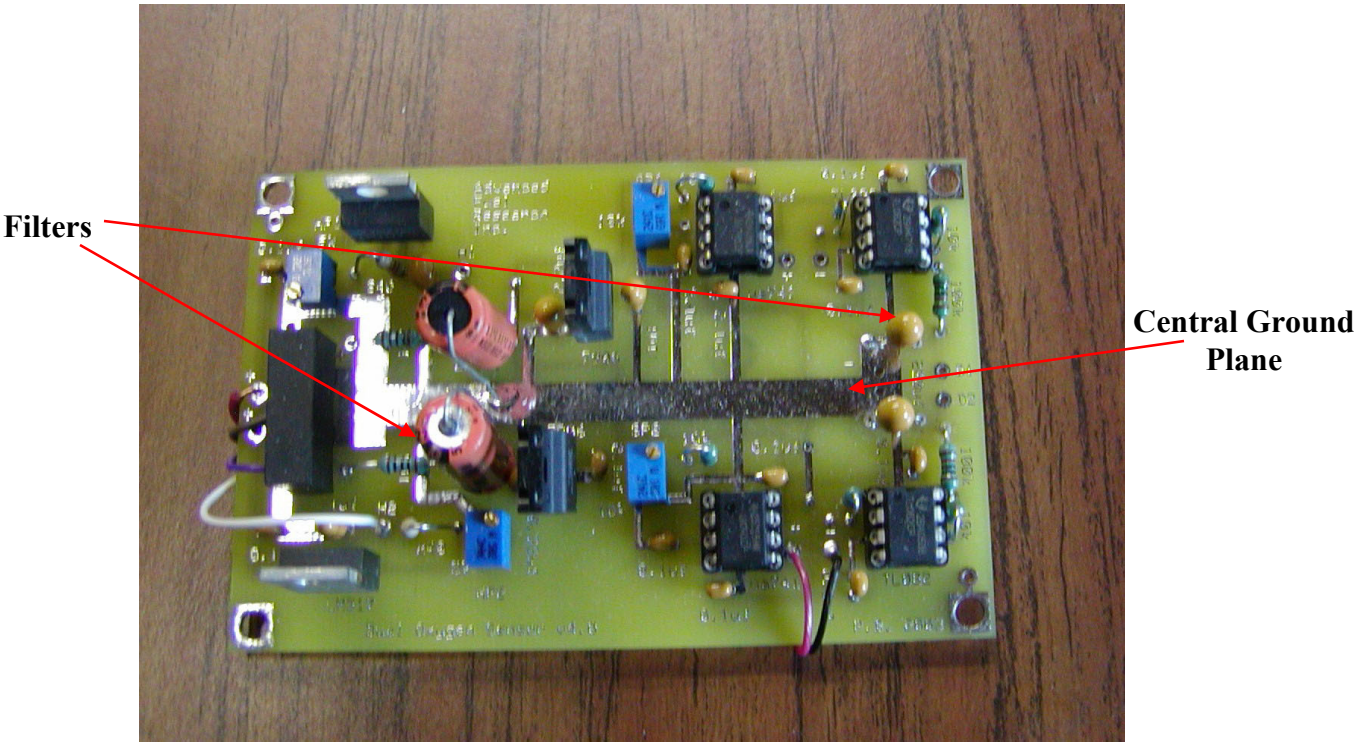

Figure 12: Close-up of PC circuit created showing filters and grounds.

The goal of this research was not only to integrate an oxygen sensor in the physical sense, but also on a software level. Two distinct programs were developed for collecting and reporting the data from the sensor. The first was a stand-alone LabView™ program that was used on the preliminary Pratt and Whitney FT-8 test. This software was completely independent of the MultiGas software and could be run on a different computer. Diagrams and screenshots of this program are available in Appendix C for review.

The second software developed was an add-on to the already existing MultiGas software. With this system, the oxygen concentration is reported simultaneously, along with all of the other gases, the cell temperature, and atmospheric pressure. This add-on also allows the user to perform calibrations though an independent sub-routine. Information on this add-on is also available for review in Appendix C.

Some care must be observed when using this type of sensor. Various reasons for fouling are known to occur. Reducing gases, H_2S and any silicon containing gases can

permanently degrade the sensor's ability to perform. In the case of H_2S, the platinum thick-film heater will be attacked and cause an inconsistent temperature, leading to drifting measurements, or failure of the heating element. Silicon can also be "pumped" through the sensor like oxygen, but becomes permanently attached to the free O2- sites in the zirconia electrolyte, severely degrading the sensor's ability to detect oxygen. This is a common cause of failure in automotive applications when coolant is released into the exhaust stream because it has silicon containing lubricants. Reducing gases can also degrade the sensor but is only a problem when not enough oxygen is present, commonly referred to as reducing atmosphere. For example, CO without any oxygen present will reduce the heated zirconia itself.

Care must also be taken that not only the sensor element, but its surroundings remain hot. This will help to prevent condensation of liquids (i.e. water, fuels) which will damage the sensor itself. This was made clear when a large amount of isopropyl-alcohol was accidentally introduced into the sampling system on the March test at AEDC/MTSU. Two internally mounted sensors that were insulated were not damaged, but an externally mounted sensor that was not insulated failed. All three sensors were from the same manufacturer. Additional information on care and operation is available in Appendix D.

It is also important to note that fuel rich conditions (Jet-A, gasoline, diesel) can cause a "non-permanent" fouling, which was observed when an Otto-cycle internal combustion engine was tested. When the amount of un-burnt hydrocarbons reached a high level (i.e. a few percent volume), the sensor stopped providing reliable results but quickly recovered once cleaner gas was flowed through the system. This is known to also occur in the automotive application with rich burning engines, known as "sluggish response". Again, even these sensors will recover once the engine is tuned properly.

Calibration and Performance Verification

In order to verify the oxygen sensor's stability and repeatability of measurement, calibration gasses were tested. The manufacturers of both the NTK and Electrovac O_2 sensors report that measurement accuracy is within +/- 0.5% of the reading of oxygen, with a measurement range of 0.1% to 95% for the NTK and 0.1% to 25% oxygen concentration for Electrovac. Technical data provided on cross sensitivities to CO_2, CO, NO_2, SO_2, CH_4, H_2S, and H_2O supports the use of this type of O_2 sensor for lean-burn turbine exhaust gas monitoring. After sensor calibration with oxygen-nitrogen mixtures, measurements with other certified gas mixtures were performed to confirm suitable operation. Stability and accuracy are shown in Figure 13. As shown in Table 1, CO_2 and CO at concentration levels not atypical of engine exhaust had negligible influence. The same was true for NO at a very high concentration. The percent differences indicated were within the oxygen concentration accuracy of the certified gas mixtures (+/- 2%).

Table 1: Measured Cross Sensitivities of O_2 Sensor.

Gas Concentrations In Mixture*	**Measured O_2 Concentration**	**% Difference (Real to Measured)**
2.95% CO_2 16.97% O_2	16.99%	+0.1%
4.5% CO_2 902 ppm CO 20.8% O_2	20.71%	-0.4%
2,790 ppm NO	0.08%	____

* certified gas mixtures, balance N_2

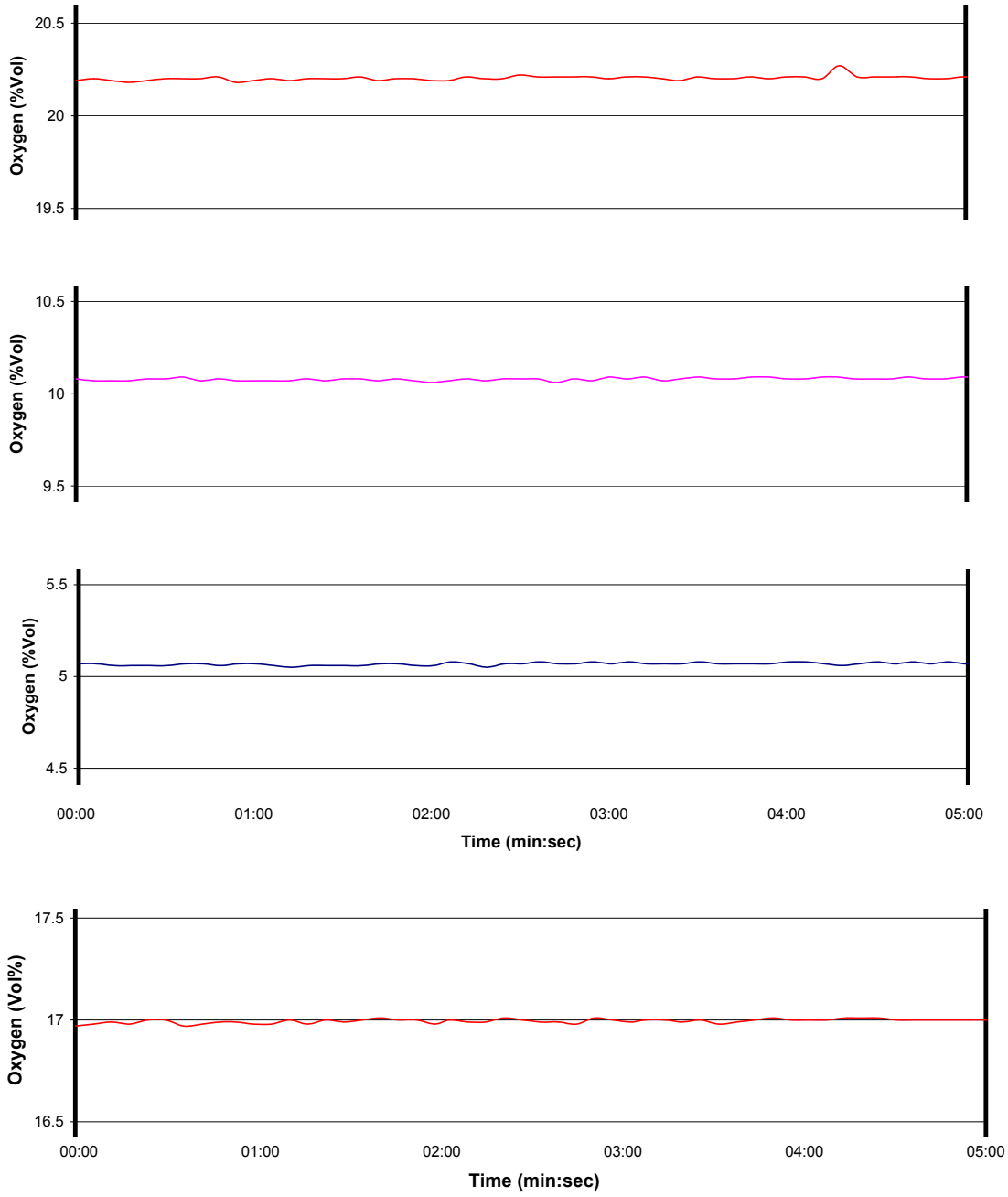

Figure 13: Signal stability of the NTK O_2 sensor when measuring three O_2 calibration standards and bottom, a certified three component gas mixture of O_2 (16.97%), CO_2 (2.95%) and nitrogen (balance).

The MultiGas system maintains a constant gas sampling temperature of 150 C. When the sensor is mounted externally, there is a potential for the exit gas to be cooled slightly. In order to verify the manufacturer's claim that the platinum-film heaters will maintain constant temperature and therefore response, a series of temperature tests were performed. The sensor was mounted in a gas sampling cell that was positioned on a heat source. A room-temperature calibration was measured to establish a baseline. The cell was then heated in roughly 50 C steps and the results recorded. In all cases the temperature gradient had little or no effect on the sensor response. Figure 14 shows the calibrations for the same sensor at the most extreme cell temperatures tested.

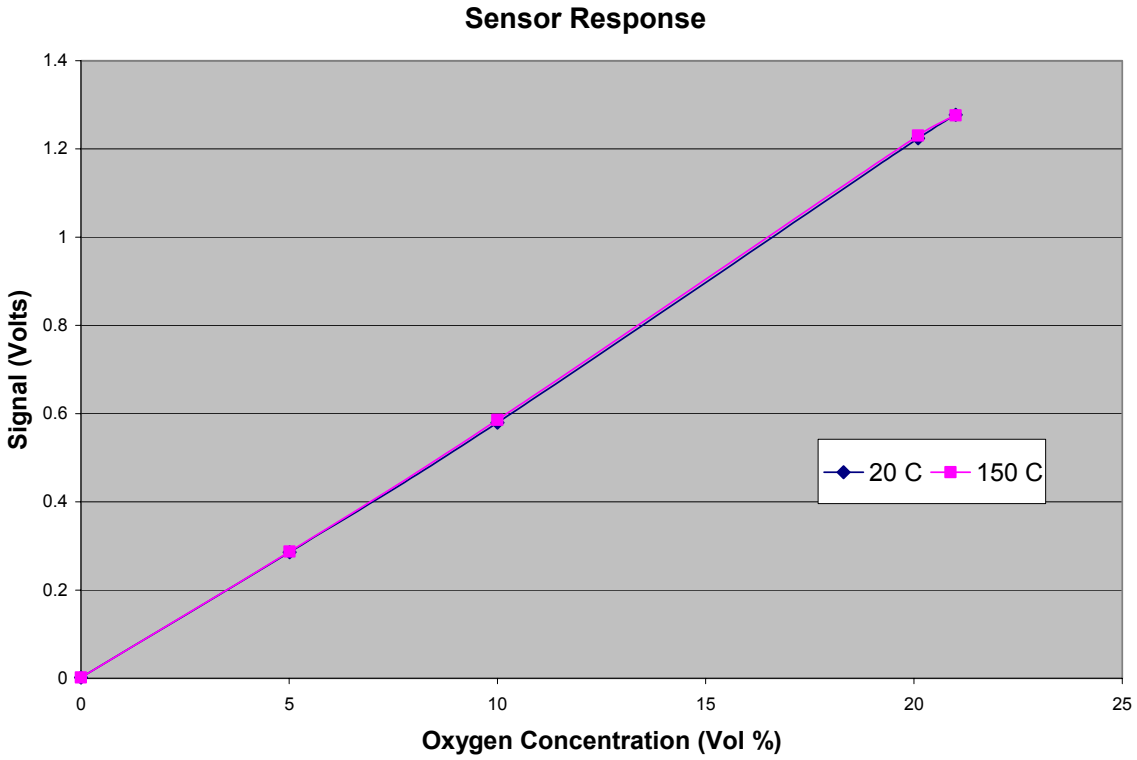

Figure 14: Oxygen sensor response as a function of concentration at 20 and 150 ºC, 10 liters/min flow rate of commercially available calibration standards.

It was observed during calibrations that pressure had some effect on the measurements. The MultiGas Analyzer normally operates at ambient pressure conditions, which can change depending on the weather. In order to document the

pressure influence, certified calibration gases were tested on both sensors over the pressure range of 0.85 to 1.1 atm. The results are shown in Figure 15.

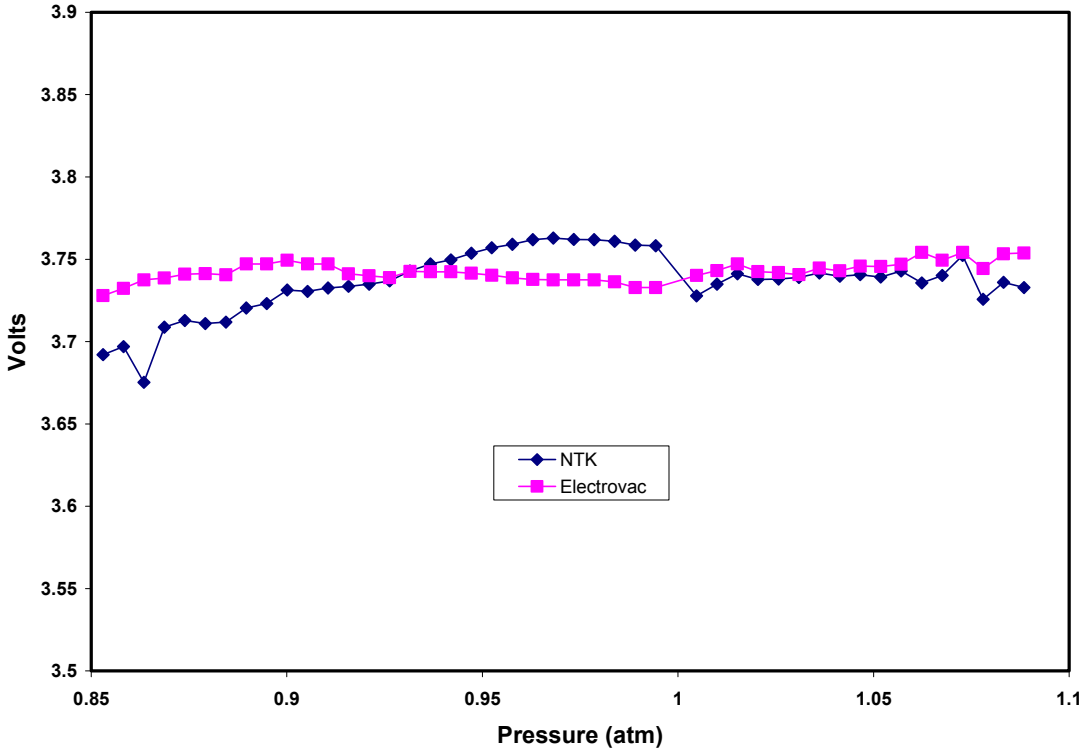

Figure 15: Pressure effects on both the NTK and Electrovac sensors.

The reported oxygen concentration was found to increase as a function of pressure in a non-linear fashion. The variations were greater with the NTK than the Electrovac. A correction is easily implemented in real time, because the MultiGas reports the pressure from a transducer in order to correct the FT-IR measurements.

Demonstrations and Testing

Pratt and Whitney FT-8 Power Plant Emissions Test, February 2003:

Though the research on the oxygen sensor was focused on an initial test at AEDC/MTSU in March, an opportunity for preliminary testing presented itself. In February 2003 Pratt and Whitney required emissions testing to be done on their FT-8 powered energy plant. It was determined that this test could provide at least some endurance and stability measurements. For this test, the prototype electronics module was used. This module did not have the DAQ mounted internally and utilized only one NTK sensor. The oxygen sensor was mounted in the flow-through assembly shown in Figure 7 and located at position #5 in Figure 6, external to the MultiGas package. This system utilized the "stand-alone" software discussed above and was not part of the MultiGas' data collection system.

The integrated gas analyzer for measuring combustion exhaust species and oxygen was connected by a heat trace sampling line to the exhaust stack of the electric power generating turbine engine. Traditional single-gas analyzers were not available for comparative measurements. Figures 16 a. and b. present measured concentrations as a function of time during firing with natural gas and liquid fuel (Jet-A), respectively.

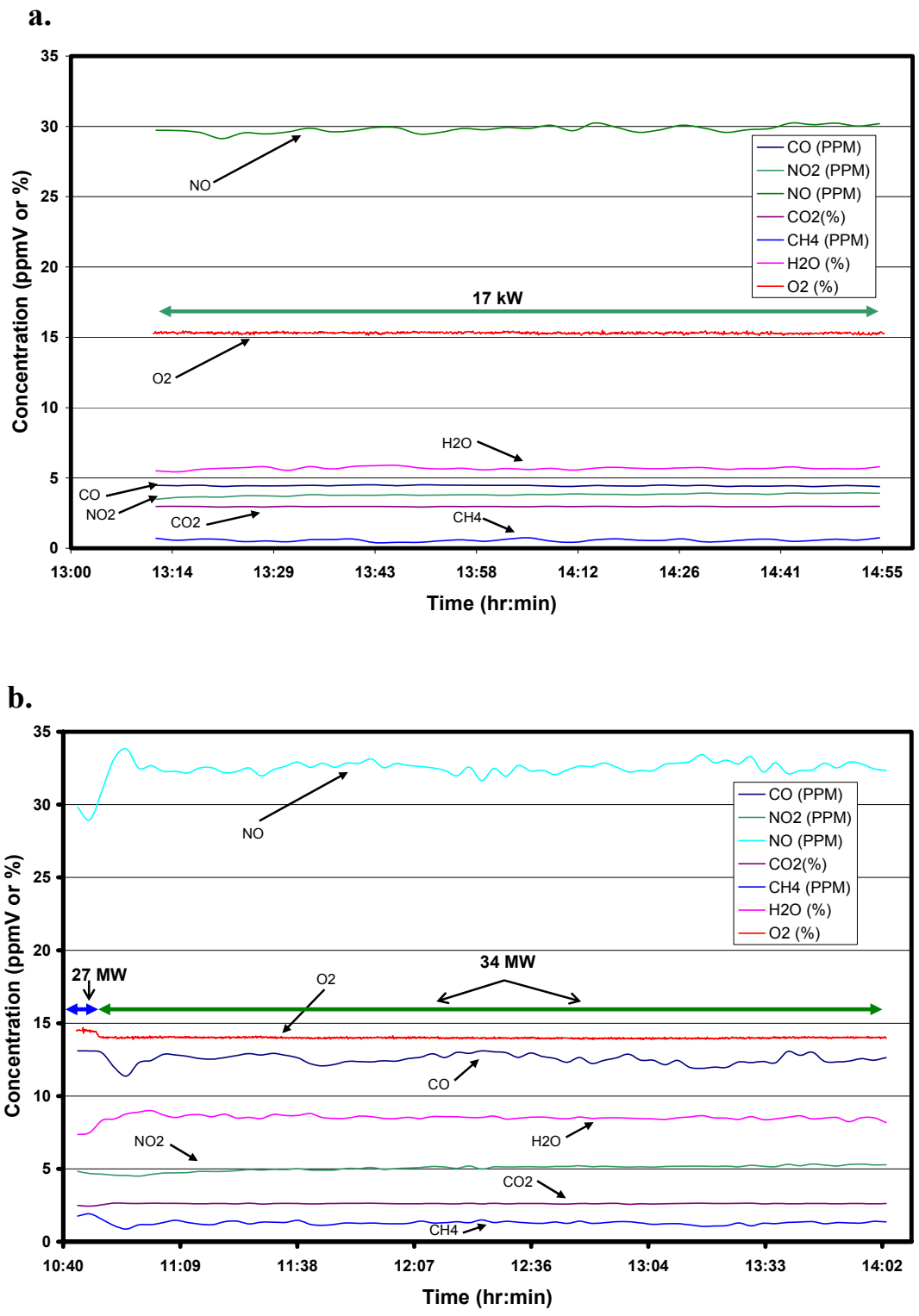

Figure 16: Concentrations of oxygen and combustion emissions measured with the integrated analyzer fired with a. natural gas and b. Jet-A.

Presented in each figure are the measured concentrations for O_2, CO_2, CO, NO, CH_4, and H_2O. The FT-IR sensor was set to collect data at 0.5 wavenumber spectral resolution (~2 scans per second) and report signal-averaged data every 3 minutes. The O_2 sensor was set to collect data at 50 Hz and report signal-averaged data every 6 seconds. It is also important to note that because the oxygen sensor was report an average value over a much shorter period than the MultiGas was, the long time averaging of the FT-IR values can result in a much smoother overall plot. During natural gas firing, the power output was increased to 34 MW after a brief time at 27 MW. The drop in O_2 concentration coincides with the rise in H_2O concentration and drop in CH_4, as expected by the reaction chemistry taking place in the turbine engine combustor. During liquid fuel firing, the power output was held constant at 17 MW, and the data traces reflect the constant operation.

The 34 MW run condition (Figure 16 b.) and the 17 MW run condition (Figure 16 a.) were held constant for ~3 hours 10 minutes and ~2 hours, respectively. During these nominally long periods of exposure to the combustion gas mixtures, the O_2 sensor maintained generally flat output response (~15.3% and 14%) in the presence of percent levels of CO_2 and H_2O. After these measurements, the O_2 sensor's response to calibration gases resulted in duplication of Figure 4. These responses provide confidence that the O_2 sensor was not being gradually poisoned by the combustion gas mixture.

Figures 17 a. and b. present expanded plots of the O_2 concentrations measured for each firing. During the periods of nominally constant power output, the peak-to-peak deviation in the O_2 traces are higher than those observed for the calibration gases in Figure 13. The liquid fueled firing exhibits a higher deviation than the natural gas firing.

a.

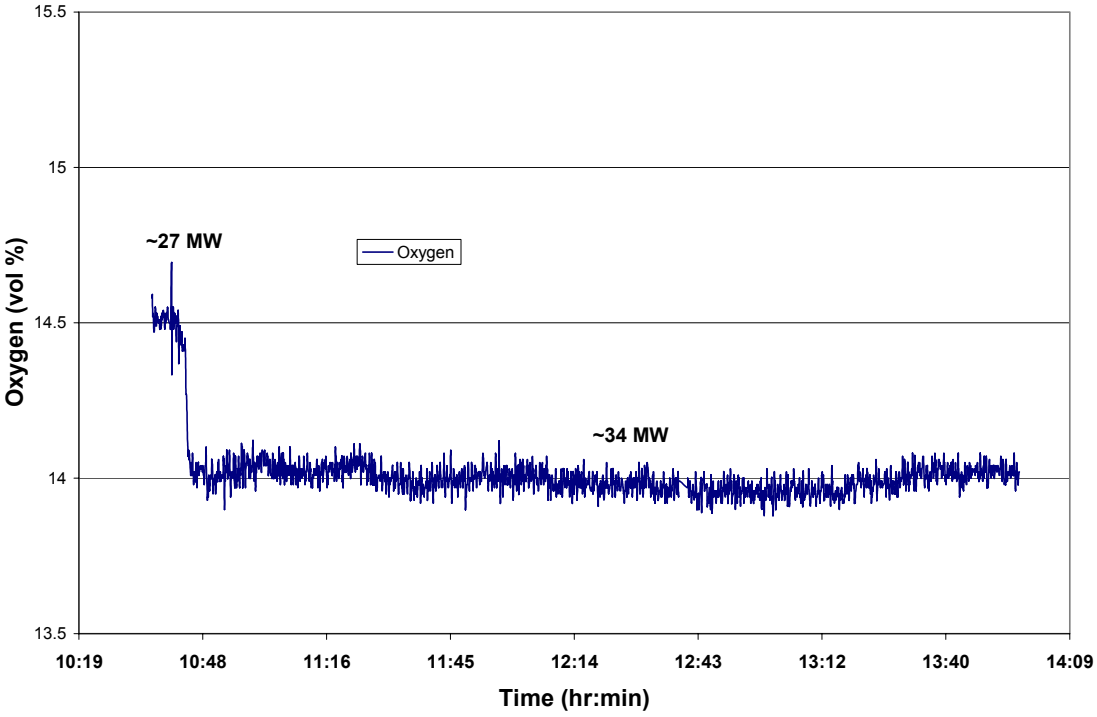

b.

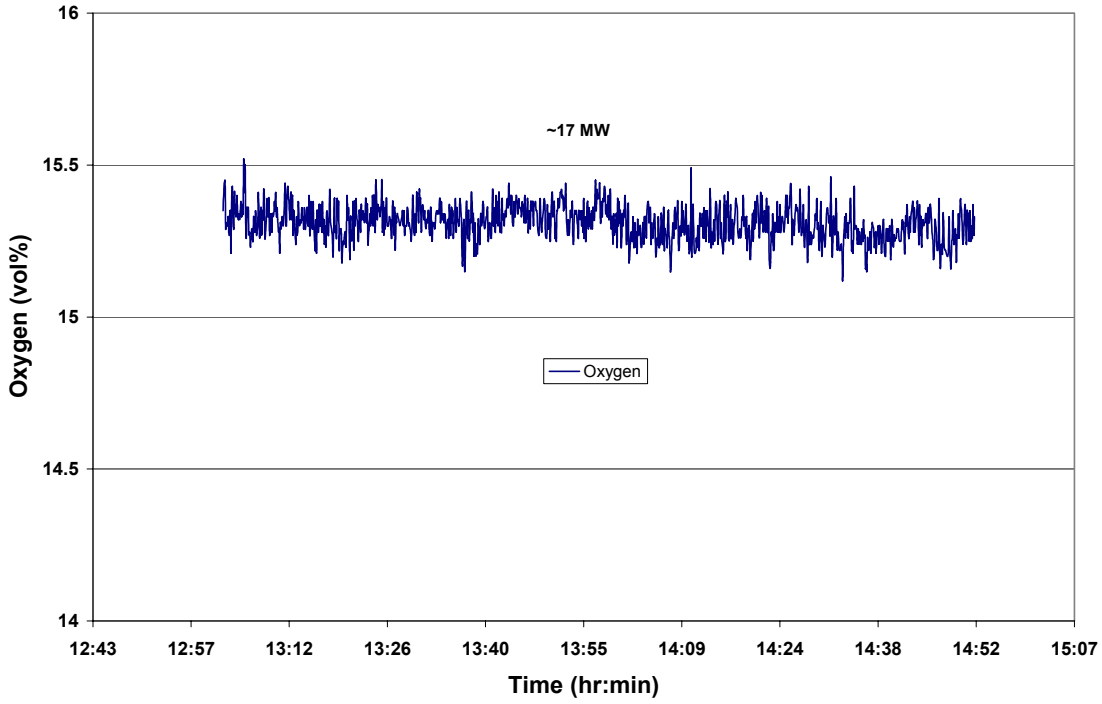

Figure 17: Expanded view of O_2 trace of Figures 16 a. and b.

AEDC/MTSU JT-12 and Continental IC Engine Test, March 2003:

Measurements were conducted on both a Pratt & Whitney JT-12 turbine engine and a Continental IC piston engine operated by the Aerospace Department at the Middle Tennessee State University (MTSU). Measurements on the JT-12 were taken 1) with the probe rake held constant at the nozzle centerline during acceleration/deceleration of the JT-12, and 2) during continuous sweep of the probe rake across the nozzle exit at constant engine power. The JT-12 can be fired with diesel fuel or Jet-A fuel, and MTSU used both fuels during the course of testing. The FT-IR sensor was set to collect data at 0.5 wavenumber spectral resolution (2 scans per second) and report signal-averaged data for every 2 seconds. The O_2 sensor was set to collect data at 50 Hz and also report signal-averaged data every 2 seconds. For this test, two NTK sensors were mounted internally in the MultiGas package.

For this test, two newly designed modules were used to collect the data from the oxygen sensors. These new modules, while not the final design, had some distinct advantages over the prototype. First the new modules did not require the 9V batteries to power the Op-Amps. This benefit allowed continuous use of the sensor, without the concern of the condition of the batteries. One other major improvement was that even though it still required an independent power supply, the DAQ module was now placed inside of the complete module, eliminating the need for custom cables and reducing overall package size.

Figure 18 overlays the measured concentrations of O_2, H_2O and CO_2 as a function of time during step-wise acceleration and deceleration, firing with diesel fuel. Note that the concentration axis for O_2 is on the right side of the plot, and that percent of full engine power is indicated at the top of the plot.

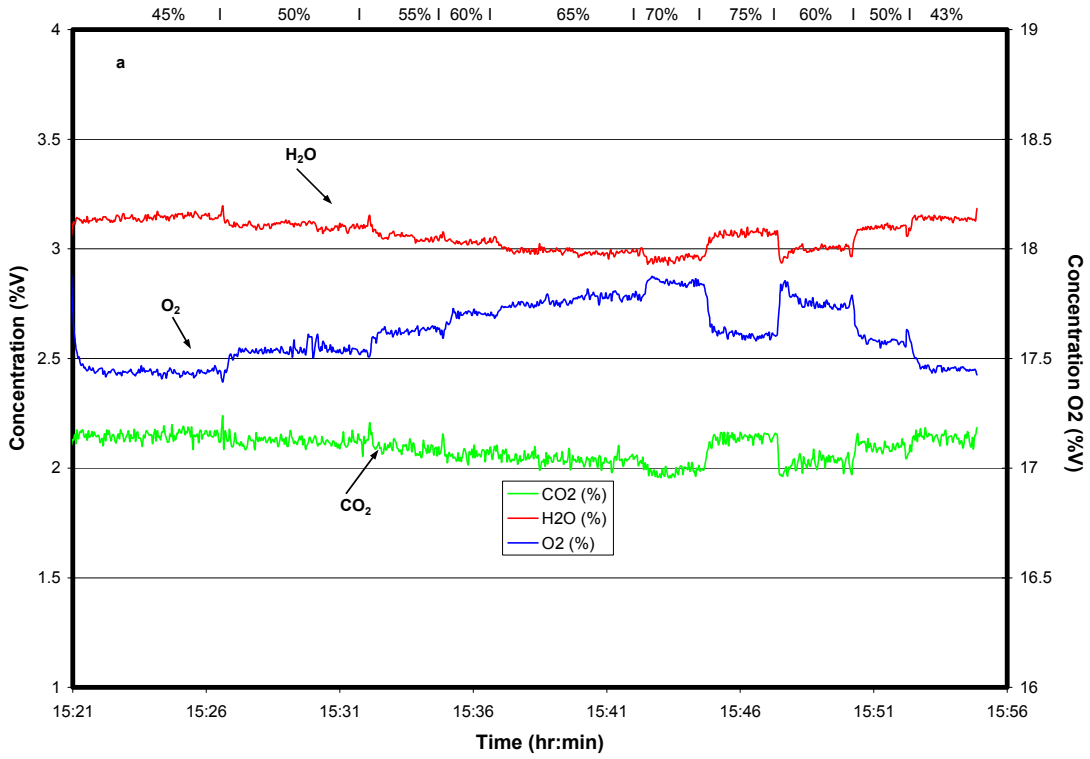

Figure 18: Oxygen balance for a stepwise power sequence at centerline.

As engine power is increased up to 70%, the excess O_2 concentration in the exhaust rises from 17.4% to 17.8% (a 2.3% increase) as more air is pulled into the engine to burn the additional fuel. According to the JT-12 maintenance manual, the automatic modulated bleed starts to close in the 70% to 75% power level range. The compressor bleed system consists of a bleed valve assembly and external linkage to the fuel control. The bleed valve assembly (bleed band) is located just downstream of the compressor. It is open at low engine speeds to dump excess air and then closes at higher power to burn more fuel. Therefore, further acceleration to 75% power results in a drop in the excess O_2 concentration and corresponding increases in H_2O and CO_2 concentrations. These trends are reversed for all three gases during deceleration.

The features of the O_2 concentration trace correlate inversely with the features of the H_2O and CO_2 concentration traces. Note the fine features at the engine power transition points, exhibited by each gas. This is an important observation since the solid oxide O_2 sensor is an independent sensor integrated into the optical FT-IR gas analyzer.

The fine features are real indications of concentrations and not simply "sensor overshoots" during rapid transitions. All three concentration traces also demonstrate reversibility from start to finish of the time (i.e., power) sequence.

Another type of test performed was continuous sweep surveys. Continuous sweep surveys are done by keeping the engine power constant but altering rake position. The sweep begins at the top of the exhaust nozzle and is dropped through the plume at a measured rate. Figure 19 presents results for an oxygen balance over four separate sweep speeds.

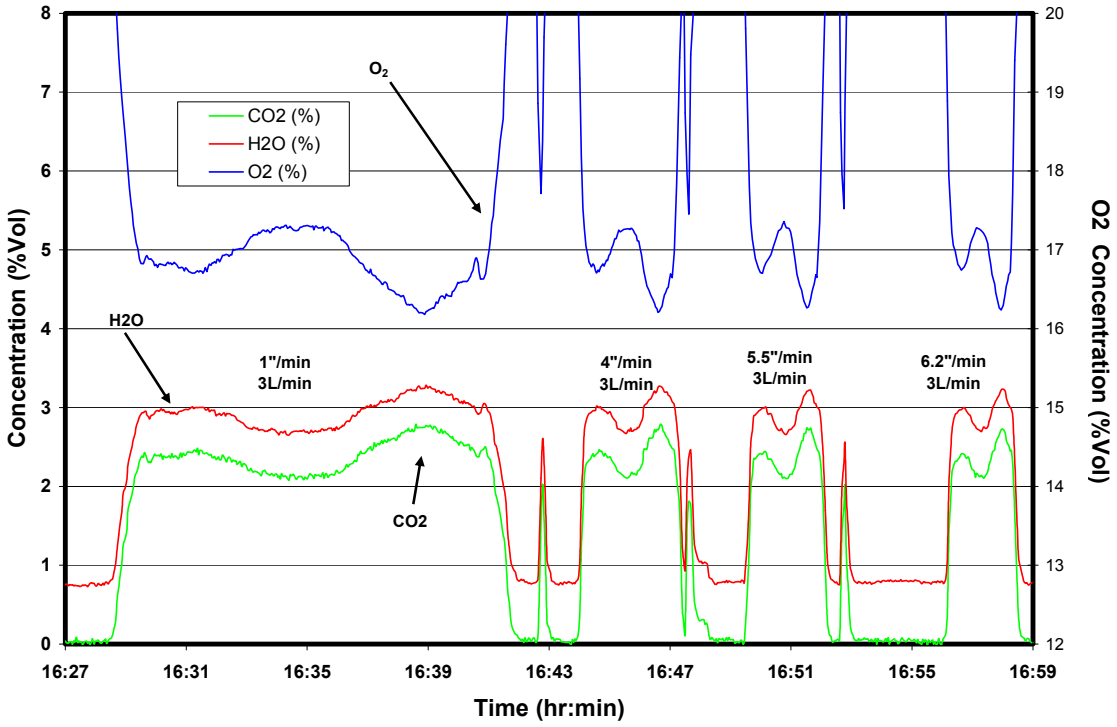

Figure 19: Oxygen balance during sweep surveys at different speeds

As the sweep speed increases, the resolution of the oxygen sensor tracks well with the FT-IR measurements. The oxygen balance is maintained even at a relatively fast rate of travel.

During the tests performed, AEDC ran the California Analytical Instruments (CAI) 100P paramagnetic oxygen analyzer. Figure 20 shows the comparison between the AFR

designed integrated oxygen sensor and the CAI during the same step-test presented above in Figure 18.

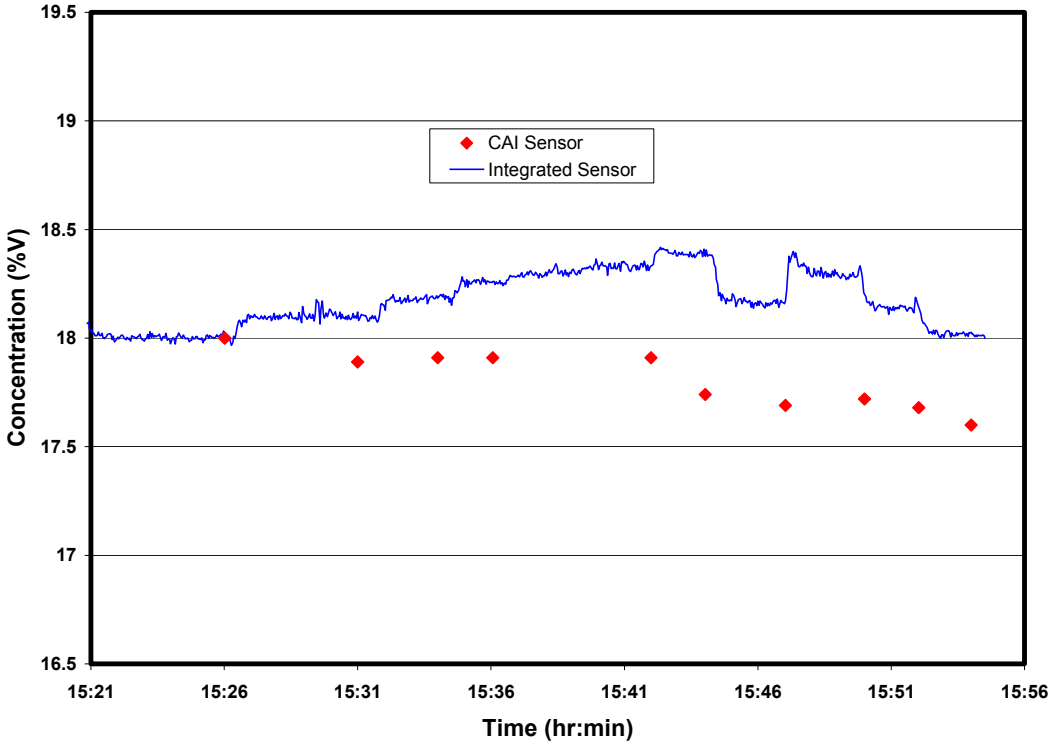

Figure 20: Comparing integrated oxygen sensor and CAI paramagnetic oxygen sensor.

The CAI levels presented in this Figure are dry basis, meaning the data from the integrated sensor has been corrected to this standard. The CAI sensor demonstrates a non-reversible trend and seems to only decrease as a function of time and violates the oxygen balance. It was later determined that the CAI system was not reporting reliably.

Previously cited, this sensor was determined to be ideal for a "lean-burn" type engine. Having a rich-burning Continental IC engine available at MTSU at the time, it was determined to be of value to test the sensors capability under rich conditions. Figure 21 shows a power sequence in RPM completed.

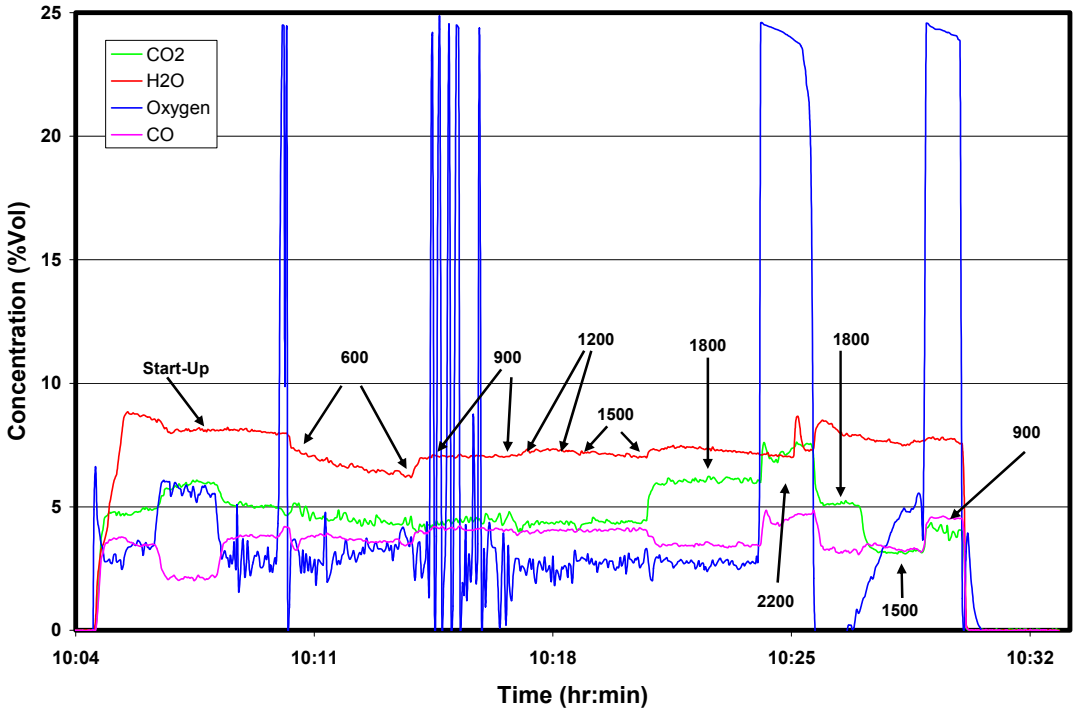

Figure 21: Oxygen balance on Continental engine. Engine speed is indicated in the plot.

With this engine, CO becomes a major contributor to the oxygen balance being roughly 80 times higher in concentration than with the JT-12. Due to the high amounts of CO and un-burnt hydrocarbons present (totaling at least 6% by volume), the sensor was not able to report the concentration of oxygen accurately. Sensor response is particularly poor when the CO and hydrocarbon levels were at their peak, registering at an off-scale value (~24%). It is important to note the even though AEDC's CAI paramagnetic oxygen analyzer was functioning, it was also reading off-scale at the same time.

June 2003 AEDC/MTSU JT-12 Test:

The June test required that six MultiGas Analyzers be equipped with oxygen sensors. Having recently procured the Electrovac sensors, it was determined that a "side-by-side" comparison could be performed. Five MultiGas model 2030 and one 2010 were equipped with sensors. Six internally mounted NTK sensors would be in series with six externally mounted Electrovac sensors. The external sensors would be well insulated to ward off formation of any condensates.

Since twelve sensors were to be tested, it was necessary to construct six modules, one for each instrument. Each module is capable of measuring two sensors simultaneously, reducing the number needed by ½. These new modules were designed so that all components were internal and employ only one power supply. Details on construction and circuitry are available in Appendices A and B.

At the June tests, continuous sweep tests were again performed. Figure 22 illustrates an oxygen balance during four tests.

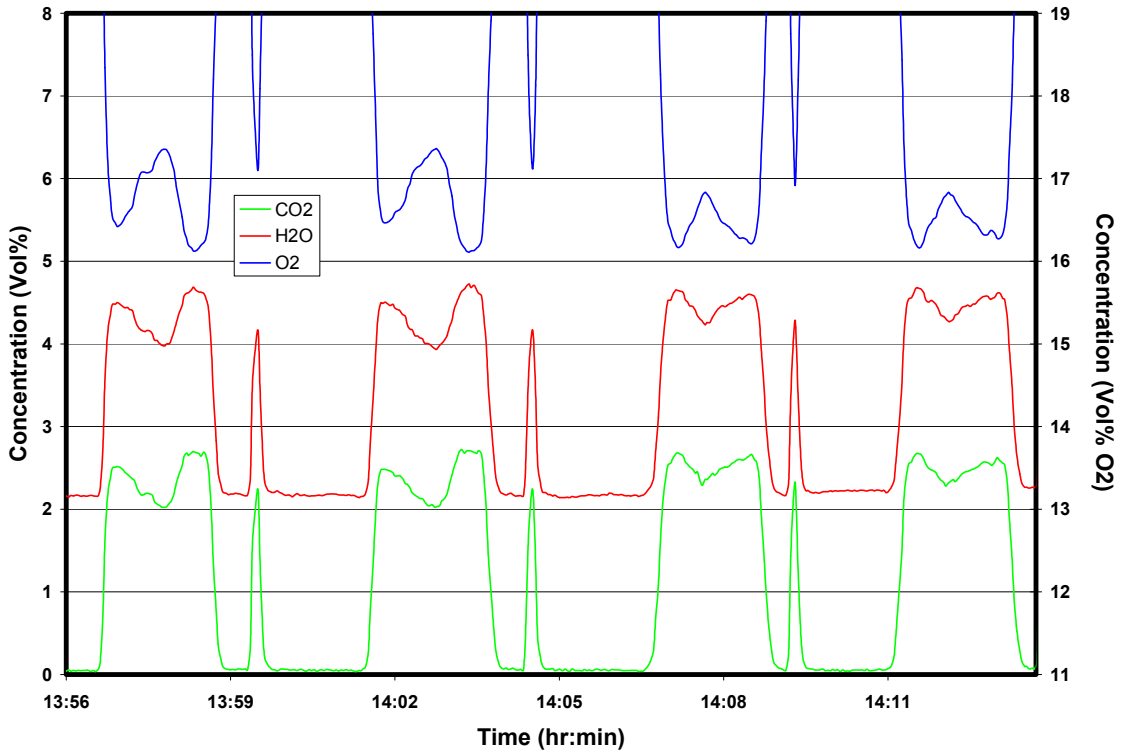

Figure 22: Oxygen balance during sweep tests.

All of these tests were performed at 45% power and a drop-rate of 6" a minute. The only difference was which position on the rake was being sampled. In all cases, the oxygen sensor tracked the response of the FT-IR based measurements. This multi-method analysis verification approach helps to confirm the results reported by the system.

During the test sequence at the MSTU airfield in June, the weather was variable. Figure 23 shows the oxygen balance on the JT-12 engine during a heavy thunderstorm.

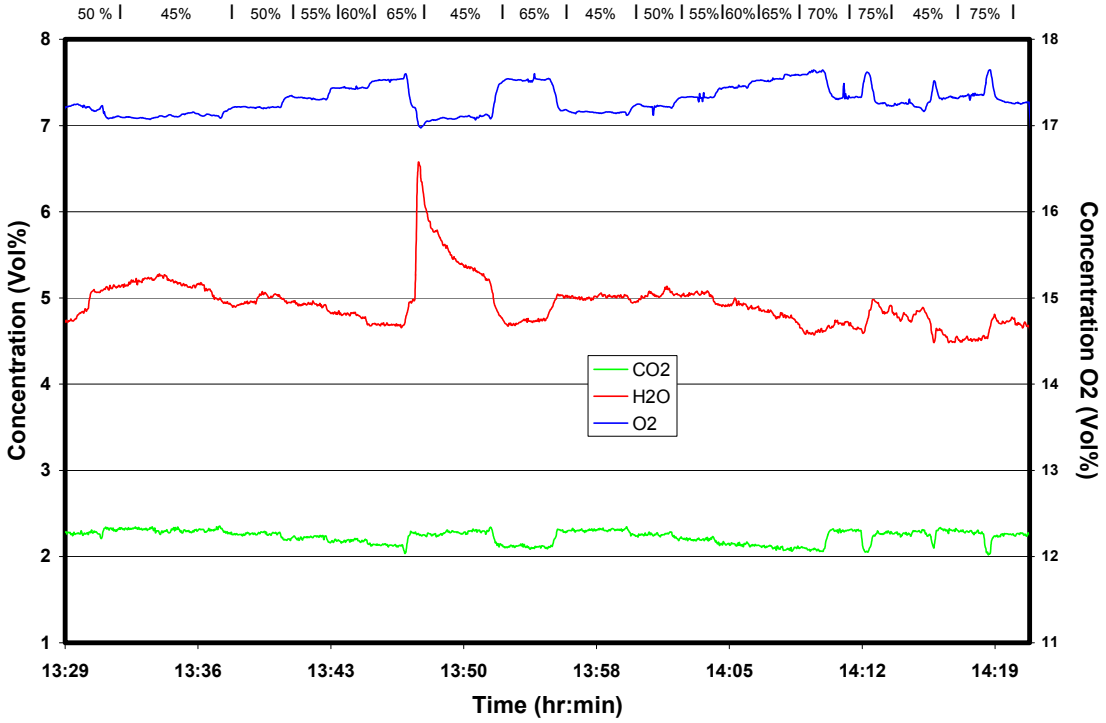

Figure 23: Oxygen balance on JT-12 engine stepwise power sequence during rainstorm.

The engine itself was tented, but during the storm liquid water was ingested by the engine at the intake. Both the FT-IR based CO_2 measurement and the oxygen sensor track each other and demonstrate reversibility, while the water measurement is mixed function of the amount of rain ingested and engine power.

Data from four MultiGas instruments was taken simultaneously with all being connected to the same sample. Figure 24 overlays the data from all four of the Electrovac sensors used in both a stepwise power sequence and two continuous sweeps.

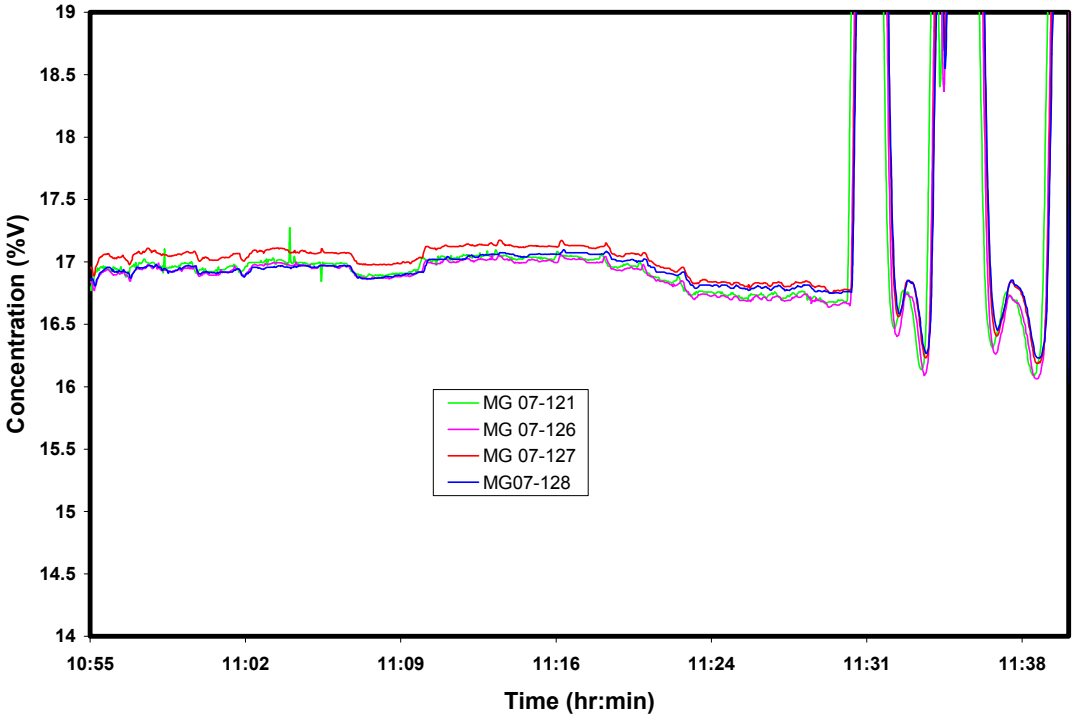

Figure 24: Overlays of four Electrovac sensors during step-test and two sweep-tests.

All four sensors tracked each other in response fairly accurately. The max deviation seen was 0.1% oxygen or 0.58% of the reading (not including three "spikes" seen in the MG 07-121 sensor). Possible sources for these small errors are: minute differences in pressure, calibrations, and/or sensor accuracy itself. Each sensor is guaranteed to be accurate within $^{+}$/- 0.5% of the reading. When comparing two sensors, this error has a range of $^{+}$/-1%, of which all of the readings fell within each other.

During the previous test at AEDC/MTSU in March, the CAI oxygen analyzer was not functioning. The dry-basis O_2 concentration is presented in Figure 25, with data points recorded from the both the traditional paramagnetic O_2 sensor and the integrated solid oxide O_2 sensor.

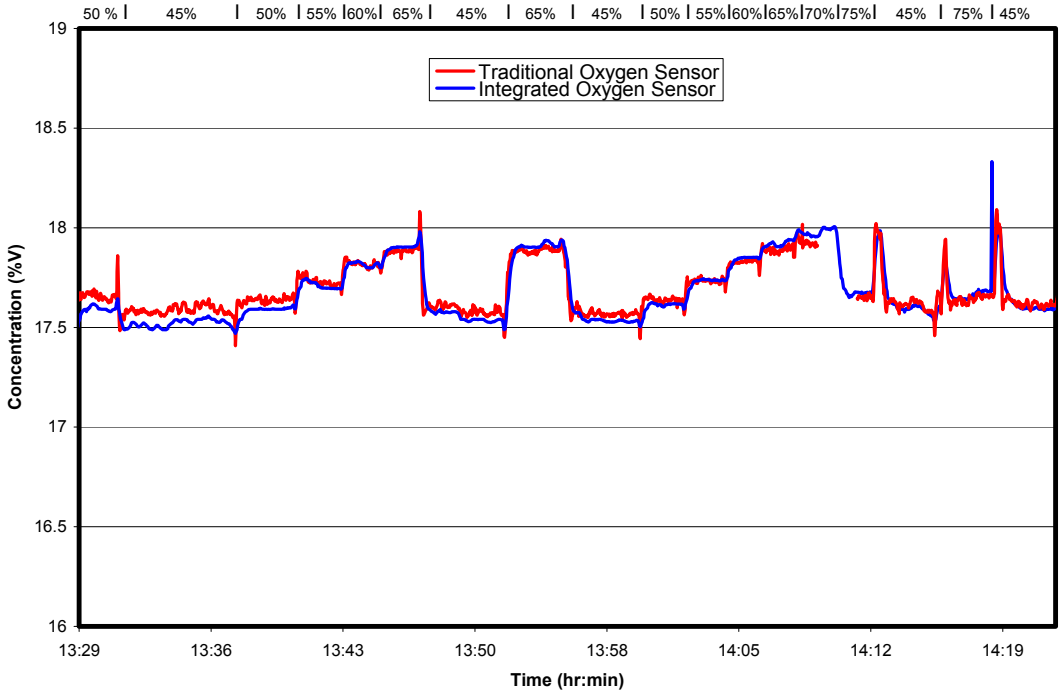

Figure 25: Oxygen concentration (dry basis) measured with the integrated O_2 sensor versus the traditional paramagnetic O2 sensor. Engine power is indicated at the top of the plot.

Throughout the power cycle, the integrated solid oxide sensor's output tracked the response the paramagnetic recorded. The maximum steady-state (constant engine power) deviation between the two instruments was approximately 0.08% oxygen, or 0.4% of the measured value. Both sensors demonstrate reversibility as a function of engine power. It is important to note that the paramagnetic sensor records a single-point measurement and the integrated sensor recorded 15 points over a one second time period and reports the average value. This, as well as some observed inherent noise within the paramagnetic sensor's response may account for the greater instability seen in its measurements. It also apparent that the data trace of the integrated sensor in Figure 25 has less apparent measurement noise than in Figure 17. The integrated sensor's electronics package was improved which increased its signal-to-noise ratio compared to when the data of Figure 17 was generated.

It has been mentioned before that paramagnetic sensors require moisture removal from the sample stream to avoid condensation in the unit. During this test, the extracted engine exhaust sample was directed through a Nafion™ tubing gas drying system. The resultant dry flow (< 0.25% moisture) was then split to offer identical samples to the O_2 sensors. The direct comparison to the traditional standard and its relationship with the independent measurements of CO_2 and H_2O, support the credibility of the integrated solid-oxide sensor to provide the measurement of exhaust excess oxygen.

Air Quality Monitoring:

The integrated oxygen sensor need not only be applied to jet engine applications. Air quality monitoring, rocket propulsion analysis and many other applications are possible. In air quality monitoring there are two needs immediately identified by AEDC, down-stream air analysis and wind tunnel for conditions for safe entry of personnel. The latter was already tested and results are discussed below.

Symptoms of oxygen deficiency in humans are well documented to begin at an atmospheric concentration of approximately 16%. The effects become progressively more severe with further reduction in oxygen content. Figure 26 plots O_2 concentration measured over a 1 hour 15 minute time period. Throughout the first 55 minutes, the O_2 concentration level is very low during the gaseous nitrogen (GN2) purge process through the cell. When the GN2 purge process is completed, a ventilation door into the cell is opened, and the O_2 level rises to about 15% in the local area of the gas extraction probe in the cell. At this time a purge blower is turned on to force air through the cell. The O_2 level drops back down to about 2% as the plug of GN2 is forced past the extraction probe. The GN2 is then displaced by air as the O_2 level recovers to the ambient air level of 20.9%.

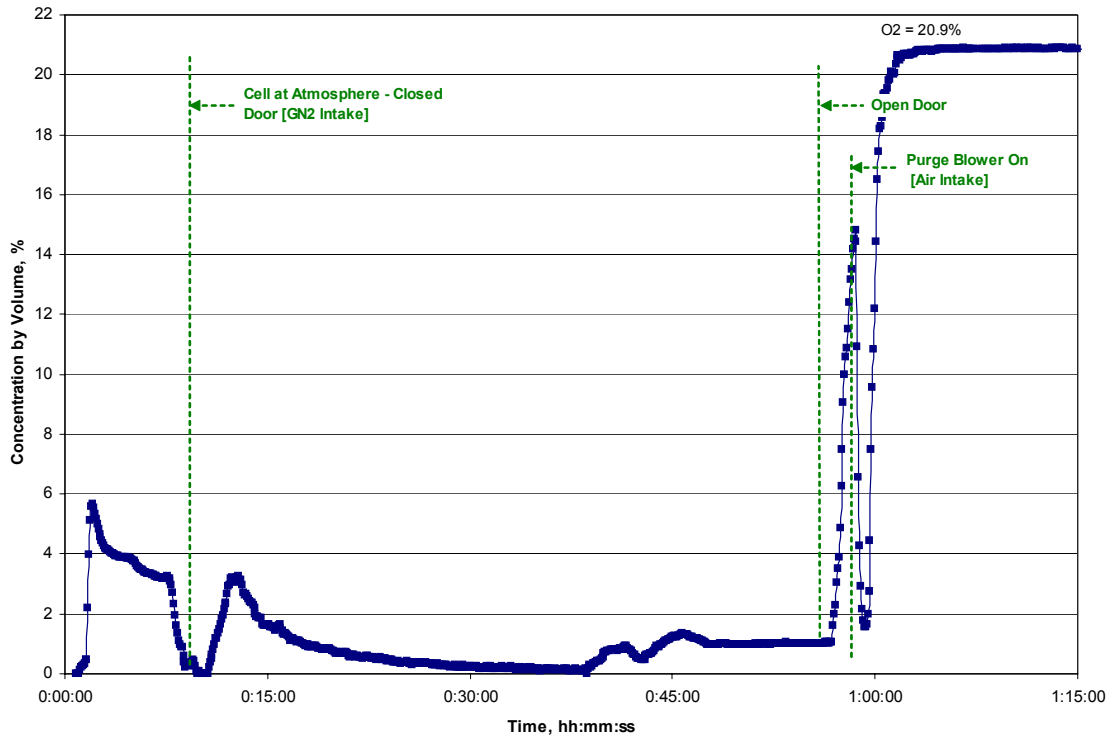

Figure 26: Oxygen concentration measured in the hypervelocity wind tunnel.

Selection of Vendor

Results of the data collected in June 2003 provided a direct comparison of the NTK and Electrovac sensors. It was agreed upon the Electrovac sensor had some distinct advantages: 1. *The Ease of Replacement and Construction*. The Electrovac sensor with its screw-thread housing requires less machining of the cell to integrate it into the MultiGas Analyzer and nine fewer service parts (four bolts, four washers and retainer plate). Replacement time is also lower because of having no additional securing hardware to remove. 2. *Reduction of Signal Noise.* This is due to the fact that the Electrovac sensor produces on the order of 20 times more current for a specific concentration of oxygen. Stray EMF affected the Electrovac response far less than the NTK, reducing the need for greater shielding. Figure 27 shows a direct real-time comparison of the two sensors.

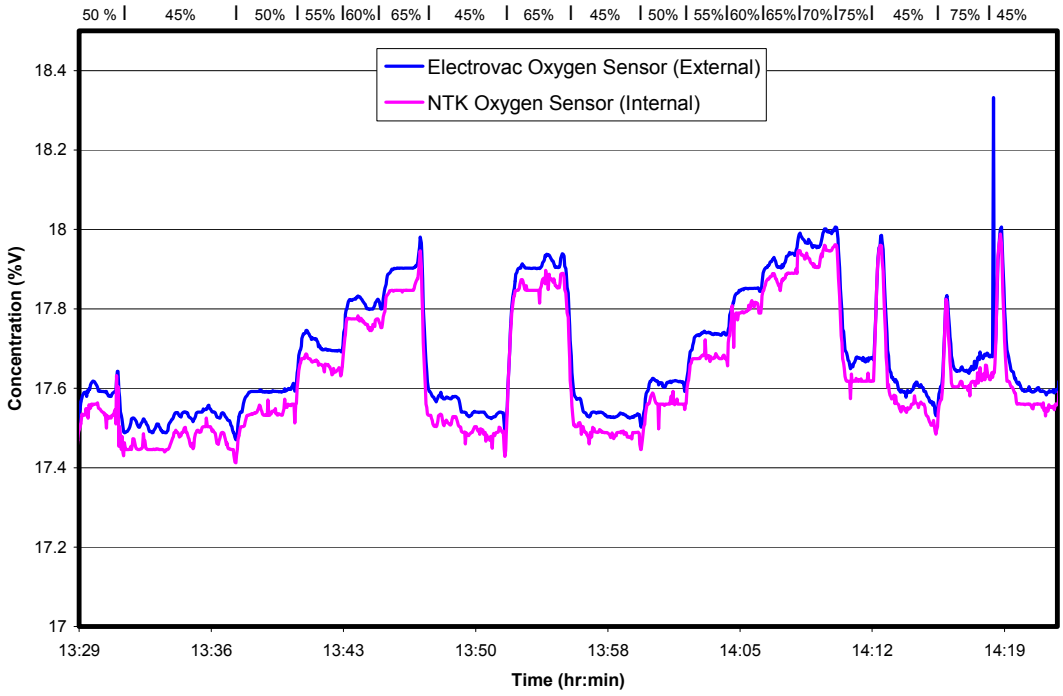

Figure 27: Comparing Sensor Response for Both the NTK and Electrovac Sensors

3. *Materials of Construction*. The NTK sensor is comprised of Teflon and PPS, both plastics with melting points of around 270 C. The Electrovac is constructed of metal, including the filter which employs a sintered metal cap. This provides a much more rugged package, desirable for long-term installations. All of these advantages made the Electrovac an ideal choice in this application. *4. Sensitivity to Pressure*. As shown in Figure 15, the Electrovac sensor demonstrates far less drift as a function of pressure. This is more suited to the application because of the need of pumping systems used to flow the sample through the FT-IR cell can slightly increase the pressure and also changes in day to day atmospheric conditions.

Conclusions

Cited literature tracks recent developments of FT-IR spectroscopy as a potential replacement for the instrumentation of the current SAE ARP for the measurement of gaseous emissions from aircraft turbine engines. Improvements in FT-IR analyzers have resulted in lower procurement and installation costs with considerably less support infrastructure. These multi-component single package analyzers also provide lower operating costs and faster response times. In addition to a major impact on cost, there is also a major impact on productivity. As part of this effort, an integrated gas analyzer has been demonstrated for the simultaneous measurement of turbine engine exhaust gases and excess oxygen. Combining the spectroscopic technique of FT-IR gas analysis with a solid-oxide (zirconia) sensor run in amperometric mode offers a "single instrument" approach for the simultaneous measurement of infrared-active combustion exhaust gases and infrared-inactive excess oxygen. The integrated instrument has also been demonstrated for other applications in the engine test cell environment, specifically for monitoring of gaseous impurities, toxics and contaminants in test cell air which can impact test article performance and test personnel safety.

References

1 Jalbert, P. and Zaccardi, V., "Improved Methodology for Turbine Engine Emissions Measurement," ASME/IGTI Paper no. GT-2002-303606.

2 Marran, D., Kenny, P., Markham, J., Jalbert, P., Moyers, R. and Gardner, D., "The Application of FT-IR Spectroscopy to Turbine Engine Exhaust Monitoring," AIAA Paper 2000-2211.

3 Oliver, W., Marran, D.F., Spartz, M.L., Lee, J.C.Y. and Nazeer, W., "Evaluation of the MKS On-Line FTIR MultiGas Analyzer for Gas Turbine Applications," ASME/IGTI Paper GT-2003-38656.

4 Griffiths, P.R. and J.J. De Haseth, Fourier Transform Infrared Spectrometry, Wiley Interscience, New York, NY (1986).

5 Adams, T.N. and Frederick, J., Kraft Recovery Boiler Physical and Chemical Processes, American Paper Institute, New York, NY (1988).

6 Dukelow, S.G., The Control of Boilers, 2nd Edition, Instrument Society of America, Research Triangle Park, NC (1991).

7 Lee, J-H., Kim, H. and Kim B.K., "Oxygen Sensing Characteristics of the Limiting Current-Type Sensors with the Microstructural and Structural Variations in Diffusion Barrier," Materials Letters, 26, 27-33 (1996).

8 Kondo, H., Saji, K., Takahashi, H. and Takeuchi, M., "Thin Film Air-Fuel Ratio Sensor," Sensors and Actuators B, 13-14, 49-52 (1993).

9 Lee J-H., Kim, H. and Kim. B-K., "Limiting Current Characteristics with Regard to Oxygen and Carbon Monoxide in Oxidizing and Reducing Atmospheres," Solid State Ionics, 86-88, 1087-1093 (1996)

10 Moses, C.A. and Stavinoha, L.L., "Gas Chromatographic Analysis of Exhaust Hydrocarbons from a Gas Turbine Combustor," Western States Section/The Combustion Institute Paper 75 – 17, Stanford Research Institute (1975).

11 Spicer, C.W., Holdren, M.W., Smith, D.L., Hughes, D.P., and Smith, M.D., "Chemical Composition of Exhaust from Aircraft Turbine Engines," Trans. ASME/Journal of Engineering for Gas Turbines and Power, **114**, 111-117 (1992).

12 Spicer, C.W., Holdren, M.W., Riggin, R.M. and Lyon T.F., Chemical Composition and Photochemical Reactivity of Exhaust from Aircraft Turbine Engines," Ann. Geophysicae **12**, 944-955 (1994).

13 Jalbert, P.A., Zaccardi, V.A., and Baker, K.P., "Recent Improvements in Near-Real Time Emissions Measurement and Analysis Capability at AEDC," SAE Paper 961309 (1996).

14 Jalbert, P.A., Zaccardi, V.A. and Baker, K.P., "Engine Emissions Measurements," Aerospace Engineering, September (1996).

15 "Procedure for the Continuous Sampling and Measurement of Gaseous Emissions from Aircraft Turbine Engines," Aerospace Recommended Practice ARP1256, Rev. B, Society of Automotive Engineers, Warrendale, PA, August 1990.

16 Gardner, D.G., Zaccardi, V.A., Jalbert, P.A., and Bryant, M.D., "Reducing the Cost of Aircraft Engine Emission Measurements," ISA vol. 443, paper 2302/IIS03-P081 (2003).

17 Markham, J.R., Bonzani, P.J., Bush, P.M., and Scire, J.J., "Integrated Gas Analyzer for Measuring Combustion Exhaust and Excess Oxygen," ISA vol. 443, paper 2303/IIS03-P080 (2003).
16 Yamada, T., Hayakawa, N., Kami, Y., and Kawai, T. "Universal Air-Fuel Ratio Heated Exhaust Gas Oxygen Sensor and Further Applications," SAE Paper no. 920234 (1992).
17 Takeuchi, T., Takahasi, H., Saji, K., Kondo, H., and Igarashi, I., "Oxygen Sensors A/F Control," SAE Paper no. 830929 (1983).
18 National Institute for Occupational Safety and Health; *Respirator Decision Logic*, NIOSH/DHHS Pub. No. 87-108, Washington, D.C., U.S. Government Printing Office, p. 21(1987).
19 American National Standards Institute, Inc., *Practices for Respiratory Protection*, Pub. No. Z88.2, NY, American National Institute Inc., p. 22 (1992).
20 Groth, R. H. and Robertson, D.J., "Reactive and Nonreactive Hydrocarbon Emissions from Gas Turbine Engines," Air & Waste Manag. Assoc., Pittsburgh, PA (1974).

Appendix A: Construction and Installation of Oxygen Sensors and Modules

The housings required to hold the zirconia sensors needed a few design considerations. *1. Low residence time.* Both the NTK and Electrovac housings had to be made in such a way as to not greatly increase sensor response time. It was also important to allow for a bypass system as top not increase the overall back-pressure of the system. In each case, the sample chambers roughly two times the size of the sensor filter elements. At 5 L/ min this allowed for a residence time far smaller than the FT-IR gas cell itself. *2. Ease of machining*. In designing the housings that were to hold the sensor, aluminum was chosen as base material. Plastic was not chosen, even though it is easier to machine, because of the high temperature of the gas (150 ºC) and of the sensor heads (~650 ºC) and that plastics can be semi-permeable to certain gasses. Some plastics can also outgas at elevated temperatures, which can alter the results of the readings. The NTK housing required two distinct parts, the base and retaining clamp. Four holes were drilled and threaded to secure the sensor through the retaining clamp. The housing for the Electrovac sensor was fabricated from a length of 1 ¼ inch bar stock, further simplifying the design. This housing was also simpler in design because the sensor itself had a means of mounting built in, by means of a threaded-housing. *3. Size and shape.* After the material was determined, the size of the housing had to be made to fit inside the MultiGas package, while minimizing the amount of modifications. *4. Preparation of housings.* In order to keep contamination of the FT-IR system at a minimum, the machined parts had to be treated. During handling and machining, oil, grit and contaminates remain on the surfaces. The first treatment was to wash the parts with soapy water to remove most of the particles remaining after machining. Then the housing was immersed in acetone and ultrasonically agitated for a minimum of 30 minutes. This would help to loosen oil and grime and dissolve it into solution. Next the housing was washed with IPA in order to remove any residue from the acetone bath. The housing was air-dried and was ready for installation. The new sample tube lines made to accommodate the housing were also rinsed out with IPA.

Sample gasses escaping from the sample can pose a health hazard to personnel. This made sealing of the sensors an important design issue. The solution for the sample lines was to drill and taper-tap 1/8 inch NPT pipe fittings into the housings, sealed with Teflon tape.

The NTK sensor itself does not have any pre-sealing considerations in the design. It was determined that the PPS base of the sensor is sealed so a Viton o-ring was sized and fitted to the sensor around the Teflon filter. This when compressed by the retaining clamp provides an adequate seal. As for the Electrovac sensor, since the package has external threads it is more simple screw-mountable. A tapered hole was tapped and a copper spacer provided the necessary sealing mechanics.

In order to prevent condensation of water and other gasses, the oxygen sensor housing has to be maintained at roughly the same temperature as the gas cell. The sensor's installation differed between the two models. In the MultiGas 2010, the sensor housing is place fully within the insulated enclosure of the gas cell. This means that the sensor is roughly at the same temperature as the gas cell. In the 2030 model, the sensor was installed in the heated output line of the instrument. In order to accommodate the change in size of the heated outlet section, a special insulated cover was created to keep both the lines and sensor heated.

When the sensors were mounted externally, it was also important to keep them well insulated. Both the sensors themselves and the heated gas contributed to keeping the housing warm, but without insulation the temperatures would dip way below 100 ºC. Heat-wraps and Melamine foam were used to insulate the exposed housings to maintain the temperatures required for non-condensing conditions.

The electronics modules themselves required some machining work to be done. In order to accommodate the electronics in a safe package, cast aluminum. Holes for cables, switches, cooling and mounting were required. The front panel contains the main power switch, monitor light and power-in jack. The rear has two oxygen sensor ports and one DB-9 serial connection. The base contains mounting holes for the PC board and fuse block. Finally, the cover has holes for both the mounting the fan and an air intake vent. Figures A.1- A.4 shows these holes and their purposes.

Figure A.1: Module Boxes before installation of components.

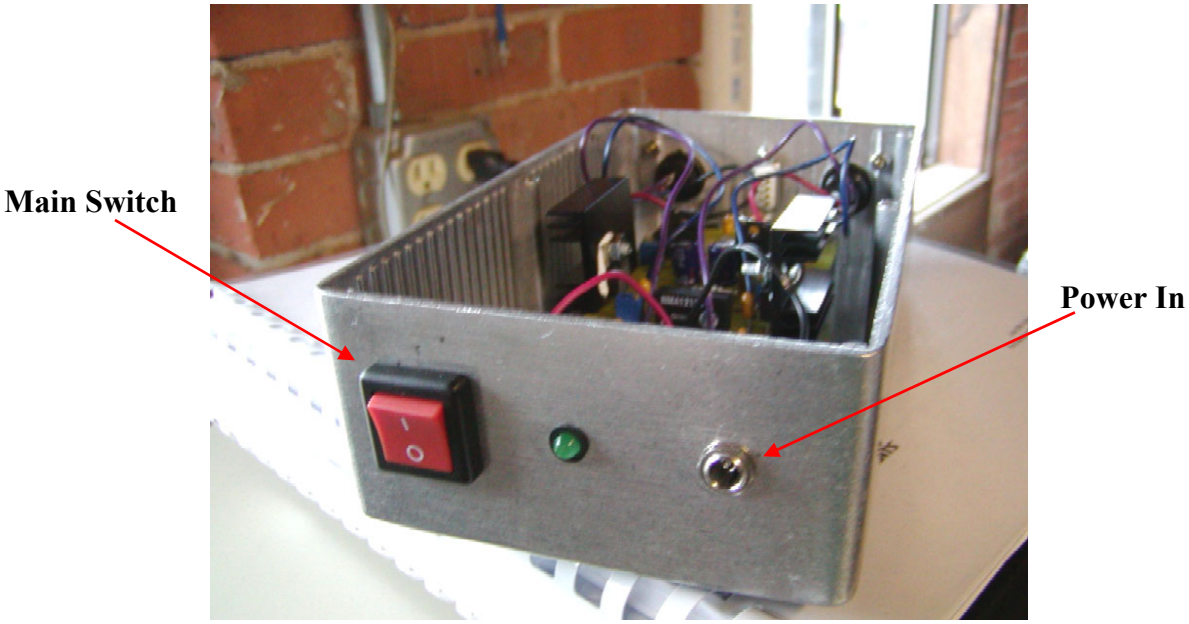

Figure A.2: Front view of a module box after installation of some components.

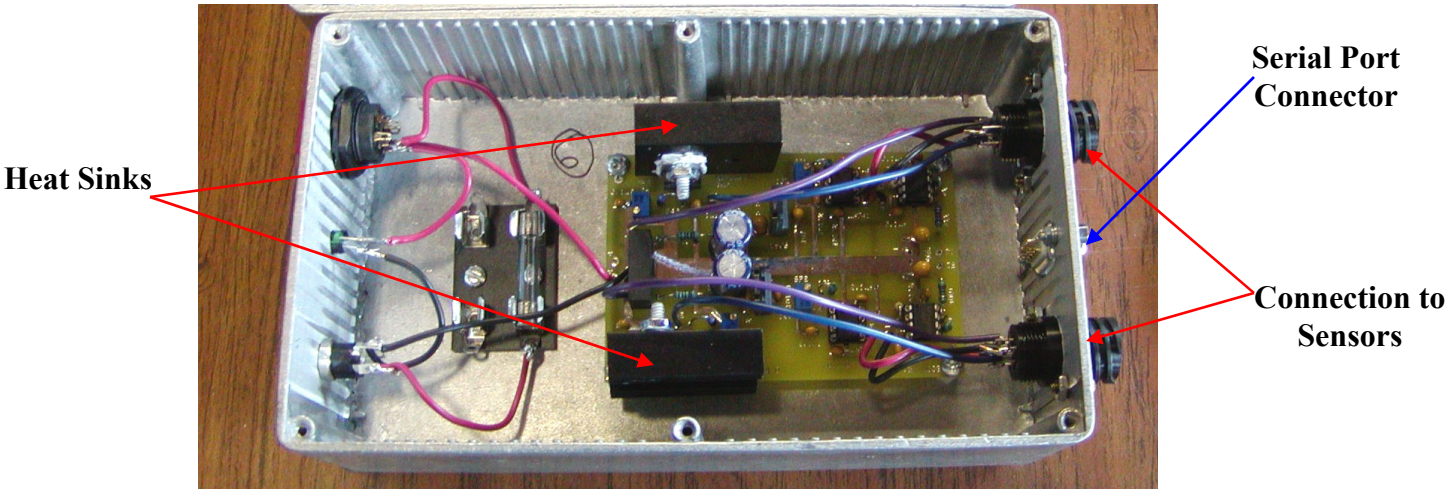

Figure A.3: Overhead of a module box with some components installed.

Figure A.4: Completed module boxes.

The sensor heaters operate around 4 volts DC in order to maintain constant prescribed temperature. This presented another design issue, how to remove the excess heat generated by the voltage regulators. Figure A.3 shows the two heat sinks employed in the sensor circuits. To remove this excess undesired heat, a micro-cooling fan was installed in the top of the module. This reduced the internal temperature from 68 ºC to ~34 ºC, well within the limits of all components used. This cooling scheme also reduced

the junction temperature of the regulators by over 60 ºC as well. This will increase greatly the lifetime of the component.

In the first prototype version of the modules, the cables were for the most part fabricated. It was determined that for reliable operation and cost reduction, pre-made cables were better. Standard connectors and shielded cables were used by the final design, except where they could not be used (i.e. the sensor interface itself). Easier to procure, more economical, simple to use and easier to assemble, four terminal AMP brand connectors replaced the "microphone" type jack connectors used in the first two versions of the modules.

The simplification of the power supplies used in this system was also a major concern. The first prototype module used four independent power supplies, two 9V batteries, 12V DC supply, and 9V DC supply. While offering noise stability, the two 9V batteries would have to be changed often and the user would have to check their status frequently. The second version created for the March 2003 AEDC/MTSU test eliminate the need for the batteries and instead utilized a multi-source power supply. In this version, the DAQ are still powered by its own power supply, reducing the number of supplies by ½.

For the latest version, a single power supply approach was taken. The multiple source supply used in the second version was both cumbersome and expensive. A single 12 volt power source was employed to power the electronics and the DAQ, eliminating the need for the independent supply. This module was also constructed to allow two sensors to be run simultaneously for comparisons of performance.

List of vendors and Suppliers:

Many vendors and suppliers were used in the fabrication of the integrated oxygen analyzer. Below is a list of all of the major vendors, followed by a brief list of items they supplied.

NTK Technologies, INC
Fine Ceramics Division
3250 N. Arlington Heights Rd.
Suite 102
Arlington Heights, IL 60004
Tel: (847) 788-9795
Fax: (847) 788-9798
www.ntktech.com

Supplied: Oxygen Sensors

Electrovac
Aufeldgasse 37-39
A-3400 Klosterneuburg, Austria
Tel: +43/2243/450-0
Fax: +43/2243/450-690
www.electrovac.com

Supplied: Oxygen Sensors

McMaster-Carr Supply
P.O. Box 440
New Brunswick, NJ, 08903-0440
Tel: (732) 329-3200
Fax: (732) 329-3772
www.mcmaster.com

Supplied: Metal, gaskets, pipe, tooling, fasteners, ect.

Digi-Key
701 Brooks Ave South
Thief River Falls, MN, 56701-0677
Tel: 1-800-344-4539
www.digikey.com

Supplied: Electronic components

Newark InOne
34 Jerome Avenue Suite 200
Bloomfield, CT 06002-2463
Tel: (860) 243-1731
Fax: (860) 242-3949
www.newark.com

Supplied: Electronic components, ect

Jameco Electronics
1355 Shoreway Road
Belmont, CA, 94002
Tel: (800) 831-4242
Fax: (800) 237-6948
www.jameco.com

Supplied: Electronic components, housings for modules, cables

B&B Electronics
707 Dayton Road
P.O. Box 1040
Ottawa, IL 61350
Tel: (815) 433-5100
Fax: (815) 433-5109
www.bb-elec.com

Supplied: Data acquisition modules

Radio Shack
200 Taylor Street, Suite 600
Ft. Worth, TX 76102
Tel: (817) 415-3200
Fax: (817) 415-3240
www.radioshack.com

Supplied: Electronic components, ect.

Express*PCB*
www.expresspcb.com

Supplied: Printed circuit boards

Appendix B: Electronic Schematics and PC Layouts

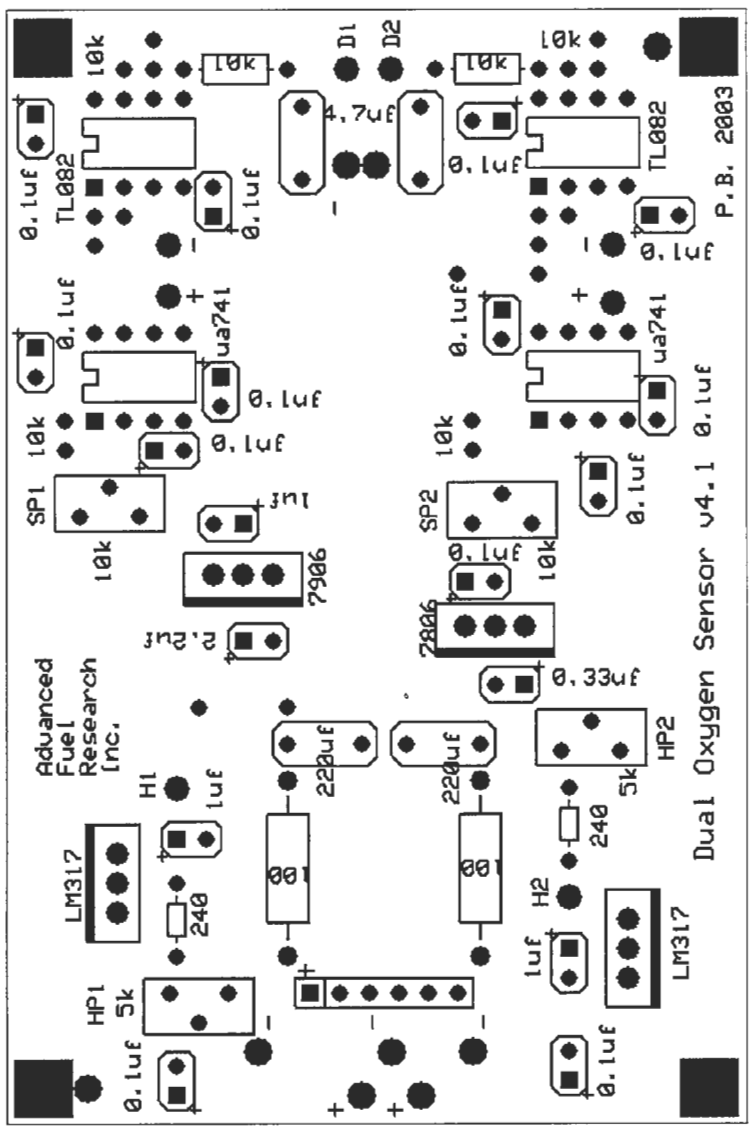

Figure B.1: Dual oxygen sensor PC layout

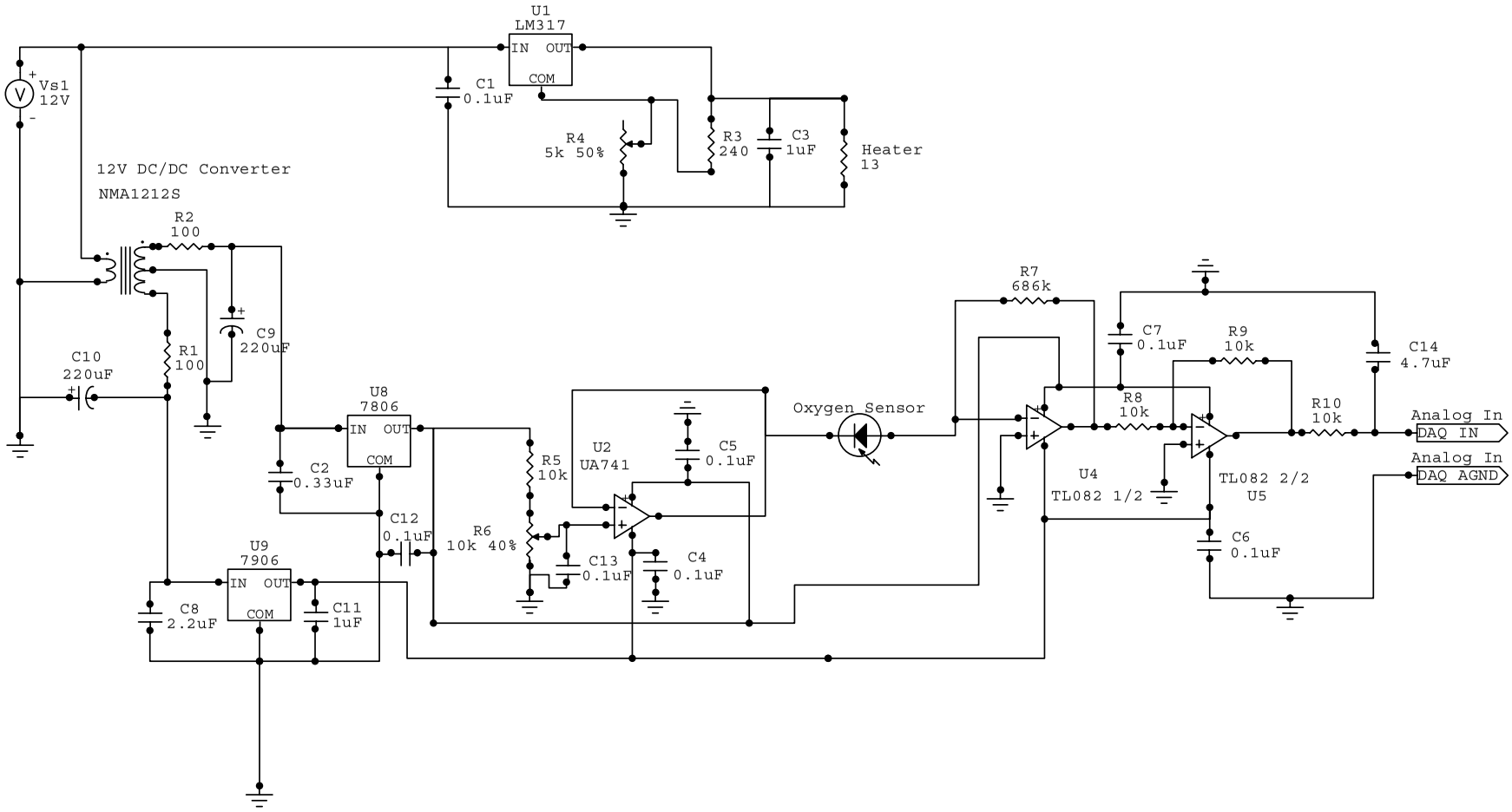

Figure B.2: Single circuit schematic

Appendix C: Software Schematics and Screenshots

During development, two different sets of software were developed. The first was a stand alone system that ran independent of the Multigas software. Figures C.1 and C.2 illustrate that software.

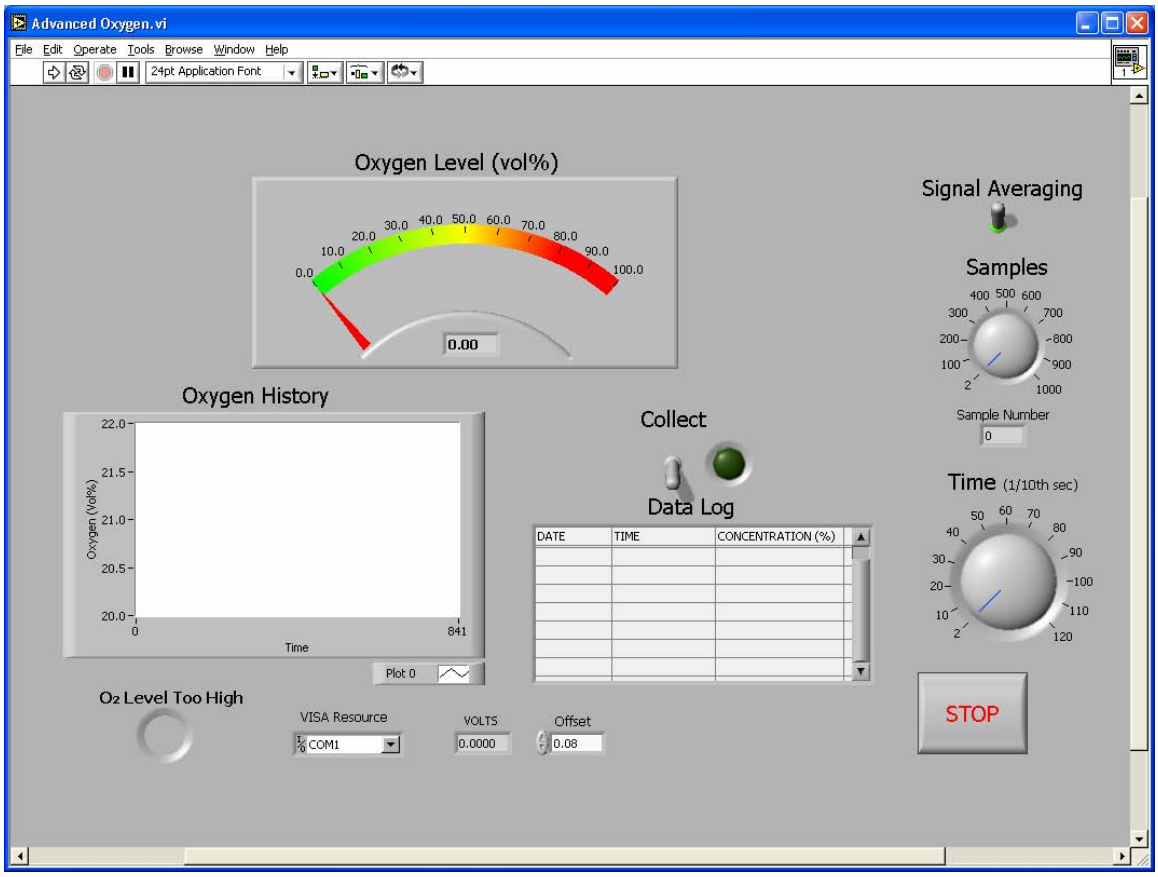

Figure C.1: Front panel for stand-alone software.

This software both reads and records the data stream. The user has to specify the number of samples number and time to average them over. This program records the averaged concentration and the exact time.

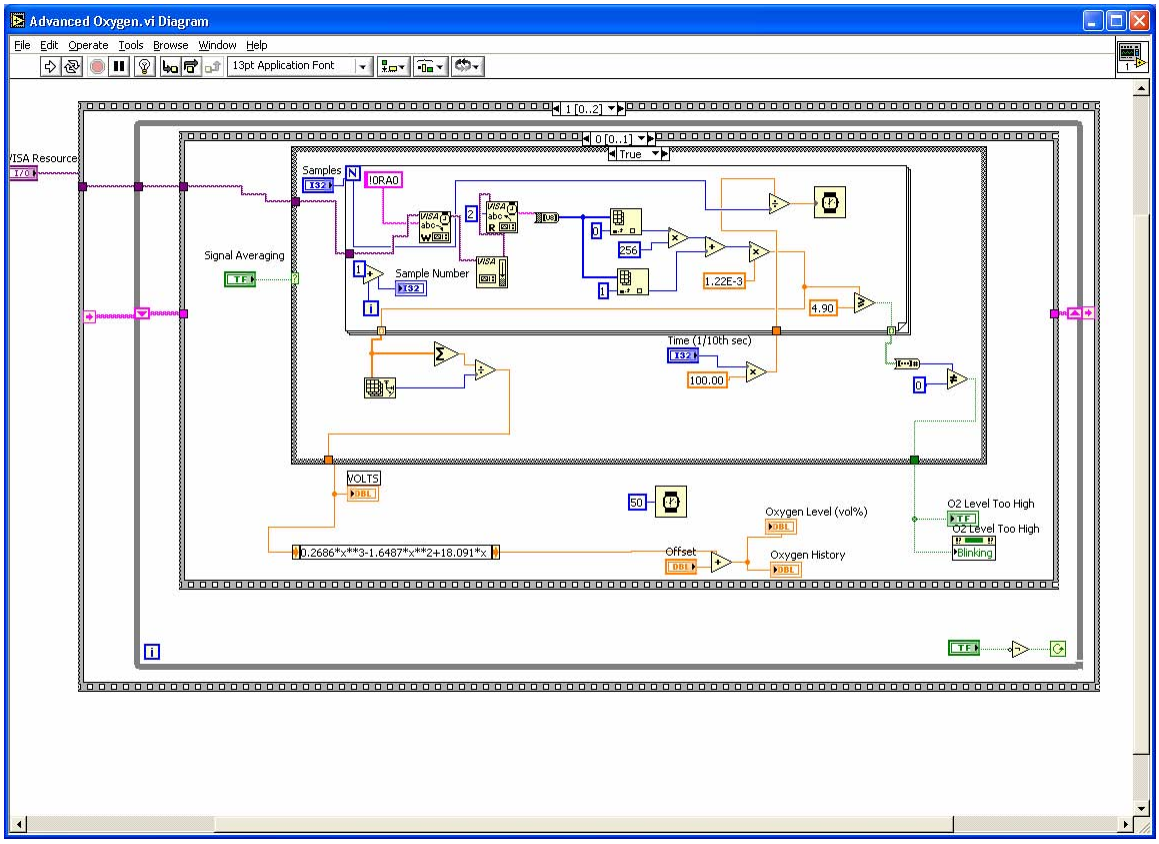

Figure C.2: Diagram for stand-alone software.

The next evolution was to integrate the software into the MKS's MultiGas package. Figures C.3, C.4, C.5 and C.6 show the software and its diagrams. Figure C.3 shows the user interface for integrating the oxygen sensor into the MultiGas data stream. When the user wishes to take a new calibration, the Sub-VI "Calibrate" can generate the necessary values and insert them into the collection routine.

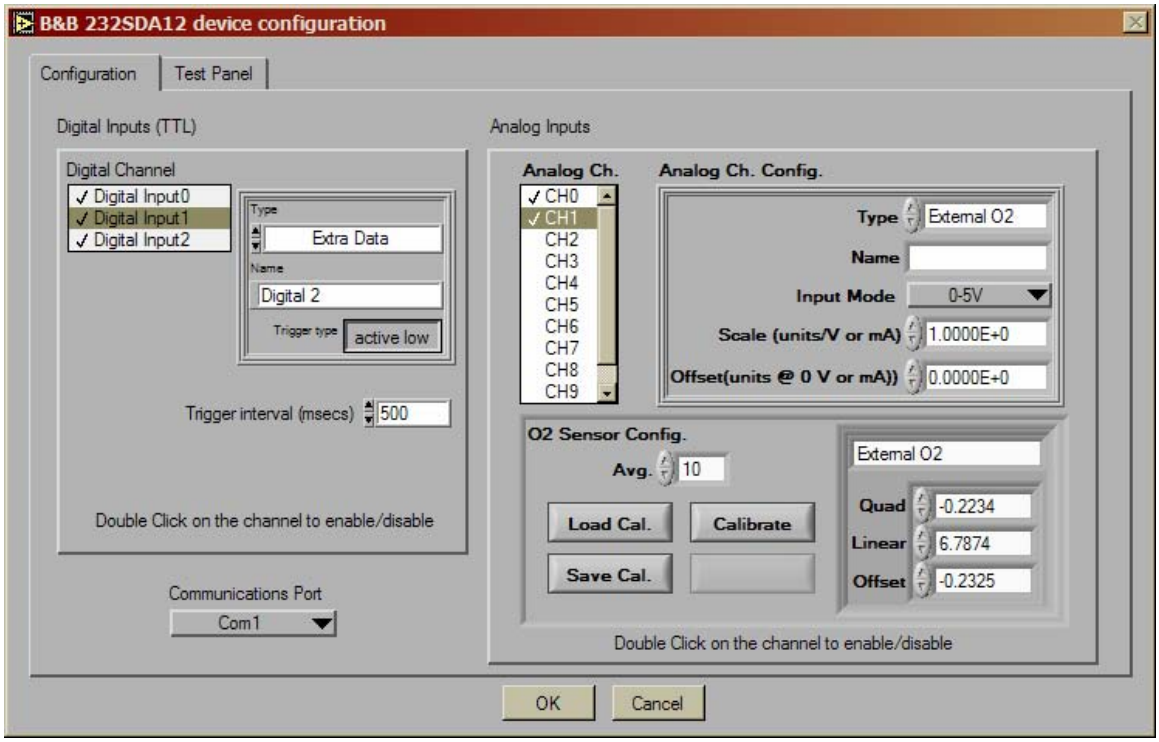

Figure C.3: Screenshot of oxygen sensor setup.

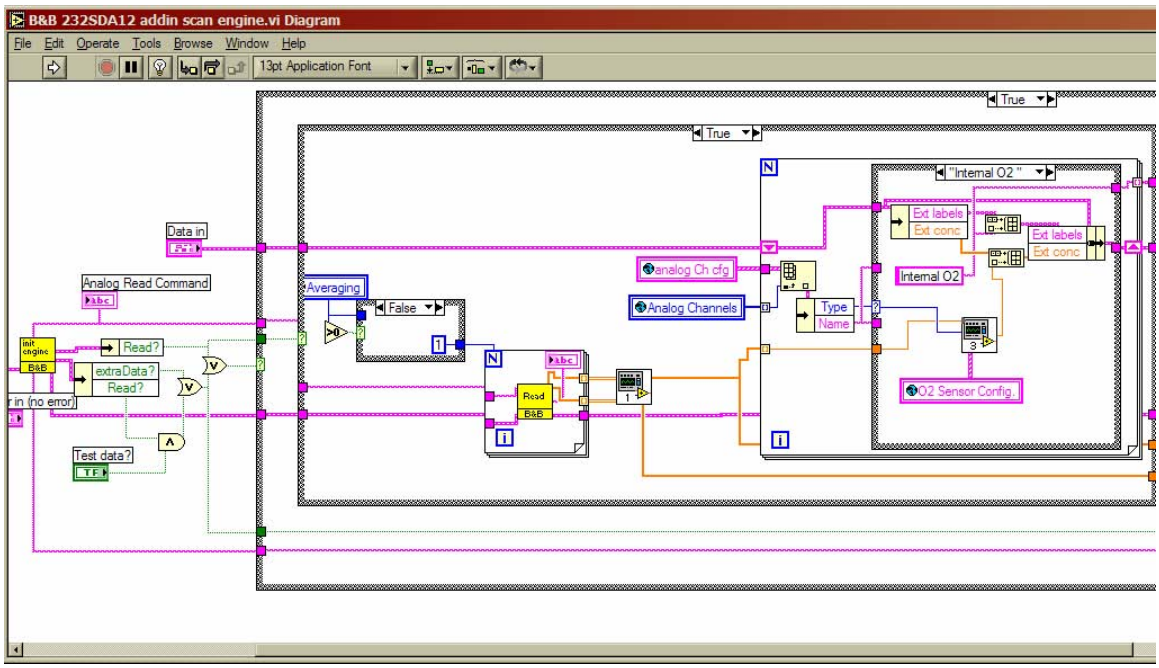

Figure C.4: Diagram of related software.

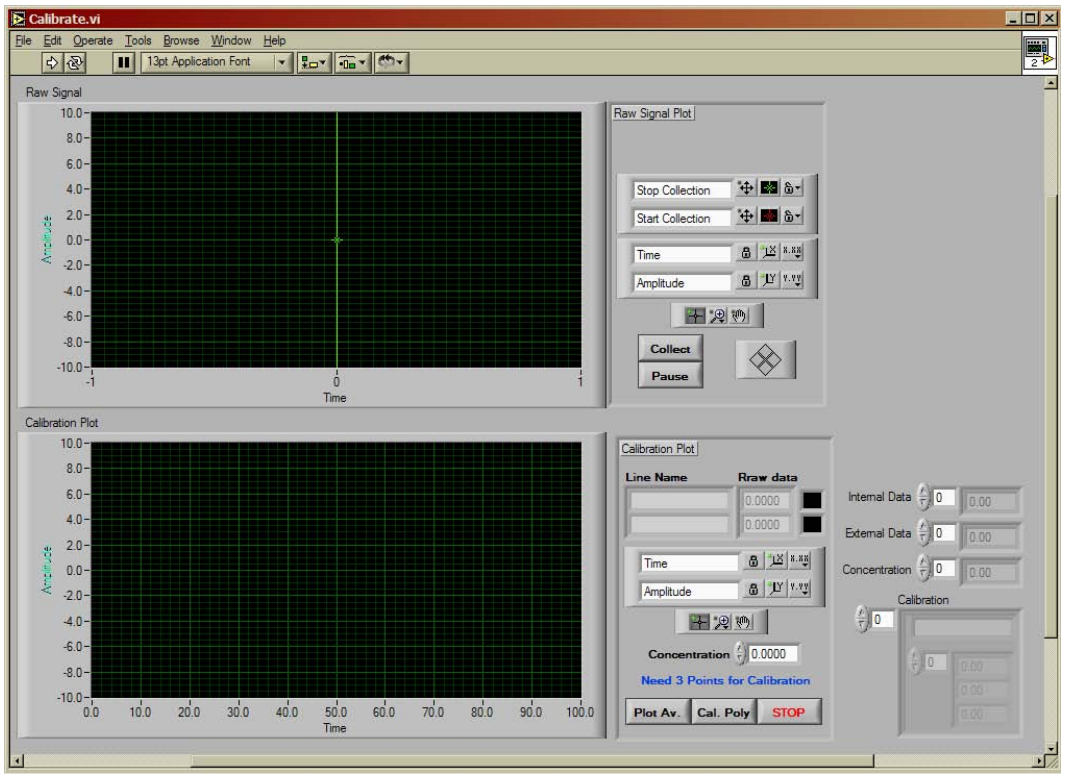

Figure C.5: View of calibration screen.

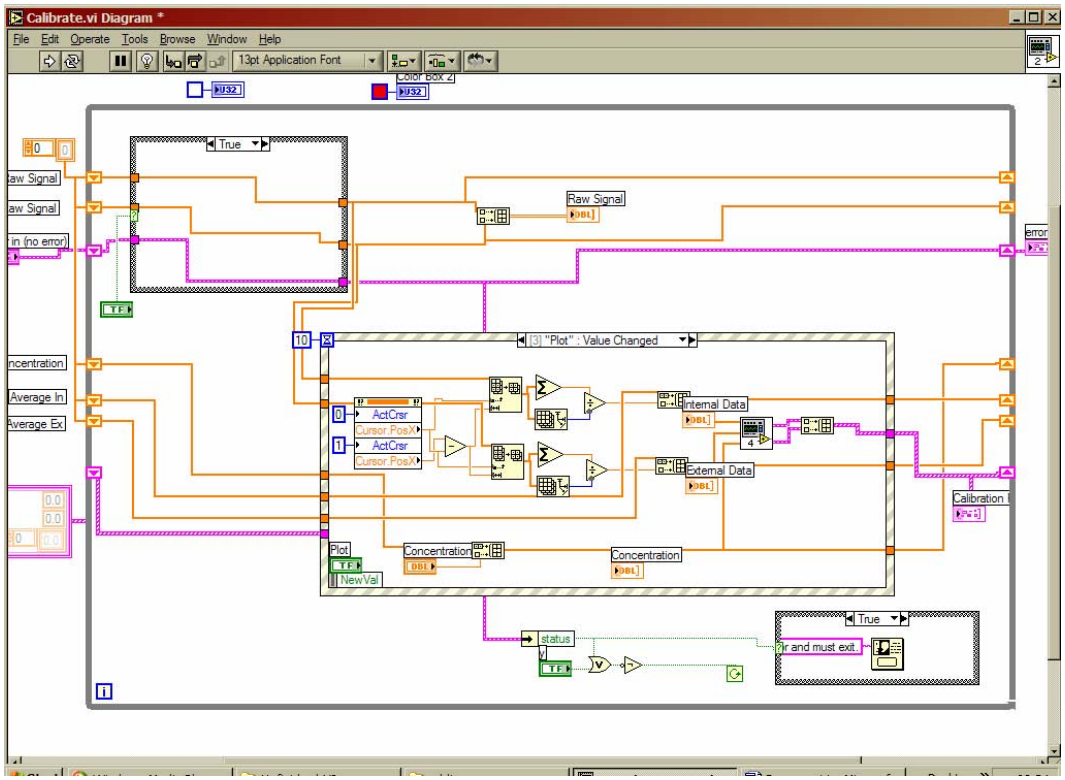

Figure C.6: Diagram of related software

Appendix D: Notes on Operation

Warm-up Procedure:

It is necessary to note that because the sensor is heated, some time for stabilization is needed. When the sensor is first powered up, the reading starts low and then increases off-scale. Within 30 seconds the sensor responds and begins to function. Ten minutes of stabilization after the sensor reaches operating temperature was found to minimize and eliminate drifting in the measurements.

Safety Concerns:

Taking into consideration the operating temperature, the internal installation of the sensor also greatly reduces the chances for operator related injuries such as burns. Temperature measurements show that both the NTK and Electrovac sensors substantially raise the temperature of the housings alone. This in combination with the sample gas temperature raises the housing temperature close to 130 ºC.

Another important consideration is the sample itself. This type of sensor should not be used where large amounts (i.e. percent volume) of flammable gas or liquid are present with oxygen. This is due to the fact that the sensor head is at ~650 ºC and this can ignite flammable mixtures. In applications where there is a potential for combustion of the sample, flame arrestors must be installed in conjunction with the sensor.

Appendix F

Final Report Document: **Prototype Stand-Alone Oxygen Sensor Unit**

The construction of the prototype stand-alone oxygen sensor unit was completed. The unit is totally self-contained, heated and insulated. The only connections needed are the sample in and out, 120V power in and serial connection to report data. The unit is self heating, which maintains the sample temperature at 150 C which is the same as the MultiGas system. In order to keep the internal electronics within recommended temperatures, a fan was used with vents to keep the non-insulated internal portion near-room temperature. The exterior surface is only slightly warm when in operation (i.e., hand-safe). The unit was calibrated and will be employed in an upcoming field test. Figures 1, 2 and 3 show the completed unit.

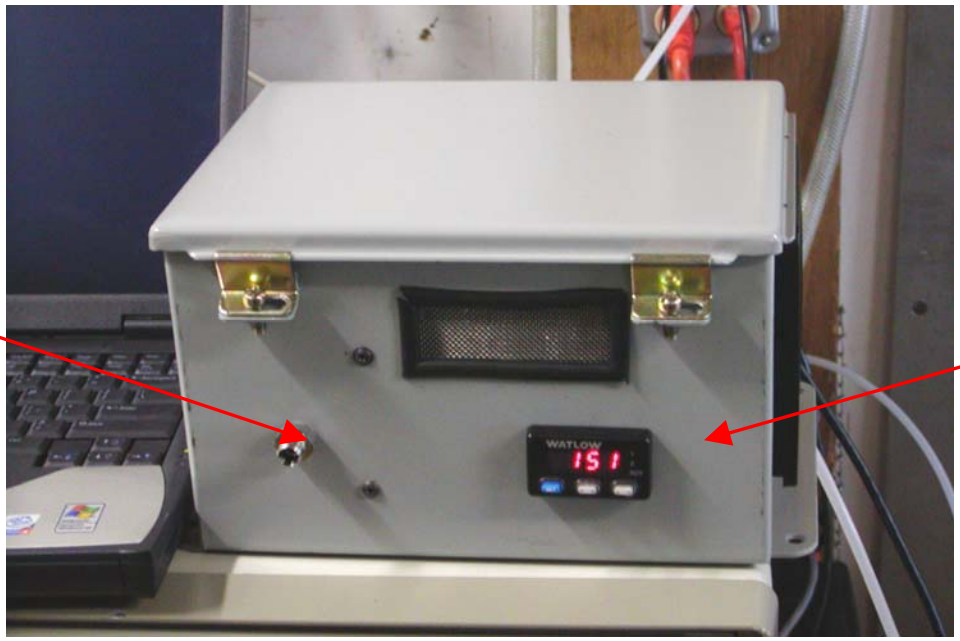

Figure 1: Front view of the stand-alone oxygen sensor unit. Dimensions: 11-inches wide x 7-inches tall x 9-inches deep (28-cm wide x 18-cm tall x 23-cm deep). Weight: 9-pounds (4.1-kilograms).

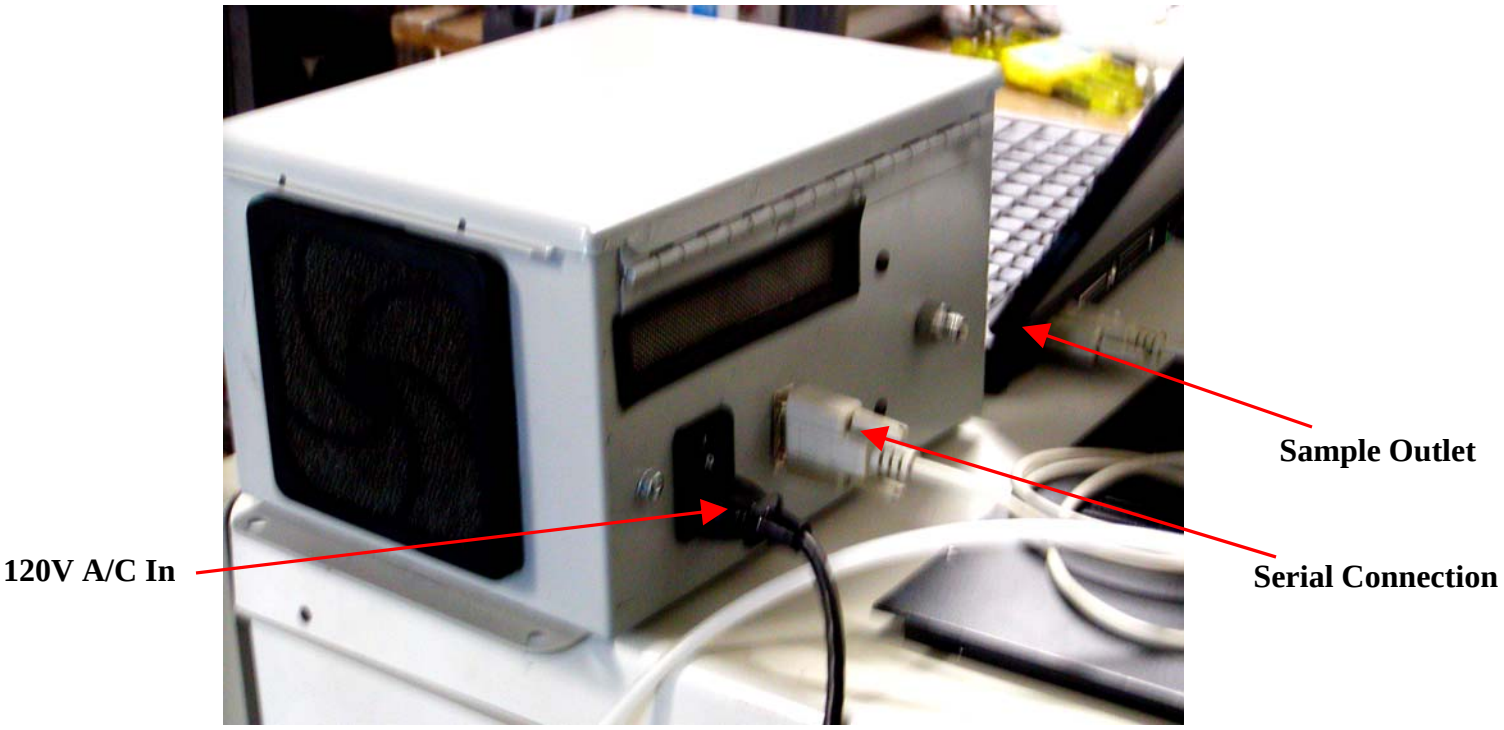

Figure 2: Rear view of unit, showing electrical connections and outlet

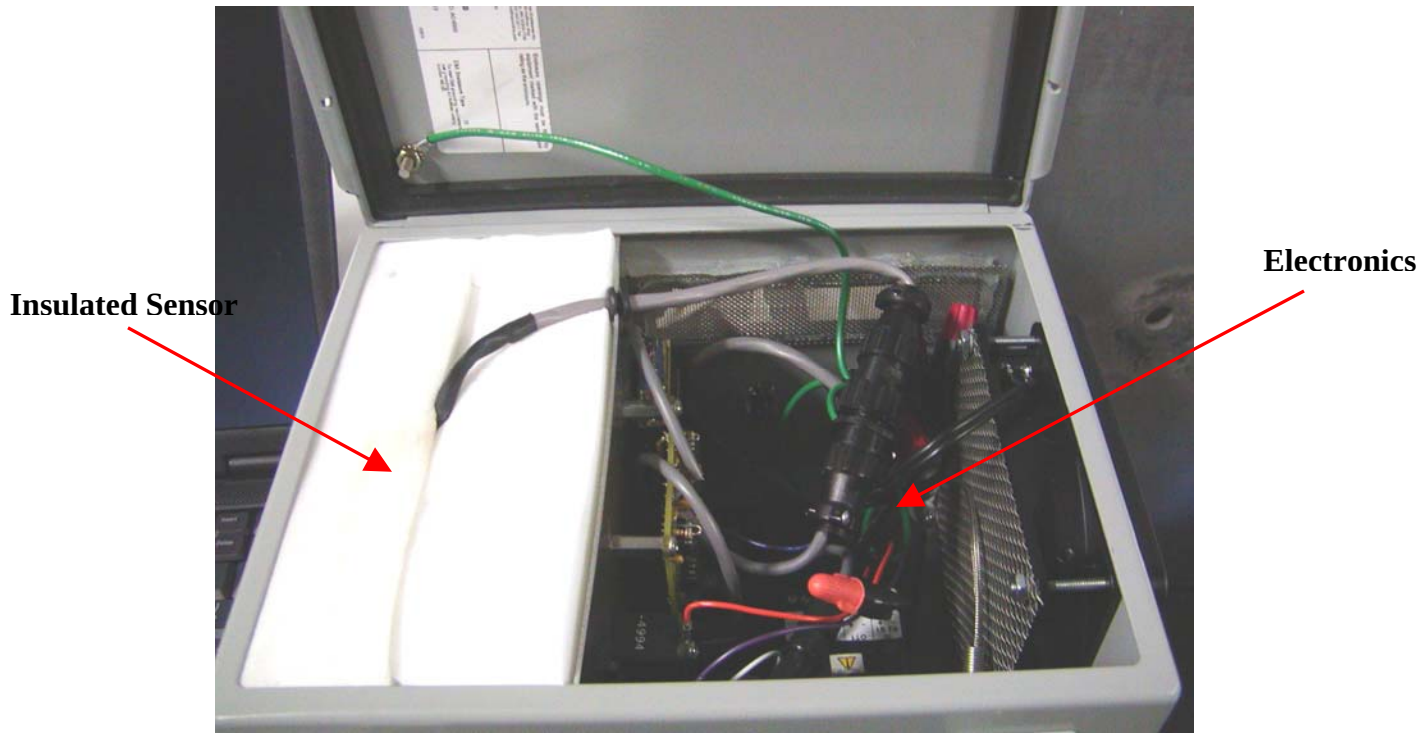

Figure 3: Internal view of stand-alone unit, showing insulated cell and electronics

Appendix G

Bush, P.M., Scire, J.J., and Markham, J.R., **"Advances in Quantifying Total Hydrocarbons and Individual Species during the Rapid, Continuous-Sweep Method of Measuring Turbine Exhaust,"** submitted to Applied Spectroscopy in April 2005. Received peer reviews in September 2005. Reviewers decline acceptance to Journal citing that MGA instrumentation was previously published by the authors and that methodology for total hydrocarbon quantification is not sufficiently innovative for publication in the journal.

Advances in Quantifying Total Hydrocarbon and Individual Species during Rapid Continuous-Sweep Measurements of Turbine Engine Exhaust

PATRICK M. BUSH, JAMES J. SCIRE, JR., and JAMES R. MARKHAM

Advanced Fuel Research, Inc., 87 Church Street, East Hartford, Connecticut 06108

Abstract

Fourier transform infrared (FT-IR) spectroscopy is known to be a useful technique for quantitative analysis of many gaseous components in turbine engine exhaust. Yet, the pursuit of FT-IR as a single, stand-alone tool to measure the complete gaseous emission profile of turbine engines has been impeded by the limited capability of FT-IR at measuring total hydrocarbon concentration (HC). In a recently demonstrated rapid, continuous-sweep measurement from the exhaust plane of a large nozzle turbine engine fired with jet fuel, traditional flame ionization detectors (FIDs) for quantifying total HC were paired with and complemented the FT-IR analyzers which quantified CO, CO_2, H_2O, NO_x, SO_x, and several low molecular weight hydrocarbons. This article presents advances in FT-IR capability for measuring total HC, achieved by increasing the number of pertinent individual hydrocarbon species in the quantitative reference library as well as considering the unburned fuel contribution. The result provides the added capability of measuring greater than 90 percent of the total hydrocarbon concentration in the gaseous exhaust emissions of turbine engines by the FT-IR method.

Introduction

The capability to provide exhaust gas analysis during development testing of aircraft turbine engines would add great value to this testing by ensuring that new engines meet regulatory requirements and therefore avoiding negative impacts on military aircraft basing. However, for new, high performance jet engines with large exhaust nozzle dimensions, run time constraints at high power conditions are not compatible with the regulatory-accepted exhaust gas measurement methods, which take hours. Therefore, the need for engine exhaust gas analysis during engine development testing requires a new methodology. In 2004, a new, continuous measurement system and methodology that demonstrated the multiple-species emissions survey of a high performance jet engine within a five-minute time scale was presented.[1] During an Air Force technology demonstrator engine test program, rapid emissions surveys were performed with results provided in near-real time during dedicated aeromechanical test periods at every altitude/Mach number tested. Valuable combustor performance and environmental emissions data over the entire flight envelope were captured. The new, continuous-sweep methodology relied on a high-temperature, translocating rake system and a rapid gas sample selection and transport system to direct flow from the engine's exhaust plane to the system of gas analyzers. The system consisted of five FT-IR gas analyzers, each simultaneously quantifying CO, CO_2, H_2O, NO_x, SO_x, and several low molecular weight hydrocarbons from the various probe-points of the rake. Each FT-IR analyzer contained an integrated solid-state sensor for the simultaneous quantification of O_2.[2] A set of flame ionization detector (FID) analyzers were used for the simultaneous quantification of the total hydrocarbon concentration (HC). In addition to combustor performance and

environmental emissions data, the system (particularly the FT-IR components) has shown potential as an engine diagnostic tool by identifying and confirming repair of an oil leak into the engine's gas path.[3] Unexpectedly, it was the SO_2 concentration in the exhaust rather than unburned hydrocarbons that was used to unambiguously identify the oil leak and confirm repair.

During previous engine testing the use of both the FT-IR and FID were necessary for individual hydrocarbon and total hydrocarbon analysis. The FT-IR analyzers provided valuable data on a number of low-molecular-weight species, including acetaldehyde, acetone, acetylene, butane, ethylene, formaldehyde, methane and propylene, but lacked the capability of measuring high-molecular-weight species and determining total HC. The FID provided total HC but lacked the capability of measuring the individual hydrocarbons. Despite the lack of discriminating techniques in the regulatory-accepted measurements, there has been a growing interest in the near-real time monitoring of certain combustion-generated hydrocarbon species that pose health hazards to the public. Certain species such as acrolein, benzene, 1,3-butadiene and formaldehyde are classified as hazardous air pollutants (HAPs) that are products of incomplete combustion of liquid based fuels. The literature indicates that the exhaust of a liquid-fuel fired turbine engine can contain dozens of hydrocarbon species. Detailed laboratory analyses of gas samples collected from liquid-fuel fired turbine engines have been performed using gas chromatography (GC).[4,5,6] This literature certainly indicates that the of later model engines contain lower levels of hydrocarbon pollutants. FT-IR spectroscopy provides similar capability as gas chromatography in discriminating individual hydrocarbon

species but in near-real time, making FT-IR technology more suitable for field testing than GC. Previously, HAPs were not measured individually for near-real time measurements, but instead by their contribution to a total HC concentration measured by an FID. Having the capability of measuring turbine engine exhaust in near-real time, using just one analyzer, for monitoring engine performance and health, as well as for monitoring environmental emissions of individual HAPs and total HC is highly desirable. Previously, for turbine combustor exhaust originating from natural gas fuel, the comparison between the FID and FT-IR methods showed good agreement.[7] However, methane accounted for 80-90 percent of the total HC. In the combustion of liquid fuels, methane is typically a minor component of the hydrocarbon distribution in the exhaust, making the comparison of the total HC between the FID and FT-IR particularly challenging. Advances in the hydrocarbon reference library for the FT-IR method are presented in this article. The result is the increased FT-IR capability of discriminating and quantifying individual hydrocarbons and determining total HC during rapid continuous-sweep measurements of turbine engine exhaust.

Instrumentation

All FT-IR spectral data were collected using the MultiGas 2030 available from MKS Instruments. The gas sampling cell in this FT-IR provides an optical path length of 5.11 meters within a sample volume of 200 cm^3 at 150 degrees Celsius.[8] A description of the advantages of this particular cell was previously presented.[7] This FT-IR was received with a rudimentary combustion-gas reference library provided by the manufacturer. Reference spectra for additional hydrocarbon species were generated using a custom gas

divider system (GDS) that also accommodates quantitative injection of liquids for vaporization. The GDS uses two digital mass flow controllers with maximum flows of 500 ccpm and 2000 ccpm. The mass flow controllers provide accurate dilution of the desired species in nitrogen to provide several concentration points in generating calibrations files for the FT-IR. Combustion species that are liquid at room temperature were calibrated by using a syringe pump to inject a constant flow of liquid into an atomizer/evaporator assembly using nitrogen as the carrier gas. The atomizer chamber was designed so that the carrier gas flows parallel to the syringe needle to minimize the potential "wicking" effect of the liquid at the needle tip, which can cause instabilities (i.e. concentration oscillations) in the measured absorption spectra recorded by the FT-IR. The atomizer/evaporator assembly is heated to 170°C to prevent condensation on cold surfaces. For the low levels of liquid introduced into the system, a slight drop in the temperature of the carrier gas occurs. The continuous, pulse-free syringe pump provides flow rates from 0.01 μLpm to 50 mlpm, which provides the capability of generating low ppm to percent level concentration spectra for liquid species. In this study, total HC data were collected using the Model 300 HFID from California Analytical Instruments, Inc.[9] This analyzer has eight selectable ranges from 10 to 30000 ppm carbon (ppmC), and exhibits a linear response between 0 and 10 volts in each range.

Configurations and Measurement Results

The total HC comparison between the FT-IR and the HFID was performed both on samples generated in the laboratory and on the exhaust produced by a Pratt & Whitney JT-12 turbine engine operated by the Aerospace Maintenance Department of the Middle

Tennessee State University (MTSU). The laboratory setup provided comparisons between the FT-IR and FID methods for individual hydrocarbons and simple hydrocarbon mixtures, and also delineated significant combustion species that contribute to the FID measured total HC. The measurements collected on the JT-12 provided a real turbine engine comparison of the two instruments. In the laboratory, the FT-IR (non-destructive analysis) and HFID (destructive analysis) were plumbed in series into the sampling line. For real turbine engine testing, the FT-IR and HFID were plumbed in parallel off of the sampling line from the JT-12 engine. The sampling system employed for measuring turbine engine exhaust from the JT-12 has been described in detail previously.[10] During the JT-12 testing, the GDS and atomizer assembly were plumbed upstream of the two instruments, providing the capability to introduce additional liquid hydrocarbons into the sampled exhaust stream. Quantitative spiking in this fashion allowed the response of the FT-IR and FID to change and be monitored while measuring the full complement of gases in turbine engine exhaust. The laboratory and engine exhaust measurements are presented in this article highlighting the advances in quantifying individual hydrocarbon species and measured total HC. Engine testing included data collected during engine power cycling with the sampling rake positioned at the centerline of the exhaust nozzle, and during vertical, continuous-sweep traverses of the sampling rake through the exhaust plume at constant power.

As mentioned above, a one-to-one correlation was previously reported between an FT-IR and FID for total HC measured from a natural gas-fired turbine combustor where 80-90 percent of the measured hydrocarbon emissions were unburned methane gas. Similar

correlation plots are presented here as examples from laboratory measurements of individual hydrocarbon species and simple mixtures of hydrocarbons. Using the GDS, several concentrations of butane and formaldehyde were measured (Figure 1), as well as several dilutions of a mixture of ethane, propane and formaldehyde (Figure 2). Generating a sample stream with either individual HC species or a simple mixture of hydrocarbons, the FT-IR and FID show a near one-to-one correlation suggesting that FT-IR has the capability of determining total HC within simple sample streams. Note that Figures 1 and 2 demonstrate that one of the species contributing to total HC is formaldehyde. In the authors' previous work, formaldehyde was measured by the FT-IR but was not used in the calculation of total HC as formaldehyde is a carbonyl compound. Manufacturers of FID analyzers have indicated that quantification of carbonyl compounds by the FID method is problematic. The data presented here shows an increased scattering of points when formaldehyde is present. However, even though formaldehyde has been previously considered problematic for FID analysis, a reasonably strong one-to-one correlation is observed here between the two methods.

In the past, the FT-IR has not compared well to the FID when measuring turbine exhaust produced from liquid fuel, due to the limited number of hydrocarbon species in the manufacturer-supplied FT-IR reference library compared to the number of hydrocarbon species within the exhaust stream. Table 1 presents the list of hydrocarbon species in the original reference library and also the limited number of species used to determine total HC. Since the measured total HC from the FT-IR originally used only five species ranging from C1-C4, figure 3a shows a poor correlation between the FT-IR and FID for

turbine engine exhaust at low engine power setting (e.g. at idle which generally produces the highest concentration of HCs over a wide distribution of molecular weights). Approximately 20-30% of the total HC was accounted for by these five species, during the two downward continuous-sweep traverses through the exit plane of the engine fired with diesel fuel at constant engine power (45%). The rake velocity was approximately 6-inches per minute through the 13.5-inch diameter engine plume. Also, the FT-IR showed a poor comparison with the FID response to the exhaust from JP-8 fuel (a kerosene base fuel) during rapid engine power cycling from 45% to 75% as seen in figure 3b (left of dashed vertical line, showing several power cycles), and for varied engine power settings from 45% to 75% at 10% increments shown in figure 3b (right of dashed vertical line) with the sampling rake located at the centerline of the engine nozzle. Breaks within the FID data trace indicate where no data points were recorded. The smaller, isolated spikes seen in the FT-IR data (figure 3a) after the traverses indicate when the sampling rake was rapidly brought back to the top position, just above the engine nozzle, at a speed faster than the measurement system's temporal resolution.

Using the GDS, the FT-IR's combustion library was expanded, with the objective of improving the capability of the FT-IR for quantifying total HC in turbine engine exhaust. Table 2 shows the expanded combustion reference library, with limits of detection indicated for most, for data averaging of 4 scans (~2.2 seconds) and 20 scans (~15 seconds). Also shown is a list of future species that will be studied using the GDS. The hydrocarbon species identified in the table with respective carbon numbers indicated are those used in this study for determining total HC. The number of hydrocarbon species for

determining total HC was expanded from the original five low molecular weight hydrocarbons (C1-C4), to nine C1-C4 species plus an unburned fuel component with a carbon value in the range of C15. As will be shown below, the unburned fuel component, with its detection limit of less than 0.5 ppm, represents a composite reference for the distribution of C5-C18 species in the exhaust. Several blends of aviation kerosene have been analyzed by carbon number resulting in a Gaussian distribution where C12 identifies the median.[11] Yet during combustion the Gaussian distribution of the unburned fuel will shift to higher carbon number due to the fact that the lower molecular weight species are more efficiently burned off, resulting in the median higher than C12.[6,12] Using the multiplying factor in the range of C15 for the unburned fuel provides a good determination of the high molecular weight hydrocarbons in turbine exhaust. Using the composite reference of unburned fuel plus the nine C1-C4 species provided a more feasible alternative for quantifying total HC in near-real time than quantifying individual species above C4.

Hydrocarbons with a carbon number of five or higher show similar absorption features in the typical spectral region for analysis, between 2800 and 3200 cm^{-1}. Figure 4 shows this spectral region for four straight chain hydrocarbons ranging from C6-C18, and illustrates the similar signatures with respect to unburned fuel vapor. Individually quantifying the components of high-molecular-weight hydrocarbon mixtures by FT-IR spectrometry is difficult because (1) the individual absorption intensities are typically weak due to the extremely low concentration of each species found in engine exhaust, typically less than 0.5 ppm[6] and (2) the broad band absorption features overlap significantly which results in

inaccurate reported concentrations (i.e. the least squares algorithm does not suitably isolate compounds present in the mixture[14]). The individual absorption features for each high molecular weight hydrocarbon are not distinguishable from the instrumental noise when collecting data at near-real time (20 seconds or faster). Yet these species contribute to a sum absorption feature that can be detected in near-real time as unburned fuel.

Evidence is provided in figure 5, which overlays the FID traces of figure 3 with the FT-IR total HC calculated with the expanded reference library. In both sets of measurements —the rapid continuous-sweep traverses at 45% engine power (figure 5a) when the engine is fired with diesel fuel, and at the nozzle centerline during cycling from 45% to 75% engine power (figure 5b) when the engine is fired with JP-8 fuel — the agreement with the FID is significantly improved. Using C16 for the diesel case and C14 for the JP-8 case as the multiplying factor for unburned fuel, the calculated total HC by the FT-IR correlates very well with the FID at all power settings. Note that a higher multiplying factor was used in the diesel case due to the fact that diesel fuel is a heavier blend than a typical kerosene. At 45% engine power the high molecular weight hydrocarbons, quantified by the composite reference, account for approximately one-third of the total HC. As engine power is increased, the concentrations of all HC species decrease.

Note that the improved total HC reported by the FT-IR (figure 5b) now maps both major and subtle changes seen by the FID significantly better than the original five species presented in figure 3b. The resulting correlation between the FT-IR and FID due to the advances in the reference library shows a near one-to-one agreement (figure 6). The

correlation plot was generated using random data points, at all power settings, taken from three separate engine tests on 10Jun03, 08Jul03 and the 10Dec04. Using three separate tests to generate the correlation indicate the reproducibility of the FT-IR in measuring total HC when compared to the traditional FID analyzer, with the advances made to the FT-IR reference library. In addition, with the advanced reference library in place, more individual hydrocarbon concentrations can be observed in near-real time during engine testing. Figure 7 compares individual hydrocarbon concentrations at 45%, 65%, and 75% engine power showing the decrease in hydrocarbons as the engine power is increased comparing the low molecular weight hydrocarbons to the high molecular weight hydrocarbons.

Conclusion

This article has presented advances in FT-IR capability for measuring total HC in turbine engine exhaust, achieved by increasing the number of pertinent individual hydrocarbon species in the quantitative reference library as well as by considering the unburned fuel contribution. The result provides the capability of measuring greater than 90 percent of the total HC, as indicated by the regulatory-accepted FID analyzer, in the gaseous exhaust of turbine engines at any power setting by the FT-IR method. This capability is particularly beneficial to the new, rapid measurement methodology currently being applied during development testing of new, high performance jet engines with large exhaust nozzle dimensions.[1] Consolidation of the broad spectrum of emissions data desired during engine development (i.e. CO, CO_2, H_2O, NO_x, SO_x, O_2, several low

molecular weight hydrocarbons C1-C4 including HAPs formaldehyde and 1,3-butadiene, and total HC) into the data stream of a single instrument has been achieved.

Acknowledgements

This work was supported under U.S. Air Force SBIR Phase III Contract F40600-02-C-0018. Gratitude is expressed to Vince Zaccardi, Paul Jalbert, Denise Bryant and Don Gardner (Aerospace Testing Alliance/AEDC), and Ron Bishel (AEDC/DOT) for their technical guidance and support; and to Bill Allen, Associate Professor in the Aerospace Maintenance Department of the Middle Tennessee State University (MTSU) for providing the gas turbine engine and test site.

---

[1] P. A. Jalbert, V. A. Zaccardi, M. D. Bryant, B. C. Winkleman, J. R. Markham, P. M. Bush and P. J. Bonzani, "Rapid, Complete Nozzle Exhaust Gas Measurement Capability for Gas Turbine Engines," *ISA vol. 451, Proceedings of the 50th International Instrumentation Symposium*, San Antonio, TX (May 9-13, 2004).

[2] J. R. Markham, P. M. Bush, P. J. Bonzani, J. J. Scire, V. A. Zaccardi, P. A. Jalbert, M. D. Bryant and D. G. Gardner, "Integrated Gas Analyzer for Complete Monitoring of Turbine Engine Test Cells," *Applied Spectroscopy*, Volume 58, Number 1, pp. 130-136, January 2004.

[3] P. A. Jalbert and J. R. Markham, "FT-IR for Turbine Engine Health Monitoring," *Applied Spectroscopy*, Volume 58, Number 12, pp. 1506-1508, December 2004.

[4] C. A. Moses and L. L. Stavinoha, "Gas Chromatic Analysis of Exhaust Hydrocarbons from a Gas Turbine Combustor," Western States Section/The Combustion Institute, Paper 75-17, Stanford Research Institute (1975).

[5] C. W. Spicer, M. W. Holdren, D. L. Smith, D. P. Hughes, and M. D. Smith, Trans. ASME/J. Eng. Gas Turbines Power, **114**, 111 (1992).

[6] C. W. Spicer, M. W. Holdren, R. M. Riggin, and T. F. Lyon, "Chemical Composition and Photochemical Reactivity of Exhaust from Aircraft Turbine Engines," Ann. Geophysicae, **12**, 994 (1994).

[7] D. Marran, P. Kenny, J. Markham, P. Jalbert, R. Moyers, and M Gardner, "The Application of FT-IR Spectroscopy to Turbine Engine Exhaust Monitoring," AIAA Paper 2000-2211 (2000).

[8] The MKS MultiGas 2030 is described at http://www.mksinst.com/GA1b.html.

[9] The Model 300 HFID is described at http://www.gasanalyzers.com/products.asp.

[10] D. G. Gardner, V. A. Zaccardi, P. A. Jalbert and M. D. Bryant, "Reducing the Cost of Aircraft Engine Emission Measurements," *ISA vol. 443, Proceedings of the 49th International Instrumentation Symposium*, Orlando, FL (May 2003).

[11] J. E. Shepherd, C. D. Nuyt, and J. J. Lee, "Flash Point and Chemical Composition of Aviation Kerosene (Jet-A)," NTSB Paper NTSB12-98-CB-0415 (2000).

[12] S. Yan, E. Eddings, R. Pugmire, and A. Sarofin, "Formulation and Some Applications of Jet Fuel Surrogates," available from the Department of Chemical & Fuels Engineering, Center for Simulation of Accidental Fires & Explosions, University of Utah.

[13] Hydrocarbon spectra downloaded from http://webbook.nist.gov/chemistry.

[14] R. L. Spellicy, "Challenges to CLS Analysis in the Real World," presented at the National Air & Waste Management Association (AWMA) conference, Salt Lake City, Utah (June 18-22, 2000).

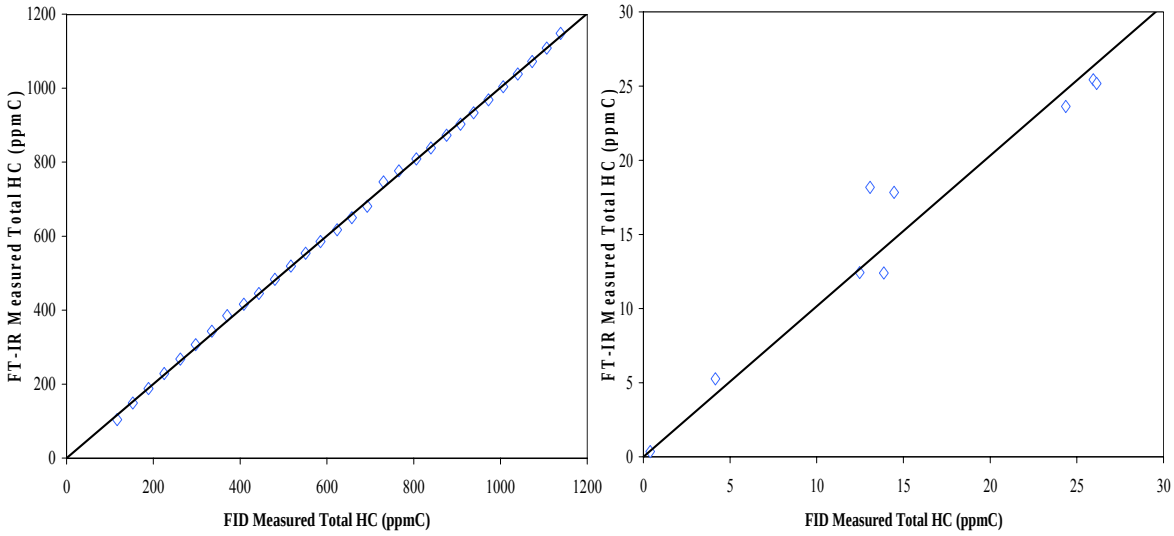

Figure 1. Correlation plots for measured total HC comparing the FID and FT-IR. The plot on the left shows several concentrations of butane gas balanced in nitrogen that spans 100-1150 ppmC. The best linear fit shown has a calculated slope of 1.0012 with a zero offset. The plot on the right shows concentrations of formaldehyde that spans 0-25 ppmC. The best linear fit shown has a calculated slope of 1.0154 with a zero offset.

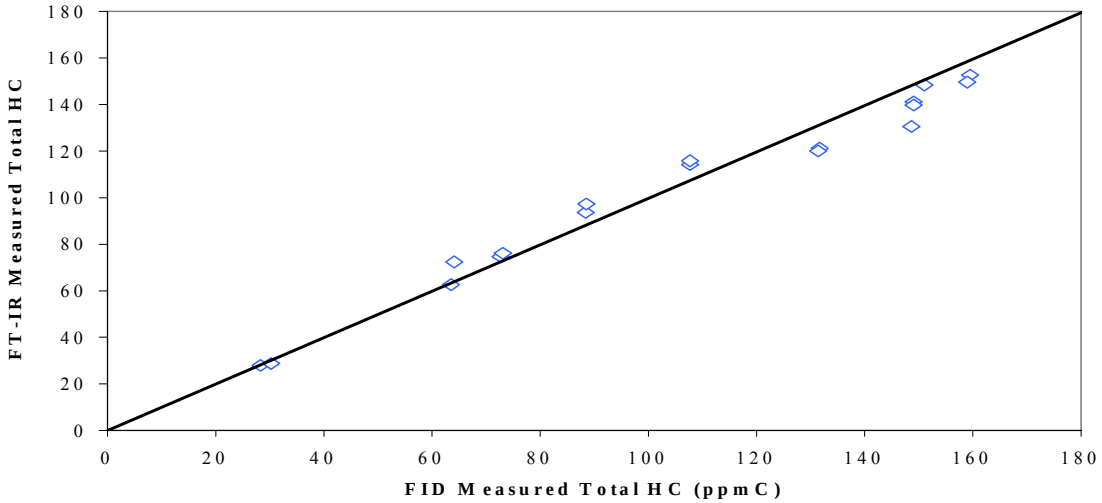

Figure 2. Correlation plot for measured total HC of a mixture containing ethane, propane and formaldehyde comparing the FID and FT-IR. The best linear fit calculated has a slope of 0.9971 with a zero offset.

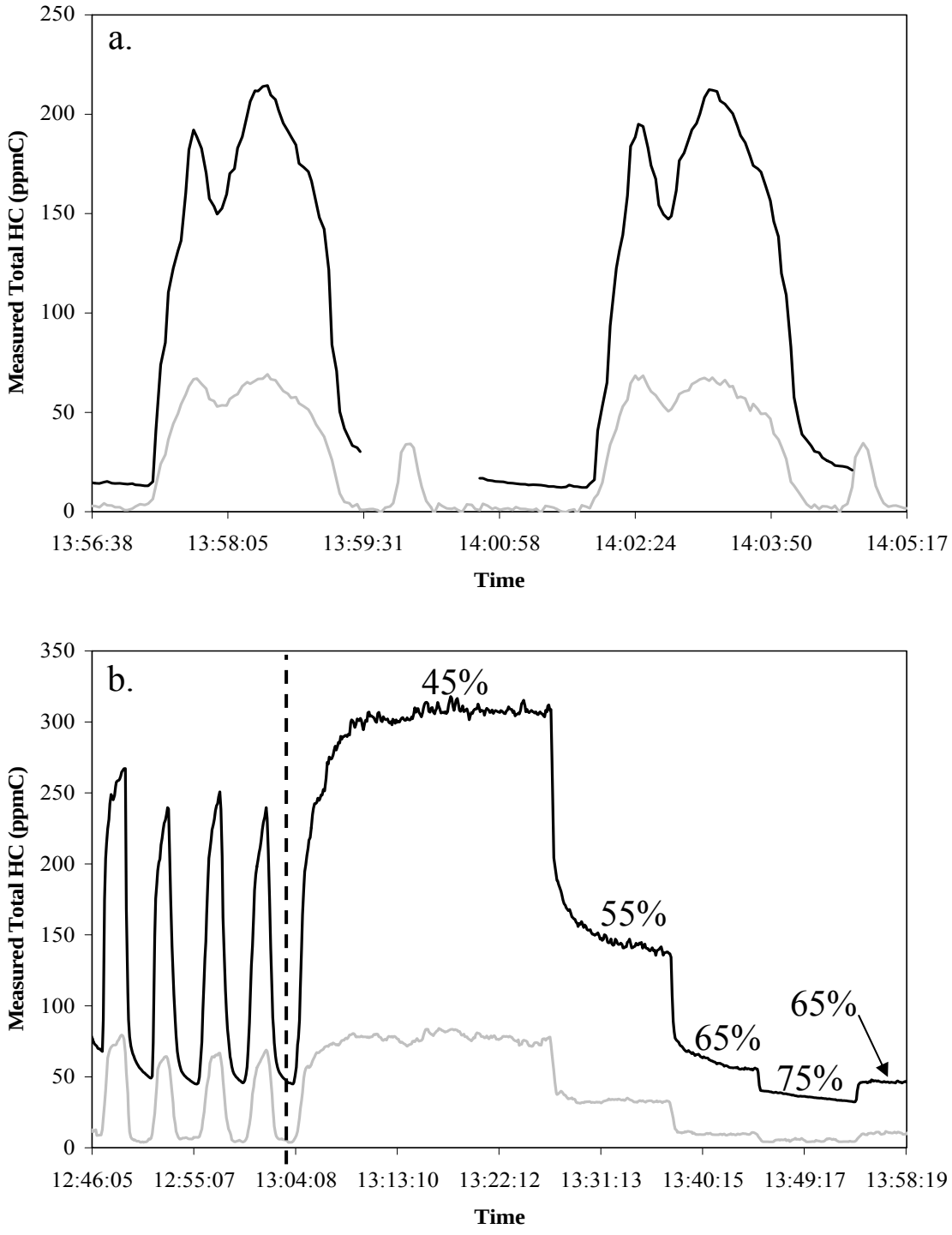

Figure 3. Using the original reference library, the FT-IR data trace (grey) for total HC compares poorly to the FID (black) data trace for two rapid traverses of the engine fired with diesel fuel at 45% engine power (plot a). The FT-IR also shows a poor comparison with the FID for rapid engine power cycling from 45% to 75% (left of dashed vertical line in plot b), and varied power steps from 45% to 75% at 10% power increments (right of dashed vertical line in plot b) with the sampling rake at the centerline of the nozzle and the engine firing with JP-8 fuel.

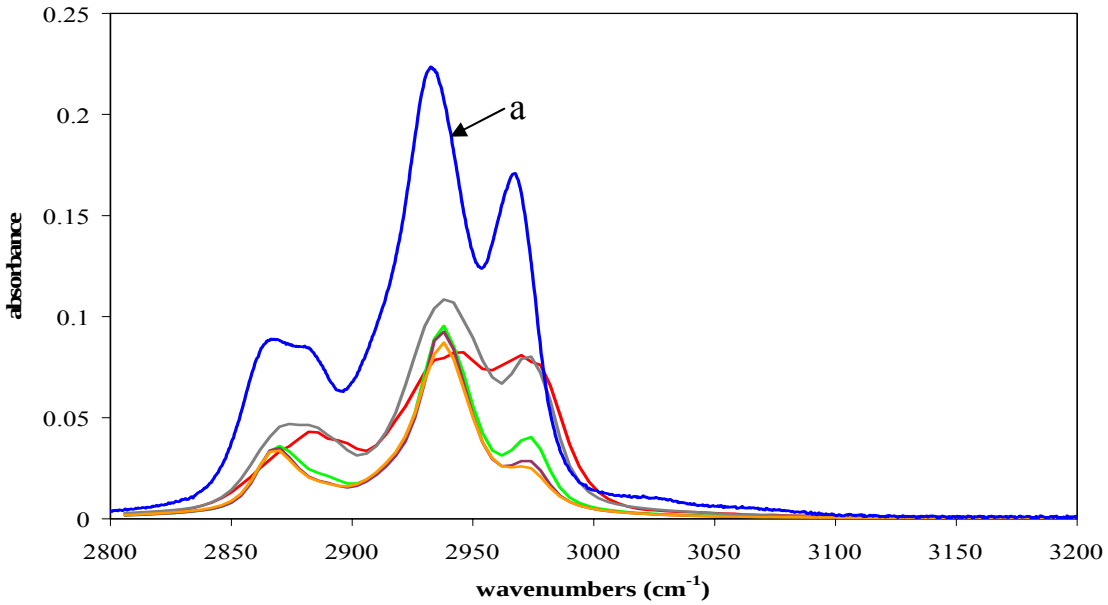

Figure 4. The spectral region between 2800 and 3200 cm^{-1} comparing the similar absorption features of straight chain hydrocarbons to unburned fuel vapor (a). The hydrocarbons identified are hexane (red), octane (gray), dodecane (green), hexadecane (purple) and octadecane (orange). Straight chain hydrocarbon spectra were downloaded from the NIST website.[13]

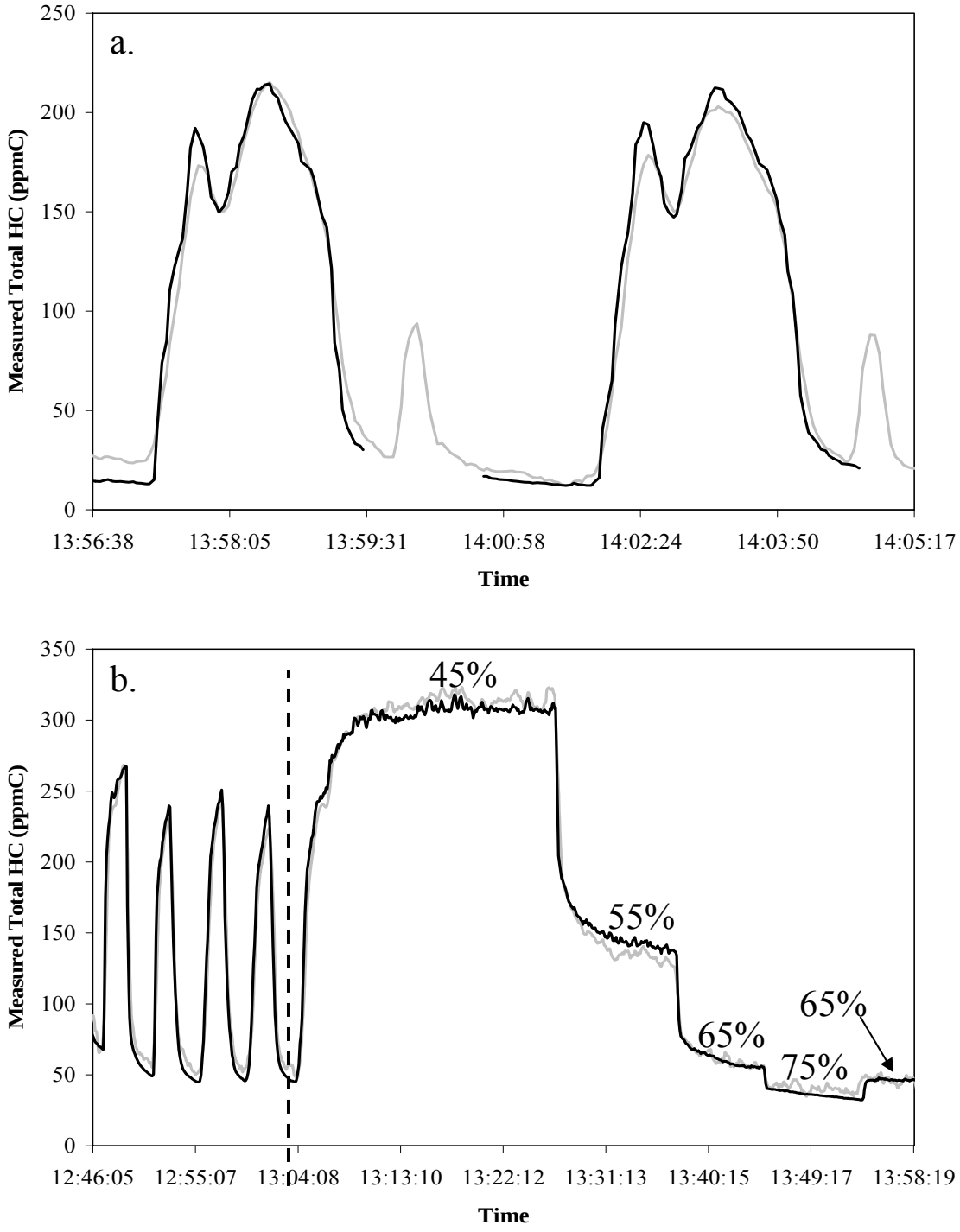

Figure 5. Using the expanded reference library, the FT-IR data trace (grey) for total HC compares well to the FID (black) data trace for two rapid sweeps of the engine fired with diesel fuel at 45% engine power (plot a). The FT-IR also shows a good comparison with the FID for rapid engine power cycling from 45% to 75% (left of dashed vertical line in plot b), and varied power steps from 45% to 75% (at 10% power increments) with the sampling rake at the centerline of the engine nozzle (right of dashed vertical line in plot b).

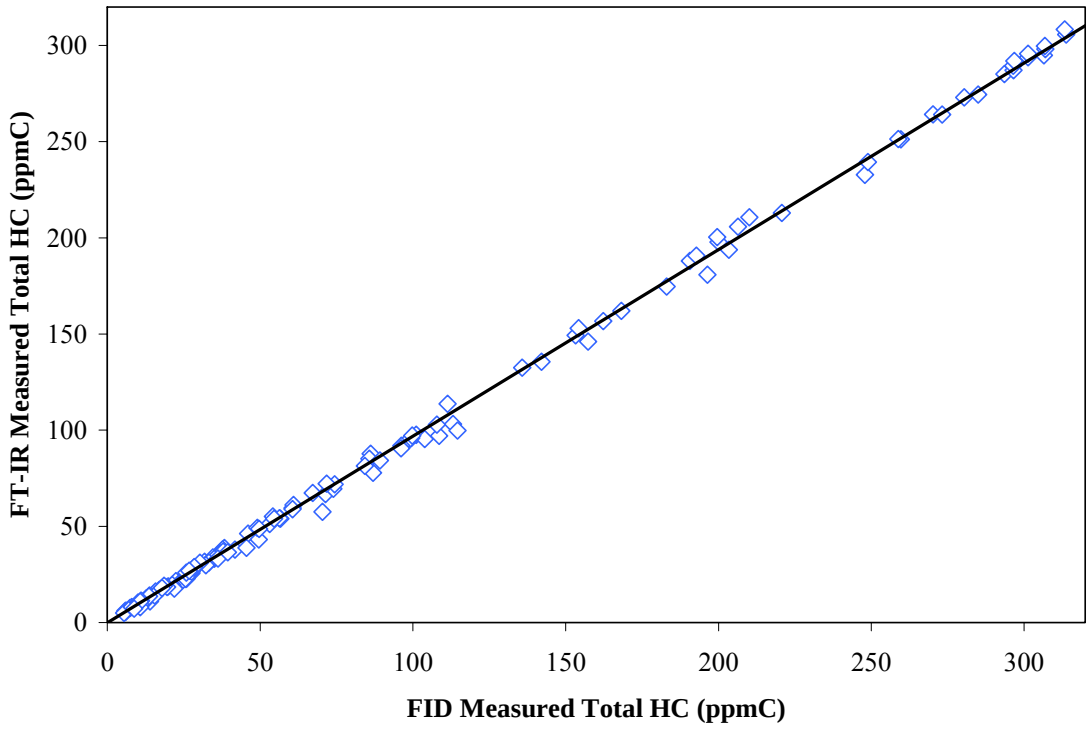

Figure 6. A Correlation plot comparing the measured total HC determined by the FT-IR using the the expanded HC species given in table 2. The best linear fit is shown with a calculated slope of 0.9696 and zero offset.

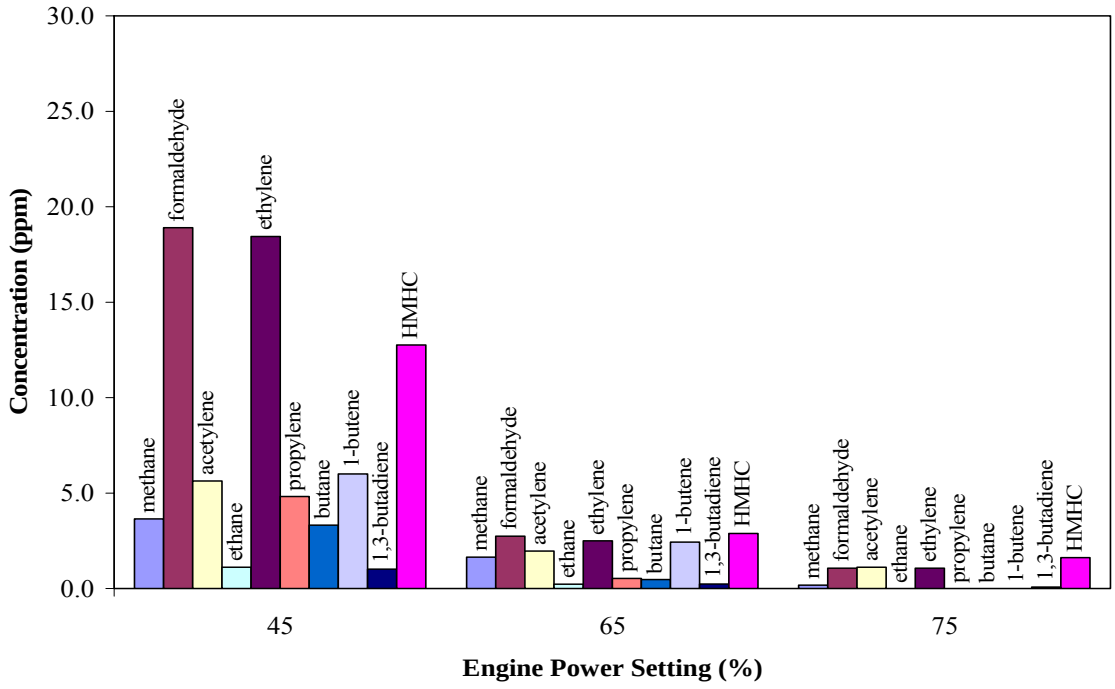

Figure 7. Distribution of Hydrocarbons observed at the exhaust nozzle centerline at 45%, 65%, and 75% engine power settings. HMHC is the total of the high molecular weight hydrocarbons.

Table 1. The original FT-IR reference library for HC compounds, and compounds for measuring total HC in turbine engine exhaust. In the column at the right, the multiplying factor of each species for determining total HC in ppmC is given.

Original HC Reference Library	Original HC Species Contributing to Measured Total HC
Acetaldehyde	Acetylene (C2)
Acetone	Butane (C4)
Acetylene	Ethylene (C2)
Butane	Methane (C1)
Ethylene	Propylene (C3)
Formaldehyde	
Methane	
Propylene	

Table 2. The expanded combustion reference library for the FT-IR, identifying detection limits (ppm) when averaging 4 scans (~2.2 seconds) and 20 scans (~15 seconds), and future combustion species to be measured to expand the reference library further. The specific unburned fuel species that have been calibrated are Jet-A, JP-8, Kerosene and Diesel (ARP - California Air Resource Board Blend and EC-D - Emission Control Diesel (BP)).

Expanded MGA Combustion Library			Future Species
	Scans		
Species	4	20	
1,3-Butadiene (C4)	0.288	0.189	1-Butyne
1-Butene (C4)	2.979	1.953	1-Heptene
Acetaldehyde	4.5	2.835	1-Hexene
Acetone	-	-	1-Octene
Acetylene (C2)	0.131	0.095	1-Pentene
Ammonia	0.182	0.095	1-Pentyne
Benzene	3.571	2.385	2-Hexene
Butane (C4)	0.523	0.374	Decane
Methane %	-	-	Diesel Blends
Methane ppm (C1)	0.212	0.144	Ethanol
Carbon Monoxide %	-	-	Gasoline Blends
Carbon Monoxide ppm	0.133	0.043	Glyoxal
Carbon Dioxide %	0.013	0.0053	Heptane
Cumene	4.864	2.871	Hexane
Cyclohexane	-	-	Isopentane
Ethane (C2)	0.143	0.071	Isobutane
Ethylene (C2)	0.326	0.224	Isoprene
Ethyl-benzene	-	-	Jet-A1
Ethylene Glycol	-	-	Jet-B
Formaldehyde (C1)	0.519	0.249	JP-4
Formic Acid	0.318	0.133	JP-5
Water %	0.025	0.0016	Nonane
Sulfur Acid	-	-	Octane
Isopropyl Alcohol	0.581	0.248	Phenol
Unburned Fuel (C14-16)	0.444	0.216	Propyl-benzene
Methanol	0.672	0.384	Propyne
m-Xylene	4.104	2.806	Styrene
Nitrous Oxide	0.375	0.126	
Nitric Oxide	0.439	0.173	
Nitrogen Dioxide	0.225	0.116	
o-Xylene	3.961	2.743	
Oxygen*	-	-	
p-Xylene	3.998	2.759	
Propylene (C3)	1.05	0.462	
Sulfur Dioxide	-	-	
Toluene	5.274	3.321	

*** Identifies species that are non-infrared active, (See ref. 2).**

Appendix H

Final Report Document: **MGA Data Collected During Measurement Trials at Solar Turbines**

Summary

Solar Turbines is interested in incorporating an emissions analyzer to their stationary turbine engines for monitoring combustion efficiency, with an emphasis on being able to measure total NOx under 1 ppm. The Multigas 2030 Analyzer, manufactured by MKS Instruments, is a suitable candidate for this application. Under the Federal Earmark FY02 funding, two MGA 2030s were purchased and lent out to Solar for a one year shake down demonstration. During the demonstration one MGA (unit 1) was installed at the University of California at San Diego for a long term durability test, while the other MGA (unit 2) was designed as a mobile unit for laboratory and field testing (when needed). Unit 1 was set up to continuously measure the emissions off a natural gas fired turbine engine before and after a SCONOx unit which removes NOx and CO from the exhaust stream. A traditional chemiluminescence detector (CLD) was also set up to only measure the emissions after the SCONOx unit for comparison. Unfortunately no CLD data was supplied to AFR for comparison. Even though it was determined that unit 1 had a small instability issue from point to point, the instrument was successful in measuring the emissions before and after the SCONOx unit, as well as, measuring accurately 4.1 and 9.01 ppm NO calibration checks (taking the overall average of all the reported concentrations). The instrument also showed sensitivity to the efficiency of the SCONOx unit by measuring lower total NOx concentrations after the system was shut down for a mandatory cleaning of the NOx scrubber unit. Unit 2 initially exhibited the same instability issue as seen in unit 1, and therefore was sent back to MKS Instruments to go through a full system upgrade, which resulted in a significant improvement in the stability of the instrument (a factor of five better than unit 1). Unit 2 was tested for reproducibility by repeating calibration checks without acquiring a new baseline each time before being shipped out to Caterpillar Technical Center (CTC) in Peoria, Illinois to measure the emission of a natural gas fueled turbine engine. Two independent CLD instruments also measured the emissions for comparison. The MGA tracks the total dry NOx concentration relatively well compared to the two CLDs. This report chronicles the work perform and discusses data obtained by both MGAs during the year long demonstration.

Work Performed

Two multigas analyzers were purchased from MKS Instruments with available funding through the FY02 federal earmark program that Advanced Fuel Research, Inc has with the United States Air Force (Project No. F40600-02-C-0018). The instruments were designed to run continuously for long durations by using a thermally-cooled mercury-cadmium-telluride (TE-cooled MCT) detector. Since these detectors do not require the use of liquid nitrogen for cooling, the MGAs can run for long durations without any interaction by an operator. Since a liquid nitrogen-cooled MCT detector requires replenishing the liquid nitrogen every eight hours, this detector was not suitable for this demonstration.

Solar Turbines designed and built two mobile carts to house each MGA (circa March 2003), along with an oxygen analyzer and the complete sampling pump system. One

mobile cart was installed at the University of San Diego for continuous emission monitoring of the SoLoNOx Titan 130 engine. Figures 1 and 2 show this mobile unit installed at UCSD in a small emission shed just outside the engine test cell. Figure 2 shows a chemiluminescence detector (CLD) instrument used for measuring total NOx located to the left of the MGA cart. The sampling system for the CLD instrument was designed to monitor the emissions after the SCONOx scrubber unit off the north and south engine. Where as, the sampling system for the MGA monitored the emissions before and after the SCONOx scrubber off the south engine only. Measuring the emissions before and after the SCONOx scrubber evaluates the capability of the MGA to detect engine level gas emissions, as well as, low ppm levels of NOx and CO without removing water from the exhaust stream. The CLD and MGA use the same sampling probe after the SCONOx scrubber on the south engine, which allows only one instrument to sample that position at any given time. Therefore no direct comparison can be made between the two instruments for total NOx concentration, since both instruments were never measuring the same exhaust gas. Scheme 1 shows a simple schematic of the sampling system used at the university. The two instruments were configured to continuously monitor the emissions by switching every seven minutes between the two sampling positions.

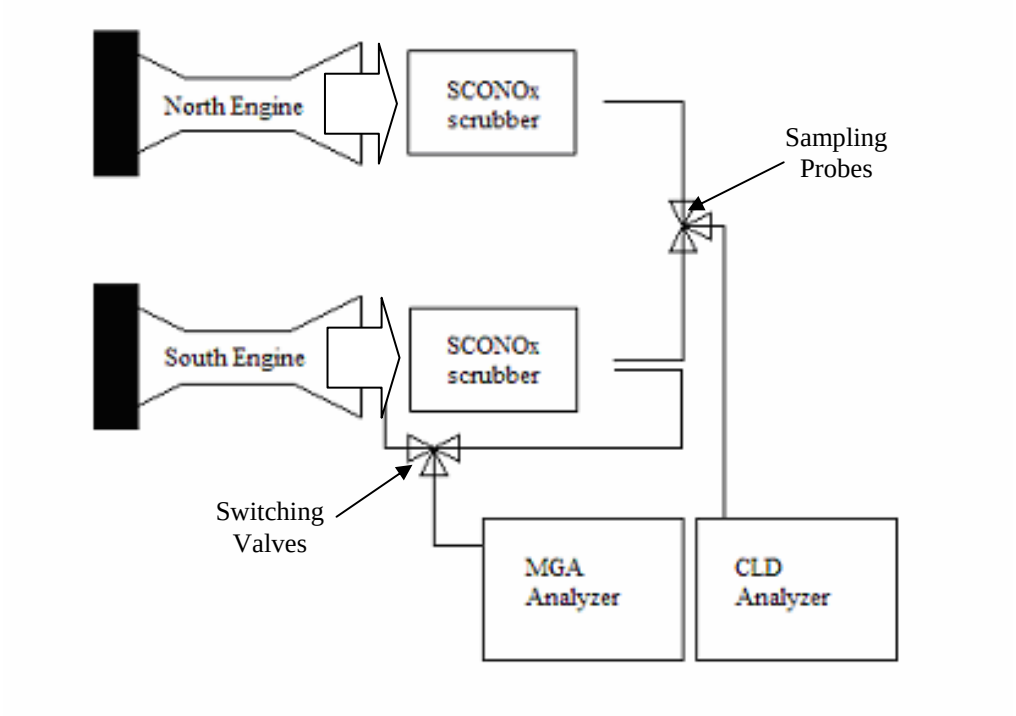

Scheme 1: Schematic of the sampling system located at UCSD.

Figure 1: Mobile unit 1 located in emission shed outside engine test cell located at the University of California at San Diego.

Figure 2: Mobile unit 1 in emission shed (right) and USCD's CLD instrument (left).

Background - The SCONOx unit is a post combustion catalytic converter that reduces both NOx and CO from the exhaust stream. The exhaust from the engine goes through an oxidation/absorption cycle where NO and CO are both oxidized to NO_2 and CO_2 respectively (formaldehyde will also be oxidized to CO_2 and H_2O if present within the exhaust stream). The combined NO_2 reacts with potassium carbonate to form potassium nitrite, potassium nitrate, and CO_2 gas. Once the potassium catalyst is saturated by NO_2, the catalyst goes through a regeneration cycle where potassium nitrite and nitrate are reduced back to potassium carbonate by flowing H_2 gas over the surface of the potassium catalyst. The majority of carbon dioxide formed during the oxidation/absorption cycle is used up during the regeneration cycle to reform potassium carbonate. Table 1 lists the chemical reactions that take place during both cycles of the SCONOx unit. [1]

Table 1: The chemical reactions that occur during the Oxidation/Absorption and Regeneration cycles of SCONOx.[1]

Oxidation/Absorption Cycle	Regeneration Cycle
$CO + ½O_2 \rightarrow CO_2$	$KNO_2 + KNO_3 + 4H_2 + CO_2 \rightarrow K_2CO_3 + H_2O + N_2$
$NO + ½O_2 \rightarrow NO_2$	
$CH_2O + ½O_2 \rightarrow CO_2 + H_2O$	
$2NO_2 + K_2CO_3 \rightarrow CO_2 + KNO_2 + KNO_3$	

To generate the H_2 gas needed during the regeneration cycle, the University uses a steam boiler which runs off of natural gas. The boiler partially oxidizes the fuel to produce high levels of H_2 and CO. Downstream of the boiler these gases are introduced into the exhaust and travel over a catalyst bed which absorbs CO. Once CO is removed from the exhaust the gas stream is introduced into the regeneration cycle to re-make the potassium carbonate catalyst. The University, at one point, was concerned about the H_2 levels being produced from the boiler and wanted to monitor the H2 concentration indirectly by measuring the CO produced. Therefore, the University used unit 1 to measure the CO levels upstream and downstream of the catalyst bed. Scheme 2 shows a simple schematic of the sampling setup during this test.

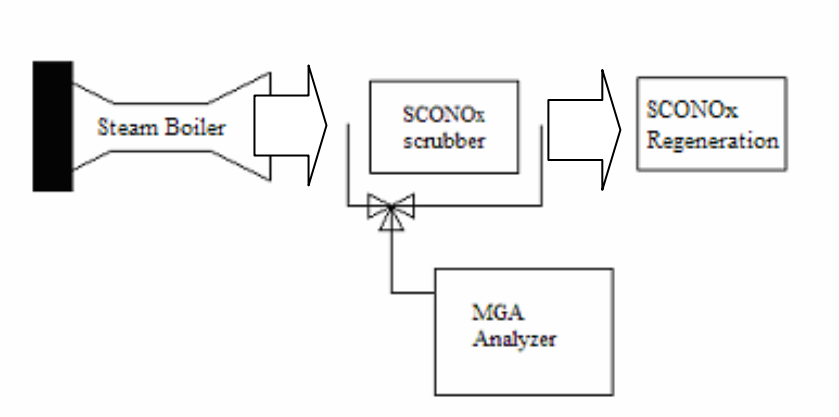

Scheme 2: Schematic of the sample system used to monitor CO levels upstream and downstream of the catalyst bed from the steam boiler (located at the University).

In May 2003, Advanced Fuel Research visited Solar Turbines to evaluate the performance of each MGA and to address some their concerns. Both instruments showed a small instability which was seen in the reported gas concentration from point to point. The majority of the instability was caused by the current electronics of the MGA and the bit size of the digitizer. Since unit 2 showed a more predominant instability than the MGA located at the university, unit 2 was shipped back to MKS Instruments for a full system upgrade. This upgrade resulted in a refurbished system using a larger digitizer on the electronics eliminating the instability caused by the electronics. The system was re-calibrated for NO, NO_2, CO, and CO_2 before being shipped back to Solar Turbines. MKS and AFR both visited Solar Turbines to perform initial installation of the system (July 2003).

Solar seemed pleased with the upgraded performance of unit 2, so the system was then installed into the mobile cart for further laboratory testing before the field test located at Caterpillar Technical Center (CTC) in Peoria, Illinois. Figure 3 shows the mobile cart designed for unit 2 during the field test at CTC. The MGA measured emissions off a full scale combustor rig burning natural gas along side two independent emission trains identified as BG and CAT-ET mobile units. The BG unit measured only total NOx using a traditional CLD instrument, where as, the CAT-ET measured total NOx using a CLD, CO and CO_2 with NDIR, and total unburned hydrocarbons with an FID instrument. All three mobile carts sampled from the same sampling probe which was divided into three separate sample streams. The sampling system was designed with only 6 feet of heated trace lines supplying sample exhaust to the BG unit, where as, the other two instruments had approximately 45 feet of heated trace lines. Scheme 3 shows a simple schematic of the sampling system used at CTC.

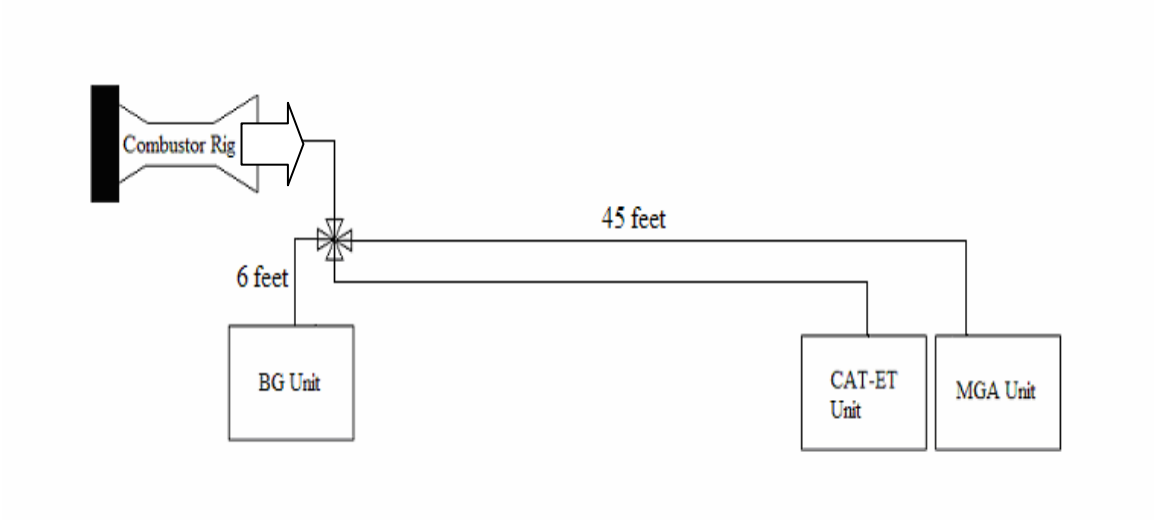

Scheme 3: Schematic of the sampling system located at CTC.

Figure 3: MGA mobile unit 2 located in emission shed at CTC.

Data Analysis

Background – The multigas analyzer is an FTIR based system that quantifies combustion gases from their distinct infrared signatures. The absorbance of each gas within the infrared spectrum is related to gas concentration through Beer's Law, which can be expressed as:

$$A = \varepsilon bc \qquad (1)$$

Where A is the absorbance measured, ε is the gas constant specific for each gas species, b is the pathlength, and c is the concentration. Therefore peak height in the absorbance spectrum can be used to monitor changes in species concentrations. Certain gases, such as atomic and symmetric diatomic gases (i.e. He, Xe, N_2, O_2, H_2) are infrared inactive and therefore can not be detected by the MGA. Whereas, non-symmetrical gas species (i.e. CO, CO_2, H_2O, NOx, etc) are infrared active and have distinctive absorption bands that can be measured by the MGA. Figure 4 shows the near infrared spectral region with

characteristic absorbance bands for six gas species typically seen in a combustion process. Note that the trace species, CO, NO, and NO_2 (NO in particular), which have been magnified for illustrative purposes, absorb in regions dominated by H_2O and CO_2. Depending upon the gas species present in the exhaust stream, overlapping absorbance bands of other gases can interfere with the calculated concentration of certain gases. Therefore the MGA is equipped with calibration routines that quantify over individually selected absorbance bands within a small spectral region to significantly reduce the "cross-talk" interferences.

The chemiluminescence detector (CLD) is typically used for measuring NO and total NOx. Chemiluminescence works by reacting NO with O_3 to form NO_2 in an excited state, which emits a photon of light as the molecule goes to ground state. The light given off in this reaction can be proportional to the NO concentration as long as O_3 is present in excess. To ensure that the entire NO sample is converted to NO_2 in the excited state, the reaction chamber is set to relatively high temperatures and O_3 is present in excess. CLD can not measure NO_2 since NO_2 present in the exhaust stream is not in the excited state. Therefore to determine total NOx, the NO_2 present within the exhaust stream is reduced to NO before entering the reaction chamber. The chemical reductants and heated metal converters typically used in CLDs are not specific to NO_2 and will reduce any nitrogen containing species present in the exhaust to NO, which results in a positive bias in the total NOx reported concentration. The conversion rate of NO_2 varies from one instrument to the next and therefore needs to be checked frequently. The baseline is also susceptible to drift, which requires that the instrument frequently be calibrated and re-zeroed. Also, CLDs are susceptible to interferences that reduce the emitted radiation by collision (known as quenching) between an excited NO_2 molecule and typically H_2O or CO_2. Therefore drying of the exhaust stream is required before sampling the gas through the CLD instrument.

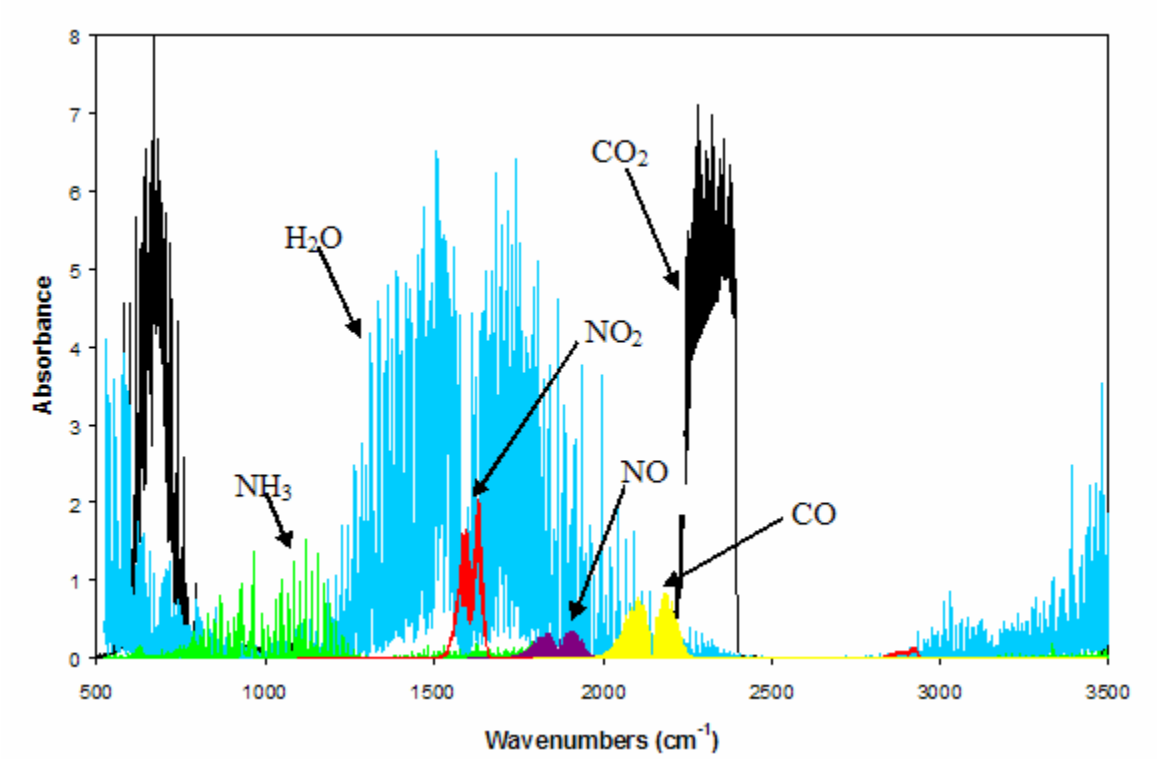

Figure 4: Infrared absorbance spectrum illustrating the "cross-talk" interferences that are present for particular gas species.

Unit 1 (MG-07-129) Results – Since optimizing the calibration routines, and the complete system upgrade of unit 2, both instruments have performed well throughout the second half of the demonstration period. Even though unit 1 never went through the necessary system upgrade to reduce the point-to-point instability, the overall average reported concentration for NO was within 2% of the manufacturer guaranteed bottle concentration when doing calibration checks for this instrument. Figure 5 shows one calibration check displaying each data point to illustrate the point-to-point instability exhibited from unit 1. Note that 75% of the total points do fall within the ±2% range (indicated by black horizontal lines) of the Manufacturer's bottle concentration of 9 ppm. However, the precision for this particular MGA does not satisfy the specification with the current system setup. Yet, analysis of the overall accuracy (average) of each calibration check ran on unit 1 indicates that the instrument is responding relatively well and that each average falls within the ±2% specification range. Figures 6 and 7 show the overall average for several calibration checks collected on unit 1 using a 4 ppm and 9 ppm calibration bottle respectively. Note that not all of the calibration checks that were acquired during the demonstration period were supplied to AFR for further analysis and reprocessing.

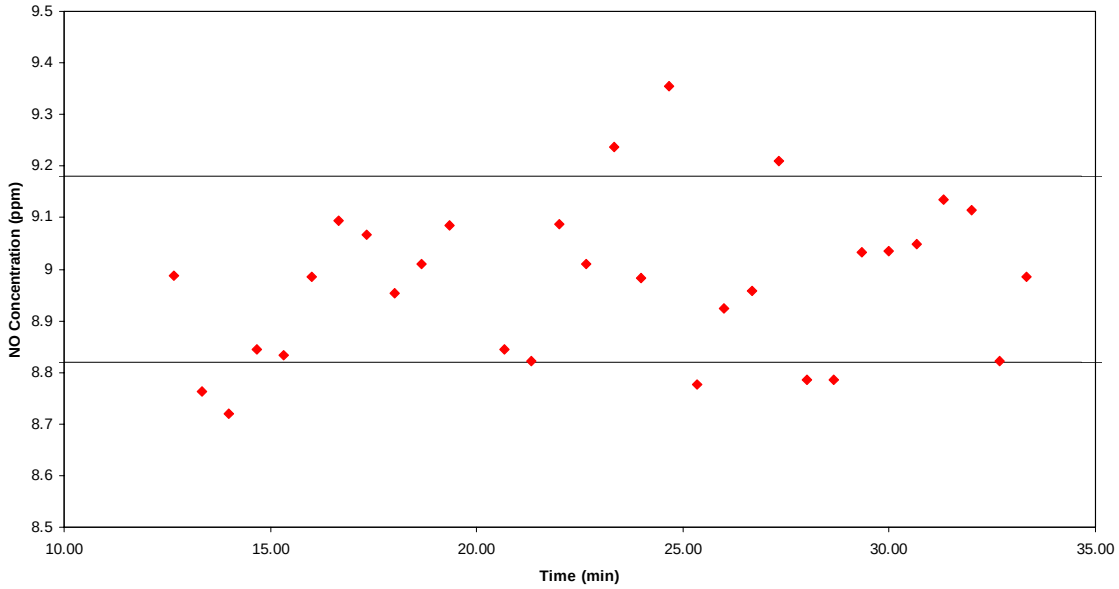

Figure 5: NO calibration check showing the point to point instability in the precision of unit 1. Measured is a certified NO sample (9 ppm ±2%) flowing through the MGA at 1.5 liters per minute. The solid lines indicate the ±2% boundary.

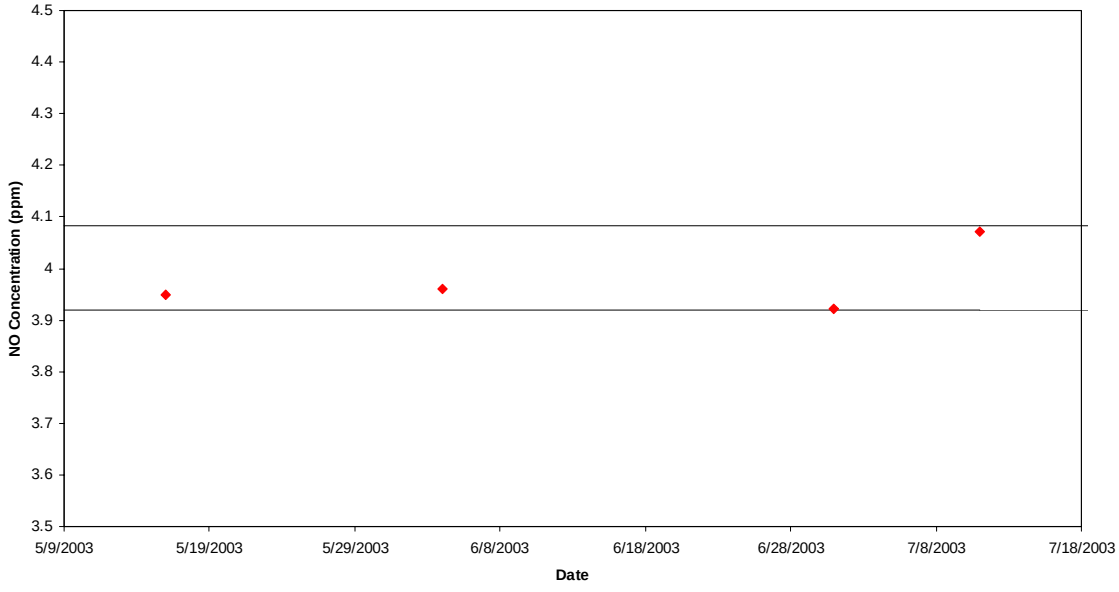

Figure 6: Overall accuracy of four daily calibration checks at 4 ppm ±2% NO concentration for unit 1.

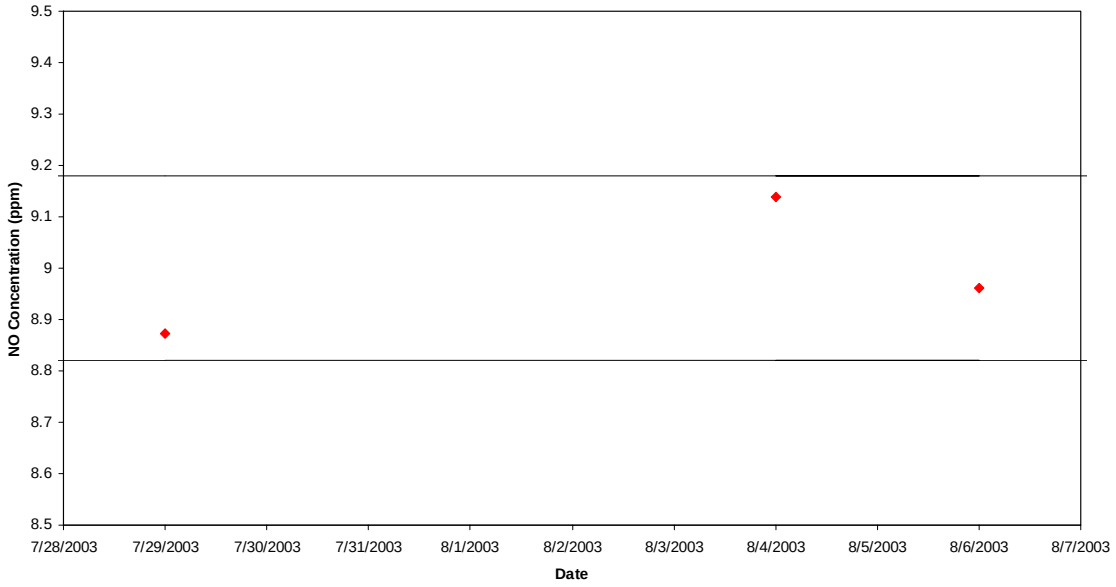

Figure 7: Overall accuracy three daily calibration checks at 9 ppm ±2% NO concentration for unit 1.

The sensitivity of unit 1 was demonstrated when the engine facility was shut down for a mandatory cleaning of the SCONOx unit. The total NOx measured by the MGA at the outlet of SCONOx and before the facility shut down ranged between 1.5 and 2.2 ppm. Once the facility came back on-line and the SCONOx scrubber unit was cleaned, the total NOx concentration reported after the scrubber went down to approximately 0.5 ppm. The NOx scrubber efficiency went from 87% before maintenance to 95% efficient after maintenance was done, a factor of two improvement in NOx emissions. Figure 8 compares data collected at the inlet and outlet of SCONOx for 7 minute intervals before (blue – 04Jun03) and after (red – 29Jul03) the maintenance shutdown. At the inlet of the SCONOx unit the MGA reported relatively the same total NOx concentration, whereas, at the outlet of the SCONOx unit the MGA showed that it is sensitive to the cleaning made on the NOx scrubber. Note that the total NOx measurements were quantified in a wet sample stream with approximately 8% water concentration present. Notice that the MGA reports a stable water concentration at the inlet of the SCONOx, whereas, the concentration fluctuates significantly at the outlet of SCONOx (Figure 9). This fluctuation is caused by the introduction of steam into the sample stream during the regeneration cycle. Steam is introduced to create the needed H_2 gas to reduce potassium nitrites and nitrates. Note that H_2O is also produced in negligible amounts during the Oxidation/Absorption cycle by oxidizing any formaldehyde present, and during the regeneration cycle of potassium carbonate. Figure 9 also shows the CO_2 concentration during the same 7 minute cycles. The fluctuation in the CO_2 concentration at the outlet of SCONOx is minimal compared to that of H_2O, indicating that the majority of CO_2 produced during the Oxidation/Absorption cycle is consumed during the regeneration cycle of the potassium carbonate catalyst (refer to Table 1 for SCONOx chemical reactions).

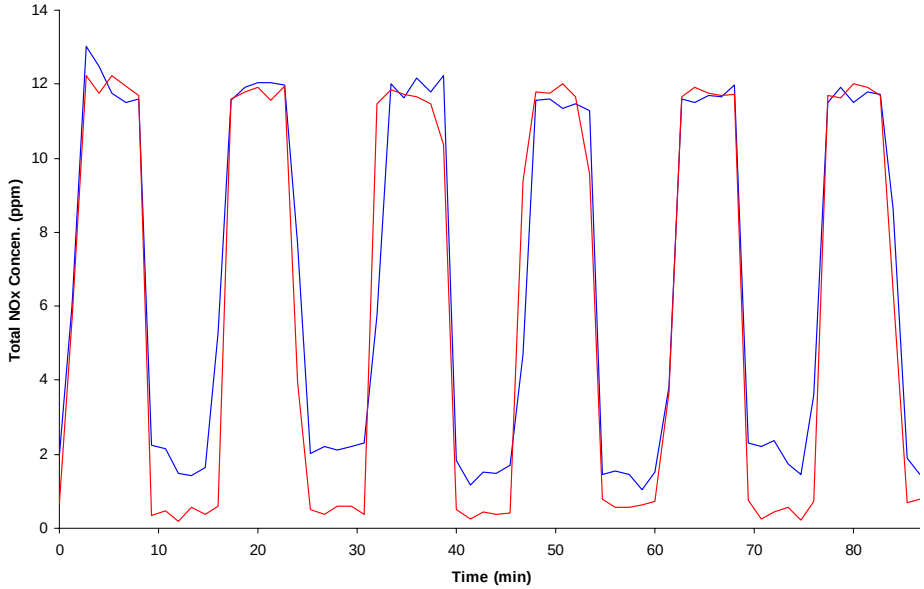

Figure 8: Measure total NOx before (blue – 04Jun03) and after (red – 29Jul03) engine shut down for mandatory SCONOx cleaning.

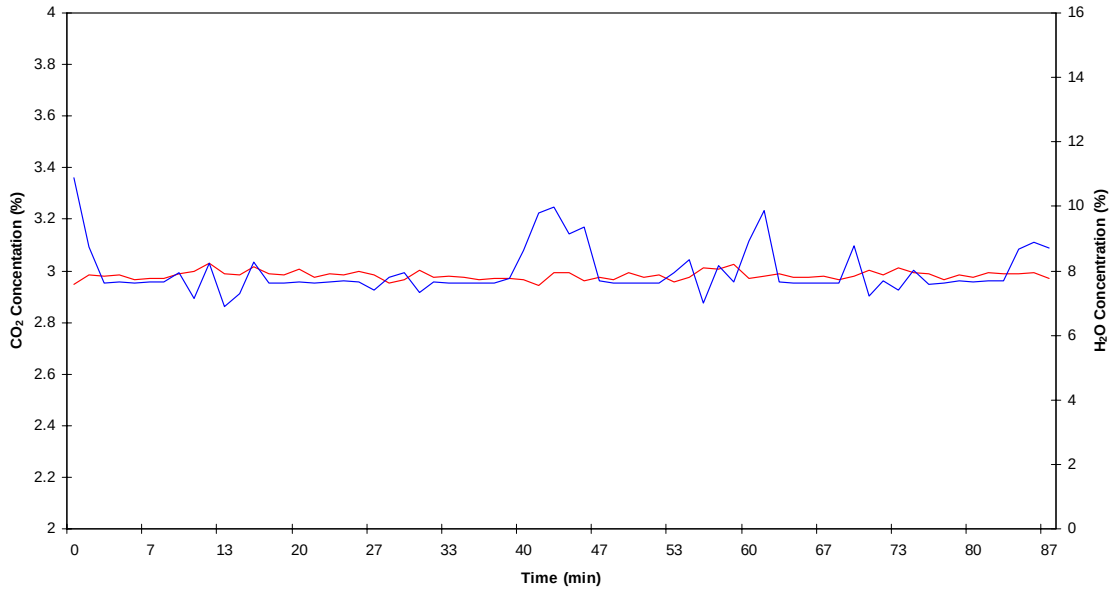

Figure 9: Measured H_2O (blue) and CO_2 (red) concentration at inlet and outlet of SCONOx unit. Fluctuations in H_2O indicate when the MGA was sampling after the SCONOx unit.

The MGA was able to detect formaldehyde at both the inlet and outlet of SCONOx averaging approximately 250 ppb and below 100 ppb respectively. The fluctuation in the formaldehyde reading is most likely due to the detection limit for formaldehyde of the TE-MCT detector. To be able to measure sub-ppm levels of formaldehyde with better stability, a liquid-nitrogen-cooled detector is needed. Yet the current instrument configuration shows sensitivity to formaldehyde by detecting a difference in the concentration between inlet and outlet of the SCONOx unit. Comparing the concentration of formaldehyde before and after the NOx scrubber, approximately 50-80% of the formaldehyde is oxidized and removed from the exhaust stream. The efficiency of oxidizing formaldehyde appears to be independent from the mandatory cleaning of the SCONOx unit, since the formaldehyde concentration before (blue – 04Jun03) and after (red – 29Jul03) the maintenance shutdown appears unchanged (Figure 10).

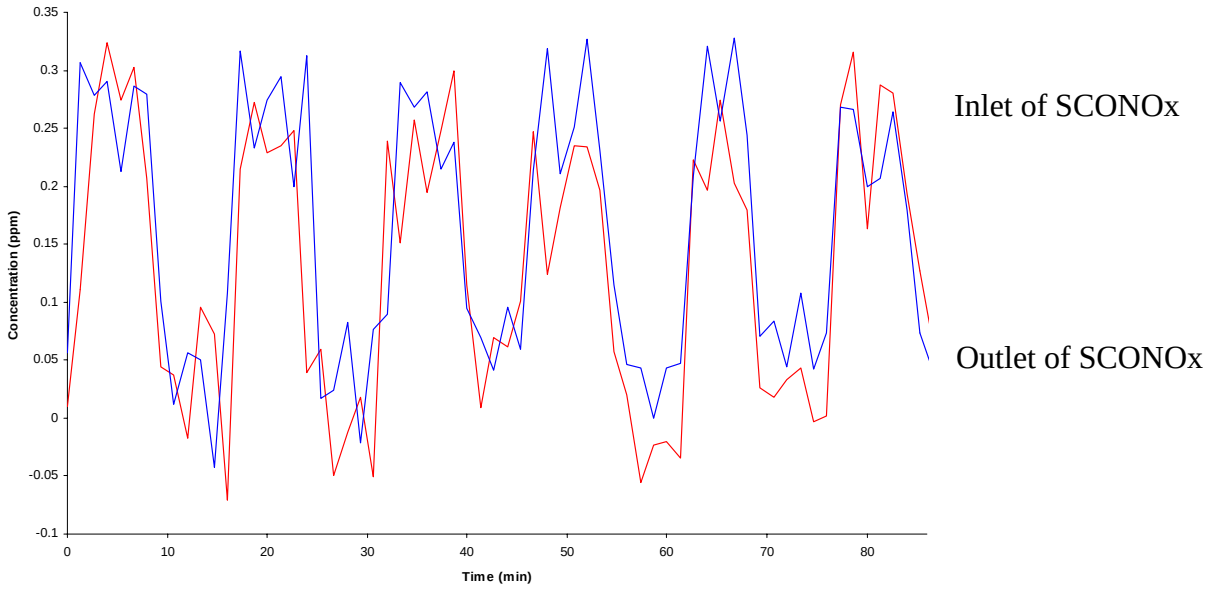

Figure 10: Formaldehyde measurement at inlet and outlet of NOx scrubber unit before (blue – 04Jun03) and after (red - 29Jul03) maintenance shut down.

Unit 2 (MG-09-131) Results – During AFR's visit at Solar Turbines in the beginning part of May, unit 2 showed significantly high point to point instability during calibration checks. Figure 11 shows data collected from a 19.2 ppm NO calibration tank on the 29Apr03, and illustrates the point-to-point instability of the instrument (standard deviation of 0.45 ppm). Even though only 30% of the data points fell within the ±2% specification, the overall average was determined to be 19.17 ppm (well within the ±2% specification) indicating that the instrument still had the capability of measuring the correct bottle concentration. Because of the point to point instability, unit 2 was shipped back to MKS for a full system upgrade, which resulted in an instrument with far less point to point instability. Figure 12 shows data collected from a 20.1 ppm NO calibration

tank on 11Jul03 (after the system upgrade). All of the data points collected fall within the ±2% specification with a standard deviation less than 0.1 ppm.

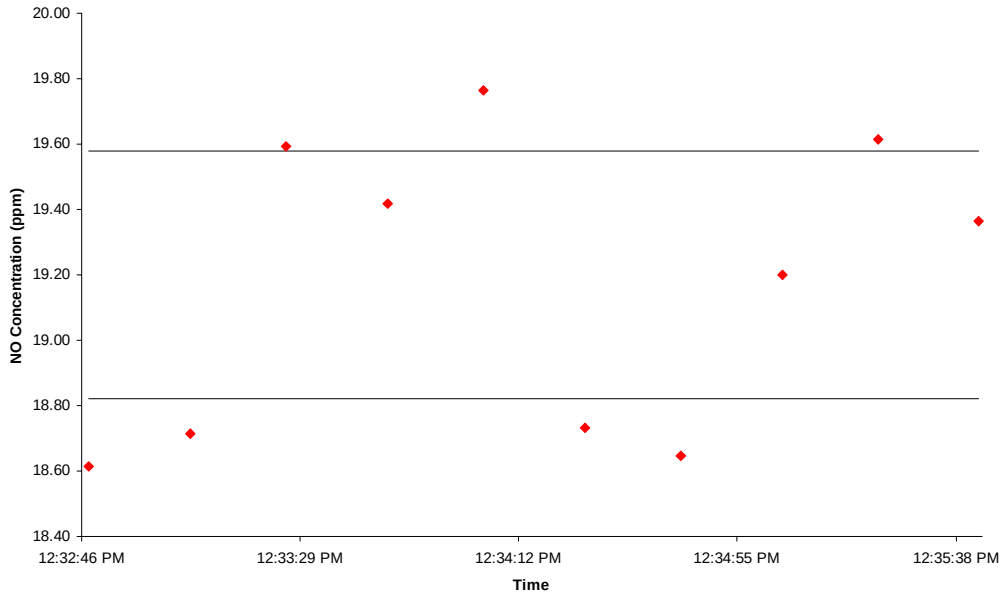

Figure 11: Calibration data showing the point to point instability of MG-09-131 before system upgrade. Data was collected from a 19.2 ppm ±2% NO calibration tank on 29Apr03.

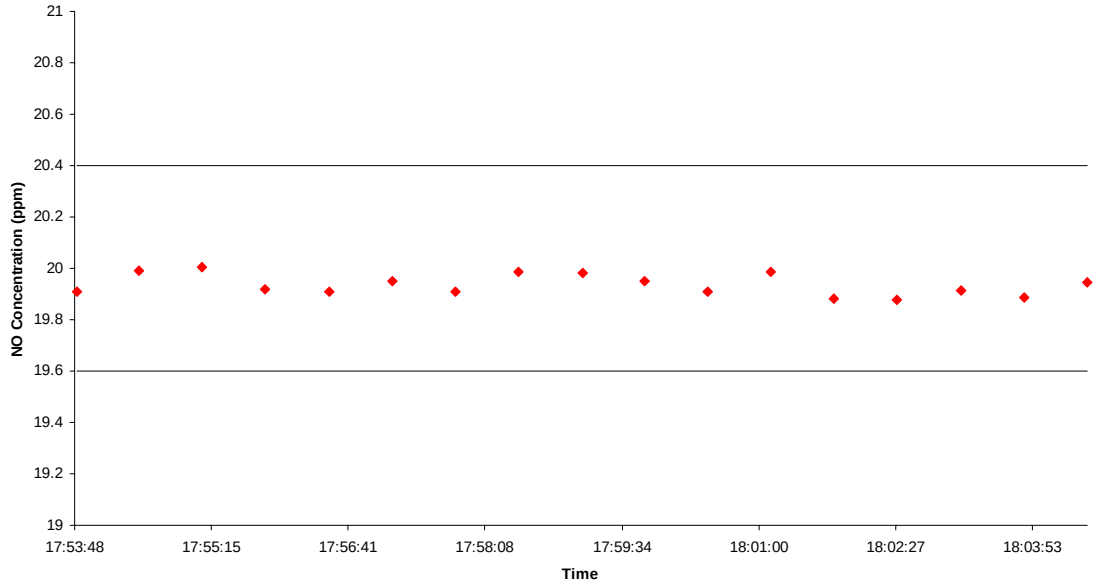

Figure 12: Calibration data showing the point to point instability of MG-09-131 after system upgrade. Data was collected from a 20.1 ppm ±2% NO calibration tank on 11Jul03.

During the month of August Solar ran reproducibility checks on the MGA by measuring the 20.1 ppm NO calibration tank several times without taking a new background each

time. The instrument was re-zeroed before the first calibration check and that background was used for each sequential calibration check. Figure 13 shows the reported average NO concentration (red) for 5 different calibration checks without taking a new background before each set. Each calibration check falls within the ±2% specification (defined by the solid black lines), but reads lower than the actual bottle concentration. If we assume that a small amount of NO is converted to NO2 inside the Teflon lines before entering the MGA, the total NOx (blue) agrees much better with the actual bottle concentration of 20.1 ppm.

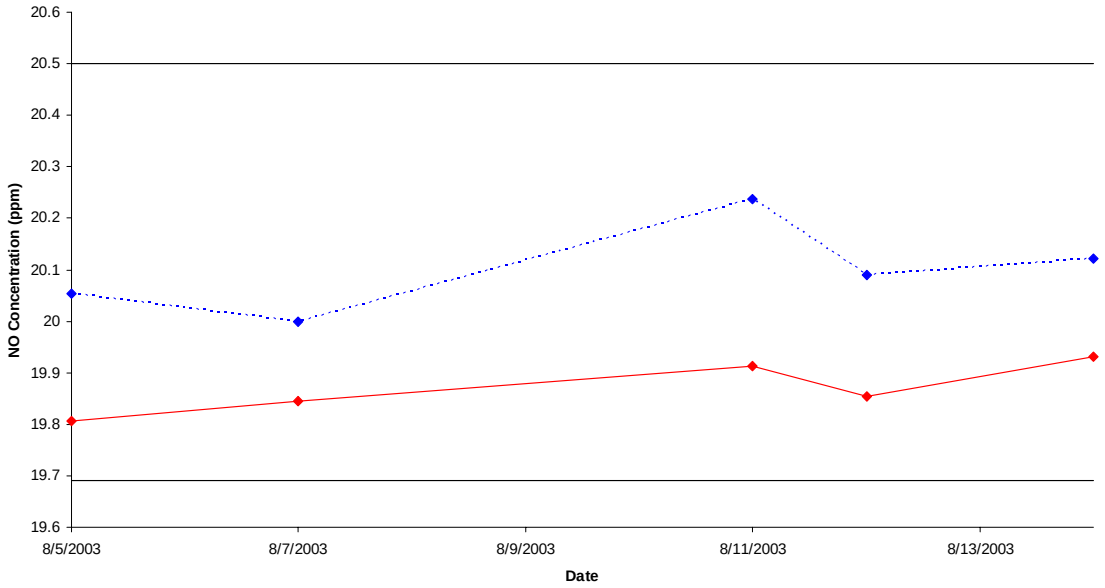

Figure 13: Reported average NO (red) and NOx (blue) concentration for several calibration checks without taking a new background each time.

Once the instrument was verified for working properly and reporting data within specification, the unit was shipped out to Caterpillar Technical Center (CTC) in Peoria, Illinois for combustor rig testing. The primary objective for this field test was the comparison of total dry NOx between the MGA and two independent chemiluminescence detectors (CLDs). The CLDs require the removal of water before measuring the total NOx and report dry NOx concentration. The MGA measures all gases on a wet basis, and therefore the total NOx concentration was corrected for water to be able to compare dry NOx. Figure 14 shows the continuous data collected for all three instruments during testing. The BG-CLD (blue) and the MGA (red) measured the sample stream continuously, where as, the ET-CLD (black) measured the sample stream at specific intervals. Note: the CLD data reported in figure 14 is not corrected for zero or span gas drifts.

At the beginning of the test all three instruments agreed with each other relatively well with approximately 5-8% difference in concentration. Towards the end of the test, the BG-CLD (blue) was reporting total NOx concentrations approximately 20% lower than the other two instruments. Also, the ET-CLD (black) showed a zero/baseline drift

several times during the test, which drifted as high as 0.5 ppm from 0 ppm at times. Yet the ET-CLD (black) and MGA (red) appear to agree with each other relatively well through the entire test. The significant difference in total NOx between the BG-CLD and the other two instruments could be a result from the difference in the heated trace lines. Both the MGA and ET-CLD instruments had approximately 7.5 times longer sample lines than the BG-CLD. Note that the two instruments with the same length in sample lines generally agree throughout the entire test.

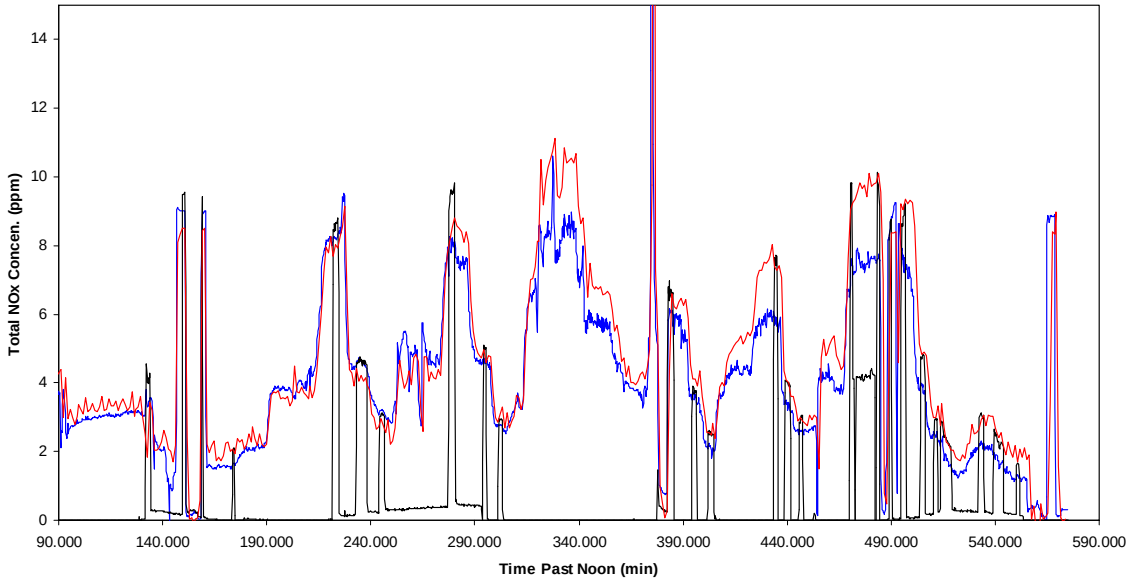

Figure 14: Continuous data comparing the MGA total dry NOx concentration to two independent CLD total NOx concentration. The BG-CLD (blue) measured the sample stream continuously and follows the same trend as the MGA (red). The ET-CLD (black) only measured the sample stream at specific intervals.

Comparing the CO2 concentration reported by the MGA and the ET-NDIR is shown in figure 15. Even through the ET-NDIR (red) measured CO_2 concentration approximately 1% higher than the MGA (blue), the two instruments track each other well. Assuming that the fuel supplied to the combustor rig is pure methane (the composition of natural gas can range from 95 -97% methane), analyzing the H_2O to CO_2 ratio (ideally a 2 to 1 ratio) can give an indication if instruments are measuring the concentrations accurately. Since the ET emission train did not measure H_2O concentration, the reported H_2O concentration from the MGA is assumed to be accurate. Making these two assumptions, the MGA reports an average ratio of 1.9 to 1 H_2O to CO_2, where as, the ET-NDIR gives an average ratio of 1.4 to 1 (Figure 16)

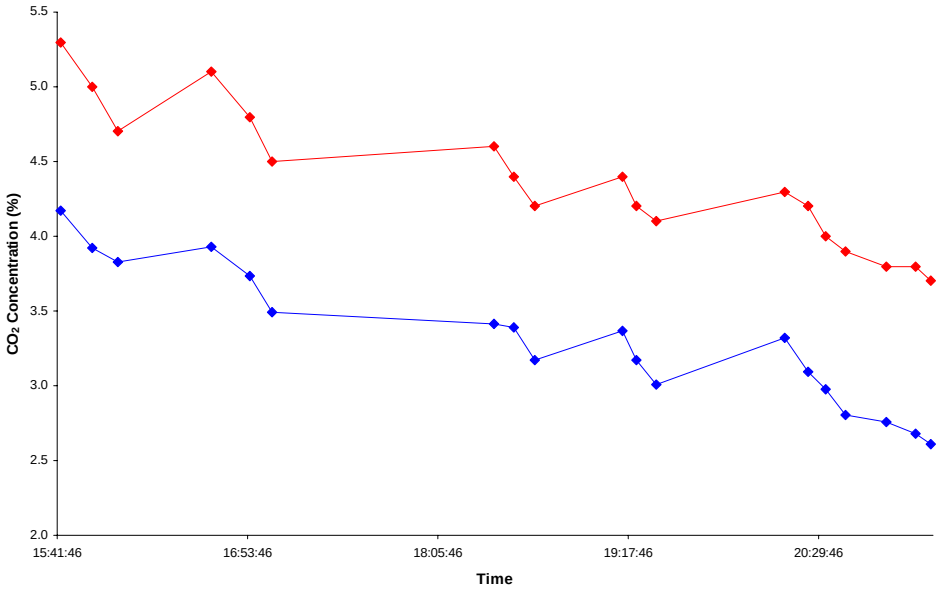

Figure 15: Comparison of CO2 concentration that is reported by the ET-NDIR (red) and the MGA (blue).

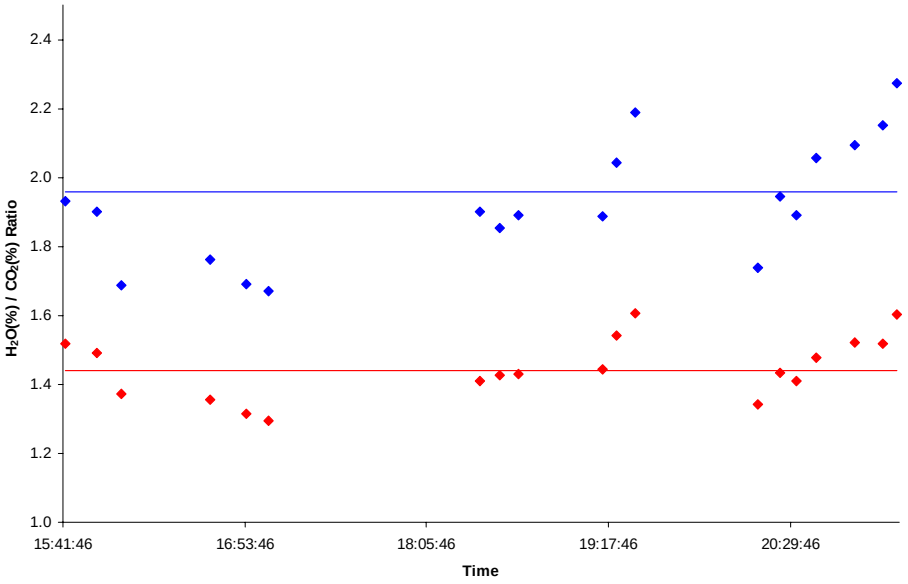

Figure 16: Comparison of the H2O/CO2 ratio calculated for both the MGA (blue) and the ET-NDIR (red) assuming the H2O concentration reported by the MGA is accurate and the fuel is pure methane. The averages are indicated by the solid lines for each instrument.

Knowing the H_2O, CO_2, and O_2 concentrations, ambient O_2 can be back calculated to ensure that the total oxygen concentration measured by the instrument balances out the ambient O_2 present during combustion (ambient O_2 is assumed to be approximately 20.9%). Again assuming the H_2O concentration reported by the MGA is accurate, the average ambient O_2 concentration calculated from the MGA data was determined to be 20.8%, whereas, using the ET-NDIR data that average was 21.9% (Figure 17). Note that the reported O_2 concentration from the ET emissions train was used to back calculate the ambient O_2 for both instruments and was assumed to be accurate.

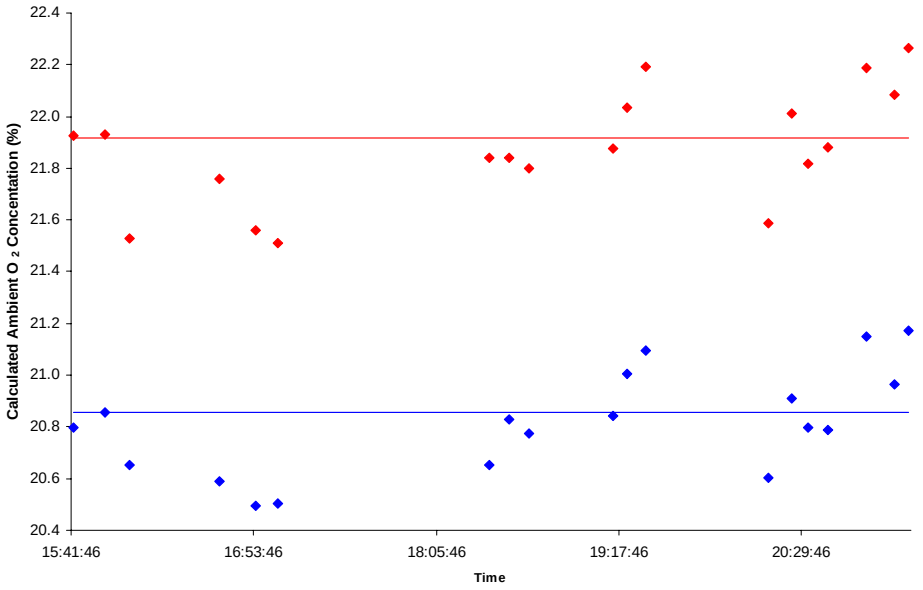

Figure 17: Comparison of the ambient O_2 concentration that was back calculated using the CO_2 data reported by both instruments. The MGA H_2O and the ET-O_2 concentrations were assumed accurate and used for both calculations. The MGA O_2 calculated concentration (blue) is more in line with a 20.9% O_2 ambient than the ET-O2 calculated concentration (red).

Conclusion

The MGA located at the University measured the combustion gases before and after the SCONOx unit continuously showing that it was sensitive enough to measure below 3 ppm total NOx. The instrument exhibited a point-to-point instability, but overall averages show that the MGA was reporting the data accurately. Each time the instrument went through a calibration check, the average reported NO concentration agreed with the calibration bottle within ±2%. The instrument also showed that it was sensitive to formaldehyde changes before and after the NOx scrubber unit, even though the levels present in the sample stream were on the border of the detection limit for the TE-cooled detector. To be able to measure sub-ppm formaldehyde without increasing the scan time, a liquid-nitrogen-cooled detector is required. The instrument was also used to measure the high levels of CO from a steam boiler and then correlated to the H2 concentration being generated for the regeneration cycle in the SCONOx unit. The data supplied to

AFR during this test has not been analyzed at this time, but the University seemed pleased with the real-time results during the test.

The second unit also exhibited the point-to-point instability, but was shipped back to MKS for a full system upgrade. The instrument was shipped back to Solar and the stability was verified by calculating the standard deviation from a 20.1 ppm NO calibration tank (standard deviation was approximately 0.1 ppm compared to the 0.4 ppm before system upgrade). The MGA showed excellent reproducibility by measuring the 20.1 ppm NO calibration tank several times without acquiring a new background each time. During combustor rig testing at CTC in Peoria, Illinois the MGA showed favorable results with the ET-CLD measuring comparable total NOx concentrations throughout the entire test. The BG-CLD data agrees relatively well at the beginning of the test, but then measures approximately 20% total NOx lower than the MGA or the ET-CLD. This difference could be caused by the difference in the heated trace lines used to supply the sample stream to all three instruments. The MGA reported H2O and CO2 concentrations agree with the expected combustion ratio when burning natural gas (ideally a 2 to 1 respectively). The MGA reported a H2O to CO2 ratio of approximately 1.9 to 1 respectively. When back calculating the ambient O2 concentration the MGA agrees relatively well averaging 20.8%, whereas, the ET-NDIR gives an average of 21.9%.

References

1. Brown-Ratafia, J., Manfredo, L., Hoffman, J., Ramezan, M. “Major Environment Aspects of Gasification-based Power Generation Technologies – Final Report.” December 2002.

Appendix I

Final Report Document: **Report on Engine Emissions Analysis, GC-MS Data Collected at MTSU**

REPORT ON ENGINE EMISSIONS ANALYSIS

To: Mr. Vince Zaccardi, AEDC/JE-Svt, 690 Second St., Arnold AFB, TN 37389-4300

From: Dr. Ngee-Sing Chong, Department of Chemistry, MTSU, Murfreesboro, TN 37130

Date: 4/5/2005

Cc: Dr. Bill Phillips, AEDC/JE-Svt, 690 Second St., Arnold AFB, TN 37389-4300

Analysis of jet engine emissions by gas chromatography-mass spectrometry (GC-MS) with solid phase microextraction (SPME) allows the detection of volatile organic compounds as shown in Figure1. The predominant hydrocarbon species found are C2-C7 compounds with the larger molecular weight compounds including polycyclic aromatic hydrocarbons (PAHs) being detected at lower levels. In general, the levels of C2-C7 hydrocarbons decreased as the engine power is increased from 45% to 55%; but the trend for 65% engine power is mixed dependent on the identity of the compounds. It is possible that the higher temperature of the emissions at 65% engine power results in a larger sampling efficiency even though the actual emissions are lower. The PAHs, acenaphthylene, fluoren-9-one, anthracene, were detected for both the Jet A and diesel emission samples collected at 45% engine power but not for the samples collected at 55% and 65% power. Although there were other semi-volatile compounds detected, their origins were questionable as to whether they are combustion-related or derived from the SPME artifacts. The SPME signals for light hydrocarbons are partially affected by the tailing of the dominant peak of carbon dioxide. Nevertheless, the peaks for the hydrocarbons can be separated and integrated successfully for quantitative analysis. In order to enhance the sensitivity of SPME sampling, the sampling device should be chilled throughout the sampling process prior to the GC-MS analysis.

Figure 1: Chromatogram of emission samples collected for 10 minutes each under different conditions of engine power using SPME silica fiber with a mixed coating of Carboxene™ and polydimethylsiloxane.

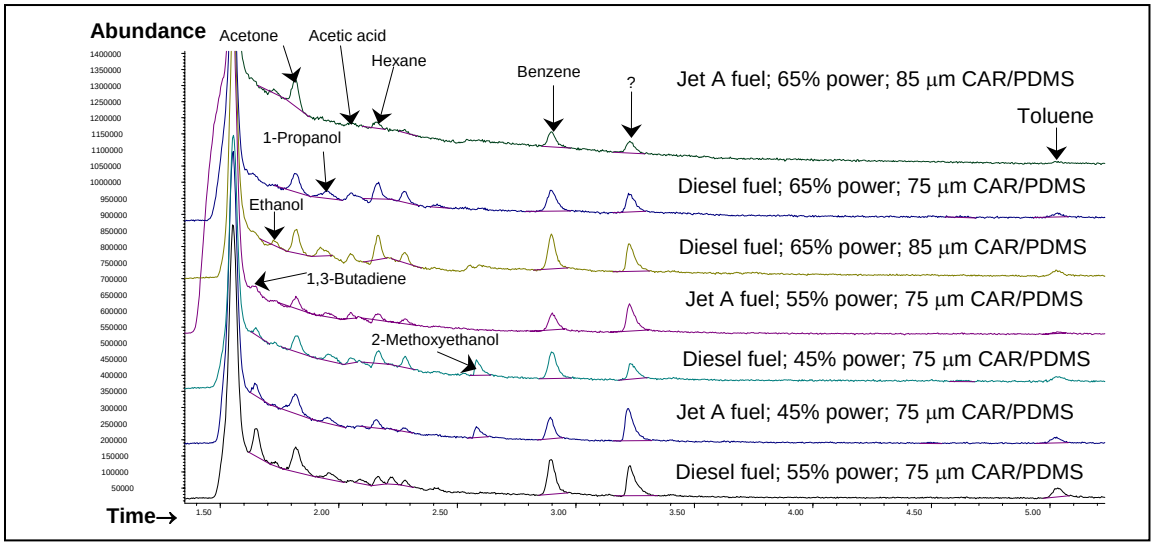

In order to avoid the chromatographic peak tailing, it may be better to either perform the GC-MS analysis in the selected ion mode or reprocess the sample data using the extracted ion mode so that the peak tailing due to carbon dioxide can be eliminated, resulting in a better accuracy of quantitative analysis. Figure 2 shows that these chromatograms are not affected adversely by the peak tailing of carbon dioxide in the extracted ion mode. The compounds corresponding to the retention times of the detected compounds are given in the attached EXCEL spreadsheet that also lists the absolute peak areas and relative distributions of hydrocarbons in engine emissions. Of all the tentatively identified compounds in the samples, the presence of methylene chloride is somewhat surprising and needs to be investigated further. The profile of organic compounds sampled by SPME also needs to be compared with other methods of sampling so that one can evaluate the strengths and limitations of the technique.

Figure 2. Extracted ion chromatograms of the emission sample for diesel at 55% engine power; chromatograms are overlaid for the extracted ions of m/z = 43, 45, 56, 58, 77, and 91.

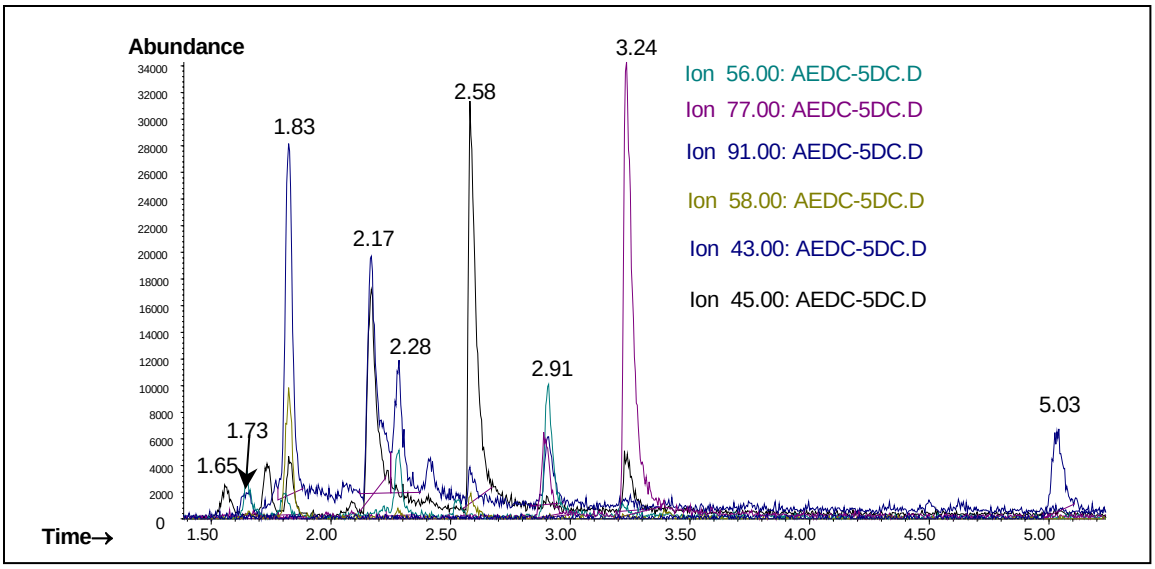

Peak Areas of Tentatively Identified Compounds in Each Sample of Jet Engine Emissions

		AEDC-4JC	AEDC-4DC	AEDC-5JC	AEDC-5DC	AEDC-6DC	AEDC-6JB	AEDC-6DB
	RT(min)	**JetA-45%**	**Diesel-45%**	**JetA-55%**	**Diesel-55%**	**Diesel-65%**	**JetA-65%**	**Diesel-65%**
1,3-Butadiene	1.65	598313	1786259	<MDL	315509	<MDL	<MDL	<MDL
Ethanol	1.73	<MDL	191866	<MDL	<MDL	<MDL	104208	198234
Acetone	1.82	1799795	2160633	716946	1214765	1477029	1807119	1606839
Methylene chloride	1.95	592469	642359	351181	679904	827107	<MDL	649422
1-Propanol	2.05	<MDL	<MDL	260016	274001	162226	<MDL	364049
Acetic acid	2.16	431941	485288	287476	557330	925231	345313	1422321
Hexane	2.28	173479	257098	336910	597282	724023	145875	641038
Ethanol, 2-methoxy	2.58	638580	<MDL	<MDL	897629	<MDL	<MDL	<MDL
Benzene	2.9	1459460	2654163	1185571	2197893	1898798	1152904	2333033
Toluene	5.03	506889	782276	112465	<MDL	322670	<MDL	<MDL
Naphthalene	18.25	138934	<MDL	<MDL	<MDL	139035	308973	450461
1,5-Dimethylnaphthalene	20.62	<MDL	609785	<MDL	<MDL	205564	<MDL	<MDL
Acenaphthylene	20.87	1500540	646840	<MDL	<MDL	<MDL	<MDL	169978
Fluoren-9-one	22.72	330984	131895	<MDL	<MDL	<MDL	<MDL	<MDL
Anthracene	22.96	4528075	462964	<MDL	<MDL	<MDL	<MDL	1112899
Phenanthrene	23.03	690946	<MDL	<MDL	<MDL	<MDL	<MDL	147422
Pyrene	24.73	927880	<MDL	<MDL	<MDL	<MDL	<MDL	<MDL
Total Peak Area		**1.43E+07**	**1.08E+07**	**3.25E+06**	**6.73E+06**	**6.68E+06**	**3.86E+06**	**9.10E+06**

Relative Distribution of Tentatively Identified Compounds in Each Sample of Jet Engine Emissions

	RT(min)	**JetA-45%**	**Diesel-45%**	**JetA-55%**	**Diesel-55%**	**Diesel-65%**	**JetA-65%**	**Diesel-65%**
1,3-Butadiene	1.65	4.18%	16.52%	<MDL	4.69%	<MDL	<MDL	<MDL
Ethanol	1.73	<MDL	1.77%	<MDL	<MDL	<MDL	2.70%	2.18%
Acetone	1.82	12.57%	19.98%	22.06%	18.04%	22.11%	46.76%	17.67%
Methylene chloride	1.95	4.14%	5.94%	10.80%	10.10%	12.38%	<MDL	7.14%
1-Propanol	2.05	<MDL	<MDL	8.00%	4.07%	2.43%	<MDL	4.00%
Acetic acid	2.16	3.02%	4.49%	8.84%	8.28%	13.85%	8.94%	15.64%
Hexane	2.28	1.21%	2.38%	10.36%	8.87%	10.84%	3.77%	7.05%
Ethanol, 2-methoxy	2.58	4.46%	<MDL	<MDL	13.33%	<MDL	<MDL	<MDL
Benzene	2.9	10.19%	24.55%	36.47%	32.64%	28.42%	29.83%	25.65%
Toluene	5.03	3.54%	7.24%	3.46%	<MDL	4.83%	<MDL	<MDL
Naphthalene	18.25	0.97%	<MDL	<MDL	<MDL	2.08%	8.00%	4.95%
1,5-Dimethylnaphthalene	20.62	<MDL	5.64%	<MDL	<MDL	3.08%	<MDL	<MDL
Acenaphthylene	20.87	10.48%	5.98%	<MDL	<MDL	<MDL	<MDL	1.87%
Fluoren-9-one	22.72	2.31%	1.22%	<MDL	<MDL	<MDL	<MDL	<MDL
Anthracene	22.96	31.62%	4.28%	<MDL	<MDL	<MDL	<MDL	12.24%
Phenanthrene	23.03	4.83%	<MDL	<MDL	<MDL	<MDL	<MDL	1.62%
Pyrene	24.73	6.48%	<MDL	<MDL	<MDL	<MDL	<MDL	<MDL

Appendix J

Final Report Document: **Significant Deliverables and Achievements**

STATUS OF CONTRACT DELIVERABLES
(Deliverables as Listed in Statement of Work Addendum FY2003, Rev. August 2003, htbiii, KS, DG, JM)

The contractor AFR is of the opinion that the Contract Deliverables have been satisfactorily met.

SOW Section and Item	Status
6.0 Deliverables	
1. Six Model 2030 FT-IR systems purchased with FY02 funds will be modified to include a quick response Oxygen Sensor. Sensor selection will be based on results of MTSU trials (AFR responsibility)	Two brands of oxygen sensors evaluated at MTSU trials. Selection made. Note that two additional FT-IR systems, not identified in the SOW, were also modified. 1. 07-121 MGA 2030: modified 2. 07-126 MGA 2030: modified 3. 07-127 MGA 2030: modified 4. 07-128 MGA 2030: modified 5. 07-129 MGA 2030: not modified†† 6. 07-131 MGA 2030: modified** 7. 07-101 MGA 2030: modified* 8. 04-008 MGA 2010: modified† †† unit significantly damaged during commercial field trial; returned to AFR, not repaired due to high cost estimate ** thermo-electrically cooled detector * pre-project unit † pre-project unit, older model, SBIR Phase II prototype
2. Measurement trials with JT-12 and/or J-85 engines at MTSU (AEDC responsibility) Trial 1 – Oxygen Sensor Investigation Trial 2 – Optimized MGA configuration for AEDC TECHMAT engine test Trial 3 – Hydrocarbon Speciation Investigation Trial 4 – Afterburner Emissions modeling Investigation	 1. Completed 2. Completed 3. Completed 4. Not Completed: trial opportunity not available during project; engine with afterburner to be relocated from MTSU (due to noise issues)
3. Measurement trials on AEDC Test Facility (AEDC & AFR Responsibility) Trial 1 – TECHMAT engine test Trial 2 – Glycol test in AEDC facility Additional Trial – AEDC Tunnel 9	 1. Completed 2. Completed 3. Completed
4. Draft Aerospace Information Report (AIR 5917) has been assigned by SAE. AEDC and AFR will jointly complete the draft AIR and present it to the SAE	Completed: AIR 5917 submitted to the SAE E-31 Committee on June 8, 2004

222

E-31 Committee for review and approval as an ARP (AEDC & AFR responsibility)	
5. Data from all laboratory trials and measurements will be copied to AFRL/MLQL to support FT-IR quantification and mixture analysis algorithm development.	Completed
6.1 Reports (AFR Responsibility)	
1. Progress reports – due quarterly 2. Operations manuals – due within 12 months after start of contract addendum 3. Maintenance manuals – delivered within 12 months after start of contract addendum - will include schematics and hardware drawing as appropriate	1. Contract change to monthly – reporting completed 2. Completed – MGA manuals shipped with units; improvement manuals included in reports draft final report, and final report 3. Completed – included with operations manuals and improvement manuals
4. Final Report – due within 12 months after start of contract addendum. Infrared spectral data and experimental data will be copied to AFRL/MLQL to support infrared spectral analysis algorithm developments.	Completed
6.2 Briefing & Test Support (AFR Responsibility)	
1. Technical Brief for Professional Group – due within 12 months after start of contract addendum	Completed at the ISA 50th International Instrumentation Symposium/PIWG Session (May 13, 2004)
2. Support performance demonstrations of the system at Arnold AFB facilities- due 6-12 months into the contract addendum	Completed
3. Technical Support - The contractor shall provide technical support for 3-6 months after the initial installation at Arnold AFB via telephone. The support period also includes one two-person trip to Arnold AFB for a maximum duration of 5 days upon client request. The contractor shall develop costing data to allow a post-deployment technical support system to be developed that will allow support for an indefinite duration	Technical support completed, including support to AEDC personnel at the 16 day NASA APEX test at Dryden Flight Research center, Edwards, CA. Costing data to allow a post-deployment technical support system to be developed was completed.

223

4. Technical data from the development effort will be captured and preserved for use in post-deployment support systems	Completed-all data and operational updates are at AFR and AEDC
6.3 Hardware (AFR Responsibility)	
1. Upgrade the 4 AEDC Model 2030 with the selected oxygen sensor before TECHMAT engine test in AEDC C-1 test stand	Completed, plus two additional AEDC units upgraded
2. Upgrade the 2 Solar Turbine Model 2030 with selected oxygen analyzer by 15 December 2003	Completed for the surviving unit in September 2004 when returned to AFR
6.4 Software (AFR Responsibility)	
1. The addition of hydrocarbon speciation calibration library will be generated and delivered to AEDC	Completed
2. Software source codes and algorithms will be documented and copies will be preserved a starting points for further developments, if necessary	Completed
6.5 Demonstration (AFR Responsibility)	
1. 50% demonstration of progress, MTSU Trials 1, 2, 3 and 4, to include report and documentation of results – due within 12 months after start of contract addendum	Completed
2. 85% demonstration of prototype system at AEDC, Trials 1 & 2, to include report and documentation of results, due within 12 months after start of contract addendum	Completed

224